UNIVERSITY OF CALIFORNIA
RIVERSIDE

Synthesis and Functionalization of Bioactive Nitrogen-Containing Heterocycles: *Lycopodium* and Isoquinoline Alkaloids

A Dissertation submitted in partial satisfaction
of the requirements for the degree of

Doctor of Philosophy

in

Chemistry

by

Andy Trinh

March 2024

Dissertation Committee:
Dr. Kevin G. M. Kou, Chairperson
Dr. Christopher Y. Switzer
Dr. Richard J. Hooley

The Dissertation of Andy Trinh is approved:

_____

_____

_____

Committee Chairperson

University of California, Riverside

ABSTRACT OF THE DISSERTATION

Synthesis and Functionalization of Bioactive Nitrogen-Containing Heterocycles: *Lycopodium* and Isoquinoline Alkaloids

by

Andy Trinh

Doctor of Philosophy, Graduate Program in Chemistry
University of California, Riverside, March 2024
Dr. Kevin G. M. Kou, Chairperson

Annotinolides A and B are 7,8-*seco*-lycopodane-derived 8,5-lactones isolated from the club moss *Lycopodium annotinum*. Preliminary investigations revealed amyloid-beta (Aβ) anti-aggregation properties that are not commonly observed in *Lycopodium* alkaloids, demonstrating potential as a therapeutic agent for Alzheimer's disease (AD). AD is characterized by progressive cognitive decline and memory loss that remains a significant challenge in modern medicine. These derivatives show promise in mitigating AD pathology by modulating neurotransmitter levels, reducing oxidative stress, and inhibiting Aβ aggregation, a hallmark of AD progression. Given the history and knowledge of *Lycopodium* alkaloids in promoting healthier connections between nerve cells in the brain, a streamlined and targeted synthesis was conceived towards annotinolides A and B. Our synthesis design features an inverse electron-demand Diels–Alder reaction to access the tricyclic lycopodine-type skeleton, bioinspired radical cyclopropanation, and

photochemical [2+2] cycloaddition. Efforts towards the synthesis of the key tricyclic intermediate will be described.

Tetrahydroisoquinoline (THIQ) alkaloids belong to another class of natural products that are ubiquitous in nature, exhibiting multifaceted pharmacological properties, including anti-inflammatory, antioxidant, and anti-apoptotic activities. More specifically, numerous studies have identified protoberberine natural products as potent modulators of AMP-activated protein kinase (AMPK), a key enzyme involved in energy metabolism regulation. Although AMPK activation is widely recognized, its counterpart remains underexplored, demanding the use of powerful synthetic tools to access novel AMPK inhibitors. To this end, a concise synthetic strategy was developed that showcases novel oxidative C–H functionalization and anionic aza-6π electrocyclization methodologies.

Heteroatom-substituted alkynes, categorized as subgroups of alkynes, have recently found extensive use in the development of synthetic methods. Ynamides in particular, characterized by their polarized triple bonds directly linked to a nitrogen atom, have recently emerged in C–H functionalization processes. The challenge of effectively and selectively transforming C−H bonds stems from their high bond dissociation enthalpy and widespread occurrence throughout organic molecules. To overcome this challenge, a common strategy involves utilizing a weakly coordinating Lewis-basic directing group. Building on the oxidative rhodium-catalyzed C−H functionalization of electron-rich alkenes (Chapter 2), the combination of *N*-methoxybenzamides with underexplored electron-rich ynamides is examined, unveiling unique regioselectivity that features cobalt-catalyzed C–H activation.

Acknowledgements

Thank you to Professor Kevin Kou for providing me with the opportunity to explore synthetic chemistry and its diverse applications at the University of California, Riverside. The expertise and technical skills he imparted have significantly influenced my development as a researcher, enabling me to take on any challenge with enthusiasm. His patience and support throughout my journey were invaluable and I am extremely thankful to have had him as an advisor.

I extend my appreciation to Professors Richard Hooley and Christopher Switzer, members of my dissertation committee, whose guidance was a crucial part in finalizing this work. Special thanks are due to the diligent staff of spectroscopists at UCR ACIF for their assistance with analytical instrumentation. I would also like to acknowledge Barbara Outzen-Hill and Christina Youhas for their coordination of exam dates and administrative tasks. Furthermore, I am grateful to Professor Hill Harman for his instruction during my short time in his group.

I am also incredibly grateful for the warm and upholding atmosphere fostered by my colleagues in the Kou lab. Thank you to Viviene Nguyen for helping me through thick and thin with her sense of humor and setting the standard for excellence. To Aaron Pan for being reliable in difficult times and accompanying me on numerous adventures. To Melody Wu for her voice of reason that typically leads me down the right path. I wish you the best in your future aspirations as a chemist. To Roni Manasi for extending his camaraderie to what has become a meaningful friendship. To Yujie Cao for being my partner through the better half of my career and keeping everyday an interesting one. I would also like to

acknowledge all of the undergraduate students I mentored—it was a privilege to guide them. Lastly, I am indebted to Elaine Bui and my family for their unconditional support, serving as the driving force behind my achievements.

Table of Contents

List of Tables

List of Figures

List of Schemes

Chapter 1 – Total Synthesis of Annotinolides A and B

1.1 Introduction

1.1.1 Background and Biological Activity

Alkaloids are a class of natural products characterized by their nitrogen-containing organic structures. Renowned for their structural complexity and pharmacological significance, alkaloids are ubiquitous in the plant kingdom and have historically played a pivotal role in the field of medicinal chemistry.[1-4] These compounds, often alkaline in nature, encompass a wide range of molecular structures, and their diverse biological activities make them intriguing subjects for scientific inquiry.

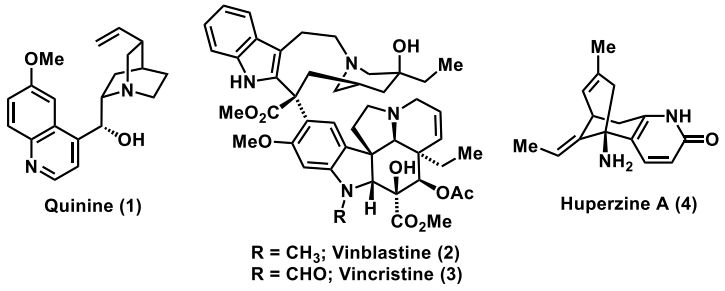

Figure 1.1: Structures of some historical alkaloids.

One of the notable contributions of alkaloids to medicine is their efficacy in treating various diseases.[1-4] For instance, the alkaloid quinine (**1**), extracted from the bark of the cinchona tree, has long been employed as an anti-malarial agent. Quinine's ability to interfere with the malaria parasite life cycle in the human body has made it an indispensable tool in the fight against this devastating tropical disease.[5-9] Additionally, vincristine (**2**) and vinblastine (**3**), derived from the Madagascar periwinkle plant, have exhibited potent anti-tumor properties, making them key components in cancer chemotherapy regimens (Figure 1.1).[5-9] The unique structural features of alkaloids contribute to their specific biological

activities, and their study remains crucial for unraveling the mysteries of medicinal plants and developing novel therapeutics. In particular, *Lycopodium* alkaloids are pyridine-, or quinolizine- and α-pyridone-type–compounds that belong to over 500 species of plants. In 1881, Bodecker isolated lycopodine from *Lycopodium* complanatum, which was confirmed as the first *Lycopodium* alkaloid upon being reisolated and characterized by Achmatowicz in 1938.[5-9] As these natural products gained popularity, a broader understanding of *Lycopodium* alkaloids led to their categorization into four structural subclasses: lycodine (**5**), phlegmarine (**6**), lycopodine (**7**), and fawcettimine (**8**).[10]

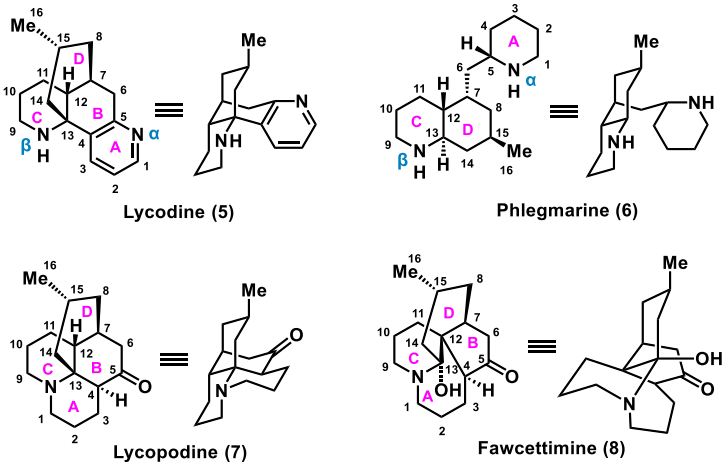

Figure 1.2: *Lycopodium* alkaloids subclasses.

While these natural products offer a vast repertoire of bioactive compounds, their isolation from natural sources can be challenging due to limitations in supply, extraction, and the ecological impact of overharvesting. Synthetic chemistry plays a crucial role in overcoming these challenges by enabling the production of natural product derivatives with enhanced efficacy and accessibility. Synthetic chemists strive to replicate and modify the complex structure of alkaloids, optimizing their pharmacological properties and addressing

issues related to supply and sustainability.[10,11] As our understanding of the intricate relationship between natural products and human health deepens, chemists increasingly explore the potential of alkaloids in addressing neurodegenerative diseases. Alzheimer's disease, characterized by the accumulation of β-amyloid (Aβ) plaques and tau tangles in the brain, represents one of the most challenging and prevalent neurodegenerative disorders.[11-14] The complexity of Alzheimer's disease necessitates multifaceted therapeutic approaches, and *Lycopodium* alkaloids are persistently emerging as promising candidates for intervention.

Interest in *Lycopodium* alkaloids surged in the mid-1980s when it was discovered that certain members of this natural product family exhibited potent acetylcholinesterase (AChE) inhibition activity.[11-14] This finding was significant because one of the prevalent markers of Alzheimer's disease in the brain is characterized by a deficiency in AChE, along with the aggregation of β-amyloid plaques and tau protein tangles. The crucial role of cholinesterases is to hydrolyze choline esters, where insufficient hydrolysis of acetylcholine in the cholinergic synapses has been associated with a decline in cognitive function.[11-14] Despite this reported relationship, the exact etiology remains unknown and continues to elude scientists in the broader understanding of Alzheimer's disease pathogenesis. Among all the *Lycopodium* alkaloids examined, it was revealed that huperzine A (HupA, **4**), isolated from the Chinese herb Qian Ceng Ta by Liu and co-workers, stood out as the most potent acetylcholinesterase inhibitor.[15-17] One significant challenge in treating neurological diseases in the central nervous system (CNS) stems from the difficulty therapeutics face in penetrating the blood-brain barrier (BBB) to access the

brain, which is essential for exerting their medicinal effects. Intriguingly, it has been demonstrated that HupA can efficiently penetrate the BBB with superior bioavailability and longer inhibition of acetylcholinesterase compared to several FDA-approved Alzheimer's disease therapeutics, including galantamine, tacrine, rivastigmine, or donepezil.[15-17] This became a focal point to further investigate HupA and therefore, found its ability to mitigate cognitive deficits in a wide range of animal models. Due to HupA's potent anti-acetylcholinesterase activity and selectivity, it was employed in studies to elucidate structure-activity relationships (SARs).[15-17] Moreover, numerous research groups have drawn inspiration from HupA, embarking on the development of derivatives and analogs with the overall purpose of enhancing potency and selectivity.

Specifically, the (–)-huperzine A enantiomer has been established as a competitive inhibitor of AChE by the Lineweaver-Burk analysis–a widely used enzyme kinetics method of determining the affinity of an enzyme for its substrate.[15-17] This potent and reversible inhibitor of AChE exhibited an estimated IC_{50} of 82 nM in the rat cortex *in vitro*. Compared to (±)-donepezil (IC_{50} = 10 nM) and the discontinued drug tacrine (IC_{50} = 93 nM), (–)-huperzine A occupied a position to supply quality treatment without irreversible damage to major human organs. Aside from its other pharmacological effects, the absolute stereochemistry of (–)-huperzine A is significant for inhibiting AChE 50 times more efficiently than its unnatural enantiomer (+)-huperzine A.[15-17] The X-ray crystallographic structure of a TcAChE (*Torpedo californica*) bound complex to (–)-huperzine A gave rise to this conclusion by depicting a favorable attraction between the charged amino group and

the aromatic rings of Trp84 and Phe330 in the active site (Figure 1.3), which was absent with (+)-huperzine A.[15-17]

Extracellular senile plaques represent a key histological feature in the brains with Alzheimer's disease. The primary constituents of these plaques are Aβ fragments, short peptides comprising 36-43 amino acids, formed through the proteolysis of the membrane-bound amyloid precursor protein (APP).[15-17] APP undergoes cleavage via two pathways, including the neurotrophic α-secretase non-amyloidogenic pathway, where peptidase proteins on disintegrin and metalloprotease families cleave APP into soluble α-APP fragments, releasing them into the extracellular media. While α-APP fragments exhibit neurotrophic and neuroprotective properties, the alternative β/γ-secretase amyloidogenic pathway results in the generation of insoluble Aβ fragments. Aβ has been implicated in triggering apoptotic responses, such as neuronal membrane blebbing and cell shrinkage, ultimately leading to cell death.[15-17] Consequently, numerous potential therapeutic approaches for AD aim to modify the β/γ-secretase amyloidogenic processing pathway.

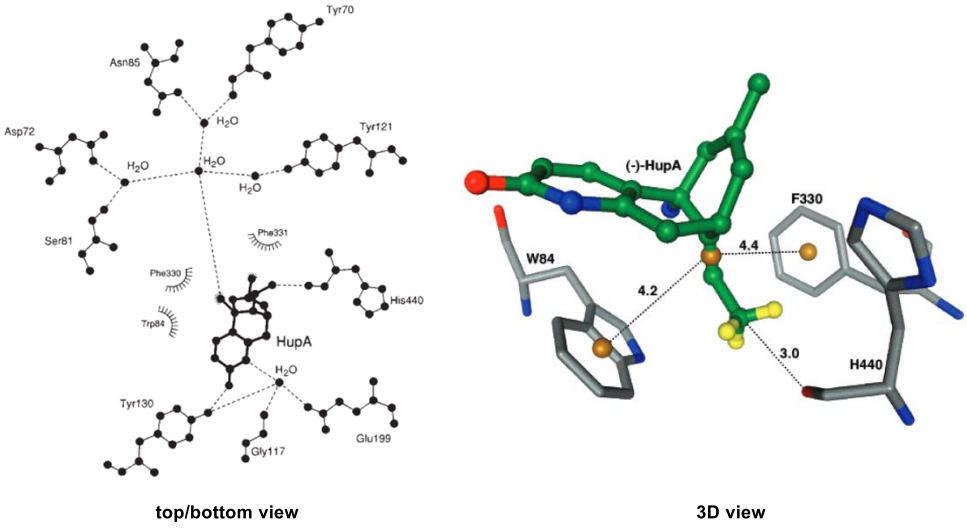

Figure 1.3: Interaction of (–)-HupA with the anionic site of *Tc*AChE.

The observed association between AChE activity and Aβ deposition suggests that (–)-hupA may influence Aβ-induced neurotoxicity.[15-17] Notably, (–)-hupA was found to mitigate Aβ-induced memory deficits and neurodegeneration in rats. In a Morris water maze test, rats received either a mixture of Aβ1-40 (intracerebroventricular infusion) and (–)-hupA (0.1 or 0.2 mg/kg, IP, once per day for 12 consecutive days), Aβ1-40 alone, or a vehicle control. The Morris water maze (MWM) is a spatial learning test for rodents, where they navigate from different start locations around a swimming arena to find a submerged escape platform using distant cues. Rats administered Aβ1-40 alone took longer to locate the platform than those receiving Aβ1-40 co-administered with (–)-hupA or the vehicle.[15-17] In a probe trial test, rats treated with (–)-hupA and Aβ1-40 spent more time in the probe quadrant than those treated with Aβ1-40 alone. The results showed that (–)-hupA significantly alleviated pathological deformations induced by Aβ1-40 in both the cortex and hippocampus of rats, while also mitigating the formation of amyloid deposits through the cortex. Despite these thorough investigations of AChE inhibitors, Alzheimer's disease remains uncurable.[15-17] The positive impacts of cholinesterase inhibitors (ChEIs) are believed to stem mainly from their capacity to enhance cholinergic neurotransmission by delaying the breakdown of ACh. However, the anticipated neuroprotective effect in Alzheimer's disease (AD) patients is absent.[15-17] Furthermore, research conducted by the Alzheimer's Disease Neuroimaging Initiative (ADNI) and the Australian Imaging, Biomarkers and Lifestyle (AIBL) study revealed a higher rate of cognitive decline in AD participants receiving long-term ChEI treatment compared to those not undergoing treatment.[15-17] This is evidence that the discovery of new synthetic targets is required to

reexamine mechanisms of action and to provide more options toward treating victims of AD. Luckily, there is more to uncover within the history between *Lycopodium* alkaloids and Alzheimer's disease, serving as inspiration for new potential therapeutics.

1.1.2 Biomimetic Inspiration

Lycopodium alkaloids are a diverse group of secondary metabolites found in various species of the *Lycopodium* genus, commonly known as club mosses.[18,19] Understanding the biosynthetic pathways of *Lycopodium* alkaloids has been a crucial area of research in natural product chemistry. Chemists, such as Ayer and Hemscheidt, have contributed to proposed biosyntheses for *Lycopodium* alkaloids over the years. The initial hypotheses revolved around identifying new members within each subclass of *Lycopodium* alkaloids, suggesting that smaller, less structurally complex, and less oxidized members might serve as intermediates en-route to more complex counterparts.[18,19] The Spenser group at McMaster University made significant contributions to this field through their groundbreaking research on feeding experiments with certain species of *Lycopodium annotinum*.[20-26] Spenser employed feeding experiments as a key methodology by providing labeled precursors to *Lycopodium annotinum*. More specifically, the objective of these experiments was to identify intermediates in the biosynthetic pathway by feeding ^{13}C- and ^{14}C radio- or stable isotope-labeled potential precursor materials to *Lycopodium* shoots.

After harvesting the fed plants one to five days later, Spenser analyzed the tissues for incorporation of the labeled potential precursors into intermediates or the end product of *Lycopodium* alkaloids.[20-26] Successfully incorporating the labeled precursors into more complex *Lycopodium* alkaloids indicated that the fed material was the correct starting

material for biosynthesis or was at least consumed and integrated at some point in the pathway. The results of his experiments provided valuable insights into the enzymatic transformations and molecular mechanisms underlying the synthesis of these bioactive compounds.[20-26] Spenser's contributions extended beyond experimental work; he played a crucial role in proposing hypotheses and developing theoretical frameworks to explain the observed biosynthetic pathways. One of the targets that piqued his interest was hupA, a known AChE inhibitor as described previously, which was included in the proposed biosynthesis of huperzinine, a related *Lycopodium* alkaloid.[20-26]

Feeding experiments involving L-lysine (**9**) revealed that the proposed biosynthetic pathway to huperzinine is initiated through lysine decarboxylase-mediated decarboxylation, resulting in the formation of cadaverine (**10**) (Scheme 1.1).[20-26] Subsequent enzymatic steps included the conversion of cadaverine to 5-aminopentanal (**11**) by diamine oxidase, and then to Δ-piperideine (**12**) through amine condensation. Δ-Piperideine was coupled with acetonedicarboxylic acid (bisCoA ester, **16**) to yield 4-(2-piperidyl) acetoacetate (4PAA, **17**) or 4-(2-piperidyl) acetoacetyl-CoA (4PAACoA, **18**), facilitated by an unidentified enzyme. This coupling partner originated from dimerization of two malonyl-CoA units by a ketosynthase enzyme. Following this, 4PAA (**17**) and/or 4PAACoA (**18**) underwent decarboxylation, mediated by an unknown decarboxylase, resulting in the formation of pelletierine (**19**), the pivotal first intermediate in the biosynthesis of various *Lycopodium* alkaloids.

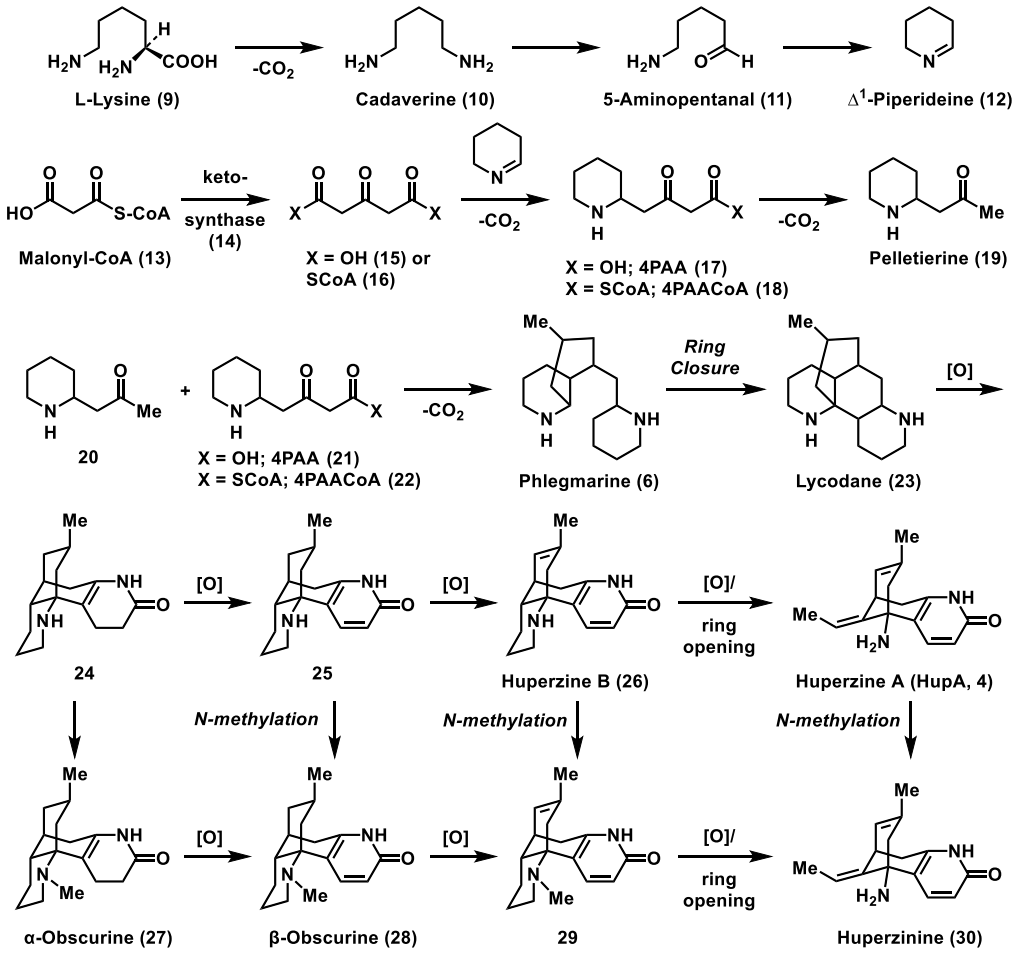

Scheme 1.1: Proposed biosynthetic pathway to Huperzinine and HupA related *Lycopodium* alkaloids.

Pelletierine then underwent coupling with 4PAA or 4PAACoA through decarboxylation, catalyzed by another unknown decarboxylase, producing phlegmarine (**6**), which played a central role in the subsequent steps.[20-26] From **6**, enzymatic processes including an oxidative ring closure, catalyzed by an enzyme related to berberine bridge enzyme, and a series of oxidases, led to the formation of lycodane (**23**).[20-26] Exposure to cytochrome P450 enzymes or 2-oxoglutarate-dependent dioxygenases gave rise to lycodine (**5**), one of the four main structural subclasses of *Lycopodium* alkaloids. Alternative oxidations of **23** resulted in the formation of huperzine B (hupB, **26**), which

could be converted to hupA through a stepwise oxidation and ring opening.[20-26] Finally, a double *N*-methylation of the primary amine affords huperzinine (**30**), which could also be isolated in its natural form and demethylated in the retrosynthetic sense as a separate method of accessing hupA. Other potential routes proposed include formation of α-obscurine (**27**) and β-obscurine (**28**), derived from a family of sarcomeric signaling proteins, through *N*-methylation of the C ring secondary amine or of the A ring enamide. Oxidation of **28** furnishes trisubstituted alkene **29**, which then a series of oxidation, ring-opening, and *N*-methylation steps would lead to the production of **30**. [20-26] Various permutations of these pathways contribute to the intricate biosynthetic routes of all *Lycopodium* alkaloids.

1.1.3 Previous Syntheses

1.1.3.1 Lycodine-Type Alkaloids

A classification by A. W. Ayer categorized *Lycopodium* alkaloids into four distinct represented by specific flagship compounds, namely lycopodine, lycodine, fawcettimine, and phlegmarine. The carbon numbering system for these alkaloids adheres to Conroy's biogenetic hypothesis, positing that the alkaloids consist of two 2-propylpiperidine units.[27] This system provides a framework that many have utilized toward the syntheses of a diverse array of *Lycopodium* alkaloids. Sarpong, for instance, has successfully accomplished 23 syntheses of various *Lycopodium* alkaloids, highlighting modern C–H functionalization methodologies to achieve concise access.[28,29] His first one was the total synthesis of lyconadin A (**39**), a lycodine-type alkaloid, finished in 2008.[28,29] However, this was after Smith and co-workers figured out their own way to synthesis lyconadin A as

well as lyconadin B (**40**) in the same method (Scheme 1.2).[30] Their synthesis involves union of iodide **31** and hydrazone **32**, followed by hydrolysis, oxidation, and generation of the cyclohexenone ring (**33**) *via* intramolecular aldol condensation. They discovered that tricyclic structure **35** could arise from a favorable 7-*endo*-trig intramolecular conjugate addition involving the enone all in one stereoselective step.[30] Although the construction of **36** contained the brute of their synthetic challenges, they utilized a series of redox reactions, protections, and deprotections to get there. The next cyclization was accessed through an iodination reaction to achieve **37**, which was then functionalized towards Lyconadins A (**39**) and B (**40**) in four steps.[30]

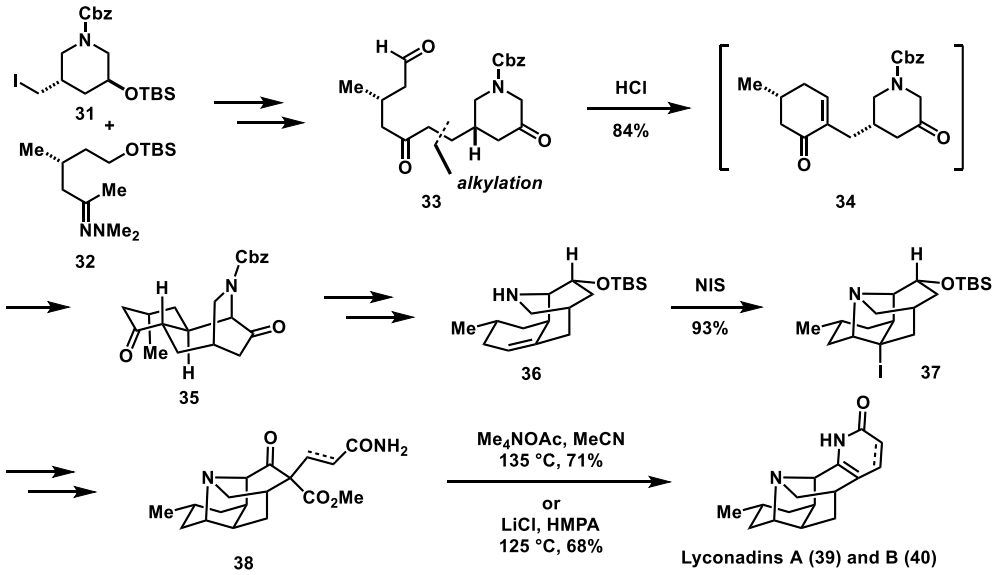

Scheme 1.2: Smith synthesis of Lyconadin A and B.

In contrast to the Smith synthesis, where the construction of the 2-pyridone moiety occurred in the final stages, their synthesis initiated with bromomethoxypicoline (**41**), a concealed 2-pyridone (Scheme 1.3).[31] The Stork–Danheiser reaction facilitated the union of vinylogous ester **42** and picoline **41**. Then, through a sequence involving cross-metathesis (CM) and Heck reactions, the Stork–Danheiser product underwent conversion

into tricyclic compound **43** featuring the desired seven-membered ring.[31] This intermediate was further developed into carbamate **44** from a Curtius rearrangement. Sarpong and collaborators employed reductive amination to establish the C13–N bond, followed by an innovative oxidative C–H amination to construct the challenging C6–N bond (**45**).[31] The methoxypyridine was subsequently transformed into the desired 2-pyridone, marking the successful culmination of their total synthesis of lyconadin A (**39**).[31]

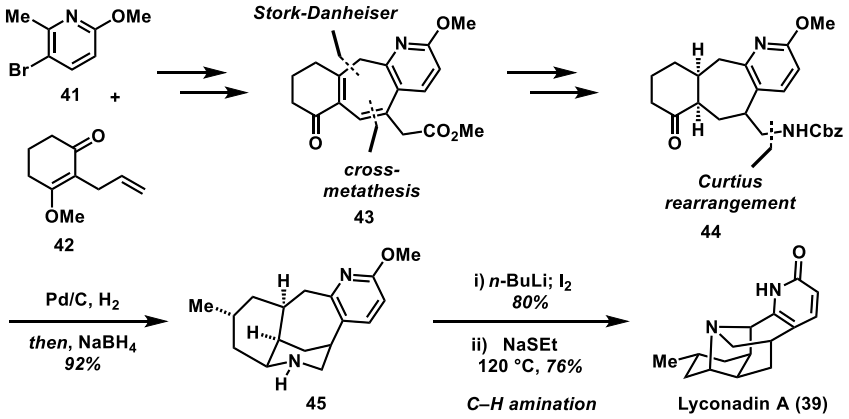

Scheme 1.3: Sarpong, Bisai, and West synthesis of Lyconadin A.

In addition to lyconadins A and B, Fukuyama and co-workers successfully developed a modular approach that allowed construction of lyconadin C as well (Scheme 1.4).[32] In their work, a Diels-Alder reaction is used to form **46** with a methylated butadiene as the diene coupling partner. This was followed by an *aza*-Prins reactions to get tricycle **47**, which was converted into key intermediate **48**.[32] Towards lyconadins A and B, the cyclopropane moiety was simply opened where one of the bromine leaving groups was eliminated to give olefin **49**.[32] Transformation from **49** incorporated a vinylogous Pummerer rearrangement where that product went through a mercury-mediated acid hydrolysis to give enone **50**. From there, lyconadin A was synthesized in two steps and

lyconadin B in 3 steps. Alternatively, cyclopropane **48** was exploited in a ring expansion to cycloheptadiene **51**.[32] Four steps after to assemble the final lactam ring then afforded lyconadin C (**52**).[32]

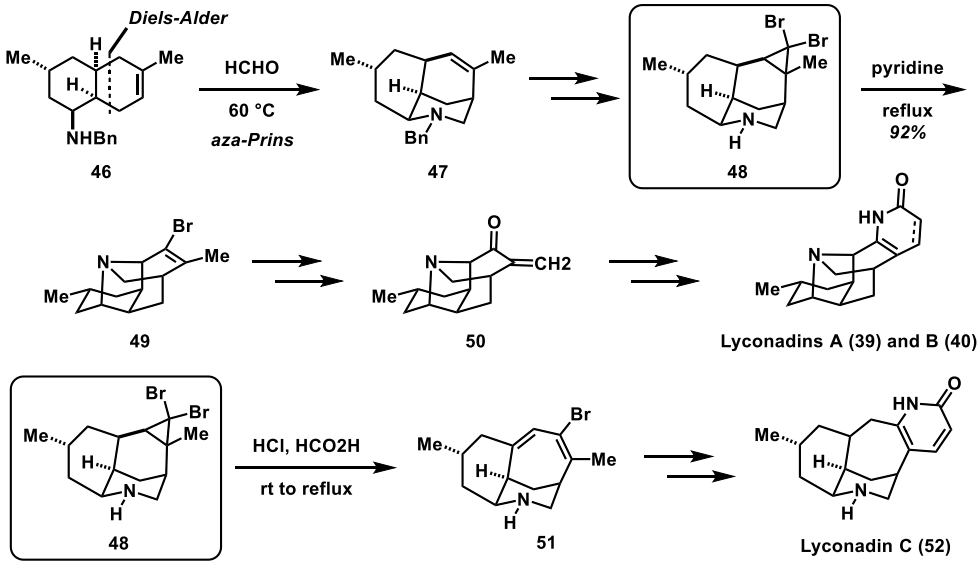

Scheme 1.4: Fukuyama synthesis of Lyconadins A-C.

Similar to Fukuyama's approach, Waters and co-workers also synthesized lyconadin C starting with a Diels–Alder reaction but instead used a silyloxy butadiene to arrive at bicycle **53**.[33] A Mannich reaction facilitated formation of cyclohexanone **54**, which was converted to diazo compound **55** by first conversion of the nitrogen protecting group and then addition by a lithiated ethyl diazoacetate.[33] Treated with rhodium-catalysis, they examined a ring expansion that was followed by triflation and a Stille cross-coupling to provide diene **56**.[33] This was turned into **52** *via* an unprecedented 6π-electrocyclization of a nonaryl dienyl isocyanate intermediate that was reduced into the desired pyridone scaffold of lyconadin C.[33]

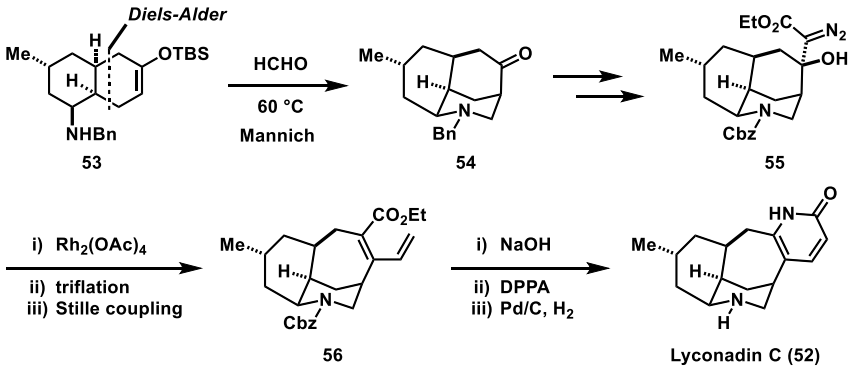

Scheme 1.5: Waters synthesis of Lyconadin C

More recently, Sarpong completed the syntheses of four other lycodine-type *Lycopodium* alkaloids: casuarinine H (**62**), lycoplatyrine B (**63**), lycoplatyrine A (**68**), and lycopladine F (**73**)–through a bioinspired late-stage diversification method (Scheme 1.6).[34] The synthetic approach features access to cross-coupling *via* a site-selective C–H borylation and an oxidative C–C bond cleavage of *N*-desmethyl-*β*-obscurine to give the robust intermediate **57**.[34] From **57**, substoichiometric quantities of RuO_2 with sodium periodate in a mixture of ^{t}BuOH and water resulted in piperidine oxidation to γ-lactam **58**. This was then hydrolyzed and underwent decarboxyolefination to give terminal alkene **60** that acted as a common intermediate toward the natural products. Palladium catalysis afforded alkylation of the terminal olefin **60** and subsequent deprotection gave 8,15-dihydrohuperzine A (**61**) in 33% yield, which has an IC_{50} = 2.6 μM towards AChE inhibition.[34] Alternatively, a simple amine deprotection with TMSI from **60** completed the first total synthesis of (–)-casuarinine H (**62**), a neuroprotective compound, which one further step of a semireduction of its pyridine moiety led to (+)-lycoplatyrine B (**63**).[34]

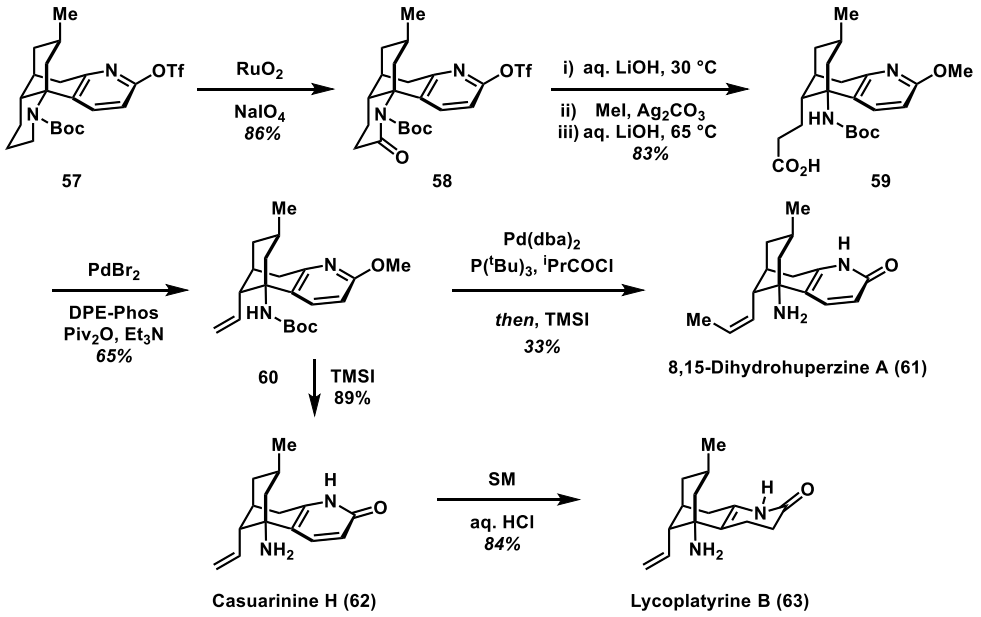

Scheme 1.6: Final transformations toward 8,15-Dihydrohyperzine A, Casuarinine H, and Lycoplatyrine B.

For the other two *Lycopodium* alkaloids, intermediate **57** was instead deoxygenated in the presence of $Pd(OAc)_2$ and ammonium formate as a reductant (Scheme 1.7).[34] The resulting *N*-boc lycodine (**64**) went through a *meta*-selective C–H borylation facilitated by an iridium catalyst, followed by a bromodeborylation to provide 2-bromolycodine (**65**). Coupled with α-hydroxy-β-lactam (**66**) formed *via* a Norrish–Yang reaction, a mild and stereospecific palladium-catalyzed C–C cross-coupling was realized at the C2 piperidine position (**67**).[34] Subsequent cleavage of the Boc and 2-oxophenylacetamide protecting groups on **67** yielded lycoplatyrine A (**68**) as a mixture of C2' epimers; however, use of enantiomerically pure lactams enabled a stereoretentive β-carbon elimination that led to the absolute configurations of this naturally occurring alkaloid.[34]

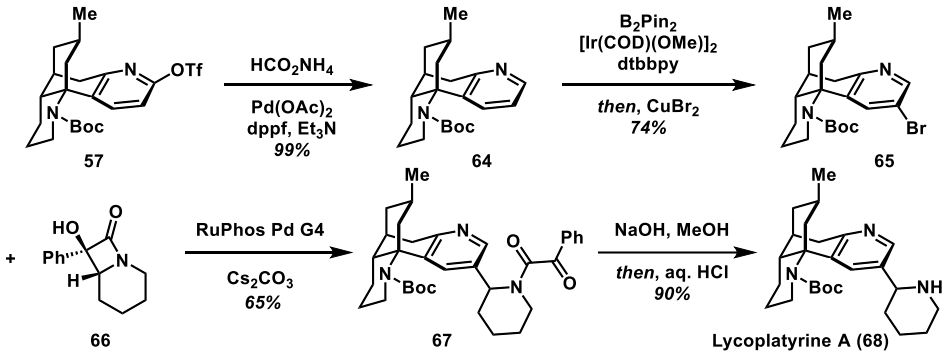

Scheme 1.7: Synthesis of Lycoplatyrine A by Sarpong and co-workers.

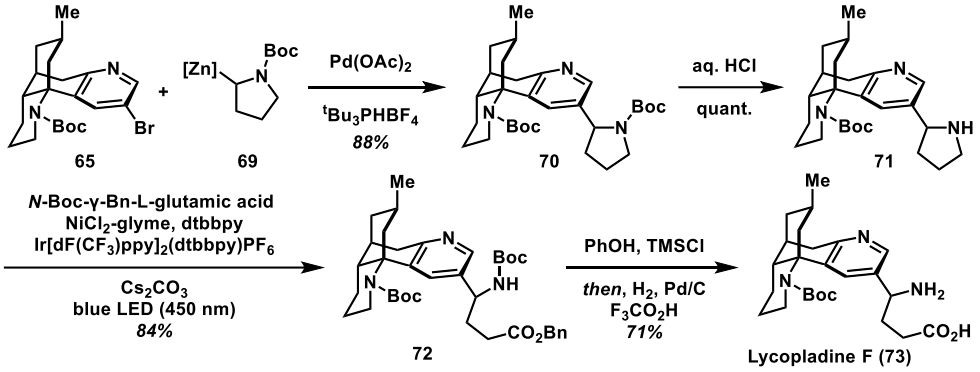

Scheme 1.8: Synthesis of Lycopladine F by Sarpong and co-workers.

Diverging from the bromopyridine intermediate **65**, a Negishi coupling with zinc pyrrolidine **69** afforded the alkylated product **70** in 88% yield.[34] Mono-cleavage of the pyrrolidine *N*-Boc was performed with aqueous HCl to give pyrrolidine **71**. This lycoplatyrine A derived intermediate (**71**) was C(sp^3)–C(sp^2) cross-coupled with *N*-Boc-*γ*-Bn-L-glutamic acid under nickel-catalyzed conditions upon activation of the amino acid moiety *via* iridium-catalyzed photoredox to produce **72**.[34] Deprotection of the primary amine and distal carboxylic acid afforded lycopladine F (**73**).

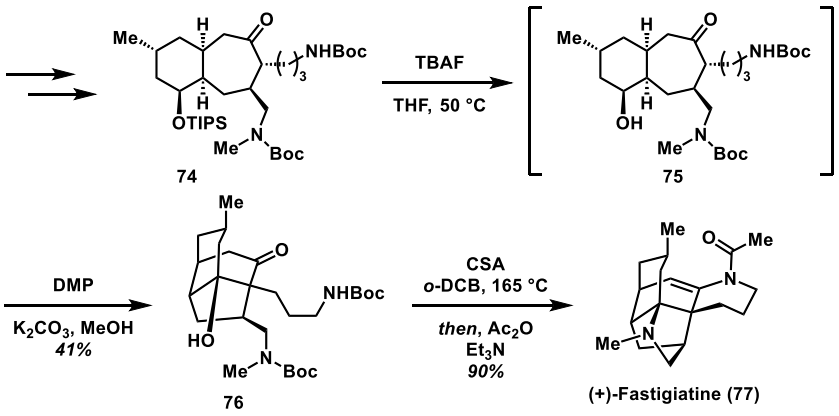

Scheme 1.9: Second generation synthesis of (+)-Fatisgiatine.

In addition to Sarpong's examples, there was another notable synthesis of a lycodine-type *Lycopodium* alkaloid called (+)-fatisgiatine (**77**) by Rychnovsky, who incorporated a biomimetic approach (Scheme 1.10).[35] In the late stages, this method employed a TBAF alcohol deprotection of silyl ether **74** that led to tricycle **76**. From there, CSA cleaved both *N*-Boc groups and induced a retro-aldol of the tricycle that facilitated the transannular aldol–Mannich cascade, finishing the synthesis.[35]

1.1.3.2 Fawcettimine-Type Alkaloids

Fawcettimine-type *Lycopodium* alkaloids were among one of the first to be pursued, where the first diastereoselective synthesis of fawcettimine, also known as Burnell's Base A, was in 1979 by Inubushi and co-workers (Scheme 1.10).[36] This was a low-yielding synthesis at an overall 0.1% over 26 steps, which resulted in some controversy about one stereocenter at the time. Almost a decade later in 1989, Heathcock not only resynthesized fawcettimine in 13 steps with a 17% overall yield, but he also designed a 6-5-9 tricycle, now known as the "Heathcock strategy", that is integrated in several syntheses of alkaloids in the fawcettimine class.[37] This landmark synthesis gave the "Heathcock

tricycle" its start as a target intermediate, where many creative strategies were developed to overcome the challenging C4 quaternary center in **81** of the tricycle located at the ring fusion. In 2014, one of the most significant breakthroughs to this issue was established by Williams and co-workers, where they performed a Diels–Alder reaction with silyloxy butadiene **82** and poorly activated enone **83** to access **87** in 10 an overall 10 steps.[38] Taniguchi and co-workers drew inspiration from this method and found success when they replaced the dienophile with a variety of alkynes.[39] They also found that altering both Diels–Alder adducts resulted in different scaffolds that granted a pathway into some racemic *Lycopodium* alkaloids such as lycopserramine T and lycopoclavamine B.

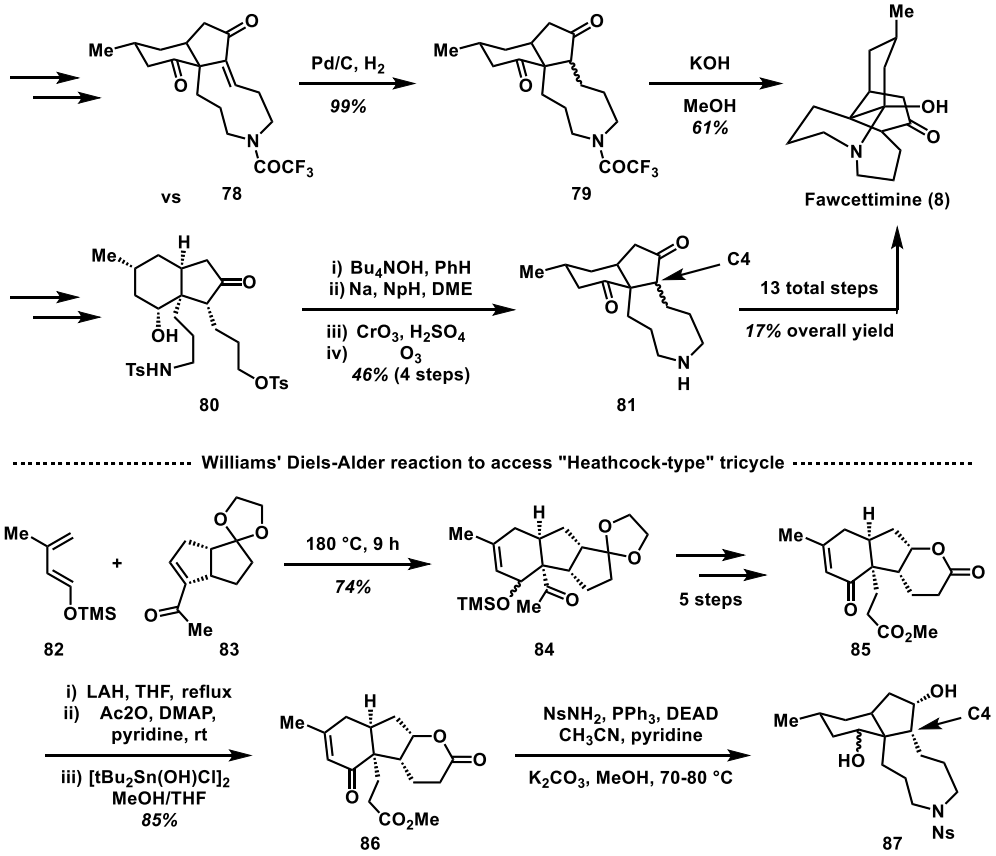

Scheme 1.10: Inubushi and Heathcock syntheses of Fawcettimine.

1.1.3.3 Lycopodine-Type Alkaloids

Disregarding the miscellaneous structural class commonly referred to as "phlegmarine", the last major subcategory of *Lycopodium* alkaloids is the lycopodine class. These typically contain a [3.3.1] framework that has proved challenging to recreate as fluidly as the Heathcock tricycle; however, Taniguchi and co-workers were able to incorporate the strategy constructing (–)-serratinine (**88**), (–)-serratine (**89**), and (–)-serratanidine (**90**).[39] In 2017, Fan and co-workers developed a novel tandem palladium-mediated oxidative dehydrogenation/hetero-Michael addition reaction in their pathway toward huperzine O (**100**), sharing a very similar tetracyclic core (**98**) and is one of few lycopodine-type natural products that have been synthesized (Scheme 1.11).[40]

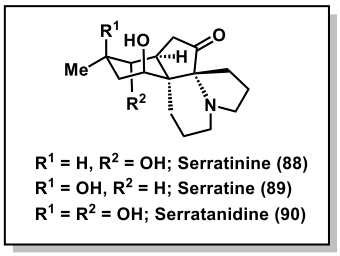

Figure 1.4: Three lycopodine-type alkaloids.

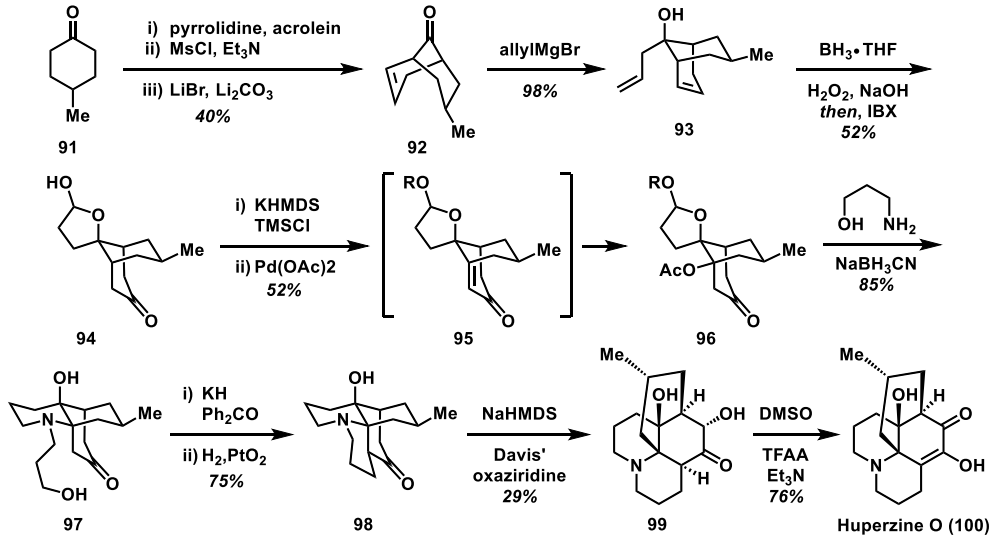

Scheme 1.11: Synthesis of Huperzine O by Fan and co-workers.

1.1.4 Annotinolides A and B

1.1.4.1 Background of *Lycopodium* Alkaloids

While our interest spans various annotinolides, our primary focus lies on two intricately structured members of the lycopodine subclass: annotinolide A (**101**) and B (**102**). These *Lycopodium* alkaloids were extracted from *Lycopodium annotinum*, a club moss indigenous to the Taibai Mountains in Shaanxi, China.[36-43] Notably, annotinolides A and B showcase compelling biological activity against Aβ-peptide aggregation, an uncommon trait among *Lycopodium* alkaloids. In a thioflavin T fluorescence assay, annotinolides A and B demonstrated significant inhibition against Aβ1-42-peptide aggregation at a concentration of only 50 μM. This inhibition surpassed that of the positive control, EGCG (epigallocatechin gallate), with annotinolide A and B registering inhibitory ratios of 42.4% and 38.1%, respectively.[36-43]

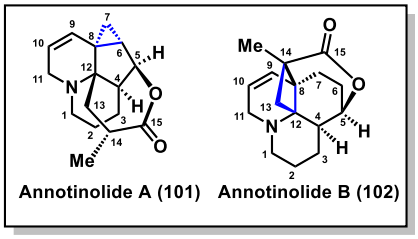

Figure 1.5: Target *Lycopodium* alkaloids that exhibit anti-aggregation activity towards amyloid-β.

Remarkably, despite an unknown mechanism of action, annotinolides A and B lack AChE activity, suggesting a novel avenue for potential Alzheimer's disease treatment. However, unraveling the therapeutic potential of annotinolides necessitates overcoming substantial synthetic challenges. Annotinolides A and B present formidable hurdles due to their structural complexity, featuring a 7,8-seco-lycopodane-derived 8,5-lactone framework with fused A-B-C rings and a bridging lactone.[41-45] Annotinolide A introduces

added complexity with a cyclopropane motif on the B-ring, while annotinolide B includes a cyclobutane structure bound through two quaternary centers.[41-45] Despite being isolated in 2016, these compounds remain unsynthesized, emphasizing the need for innovative synthetic approaches to unlock their therapeutic potential. Laying the groundwork, Synder and co-workers completed the total synthesis of annotinolides C (**119**) and D (**122**).[46]

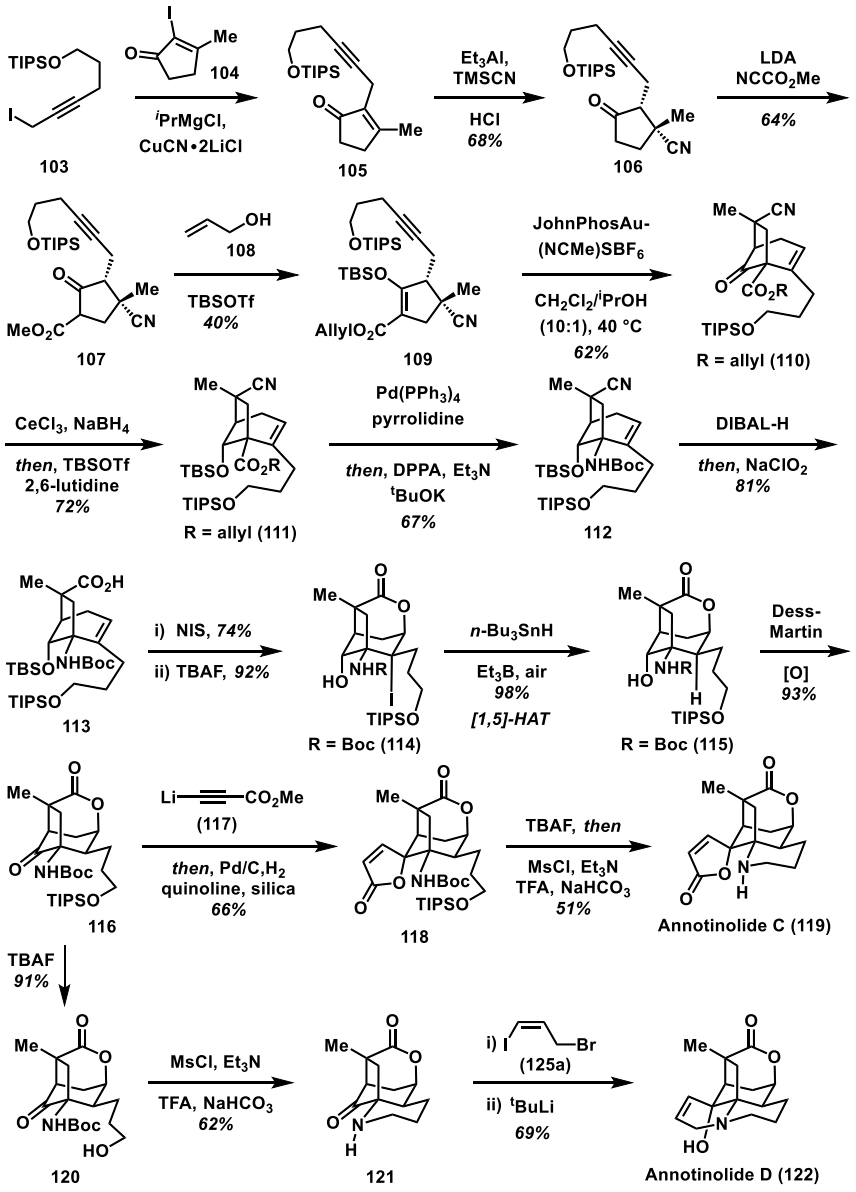

Scheme 1.12: Syntheses of Annotinolides C and D by Synder and co-workers.

1.1.4.2 Synthesis of Annotinolides C and D

The unified approach towards these two *Lycopodium* alkaloids began with preparation of propargyl iodide **103** in 3 steps, coupled with disubstituted α-iodocyclopentenone **104** catalyzed by copper and ^{i}PrMgCl.[46] This was followed by a stereoselective 1,4-cyano addition facilitated by an *in situ* generated Nagata's reagent.[46] Carbonylation to 1,3-ketoester **107** was achieved by lithium diisopropylamide (LDA) treatment followed by Mander's reagent. Then, cyclopentanone **107** underwent allylation to set the stage for a Conia-ene transformation that was most successful with JohnPhosAu(NCMe)SBF_6 and an essential mixed solvent system (CH_2Cl_2/^{i}PrOH; 10:1).[46] From there, exposed ketone **110** was reduced and silylated to avoid issues with the subsequent Curtius rearrangement to Boc-protected amine **112**.[46] A reduction/Pinnick oxidation sequence was performed to convert the nitrile into carboxylic acid **113**, which was then used to form tricycle **114** through lactonization.

The neighboring silyl protecting group in **113** was also removed with tetra-n-butylammonium fluoride (TBAF) after cyclization, and then exposed to radical conditions.[46] This induced a 1,5-hydrogen atom transfer that removed the superfluous iodine in **114**, replacing it with a hydrogen atom in an overall deiodination (**115**). Secondary alcohol **115** was then oxidized *via* Dess–Martin oxidation to the desired core intermediate **116**.[46] Toward annotinolide D (**122**), the silyl group on **116** was cleaved and followed up by a one-pot mesylate formation, Boc-removal, and intramolecular S_N2 cyclization to **121**. The final ring was then assembled by an initial *N*-alkylation and then intramolecular, diastereoselective 1,2-addition.[46] Alternatively, annotinolide C (**119**) was

accessed from intermediate **116** through diastereoselective addition of lithium propiolate **117** for the initial ring closure, which was then reduced with Lindlar's catalyst to afford lactone **118**.[46] Finally, a similar desilylation/S_N2 sequence was carried out to ring-close and complete the second target in the same 20 steps.[46]

1.1.5 Retrosynthetic Proposal

We sought a common intermediate that would allow access to both annotinolides A and B, so we began by retrosynthetically simplifying each target to identify a simple common intermediate that may be readily accessible (Scheme 1.13). *Lycopodium* alkaloid **101** could be disconnected at the lactone to keto-ester **123**, which could be formed by the radical alkylation of cyclopropane **124** trapped with a methacrylate derivative (**125**). In the forward sense, tricyclic quinolinone **126** would undergo a radical-mediated cyclopropanation to give radical **124**. Key intermediate **127** could then be constructed by two different targeted precursors, enaminone **128** or tetrahydroquinolone **129.** The dialkylation of **129** was our first attempt towards tricycle **127**, which slowly introduced **128** as another potential transform along the way. Tetrahydroquinolone **129** was envisioned as the product of an inverse-electron demand Diels–Alder (IEDDA) reaction with 1,2,3-triazine (**133**) as an azadiene paired with *in situ* formed enamine between vinylogous ester **134** and pyrrolidine. These two cycloaddition partners would then be synthesized from commercially available materials. Alternatively, disconnection of the cyclobutane ring on annotinolide B (**102**) opens the structure to a similar methacrylate derivative (**130**), which could be constructed by olefination and esterification of shared intermediate **126**.

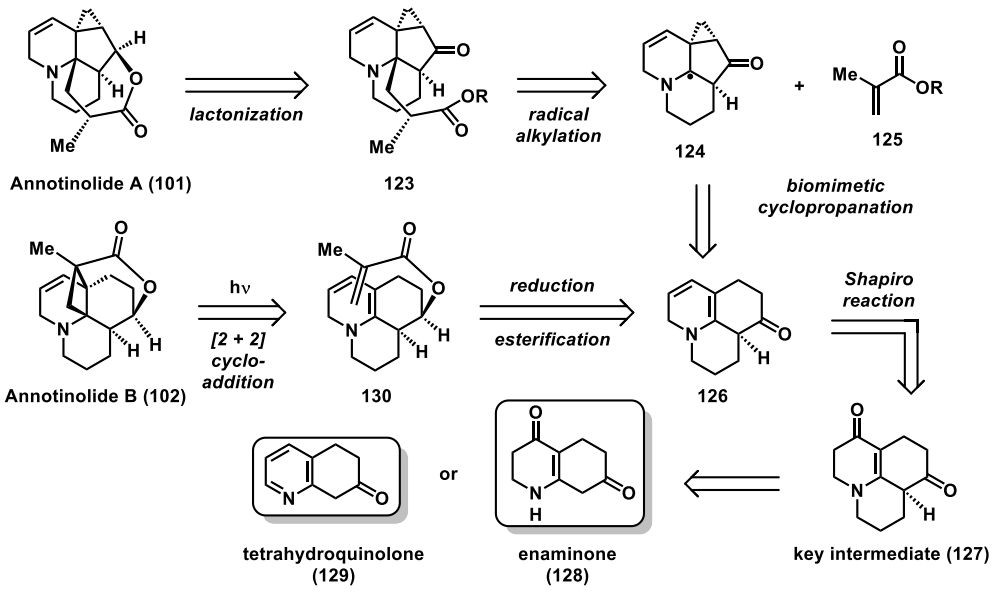

Scheme 1.13: Retrosynthetic proposal towards Annotinolides A and B.

The proposed total synthesis route for annotinolides A and B presented several notable features and challenges. Initial hurdles arose from the intricate structural complexity inherent in the polycyclic frameworks of these *Lycopodium* alkaloids. Installation of the strained cyclopropane ring in annotinolide A and cyclobutane ring in annotinolide B presented certain issues in our synthetic strategies. Furthermore, the labile bridging lactone rings posed challenges due to concerns regarding decomposition, and the highly susceptible 6,6,5- and 6,6,6-tricyclic scaffolds were prone to over oxidation, particularly of the nitrogen-containing C-ring. Despite these concerns, the cyclopropanation required for accessing annotinolide A was intriguing, as it involved a biomimetic radical pathway reliant on the electronic properties of the substrate to influence multiple C–C bond formations that includes a strained ring system. The interest in annotinolide B lied within an intramolecular and regioselective [2 + 2] cycloaddition to achieve the target cyclobutane ring. Given the significant hurdles posed by the total

synthesis of annotinolides A and B, a strategically designed divergent synthesis approach was employed, enabling the synthesis of both alkaloids from a shared intermediate. Consequently, the primary objective was to access this key, tricyclic quinolinone intermediate.

1.2 Results and Discussion

1.2.1 Inverse Electron Demand Diels–Alder

The construction of these azabicyclic moieties commenced with the preparation of 1,2,3-triazine (**133**) in 25% yield, which is most directly obtained by *N*-amination of pyrazole (**131**) to aminopyrazole **132**, followed by an oxidative ring expansion (Scheme 1.17). Based on the precedence from Boger, this unsubstituted triazine **133** supposedly participates in an inverse electron demand Diels–Alder reaction as an electron deficient diene unit.[47] A one-pot, cascade condensation/[4+2] cycloaddition was anticipated towards a bridged intermediate, which could subsequently undergo a retro [4+2] cycloaddition to the desired tetrahydroquinolone (**138**) and produce N_2 gas as a byproduct upon rearomatization. Starting from 1,3-cyclohexanedione, only 38% yield of 3-methoxy-2-cyclohexe-1-one (**134**) was isolated, so we tested different solvents to arrive at a consistent 57% yield with benzene. One concern was from the possibility of evaporating off the vinylogous ester along with the solvent, therefore we used ether to complete solvent transfers when necessary. This minor detail was not enough to change the yield significantly, and it turned out that the product was not labile after testing 2 mL under vacuum. Instead, it seems likely to hydrolyze when not sealed under N_2 gas and properly stored in a freezer. When subjecting it to the IEDDA, we unfortunately discovered that the

predominant product was a β-amino enal (**135**) formed through the Michael addition of pyrrolidine into 1,2,3-triazine ensued by a retro [4 + 2] cycloaddition and hydrolysis.

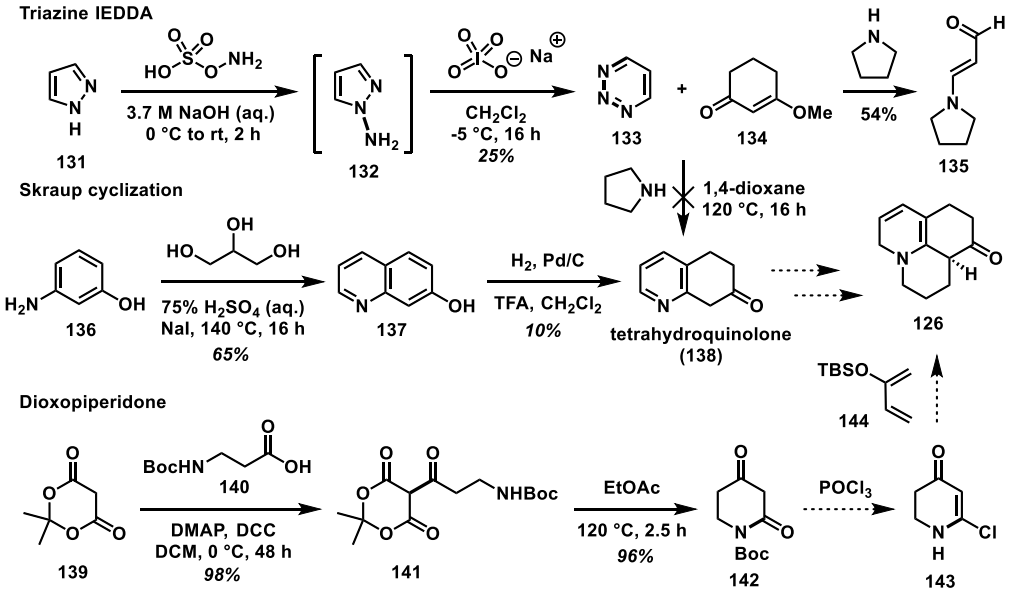

Scheme 1.14: Previous attempts to synthesize tetracyclic key intermediate.

1.2.2 Skraup Quinoline Synthesis

Thus, focus was turned to constructing **138** from 3-aminophenol (**136**) through the Skraup quinoline cyclization and electrophilic aromatic substitution (EAS)-type reaction sequence. This quinoline synthesis involved *in situ* formation of acrolein from the repetitive dehydration of glycerol and underwent 1,4-conjugate addition with the aniline portion of **136**. The EAS proceeded by addition into the tethered aldehyde and the pyridine was rearomatized under acidic conditions. Oxidation with excess acid and sodium iodide encouraged the formation of hydroxy quinoline **137**.

In first attempts at the Skraup quinoline synthesis, we found that using *m*-anisidine gave isomers of the target compound. Also, literature preparations all required subsequent additions of reagents at various temperatures at a time. This is difficult to do while working

with glycerol, which is tremendously viscous. After optimizing conditions for the Skraup, we found that the best yield of 65% for desired isomer **137** came from the specific apparatus of using a microwave vial and irradiation at 150°C with maximum stirring. In order to reduce the quinoline into **138**, we first approached it with a Birch reduction but overlooked its selectivity towards the pyridine ring. From here, the work of Jiang and co-workers was the inspiration for attempting a selective, partial hydrogenation to tetrahydroquinolone **138**. Although there were some initial results with 10% yield of the desired product, most scenarios ended with starting material or over hydrogenation. After numerous attempts to develop this reduction strategy (Table 1.1), efforts were centralized around a more paradigmatic pathway.

1.2.3 Alternative Diels–Alder Methods

Faced with these challenges, we looked toward a similar key intermediate with inspiration from the work of Roberts and co-workers. This approach started with the acylation of Meldrum's acid (**139**) with Boc-β-alanine (**140**) in 98% yield of **141** and subsequent intramolecular, 6-exo-trig cyclization to dioxopiperidone **142** in 96% yield. A chloroimidate (**143**) would then be constructed using phosphoryl chloride, as a precursor to a [4+2] cycloaddition with silyloxy butadiene **144**. However, there was no indication of **143** formation despite isolation of the cyclohexanone derivative since 1987. We envisioned the β-ketone on **142** to improve acidity of the bisecting α-proton towards elimination, but only starting material remained. We then cleaved the Boc protecting group to increase nucleophilicity of the amide into the chlorinating agent but fell short yet again with no reactivity. Lastly, our efforts to protect the ketone and then form the chloroimidate after

yielded the same results, therefore we took another look at the synthetic plan and stumbled upon a similar intermediate through a more established method.

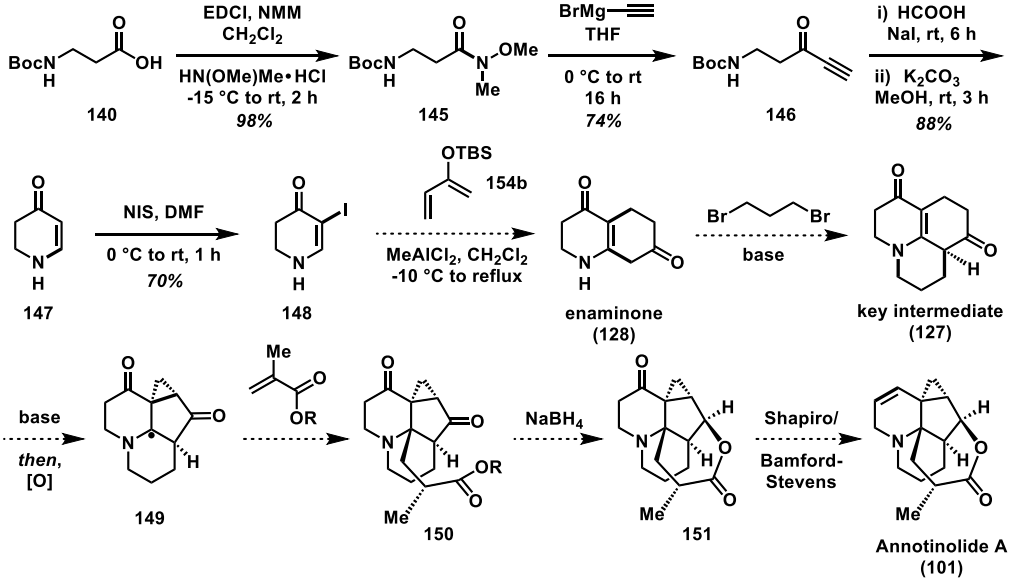

Scheme 1.15: Alternative dienophile approach *via* ynone intermediate.

Starting from Boc-β-alanine (**140**), we were able to replicate the transformation done by Georg and co-workers from carboxylic acid into Weinreb amide **145** in 98% yield. A subsequent Grignard addition was performed with ethynyl magnesium bromide, isolating ynone **146** in 74% yield. Upon deprotection of the primary amine, a 6-endo-trig cyclization into the ynone gave unsubstituted enaminone **147** in 88% yield. This was treated with iodine, providing α-iodoenaminone **148** in 70% yield to be used as the dienophile in a Diels–Alder reaction. It was not until our efforts to make copious amounts of **148** that we realized the poor atom economy. As we reconsidered the options, the choice was made to silylate and then oxidize the readily available 1-Boc-4-piperidone *via* Saegusa–Larock conditions in 95% yield. We cleaved the Boc protecting group to afford a more electron rich alkene when executing the [4 + 2] cycloaddition; however, no

significant results were obtained. Instead of optimizing substrates for this pericyclic reaction, we ultimately explored alternatives to form the sought-after quinolone.

Then, enolization of the more accessible α-position on the cyclohexanone would invite a single electron oxidation, promoting the formation of a cyclopropane ring through homolytic cleavage of the enamine double bond to create tertiary radical **149**. A methacrylate derivative would then be inserted to encourage a radical conjugate addition to assemble **150** that could undergo lactonization following the reduction of the cyclopentanone portion to the secondary alcohol. This pathway to annotinolide A (**101**) could then be altered at the key intermediate by reduction and esterification in the presence of a methacrylate derivative or acyl chloride. This would set the stage for an intramolecular, photochemical [2+2] cycloaddition to construct the cyclobutane ring of annotinolide B (**102**). Despite the lack of reported [2+2] cycloaddition reactions between cyclic enamines and acrylates, this interaction would be promising upon excitation of the methacrylate olefin. The main reason is that the desired regioselectivity would come from the more electrophilic α-position of the α,β-unsaturated ester interacting with the nucleophilic β-carbon of the enamine alkene in 138 due to donation of electron density from the nitrogen.

1.2.4 Tandem Cyclization/Hydrolysis/Decarboxylation

Inspired by Beshore and co-workers in their synthesis of (+)-lycondain A, we examined a Michael addition of vinylogous diester **153** with propiolamide (**154**) in preparation of forming a 2-pyridone (**156**) ring upon cyclization. First off, 3-methoxy-2-cyclohexen-1-one (**134**) was previously made and confirmed still viable to undergo α-acylation with ethyl cyanoformate **152** at 88% yield. When diester **153** was subjected to a

Michael addition with propiolamide, no reaction was observed at room temperature. After encouraging reactivity with 100 °C, the reaction proceeded with an 82% yield of scaffold **155**, paving the way for assembling the bicyclic, tetrahydroquinolinone **156**. We then faced the main transformation towards the key intermediate–a tandem reaction sequence involving cyclization, ester hydrolysis, and decarboxylation (Scheme 1.16). Unfortunately, the reaction worked too well and ended up fully oxidizing to the readily accessible and affordable 2,7-dihydroxyquinoline (**157**).

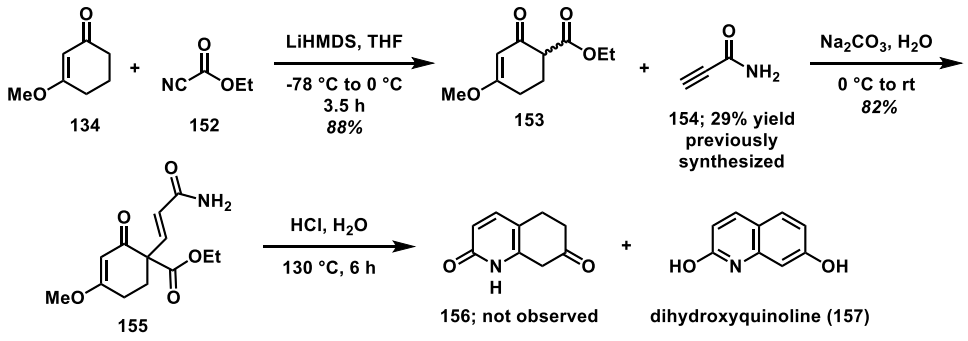

Scheme 1.16: Tandem cyclization/hydrolysis/decarboxylation approach.

1.3 Conclusion and Future Direction

As of the moment, we are surveying more mild conditions to perform this tandem sequence and avoid over oxidation, which could then be readily alkylated into the key, tricyclic quinolinone intermediate. However, we have made some progress on an alternate route employing 5-bromopentanoic acid (**158**) as an affordable precursor (Scheme 1.20). This carboxylic acid was converted into Weinreb amide **159** in quantitative yield, which was then used as a tether when coupled with 4-hydroxypyridine (**160**) through substitution giving **161** in 85% yield. The tethered Weinreb amide could then be substituted for a vinyl group through Grignard addition to give an α,β-unsubstituted ketone, followed by silylation

to a silyloxy butadiene intermediate. The intramolecular [4+2] cycloaddition between this diene and pyridone dienophile could then yield isomer **162** of the target intermediate (**127**) in four swift steps.

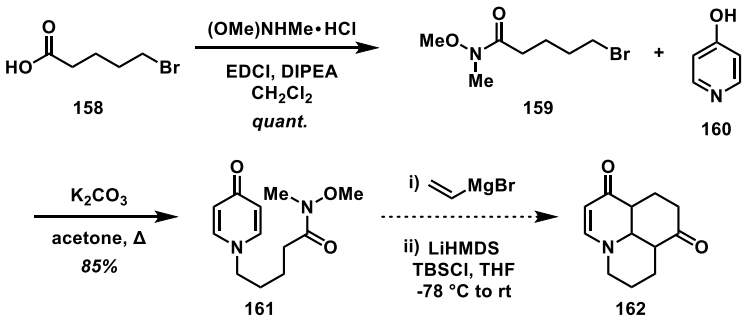

Scheme 1.17: Pyridone functionalization approach.

1.4 Experimental

1.4.1 General Information

1.4.1.1 Solvents and Reagents

Commercial reagents were purchased from MilliporeSigma, Acros Organics, Chem-Impex, TCI, Oakwood, and Alfa Aesar, and used without additional purification. Solvents were purchased from Fisher Scientific, Acros Organics, Alfa Aesar, and Sigma Aldrich. Tetrahydrofuran (THF), diethyl ether (Et_2O), acetonitrile (MeCN), dichloromethane (CH_2Cl_2), benzene, 1,4-dioxane, and triethylamine (Et_3N) were sparged with argon and dried by passing through alumina columns using argon in a Glass Contour (Pure Process Technology) solvent purification system. Dimethylformamide (DMF), dimethyl sulfoxide (DMSO), and dichloroethane (DCE) were purchased in Sure/Seal or AcroSeal bottling and dispensed under N_2. Deuterated solvents were obtained from Cambridge Isotope Laboratories, Inc. or MilliporeSigma.

1.4.1.2 Reaction setup, progress monitoring, and product purification

In general, the catalytic reactions are not air- or moisture-sensitive; however, the iron and zinc salts are hygroscopic and quickly change color when being weighed and added to the reaction vessel. This influences how much metal catalyst is being added because their molecular weights increase on hydration. For consistency and rigor, the iron and zinc salts were weighed and added to vials inside a nitrogen-filled glovebox. All other reagents, including the solvent, were added outside the glovebox under open air. Reaction progresses were monitored using thin-layer chromatography (TLC) on EMD Silica Gel 60 F254 or Macherey–Nagel SIL HD (60 Å mean pore size, 0.75 mL/g specific pore volume, 5–17 μm particle size, with fluorescent indicator) silica gel plates. Visualization of the developed plates was performed under UV light (254 nm). Purification and isolation of products were performed via silica gel chromatography (both column and preparative thin-layer chromatography). Organic solutions were concentrated under reduced pressure on IKA® temperature-controlled rotary evaporator equipped with an ethylene glycol/water condenser.

1.4.1.3 Analytical instrumentation

Melting points were measured with the MEL-TEMP melting point apparatus. Proton nuclear magnetic resonance (^{1}H NMR) spectra, carbon nuclear magnetic resonance (^{13}C NMR) spectra and fluorine nuclear magnetic resonance (^{19}F NMR) spectra were recorded on Bruker Avance NEO 400 (not ^{1}H decoupled) or Bruker Avance 600 MHz spectrometers (^{1}H decoupled). Chemical shifts (δ) are reported in ppm relative to the residual solvent signal (δ 7.26 for ^{1}H NMR, δ 77.16 for ^{13}C NMR in $CDCl_3$).[1] Data for ^{1}H

NMR spectroscopy are reported as follows: chemical shift (δ ppm), multiplicity (s = singlet, d = doublet, t = triplet, q = quartet, m = multiplet, br = broad, dd = doublet of doublets, dt = doublet of triplets), coupling constant (Hz), integration. Data for ^{13}C and ^{19}F NMR spectroscopy are reported in terms of chemical shift (δ ppm). IR spectroscopic data were recorded on a NICOLET 6700 FT-IR spectrophotometer using a diamond attenuated total reflectance (ATR) accessory. Samples are loaded onto the diamond surface either neat or as a solution in organic solvent and the data acquired after the solvent had evaporated. High resolution accurate mass (ESI) spectral data were obtained from the Analytical Chemistry Instrumentation Facility at the University of California, Riverside, on an Agilent 6545 Q-TOF LC/MS instrument (supported by NSF grant CHE-1828782).

1.5 Experimental Procedures and Characterization Data

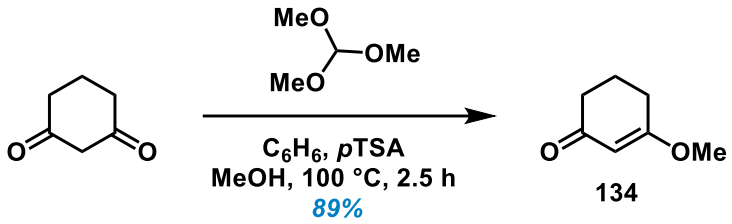

3-Methoxycyclohex-2-en-1-one (134).[49] According to Chandrasekhar and co-workers, 1,3-cyclohexadione (5.01 g, 51.0 mmol, 1.6 equiv) was dissolved in benzene (85 mL, 0.37 M) at rt. After adding *p*-toluenesulfonic acid (0.21 mg, 0.1 mol%) and MeOH (17 mL, 1.8 M), the reaction mixture was stirred for 15 min before pipetting in trimethyl orthoformate (5.2 mL, 31.3 mmol, 1.0 equiv). The reaction was heated to reflux (80–85°C) with a water condenser for 16 h and then cooled to rt. The mixture was washed with 10% aq. NaOH solution (2 × 20 mL), brine (1 × 20 mL), dried, and concentrated *in vacuo* to give the yellow oil (2.51 g, 89%). ^1H NMR (600 MHz, $CDCl_3$) δ 5.27 (s, 1H), 3.57 (s, 3H), 2.30 (t, J = 6.3

Hz, 2H), 2.24 (t, J = 6.6 Hz, 2H), 1.87 (qn, J = 6.6 Hz, 2H). ^{13}C NMR (400 MHz, $CDCl_3$) δ 199.8, 178.8, 128.4, 102.5, 55.7, 36.9, 28.9, 21.3. All other spectroscopic data are in accord with previously reported literature.

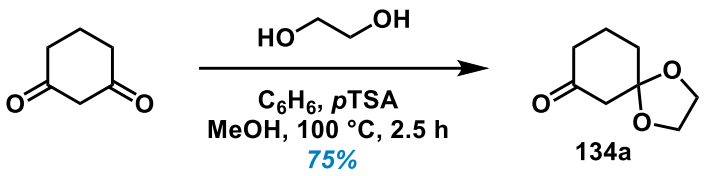

1,4-Dioxaspiro[4.5]decan-7-one (134a).[50] According to Beaver and co-workers, ethylene glycol (2.08 mL, 37.9 mmol, 1.0 equiv) was added to a stirring solution of 1,3-cyclohexadione (5.00 g, 44.6 mmol, 1.2 equiv) and benzene (100 mL, 0.45 M) at rt. After adding *p*-toluenesulfonic acid (0.21 mg, 0.1 mol%), the reaction was heated to 85 °C for 1.5 h and then cooled to rt. The mixture was washed with 10% aq. NaOH solution (2 × 50 mL), brine (1 × 75 mL), dried, and concentrated *in vacuo*. Purification by silica gel flash column chromatography (25% acetone/CH_2Cl_2, R_f = 0.54). The product was isolated as a clear oil (4.43 g, 75%). ^{1}H NMR (600 MHz, $CDCl_3$) δ 3.97–3.94 (m, 4H), 2.59 (s, 2H), 2.33 (t, J = 6.4 Hz, 2H), 2.00–1.83 (m, 4H). All other spectroscopic data are in accord with previously reported literature.

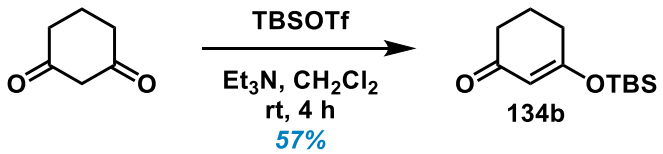

3-((Tert-butyldimethylsilyl)oxy)cyclohex-2-en-1-one (134b).[51] According to Park and co-workers, triethylamine (840 µL, 6.00 mmol, 1.2 equiv) was added to a stirring solution of 1,3-cyclohexadione (561 mg, 5.00 mmol, 1.0 equiv) and CH_2Cl_2 (10 mL, 0.5 M) at rt in a flame-dried 50 mL round-bottom flask equipped with a stir bar. The mixture was stirred

at rt for 1 h before adding TBSOTf (1.26 mL, 5.50 mmol, 1.1 equiv) dropwise. The resulting solution was stirred at rt for 3 h and then quenched with cold sat. aq. NH_4Cl (10 mL). The organic layer was removed in a separatory funnel and the remaining aqueous layer was extracted with Et_2O (3 × 10 mL). The combined organic extract was dried over anhydrous Na_2SO_4, filtered, and concentrated *in vacuo*. Purification by silica gel flash column chromatography (50% acetone/hex, $R_f = 0.72$). The product was isolated as a clear oil (644 mg, 57%). ^1H NMR (400 MHz, $CDCl_3$) δ 5.29 (s, 1H), 2.45–2.27 (m, 4H), 1.95 (qn, $J = 6.5$ Hz, 2H), 0.90 (s, 9H), 0.08 (s, 6H). All other spectroscopic data are in accord with previously reported literature.

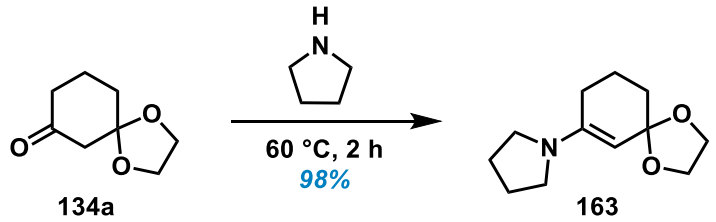

134a 163

1-(1,4-Dioxaspiro[4.5]dec-7-en-7-yl)pyrrolidine (163). Dioxolane **134a** (15.0 μL, 0.096 mmol, 1.0 equiv) and pyrrolidine (9.5 μL, 0.115 mmol, 1.2 equiv) were added to a 4 mL screw cap vial equipped with a stir bar. The vial was sealed and the mixture was stirred and heated at 110 °C for 2 h before concentrated *in vacuo*. Purification by silica gel flash column chromatography (50% acetone/hex, $R_f = 0.45$). The product was isolated as a dark brown solid (19.6 mg, 98%). ^1H NMR (600 MHz, $CDCl_3$) δ 5.02 (s, 1H), 3.65 (s, 4H), 3.42 (t, $J = 6.4$ Hz, 2H), 3.20 (t, $J = 6.4$ Hz, 2H), 2.42 (t, $J = 6.3$ Hz, 2H), 2.25 (td, $J = 7.0, 5.8, 1.7$ Hz, 2H), 1.94 (qd, $J = 6.0, 5.6, 2.3$ Hz, 6H). HRMS (ESI): *m/z* $[M+H]^+$ calculated for $C_{12}H_{19}NO_2$: 209.1416; found: 210.1493.

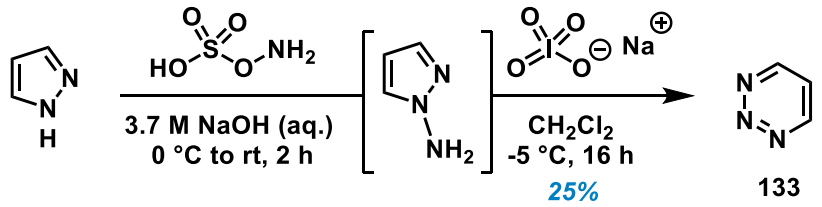

1,2,3-Triazine (133).[48] As a modified procedure to Boger and coworkers, pyrazole (8.68 g, 128 mmol, 1.0 equiv) was added to a stirring solution of 3.7 M NaOH (207 mL, 17.9 mol, 140 equiv NaOH) and chilled at 0 °C for 15 min before adding hydroxylamine-O-sulfonic acid (HOSA, 43.3 g, 383 mmol, 3.0 equiv) in small portions, waiting for the solution to turn transparent before adding the next portion. After all of the HOSA was added, the reaction mixture was stirred at 0 °C for an additional 30 min, after which the ice bath was removed and the reaction mixture was stirred at ambient temperature for 1 h to give a vibrant yellow solution. Full conversion was confirmed by TLC analysis before transferred to a separatory funnel and extracted with CH_2Cl_2 (3 × 70 mL). The combined organic extract was washed with saturated aq. NaCl (1 × 75 mL), dried over anhydrous Na_2SO_4, filtered, and concentrated *in vacuo*. This yellow oil was reconstituted in CH_2Cl_2 (352 mL, 0.36 M) and stirred vigorously at rt before adding H_2O (132 mL, 0.97 M). While stirring, the heterogeneous mixture was cooled between –5 °C and –10 °C with a cryostat, monitored with a thermometer, for 30 min before adding $NaIO_4$ (54.79 g, 257 mmol, 2.0 equiv) over 10 min in small portions. The vessel was left to stir vigorously overnight (18 h) at approximately –5 °C and then warmed to rt. The organic layer was separated and the aqueous layer extracted with CH_2Cl_2 (3 × 50 mL). The combined organic extract was washed with saturated aq. NaCl (1 × 100 mL), dried over anhydrous Na_2SO_4, filtered, and concentrated *in vacuo*. Purification by silica gel flash column chromatography (70%

EtOAc/hex, R_f = 0.32). The product was isolated as a tan solid (2.59 g, 25%). ^{1}H NMR (600 MHz, $CDCl_3$) δ 9.09 (d, *J* = 5.6 Hz, 1H), 7.43 (t, *J* = 5.6 Hz, 1H). ^{13}C NMR (400 MHz, $CDCl_3$) δ 149.9, 117.9. HRMS (ESI): *m/z* $[M+H]^+$ calculated for $C_3H_3N_3$: 81.0327; found: 82.0335. All other spectroscopic data are in accord with previously reported literature.

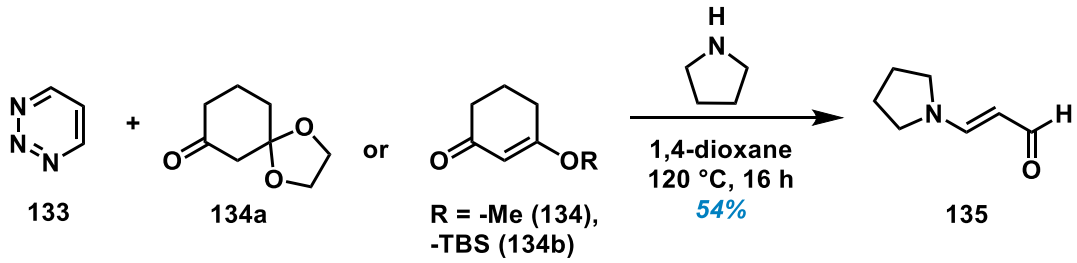

(E)-3-(Pyrrolidin-1-yl)acrylaldehyde (135).[48] 1,2,3-Triazine (200 mg, 2.45 mmol, 1.5 equiv) was dissolved in 1,4-dixoane (4 mL, 0.41 M) in a 10 mL microwave vial equipped with a stir bar. Ketal **134a** or either vinylogous ester (**134** or **134b**) (1.63 mmol, 1.0 equiv) and pyrrolidine (150 µL, 1.80 mmol, 1.1 equiv) was added to the solution. The microwave vial was tightly sealed and heated at 120 °C for 16 h before cooling, transferring with CH_2Cl_2 (5 mL), and concentrated *in vacuo*. Purification by silica gel flash column chromatography (50% acetone/hex, R_f = 0.32). The product was isolated as a tan solid (166 mg, 54%). ^{1}H NMR (400 MHz, DMSO-d_6) δ 8.92 (d, *J* = 8.6 Hz, 1H), 7.52 (d, *J* = 12.6 Hz, 1H), 4.89 (dd, *J* = 12.6, 8.6 Hz, 1H), 3.49 (t, *J* = 6.6 Hz, 2H), 3.11 (t, *J* = 7.0 Hz, 2H), 1.93 (qn, *J* = 7.0 Hz, 2H), 1.85 (qn, *J* = 6.6 Hz, 2H). ^{13}C NMR (400 MHz, DMSO-d_6) δ 187.3, 156.5, 101.2, 51.7, 46.7, 30.7, 24.8, 24.6. HRMS (ESI): *m/z* $[M+H]^+$ calculated for $C_7H_{11}NO$: 125.0841; found: 126.0847.

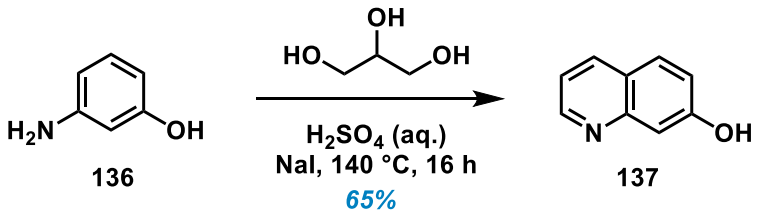

136 137

7-Hydroxyquinoline (137).[55] As a modified procedure to Li and coworkers, a mixture of 3-aminophenol (4.00 g, 37 mmol, 1.0 equiv), 75% H_2SO_4 (11.0 mL, 150 mmol, 4.1 equiv), glycerol (2.95 mL, 40 mmol, 1.1 equiv), and NaI (22.5 mg, 0.15 mmol, 0.01 equiv) was sealed in a pressure vessel equipped with a stir bar. The potential heat pockets were removed by sonication before heated at 130 °C for 16 h. After cooling to ambient temperature, the viscous mixture was transferred to a large Erlenmeyer flask with H_2O and the residue was removed by small portions of 10 M NaOH while periodically sonicating. The solution was diluted with H_2O and then titrated to pH 7 with 10 M NaOH while stirring vigorously. CH_2Cl_2 (150% aq. volume) was added to the aqueous solution and left to stir for 10 minutes before filtering through a fritted funnel packed with Celite. The organic layer was removed and the aqueous layer filtered through Celite once more while rinsing with more CH_2Cl_2 (20 mL). The resulting mixture was extracted with CH_2Cl_2 (3 × 50 mL) and the combined organic extract was washed with saturated aq. NaCl (1 × 75 mL), dried over anhydrous Na_2SO_4, filtered, and concentrated *in vacuo*. Purification by alumina flash column chromatography (70% EtOAc/hex, R_f = 0.18). The product was isolated as a tan solid (3.46 g, 65%). ^{1}H NMR (600 MHz, DMSO-d_6) δ 10.19 (s, 1H), 8.73 (dd, J = 4.2, 1.8 Hz, 1H), 8.20 (dd, J = 8.2, 1.8 Hz, 1H), 7.81 (d, J = 8.8 Hz, 1H), 7.28 (dd, J = 8.2, 4.2 Hz, 1H), 7.24 (d, J = 2.4 Hz, 1H), 7.16 (dd, J = 8.8, 2.4 Hz, 1H). HRMS (ESI): *m/z* $[M+H]^+$

calculated for C_9H_7NO: 145.0528; found: 146.0562. All other spectroscopic data are in accord with previously reported literature.

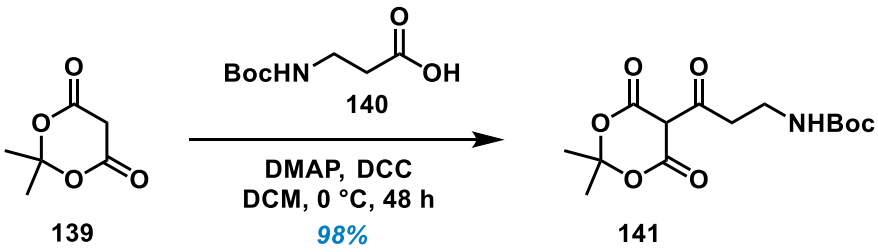

Tert-butyl (3-(2,2-dimethyl-4,6-dioxo-1,3-dioxan-5-yl)-3-oxopropyl)carbamate (141).[53] As a modified procedure to Sevilla and coworkers, Boc-β-alanine (1.00 g, 5.29 mmol, 1.0 equiv), Meldrum's acid (762 mg, 5.29 mmol, 1.1 equiv), and dimethylaminopyridine (DMAP, 710 mg, 5.81 mmol, 1.1 equiv) were added to a flame dried round-bottom flask equipped with a stir bar. The collection of solids was dissolved in CH_2Cl_2 (20 mL) and stirred at 5 °C for 1 h before adding dicyclohexylcarbodiimide (DCC, 1.20 g, 5.81 mmol, 1.1 equiv). The mixture was stirred at 5 °C for 48 h and then filtered through a fritted funnel with cold dichloromethane (10 mL). The reaction mixture was washed with 10% w/v $KHSO_4$ (3 × 20 mL) and brine (1 × 30 mL). The resulting organic extract was dried over anhydrous Na_2SO_4, filtered, and concentrated under reduced pressure. The yellow solids were taken up in ether and then concentrated *in vacuo*. Purification by silica gel flash column chromatography (25% EtOAc/hex, $R_f = 0.27$). The product was isolated as a white solid (1.58 g, 98%). ^{1}H NMR (400 MHz, $CDCl_3$) δ 4.82 (s, 1H), 3.59–3.51 (m, 2H), 3.30 (t, $J = 6.3$ Hz, 2H), 1.75 (s, 6H), 1.42 (s, 9H). HRMS (ESI): *m/z* $[M+H]^+$ calculated for $C_{14}H_{21}NO_7$: 315.1318; found: 316.1356. All other spectroscopic data are in accord with previously reported literature.

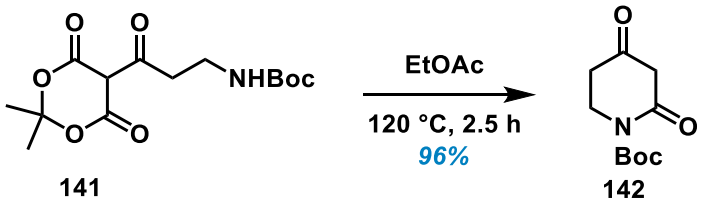

Tert-butyl 2,4-dioxopiperidine-1-carboxylate (142).[53] As a modified procedure to Sevilla and co-workers, carbamate **141** (500 mg, 1.59 mmol, 1.0 equiv) was dissolved in EtOAc (2 mL, 0.80 M) and heated at 120 °C for 2.5 h. The reaction mixture was cooled to rt, filtered through a fritted funnel, and then concentrated *in vacuo*. Purification by silica gel flash column chromatography (40% acetone/hex) gave the title product as a white solid (325 mg, 96%). ^{1}H NMR (500 MHz, $CDCl_3$) δ 4.10 (t, J = 6.0 Hz, 2H), 3.51 (s, 1H), 2.63 (t, J = 6.0 Hz, 2H), 1.55 (s, 9H). HRMS (ESI): *m/z* $[M+H]^+$ calculated for $C_{10}H_{15}NO_4$: 213.1001; found: 214.1029. All other spectroscopic data are in accord with previously reported literature.

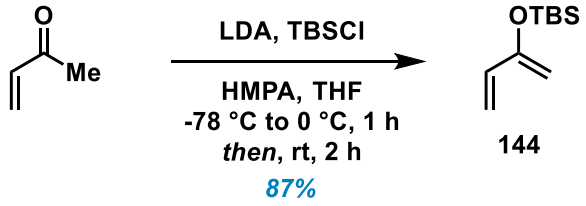

(Buta-1,3-dien-2-yloxy)(tert-butyl)dimethylsilane (144). A solution of methyl vinyl ketone (1.00 mL, 12.1 mmol, 1.0 equiv) in THF (12.0 mL, 1.0 M) was cooled to –78 °C in a flame dried round-bottom flask equipped with a stirbar. 2M LDA in THF (6.70 mL, 13.5 mmol, 1.1 equiv) was added dropwise and stirred at –78 °C for 0.5 h. Then, HMPA (1.70 mL, 9.70 mmol, 0.8 equiv) and TBSCl (2.01 g, 13.5 mmol, 1.1 equiv) in THF (5.00 mL) was added in that specific order and stirred at rt for 2 h. Reaction was quenched with sat.

aq. $NaHCO_3$ (20 mL) and the organic layer was removed in a separatory funnel. The remaining aqueous layer was extracted with hexanes (3 × 30 mL) and the combined organic extract was washed with saturated aq. NaCl (1 × 20 mL), dried over anhydrous Na_2SO_4, filtered, and concentrated *in vacuo*. Purification by silica gel flash column chromatography (100% hex, $R_f = 0.77$). The product was isolated as a clear oil (1.96 g, 87%). ^1H NMR (600 MHz, $CDCl_3$) δ 6.19 (ddd, J = 16.9, 10.5, 1.5 Hz, 1H), 5.51 (d, J = 16.9 Hz, 1H), 5.08 (dd, J = 10.5, 1.9 Hz, 1H), 4.34 (s, 1H), 4.32 (s, 1H), 0.97 (s, 6H), 0.18 (s, 3H). HRMS (ESI): *m/z* $[M+H]^+$ calculated for $C_{10}H_{20}OSi$: 184.1283; found: 185.1342. All other spectroscopic data are in accord with previously reported literature.

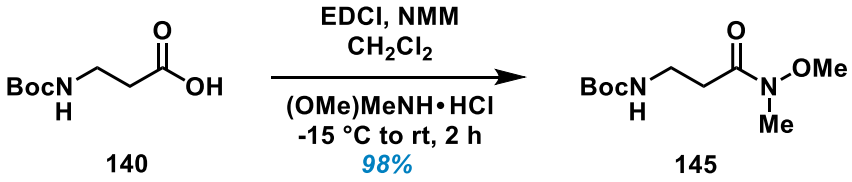

Tert-butyl (3-(methoxy(methyl)amino)-3-oxopropyl)carbamate (145).[57] As a modified procedure to Georg and co-workers, *N*-methylmorpholine (NMM, 3.20 mL, 29.1 mmol, 1.1 equiv), EDCI (5.57 g, 29.1 mmol, 1.1 equiv), and HN(OMe)Me • HCl (2.84 g, 29.1 mmol, 1.1 equiv) were added to a cooled (–15 °C), stirring solution of Boc-β-alanine (5.00 g, 26.4 mmol, 1.0 equiv) in CH_2Cl_2 (500 mL, 0.05 M). The mixture was stirred at rt for 2 h and then cooled to 0 °C before quenching with cold 10% aq. HCl solution. The solution was stirred at 0 °C for an additional 5 min and then diluted with H_2O (250 mL). The organic layer was separated and the aqueous layer extracted with CH_2Cl_2 (3 × 75 mL). The combined organic extract was washed with saturated aq. $NaHCO_3$ (1 × 100 mL), dried over anhydrous Na_2SO_4, filtered, and concentrated *in vacuo*. Purification by silica gel flash

column chromatography (eluting with 25-75% EtOAc/hex). The product was isolated as a clear oil (6.02 g, 98%). R_f = 0.34 (75% EtOAc/hex). ^{1}H NMR (500 MHz, $CDCl_3$) δ 5.23 (s, 1H), 3.66 (d, *J* = 3.1 Hz, 3H), 3.41 (p, *J* = 5.8, 5.1 Hz, 2H), 3.17 (d, *J* = 3.1 Hz, 3H), 2.63 (s, 2H), 1.41 (s, 9H). HRMS (ESI): *m/z* $[M+H]^+$ calculated for $C_{10}H_{20}N_2O_4$: 232.1345; found: 233.1358. All other spectroscopic data are in accord with previously reported literature.

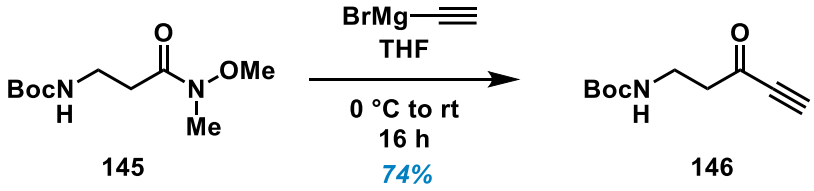

Tert-butyl (3-oxopent-4-yn-1-yl)carbamate (146).[57] As a modified procedure to Georg and co-workers, Weinreb amide **145** (1.55 g, 6.67 mmol, 1.0 equiv) was added to a flame-dried flask equipped with a magnetic stir bar and gently stirred under vacuum for 15 min and then diluted with anhydrous THF (35 mL, 0.19 M). The mixture was cooled to 0 °C and ethynyl magnesium bromide (0.4 M in THF, 100 mL, 5.0 equiv) was added slowly. The solution was then stirred at rt for 16 h and then quenched with cold 1 M aq. HCl (20 mL) solution. The reaction mixture was extracted with EtOAc (3 × 35 mL) and then the combined organic extract was washed with saturated aq. $NaHCO_3$ (1 × 50 mL), dried over anhydrous Na_2SO_4, filtered, and concentrated *in vacuo*. Purification by silica gel flash column chromatography (eluting with 10-50% EtOAc/hex). The product was isolated as a yellow oil (976 mg, 74%). R_f = 0.48 (50% EtOAc/hex). ^{1}H NMR (600 MHz, $CDCl_3$) δ 4.92 (s, 1H), 3.41 (t, *J* = 6.0 Hz, 2H), 3.28 (s, 1H), 2.84 (t, *J* = 6.0 Hz, 2H), 1.41 (s, 9H).

HRMS (ESI): *m/z* $[M+H]^+$ calculated for $C_{10}H_{15}NO_3$: 197.1052; found: 198.1083. All other spectroscopic data are in accord with previously reported literature.

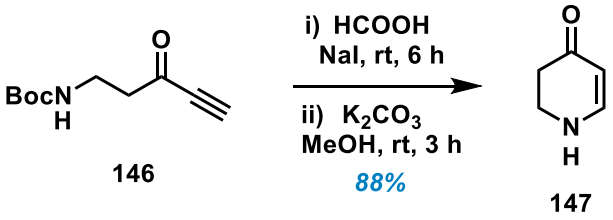

2,3-Dihydropyridin-4(1H)-one (147).[57] According to Georg and co-workers, NaI (.228 g, 1.52 mmol, 3.0 equiv) was added to a solution of ynone **146** (.100 g, 0.507 mmol, 1.0 equiv) in 98% HCOOH (0.1 M, 5.1 mL, 19.6 mmol) while stirring in a flame-dried flask at rt. The mixture was stirred at rt for 6 h and then the solvent was removed by blowing air directly into the solution. After most of the solvent was gone, the flask was placed under vacuum for 20 min and then diluted with MeOH (0.02 M, 25 mL). Excess K_2CO_3 (at least 5.0 equiv) was added to the solution and then stirred at rt for 3 h. The mixture was then dissolved with CH_2Cl_2, vacuum filtered, and then concentrated *in vacuo*. Purification by silica gel flash column chromatography (eluting with 10% MeOH/EtOAc). The product was isolated as an orange solid (45.8 mg, 93%). R_f = 0.22 (10% MeOH/EtOAc). ^{1}H NMR (500 MHz, MeOD) δ 7.42 (d, *J* = 7.2 Hz, 1H), 4.92 (d, *J* = 7.2 Hz, 1H), 3.55 (t, *J* = 8.1 Hz, 2H), 2.42 (t, *J* = 8.1 Hz, 2H). All other spectroscopic data are in accord with previously reported literature.

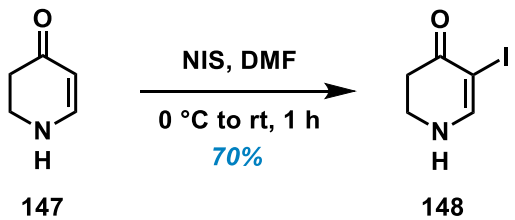

5-Iodo-2,3-dihydropyridin-4(1H)-one (148).[66] As a modified procedure to Guinchard and co-workers, K_2CO_3 (171 mg, 1.24 mmol, 1.2 equiv), I_2 (392 mg, 1.54 mmol, 1.5 equiv), and DMAP (25.1 mg, 0.206 mmol, 0.2 equiv) was added slowly, in the respective order, to a stirring solution of enaminone **147** (100 mg, 1.03 mmol, 1.0 equiv) in a mixture of THF:H_2O (1:1, 6.0 mL, 0.21 M) at 0 °C. The mixture was then stirred at rt for 2 h. The solution was concentrated *in vacuo* and the residue was then taken up in sat. aq. sodium thiosulfate (10 mL) and neutralized with aq. 2 M HCl to a pH of 5. The mixture was extracted with CH_2Cl_2 (3 × 10 mL), dried over anhydrous Na_2SO_4, filtered, and then concentrated *in vacuo*. Purification by silica gel flash column chromatography (eluting with 10-50% acetone/hex). The product was isolated as a white solid (68.9 mg, 70%). R_f = 0.33 (50% acetone/hex). ^{1}H NMR (600 MHz, DMSO-d_6) δ 8.12 (s, 1H), 7.79 (s, 1H), 3.49 (t, J = 7.8 Hz, 2H), 2.43 (t, J = 7.8 Hz, 2H). ^{1}H NMR (500 MHz, $CDCl_3$) δ 7.67 (d, J = 6.7 Hz, 1H), 3.70 (td, J = 7.7, 2.6 Hz, 2H), 2.74 (t, J = 7.7 Hz, 2H). ^{13}C NMR (600 MHz, DMSO-d_6) δ 184.8, 157.5, 60.3, 40.8, 34.9. HRMS (ESI): *m/z* $[M+H]^+$ calculated for C_5H_6INO: 222.9494; found: 223.9498. IR: 3244, 2966, 2852, 1615, 1540, 1498, 1144, 1003, 644 cm^{-1}.

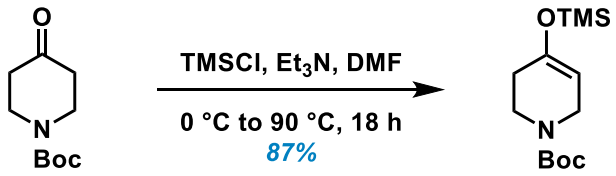

164

Tert-butyl 4-((trimethylsilyl)oxy)-3,6-dihydropyridine-1(2H)-carboxylate (164).[68] As a modified procedure to Steven and co-workers, triethylamine (14.2 mL, 100 mmol, 2.0 equiv) was added slowly to a stirring solution of 1-Boc-4-piperidone (10.0 g, 50.2 mmol,

1.0 equiv) in anhydrous DMF (100 mL, 0.5 M) at 0 °C. Chlorotrimethylsilane (12.8 mL, 100 mmol, 2.0 equiv) was then added to the reaction mixture before attaching a reflux condenser. The reaction was stirred at 90 °C for 18 h. Once cooled, the stir bar was removed and the reaction mixture was concentrated *in vacuo*. The residue was dissolved in EtOAc (145 mL) and then washed with H_2O (1 × 50 mL) and a 10% aq. $NaHCO_3$ solution (1 × 50 mL). The organic extract was dried over anhydrous Na_2SO_4, filtered, and concentrated *in vacuo*. Purification by silica gel flash column chromatography (eluting with 100% hex). The product was isolated as a yellow oil (11.9 g, 87%). R_f = 0.63 (100% hex). ^1H NMR (500 MHz, $CDCl_3$) δ 4.78 (s, 1H), 3.86 (s, 2H), 3.51 (t, J = 6.0 Hz, 2H), 2.09 (s, 2H), 1.46 (s, 9H), 0.19 (s, 9H). All other spectroscopic data are in accord with previously reported literature.

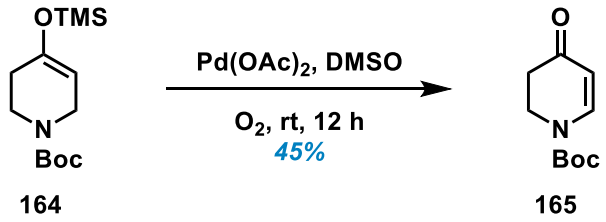

Tert-butyl 4-oxo-3,4-dihydropyridine-1(2H)-carboxylate (165).[69] As a modified procedure to Luu and co-workers, a mixture of silyl enol ether **164** (.100 g, 0.368 mmol, 1.0 equiv) and $Pd(OAc)_2$ (41.4 mg, 0.184 mmol, 50 mol %) was diluted with anhydrous DMSO (1.4 mL, 0.27 M) in a reaction vial equipped with a stir bar. The cap was taken off and the reaction mixture was left to stir at rt for 6 h before quenching with H_2O at 0 °C. The solution was filtered through celite and extracted with EtOAc (3 × 5 mL) before concentrated *in vacuo*. Purification by silica gel flash column chromatography (eluting with 0-40% EtOAc/hex). The product was isolated as a brown solid (32.7 mg, 45%). R_f =

0.31 (40% EtOAc/hex). ^{1}H NMR (600 MHz, $CDCl_3$) δ 7.80 (s, 1H), 5.29 (s, 1H), 3.96 (t, J = 7.3 Hz, 2H), 2.54 (t, J = 7.3 Hz, 2H), 1.53 (s, 9H). All other spectroscopic data are in accord with previously reported literature.

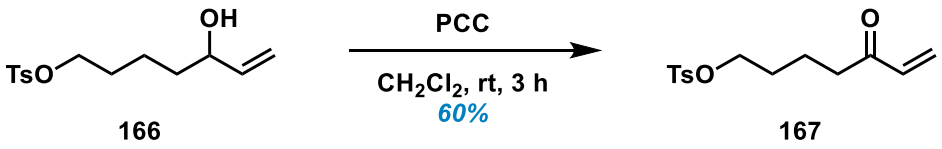

5-Oxohept-6-en-1-yl 4-methylbenzenesulfonate (167). A solution of 5-hydroxyhept-6-en-1-yl 4-methylbenzenesulfonate (.200 g, 0.703 mmol, 1.0 equiv) in CH_2Cl_2 (2.0 mL, 0.35 M) was added into a stirring mixture of PCC (0.2 M in CH_2Cl_2, 303 mg, 1.41 mmol) in CH_2Cl_2 (1.5 mL) by cannula. The reaction was stirred at rt for 3 h and then diluted with CH_2Cl_2 (10 mL). The solution was decanted and the resin rinsed with CH_2Cl_2 (3 × 5 mL). The combined organic extract was washed with 2 M aq. NaOH (2 × 10 mL), 2 M aq. HCl (1 × 10 mL), and sat. aq. Na_2CO_3 (1 × 10 mL). The solution was dried over anhydrous Na_2SO_4, filtered, and concentrated *in vacuo*. Purification by silica gel flash column chromatography (eluting with 0-25% EtOAc/hex). The product was isolated as a yellow oil (.101 g, 60%). R_f = 0.48 (25% EtOAc/hex). ^{1}H NMR (600 MHz, $CDCl_3$) δ 7.78 (d, J = 8.0 Hz, 2H), 7.34 (d, J = 7.9 Hz, 2H), 6.31 (dd, J = 17.7, 10.6 Hz, 1H), 6.19 (d, J = 17.6 Hz, 1H), 5.83 (d, J = 10.6 Hz, 1H), 4.03 (t, J = 5.8 Hz, 2H), 2.56 (t, J = 6.7 Hz, 2H), 2.45 (s, 3H), 1.75 – 1.58 (m, 4H). HRMS (ESI): *m/z* $[M+H]^+$ calculated for $C_{14}H_{18}O_4S$: 282.0926; found: 283.0971.

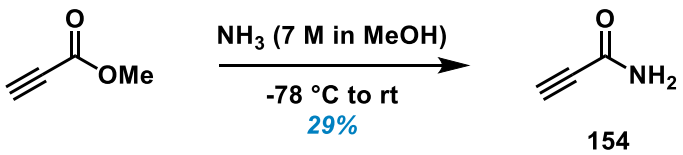

Propiolamide (154).[73] Methyl propiolate (3.2 mL, 35.7 mmol, 1.0 equiv) was added dropwise to a stirring solution of NH_4OH (2.6 mL, 35.7 mmol, 1.0 equiv) at -78 °C. After 10 min, the reaction was allowed to gradually warm to rt and stirred at rt for 2 h. The reaction mixture was then quenched with H2O (20 mL) and transferred to a separatory funnel where the organic layer was isolated. The aqueous was then extracted with EtOAc (3 × 10 mL). The combined organic extract was dried over anhydrous Na2SO4, filtered, and then concentrated *in vacuo*. Purification by silica gel flash chromatography (eluting with 50% EtOAc/hex). The product was isolated as a colorless oil (704 mg, 29%). R_f = 0.22 (50% EtOAc/hex). ^{1}H NMR (500 MHz, $CDCl_3$) δ 5.98 (s, 1H), 5.85 (s, 1H), 2.86 (s, 1H). All other spectroscopic data are in accord with previously reported literature.

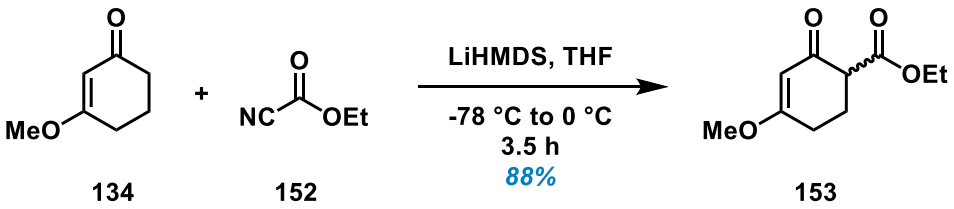

134 152 153

Ethyl 4-methoxy-2-oxocyclohex-3-ene-1-carboxylate (153).[73] 1 M LiHMDS (38.1 mL, 38.1 mmol, 1.2 equiv) was added dropwise to a stirring solution of 3-methoxy-2-cyclohexen-1-one (4.00 g, 31.7 mmol, 1.0 equiv) in THF (99 mL, 0.32 M) at -78 °C. The mixture was stirred at -78 °C for 30 min before adding ethyl cyanoformate (3.45 mL, 34.9 mmol, 1.1 equiv). This solution was stirred at -78 °C for 1 h and then switched to an ice bath before letting the reaction stir to rt o/n, which was then quenched with sat. aq. $NaHCO_3$ (99 mL). The crude reaction mixture was transferred to a separatory funnel and extracted with EtOAc (3 × 120 mL), dried over anhydrous Na_2SO_4, filtered, and concentrated *in vacuo*. Purification by silica gel flash column chromatography (eluting with 0-40%

EtOAc/hex). The product was isolated as a pale, yellow oil (5.53 g, 88%). R_f = 0.36 (40% EtOAc/hex). ^{1}H NMR (500 MHz, $CDCl_3$) δ 5.40 (s, 1H), 4.20 (q, *J* = 7.1 Hz, 2H), 3.70 (s, 3H), 3.31 (dd, *J* = 9.0, 5.0 Hz, 1H), 2.56 (ddd, *J* = 17.4, 6.5, 5.0 Hz, 1H), 2.47 – 2.28 (m, 2H), 2.16 (ddt, *J* = 13.6, 6.7, 5.1 Hz, 1H), 1.27 (t, *J* = 7.2 Hz, 2H). All other spectroscopic data are in accord with previously reported literature.

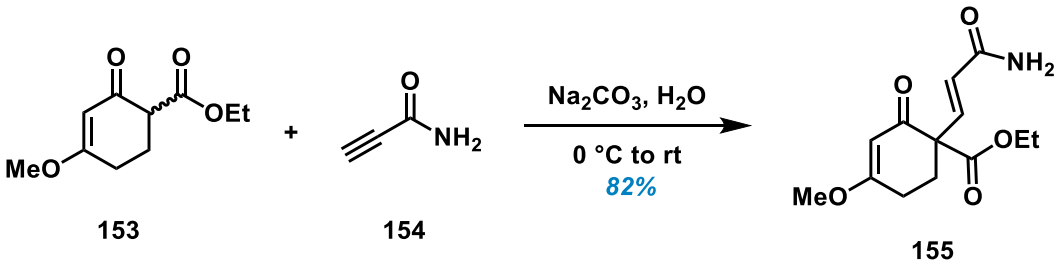

Ethyl (E)-1-(3-amino-3-oxopropenyl)-4-methoxy-2-oxocyclohexene carboxylate (155).[73] Diester **153** (100 mg, 0.505 mmol, 1.0 equiv), propiolamide (59.6 mg, 0.863 mmol, 1.7 equiv), and K_2CO_3 (140 mg, 1.01 mmol, 2.0 equiv) was added to a vial before diluting with DMF (1.0 mL, 0.5 M) at rt. The reaction mixture was stirred at 100 °C for 18 h and then quenched with H_2O (3.0 mL). The solution was extracted with CH_2Cl_2 (3 × 5 mL). The combined organic extract was dried over anhydrous Na_2SO_4, filtered, and concentrated *in vacuo*. Purification by silica gel flash chromatography (eluting with 10-50% acetone/hex). The product was isolated as a colorless oil (109 mg, 82%). R_f = 0.27 (50% acetone/hex). ^{1}H NMR (500 MHz, $CDCl_3$) δ 7.00 (d, *J* = 16.0 Hz, 1H), 5.93 (m, 3H), 5.42 (s, 1H), 4.19 (q, *J* = 7.1 Hz, 2H), 3.71 (s, 3H), 2.63 (ddd, *J* = 13.2, 8.0, 5.0 Hz, 1H), 2.56 – 2.47 (m, 1H), 2.41 (ddd, *J* = 18.1, 8.1, 5.2 Hz, 1H), 2.11 (ddd, *J* = 13.5, 6.8, 5.1 Hz, 1H), 1.24 (t, *J* = 7.1 Hz, 3H). HRMS (ESI): *m/z* $[M+H]^+$ calculated for $C_{13}H_{17}NO_5$: 267.1108; found: 268.1181.

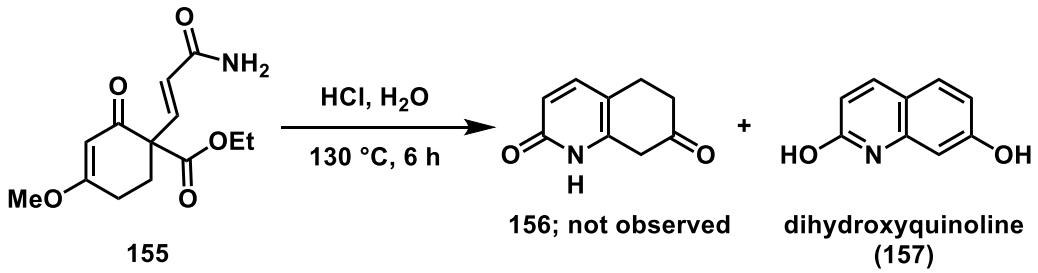

155

156; not observed

dihydroxyquinoline (157)

2,7-Dihydroxyquinoline (157).[73] Concentrated HCl (0.3 mL, 3.10 mmol, 33.0 equiv) was added dropwise to carboxylate **155** (25.0 mg, 0.094 mmol, 1.0 equiv) in a microwave vial equipped with a stir bar at rt. The reaction was stirred at 130 °C for at least 6 h before it was poured directly on ice. The solution was titrated to pH = 7 with sat. aq. $NaHCO_3$ and then extracted with EtOAc (3 × 2 mL). The combined organic extract was dried over anhydrous Na_2SO_4, filtered, and concentrated *in vacuo*. Purification by silica gel flash chromatography (eluting with 100% EtOAc). The product was isolated as a (12.4 mg, 82%). R_f = 0.44 (100% EtOAc). ^{1}H NMR (500 MHz, $CDCl_3$) δ 7.64 (d, *J* = 9.4 Hz, 1H), 7.36 (d, *J* = 8.4 Hz, 1H), 6.84 (d, *J* = 2.5 Hz, 1H), 6.80 (dd, *J* = 8.5, 2.4 Hz, 1H), 6.26 (d, *J* = 9.5 Hz, 1H). All other spectroscopic data are in accord with previously reported literature.

1.6 NMR Spectra

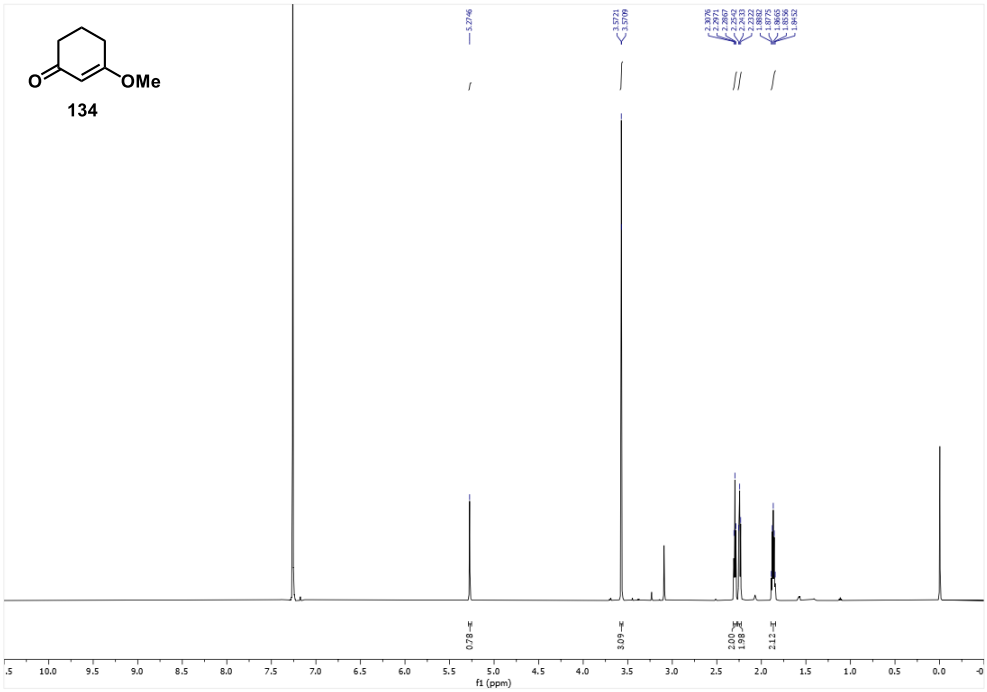

Figure 1.6: 3-Methoxy-2-cyclohexe-1-one (**134**); ^{1}H NMR (600 MHz, $CDCl_3$) at 24.8 °C.

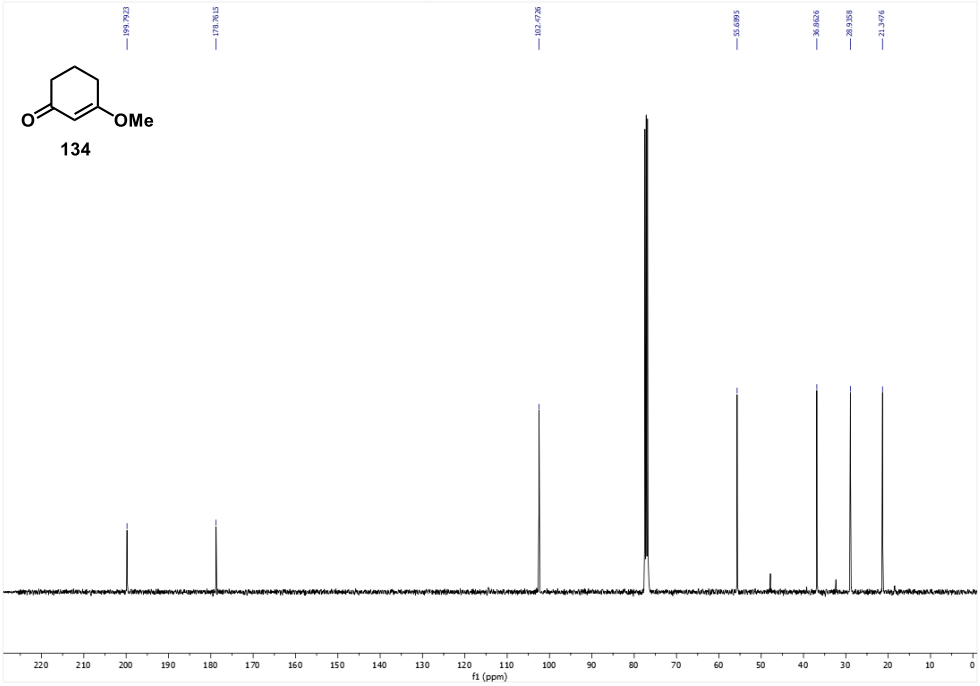

Figure 1.7: 3-Methoxy-2-cyclohexe-1-one (**134**); ^{13}C NMR (600 MHz, $CDCl_3$) at 24.8 °C.

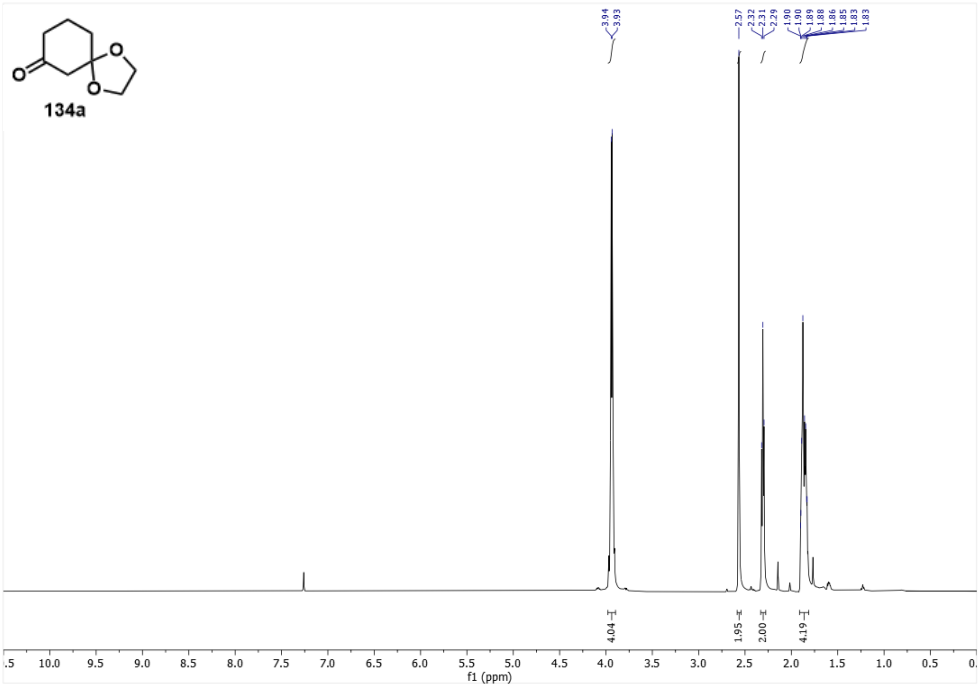

Figure 1.8: 1,4-Dioxaspiro[4.5]decan-7-one (**134a**); ^{1}H NMR (600 MHz, $CDCl_3$) at 24.8 °C.

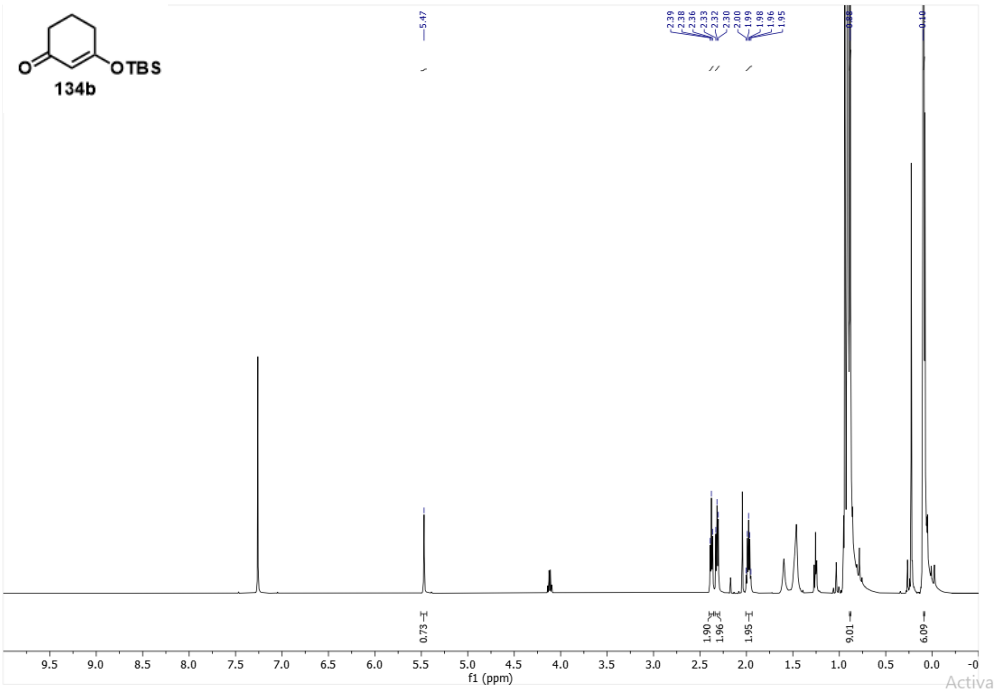

Figure 1.9: 3-((Tert-butyldimethylsilyl)oxy)cyclohex-2-en-1-one (**134b**); ^{1}H NMR (400 MHz, $CDCl_3$) at 21.9 °C.

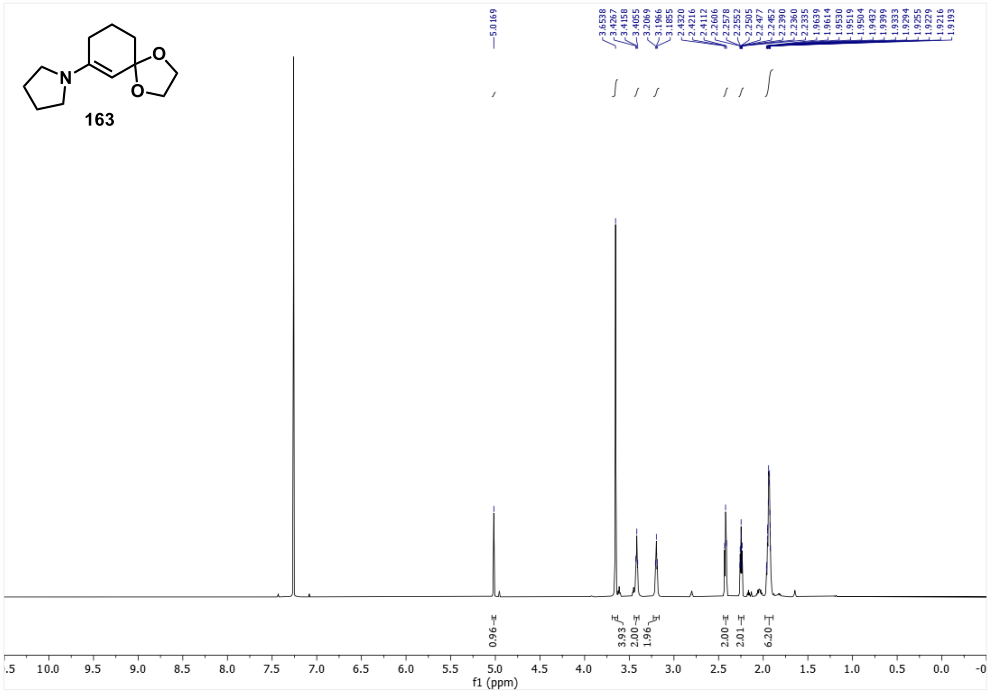

Figure 1.10: 1-(1,4-Dioxaspiro[4.5]dec-7-en-7-yl)pyrrolidine (**163**); ^{1}H NMR (600 MHz, $CDCl_3$) at 24.8 °C.

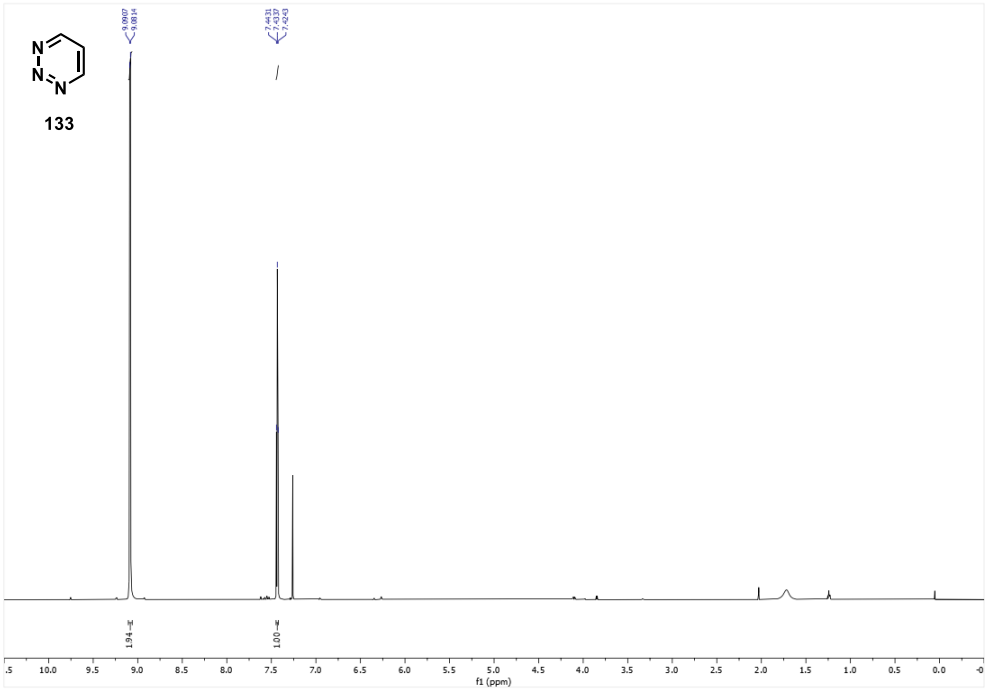

Figure 1.11: 1,2,3-Triazine (**133**)*;* ^{1}H NMR (600 MHz, $CDCl_3$) at 24.8 °C.

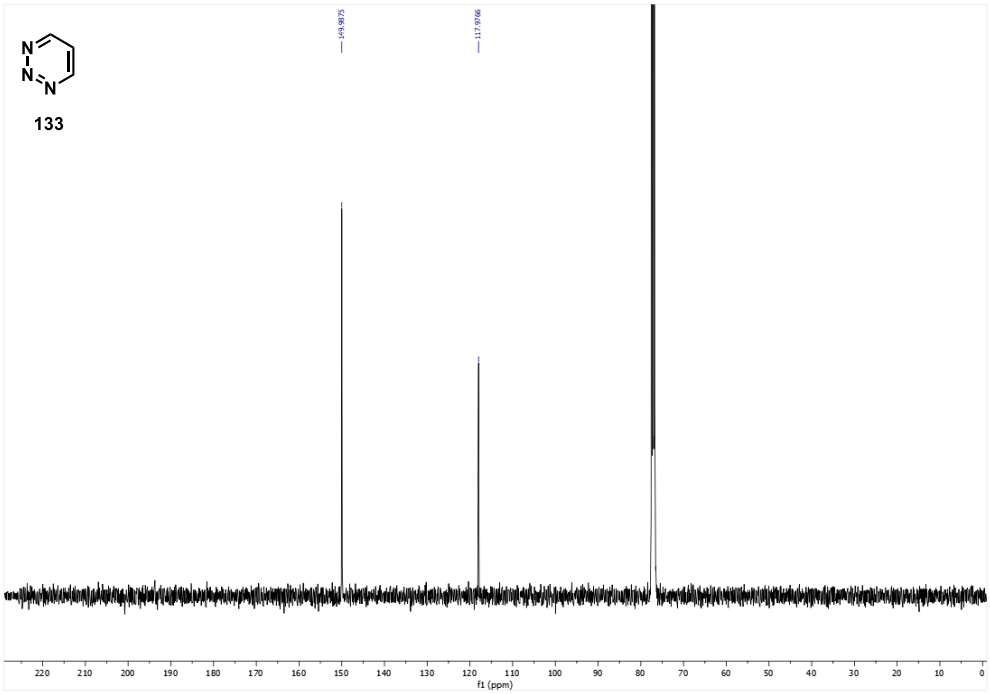

Figure 1.12: 1,2,3-Triazine (**133**)*;* ^{13}C NMR (600 MHz, $CDCl_3$) at 24.8 °C.

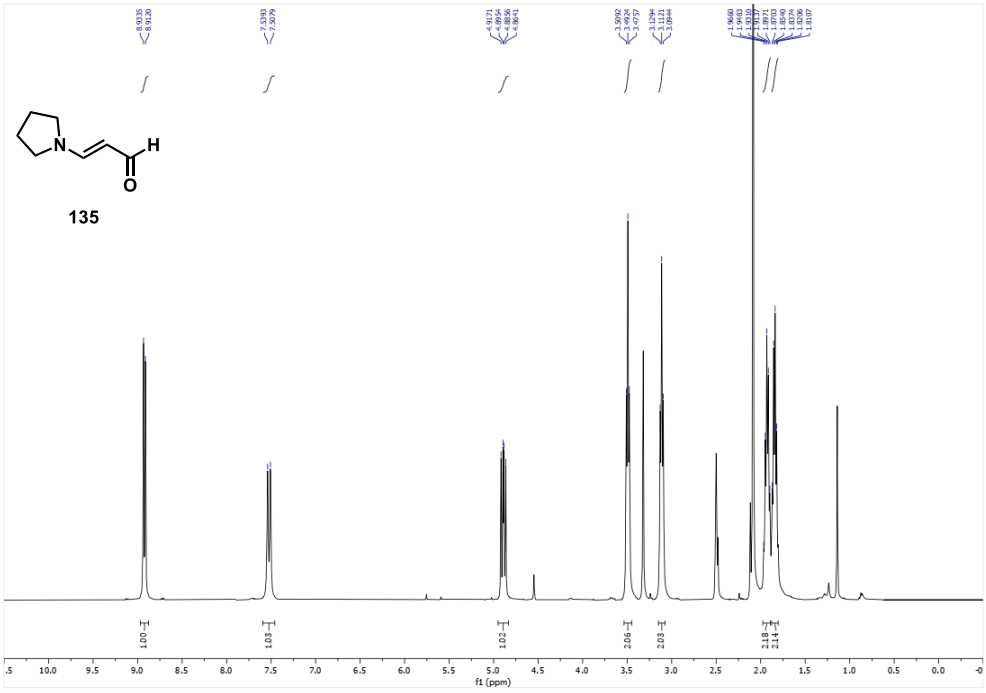

Figure 1.13: (*E*)-3-(Pyrrolidin-1-yl)acrylaldehyde (**135**); ^{1}H NMR (400 MHz, DMSO-d_6) at 21.9 °C.

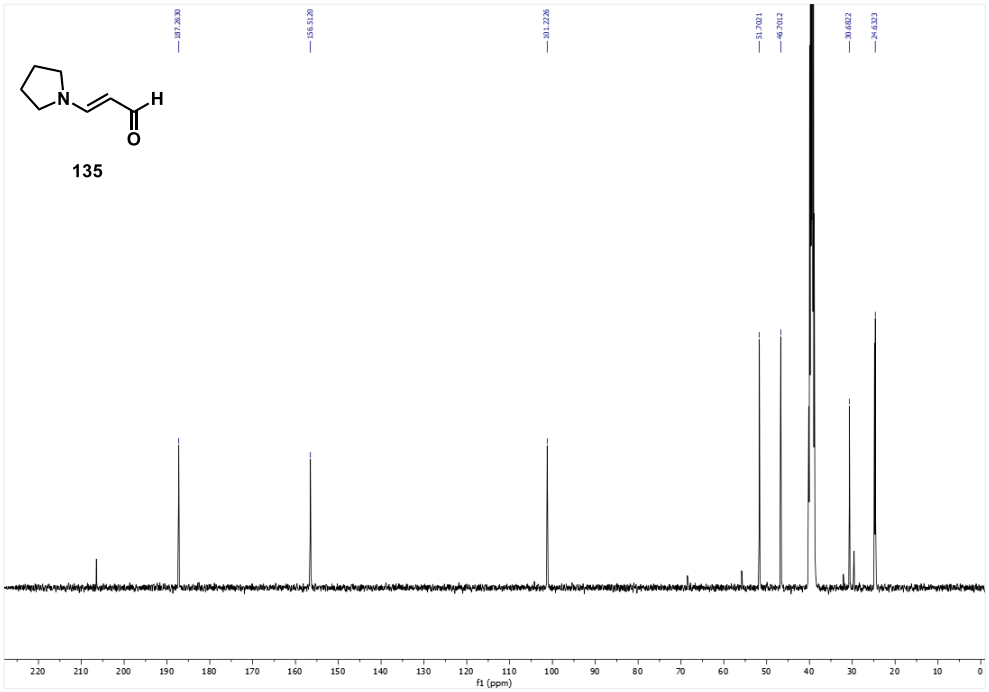

Figure 1.14: (*E*)-3-(Pyrrolidin-1-yl)acrylaldehyde (**135**); ^{13}C NMR (400 MHz, DMSO-d_6) at 21.9 °C.

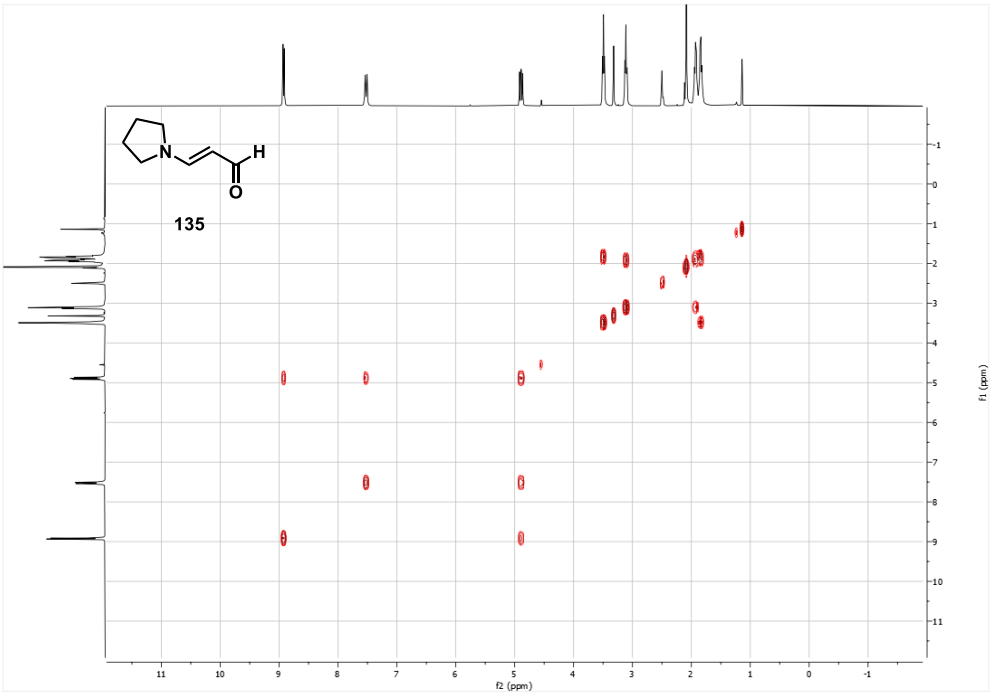

Figure 1.15: (*E*)-3-(Pyrrolidin-1-yl)acrylaldehyde (**135**); COSY (400 MHz, DMSO-d_6) at 21.9 °C.

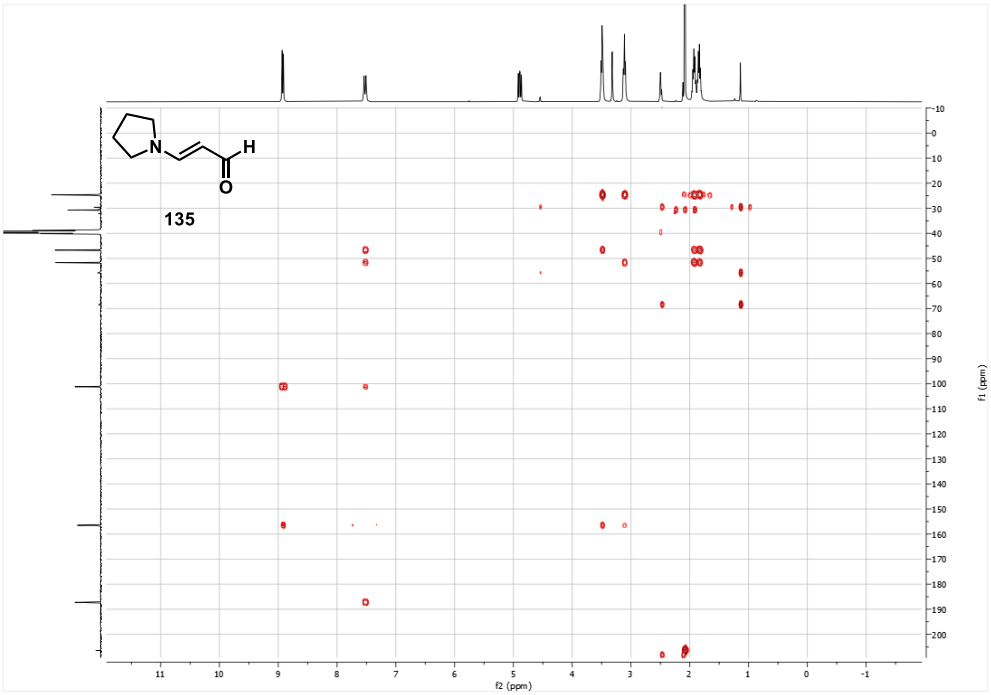

Figure 1.16: (*E*)-3-(Pyrrolidin-1-yl)acrylaldehyde (**135**); HMBC (400 MHz, DMSO-d_6) at 21.9 °C.

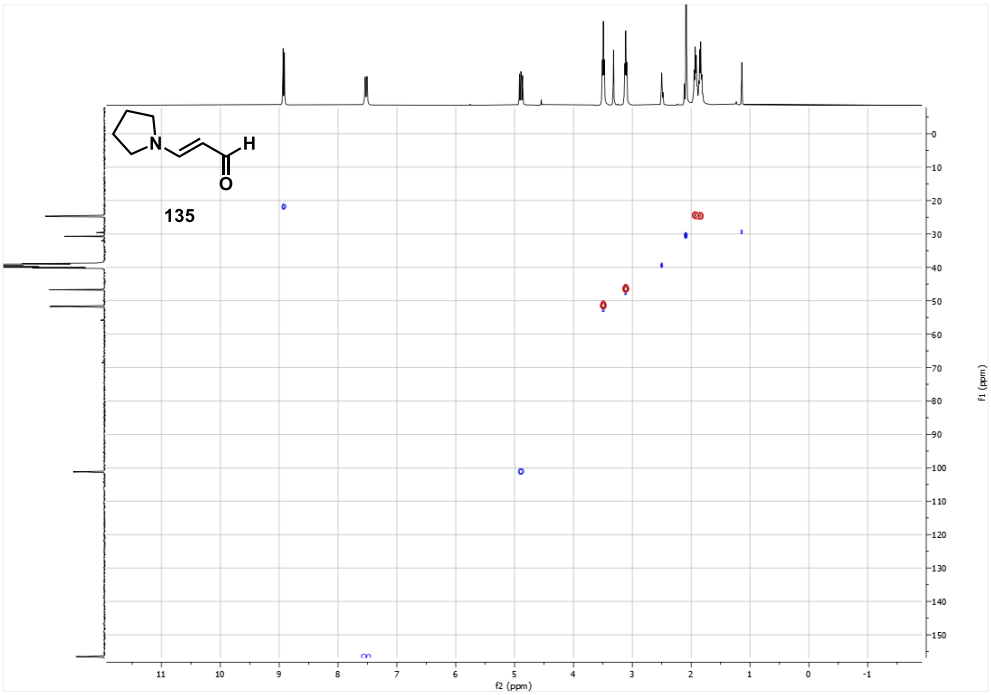

Figure 1.17: (*E*)-3-(Pyrrolidin-1-yl)acrylaldehyde (**135**); HSQC (400 MHz, DMSO-d_6) at 21.9 °C.

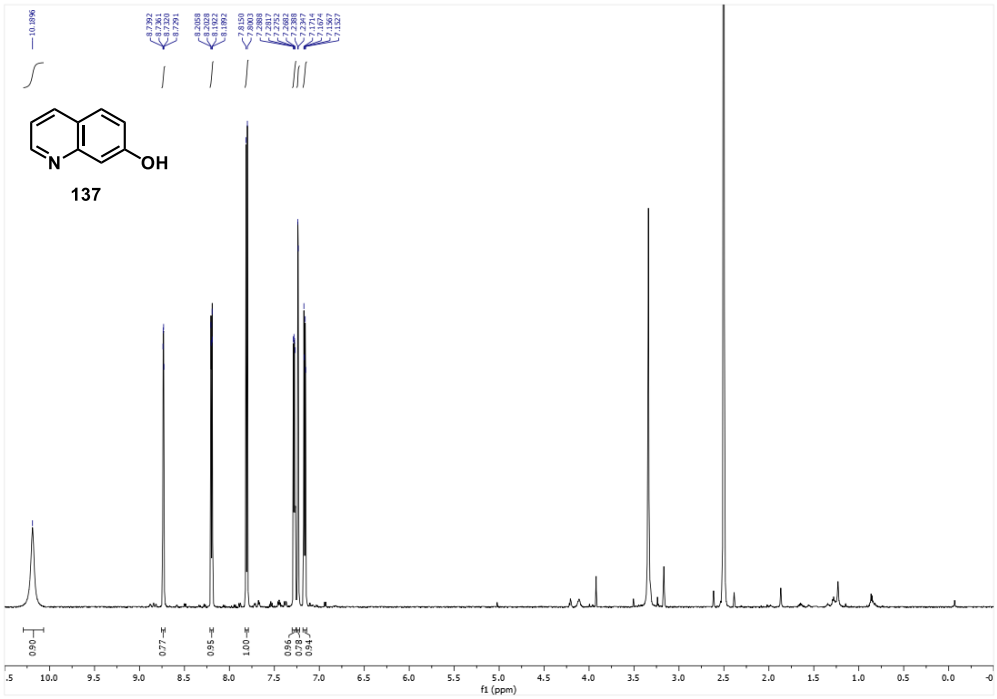

Figure 1.18: 7-Hydroxyquinoline (**137**); ^{1}H NMR (600 MHz, DMSO-d_6) at 24.8 °C.

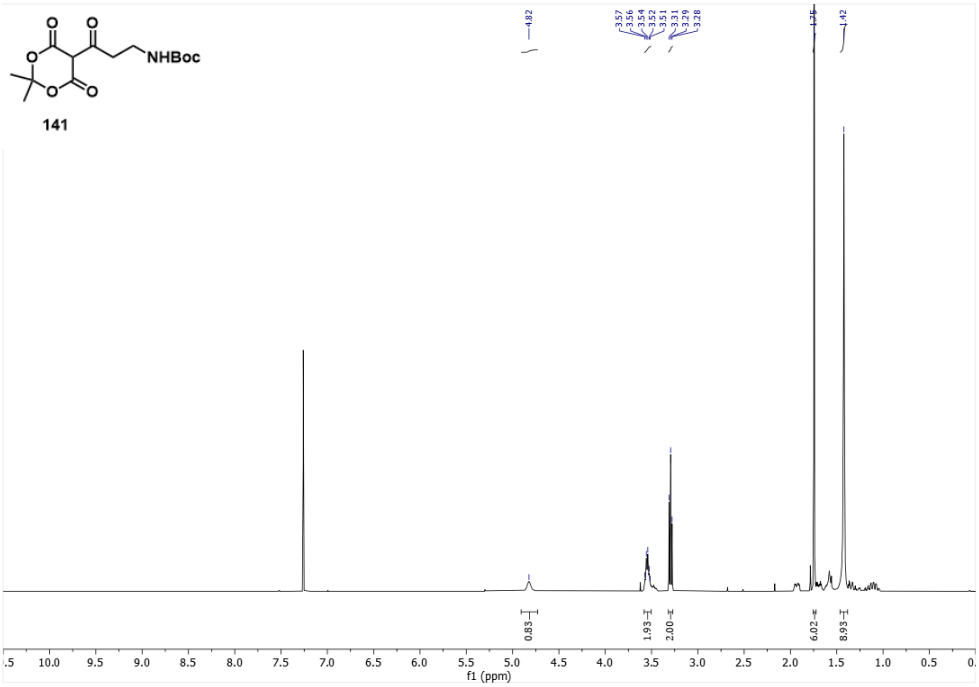

Figure 1.19: Tert-butyl (3-(2,2-dimethyl-4,6-dioxo-1,3-dioxan-5-yl)-3-oxopropyl)carbamate (**141**); ^{1}H NMR (400 MHz, $CDCl_3$) at 21.9 °C.

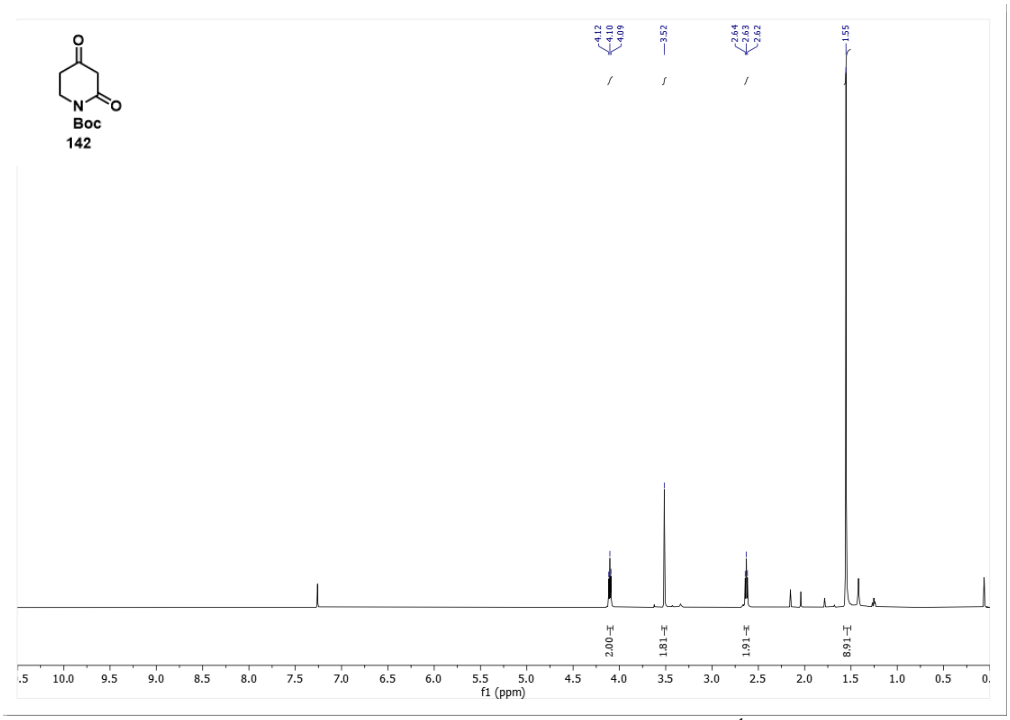

Figure 1.20: Tert-butyl 2,4-dioxopiperidine-1-carboxylate (**142**); ^{1}H NMR (500 MHz, $CDCl_3$) at 24.8 °C.

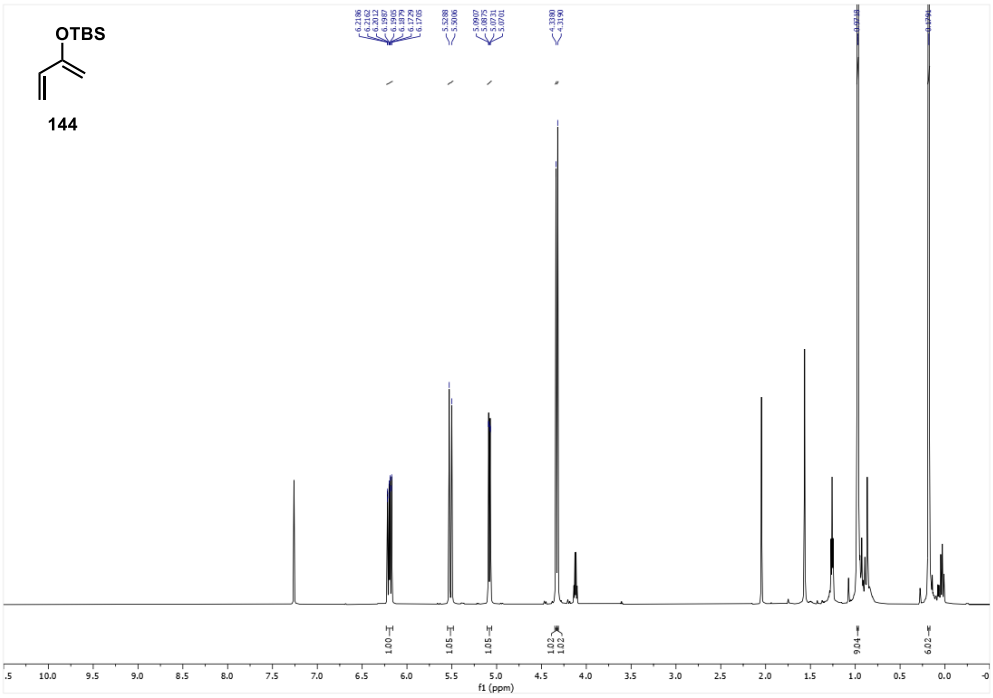

Figure 1.21: (Buta-1,3-dien-2-yloxy)(tert-butyl)dimethylsilane (**144**); ^{1}H NMR (600 MHz, $CDCl_3$) at 24.8 °C.

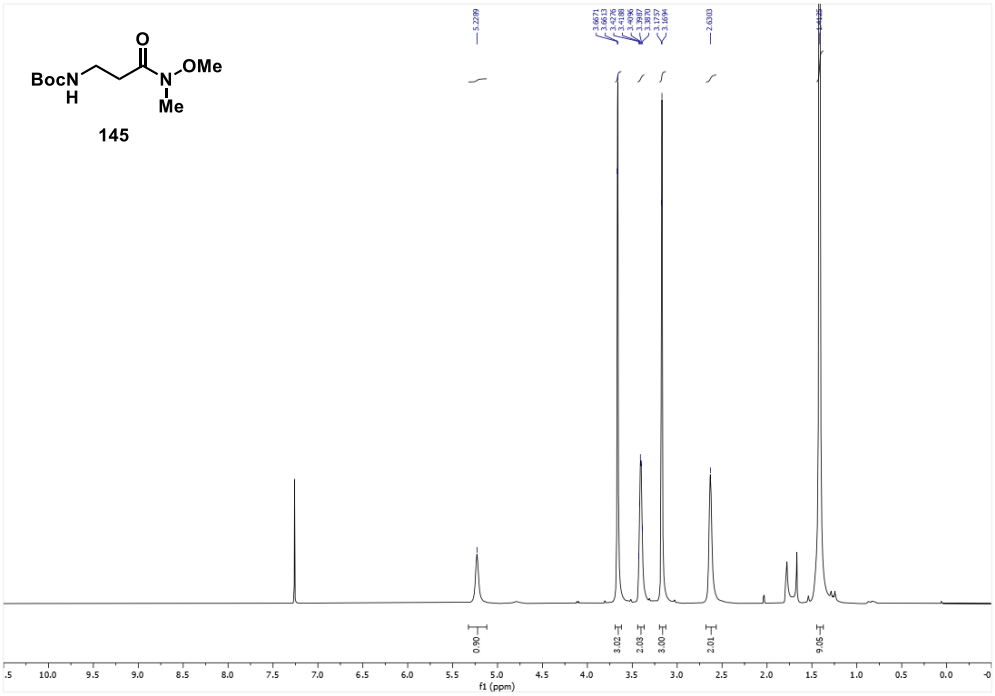

Figure 1.22: Tert-butyl (3-(methoxy(methyl)amino)-3-oxopropyl)carbamate (**145**); ^{1}H NMR (500 MHz, $CDCl_3$) at 24.8 °C.

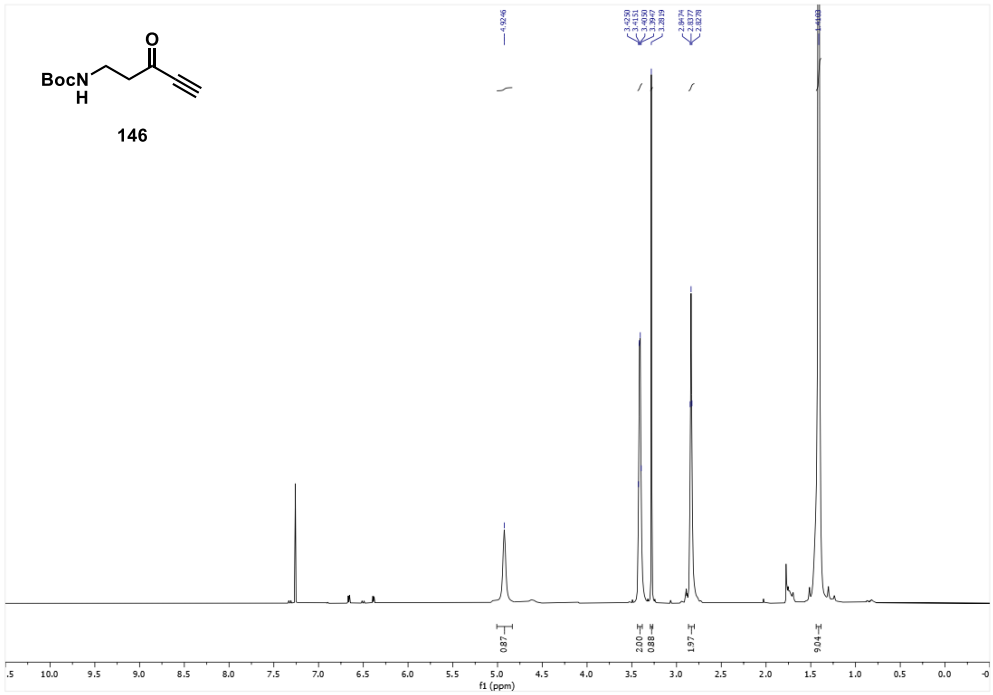

Figure 1.23: Tert-butyl (3-oxopent-4-yn-1-yl)carbamate (**146**); ^{1}H NMR (600 MHz, $CDCl_3$) at 24.8 °C.

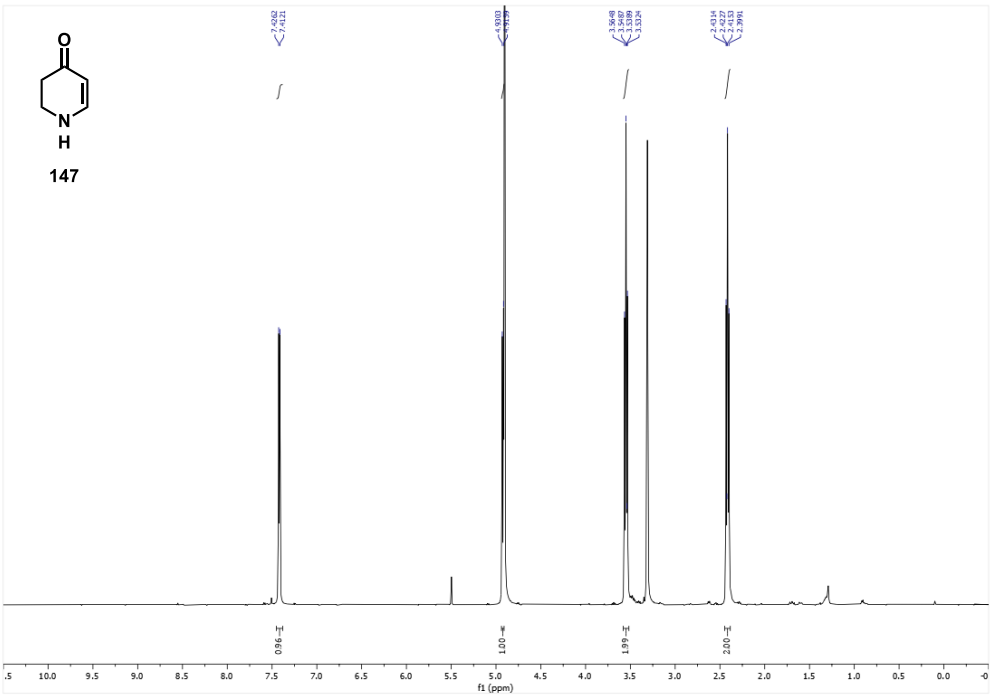

Figure 1.24: 2,3-Dihydropyridin-4(1H)-one (**147**); ^{1}H NMR (500 MHz, MeOD) at 24.8 °C.

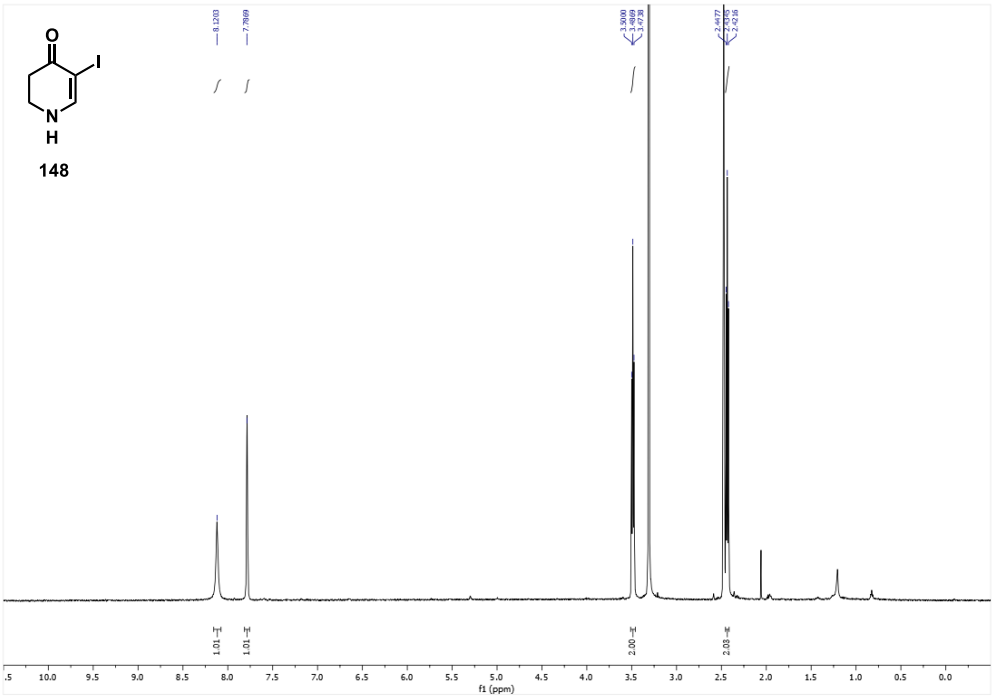

Figure 1.25: 5-Iodo-2,3-dihydropyridin-4(1H)-one (**148**); ^{1}H NMR (600 MHz, DMSO-d_6) at 24.8 °C.

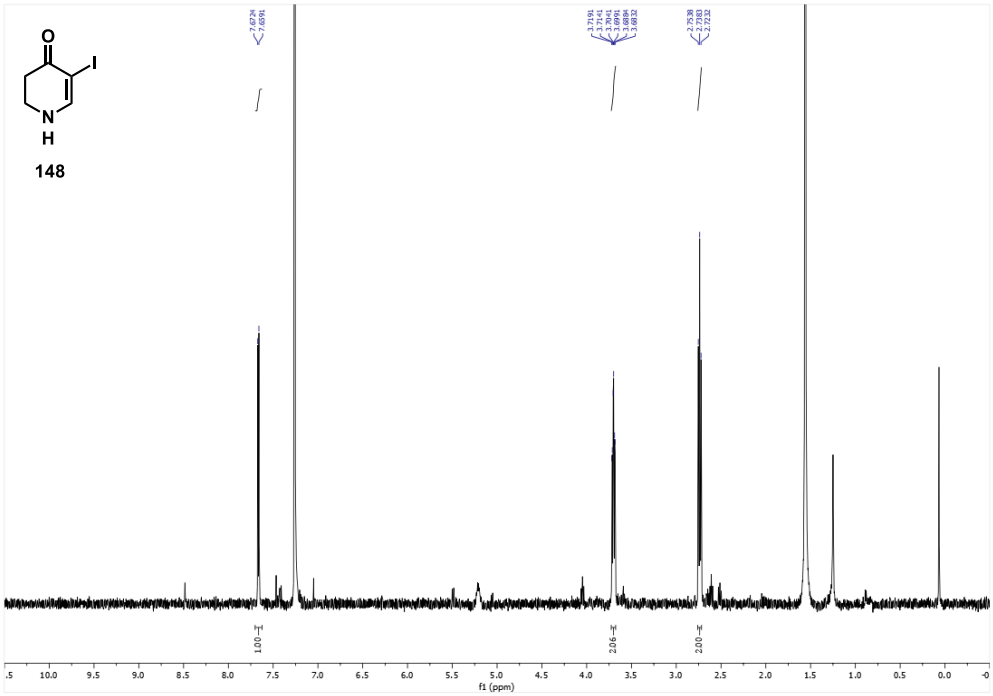

Figure 1.26: 5-Iodo-2,3-dihydropyridin-4(1H)-one (**148**); ^{1}H NMR (500 MHz, $CDCl_3$) at 24.8 °C.

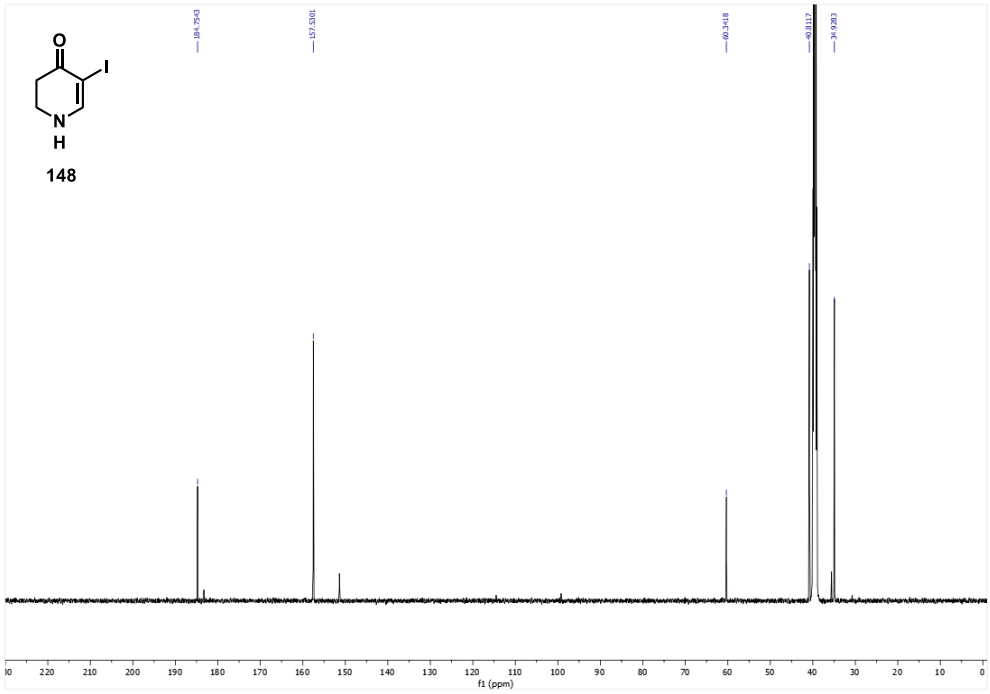

Figure 1.27: 5-Iodo-2,3-dihydropyridin-4(1H)-one (**148**); ^{13}C NMR (600 MHz, DMSO-d_6) at 24.8 °C.

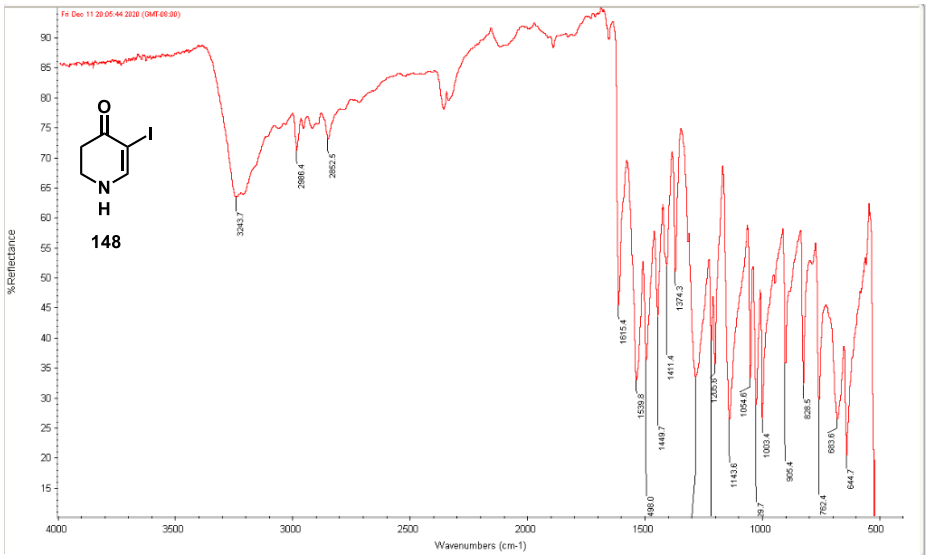

Figure 1.28: 5-Iodo-2,3-dihydropyridin-4(1H)-one (**148**); IR Spectrum.

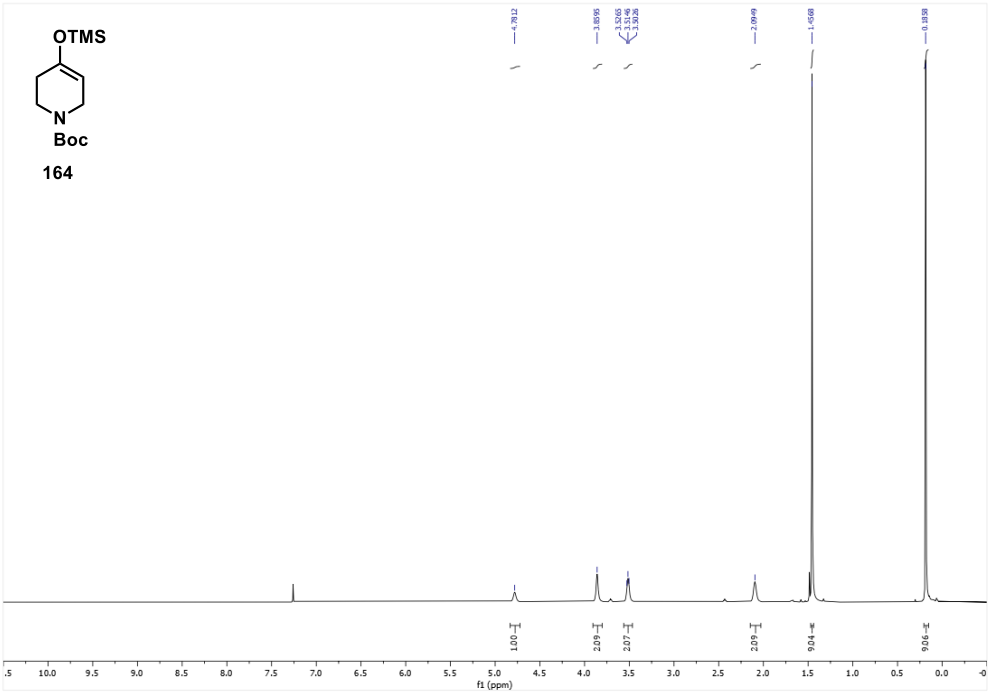

Figure 1.29: Tert-butyl 4-((trimethylsilyl)oxy)-3,6-dihydropyridine-1(2H)-carboxylate (**164**); ^{1}H NMR (500 MHz, $CDCl_3$) at 24.8 °C.

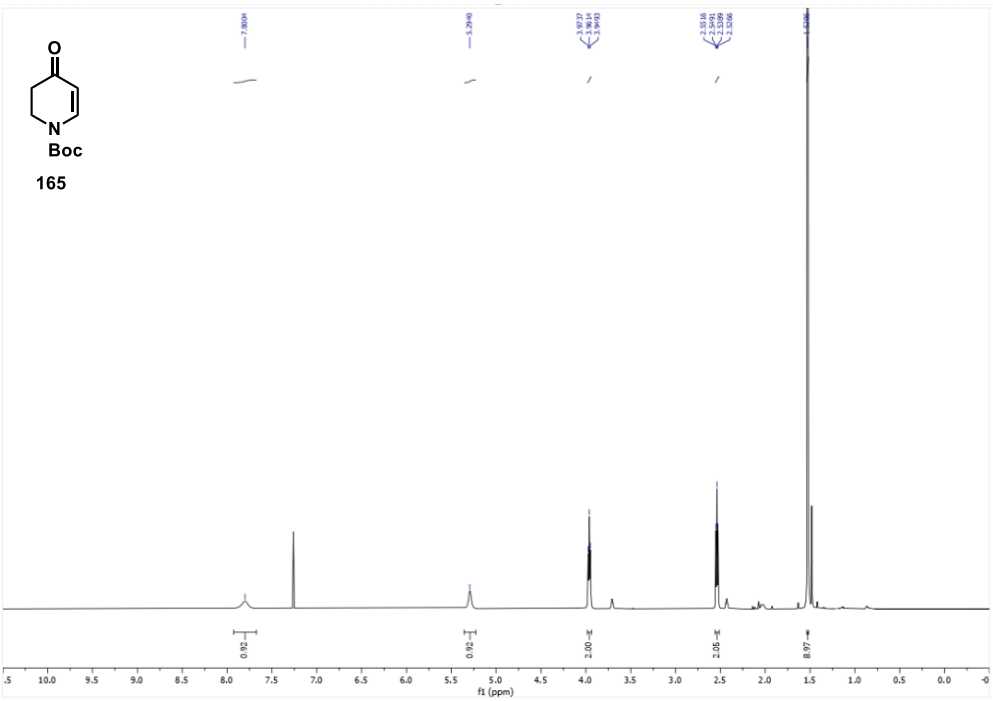

Figure 1.30: Tert-butyl 4-oxo-3,4-dihydropyridine-1(2H)-carboxylate (**165**); ^{1}H NMR (600 MHz, $CDCl_3$) at 24.8 °C.

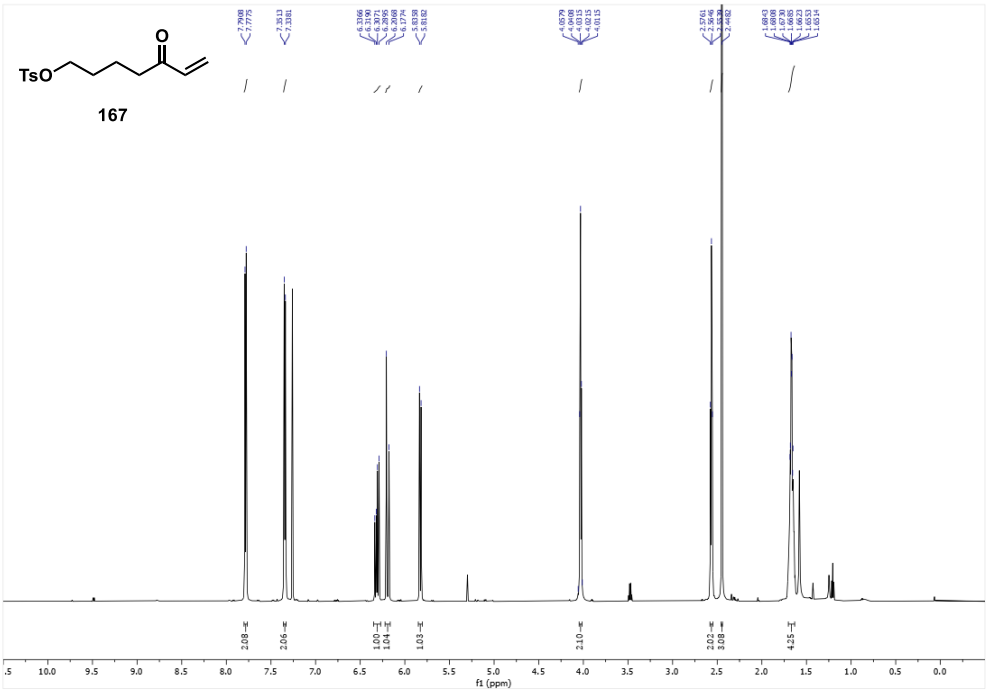

Figure 1.31: 5-Oxohept-6-en-1-yl 4-methylbenzenesulfonate (**167**); ^{1}H NMR (600 MHz, $CDCl_3$) at 24.8 °C.

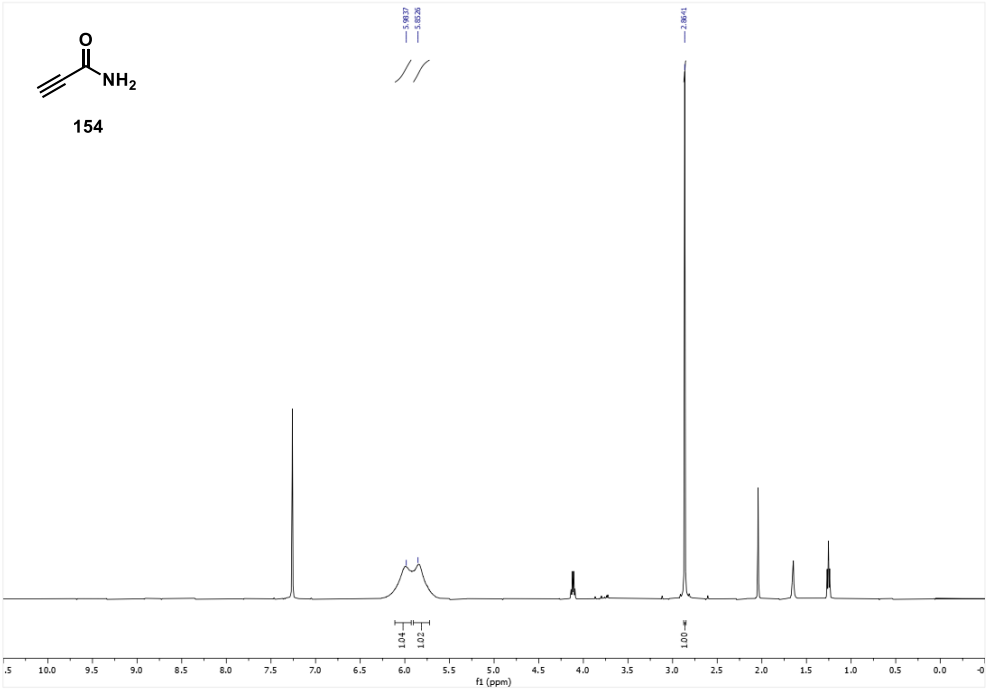

Figure 1.32: Propiolamide (**154**); ^{1}H NMR (500 MHz, $CDCl_3$) at 24.8 °C.

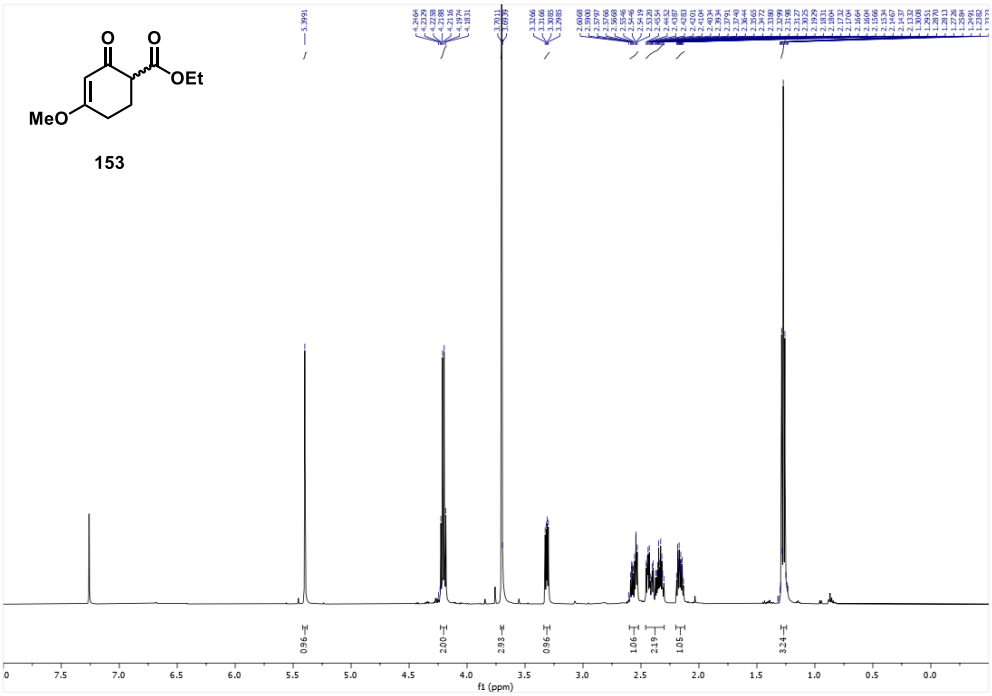

Figure 1.33: Ethyl 4-methoxy-2-oxocyclohex-3-ene-1-carboxylate (**153**); ^{1}H NMR (500 MHz, $CDCl_3$) at 24.8 °C.

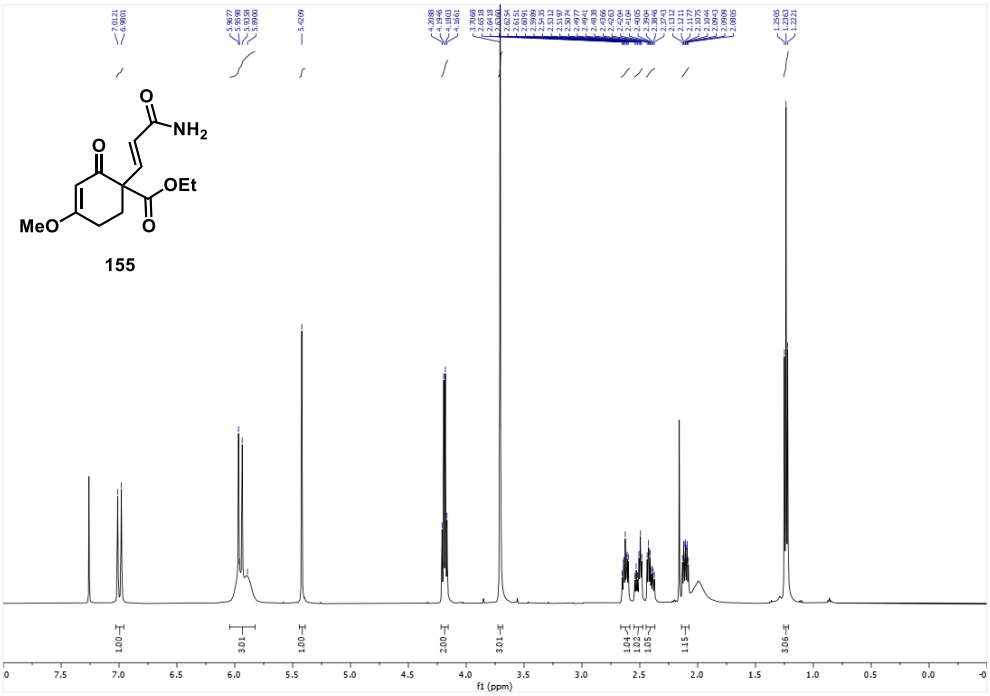

Figure 1.34: Ethyl (E)-1-(3-amino-3-oxopropenyl)-4-methoxy-2-oxocyclohexene carboxylate (**155**); ^{1}H NMR (500 MHz, $CDCl_3$) at 24.8 °C.

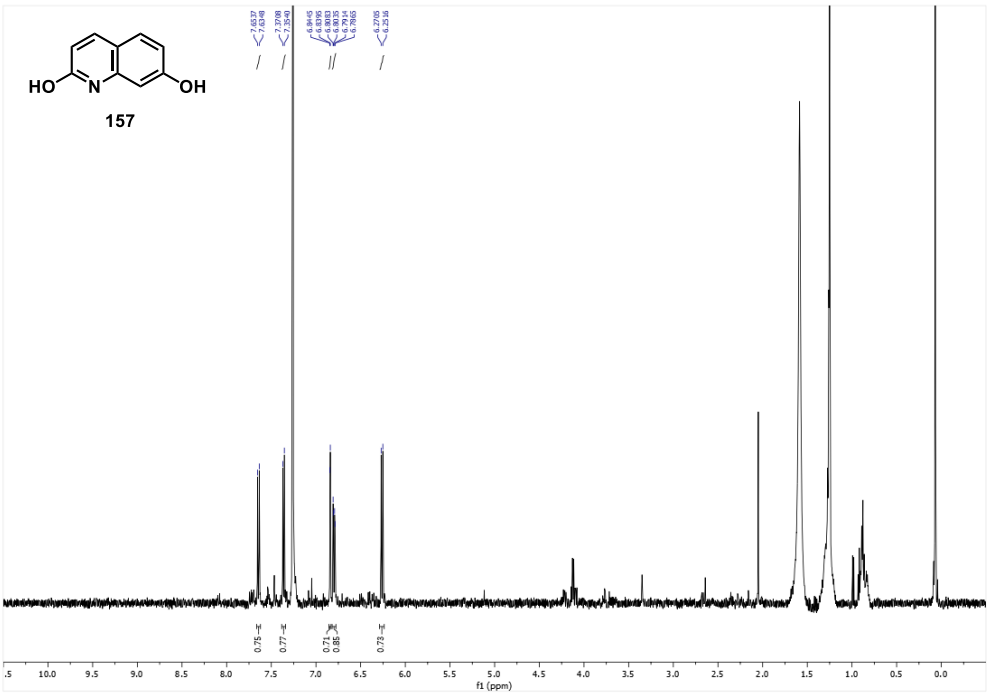

Figure 1.35: 2,7-Dihydroxyquinoline (**157**); ^{1}H NMR (500 MHz, $CDCl_3$) at 24.8 °C.

1.7 References

(1) Heinrich, M.; Mah, J.; Amirkia, V. Alkaloids Used as Medicines: Structural Phytochemistry Meets Biodiversity—an Update and Forward Look. *Molecules* **2021**, *26* (7), 1836. DOI: 10.3390/molecules26071836

(2) Rajput, A.; Sharma, R.; Bharti, R. Pharmacological Activities and Toxicities of Alkaloids on Human Health. *Mater. Today Proc.*, **2022**, *48* (5), 1407–1415. DOI: 10.1016/j.matpr.2021.09.189

(3) Faisal, S.; Badshah, S. L.; Kubra, B.; Emwas, A.-H.; Jaremko, M. Alkaloids as Potential Antivirals. A Comprehensive Review. *Nat. Prod. and Bioprospect.*, **2023**, *13* (1). DOI: 10.1007/s13659-022-00366-9

(4) Patil, S. P. Recently Isolated Lycodine-Type Lycopodium Alkaloids and Their Total Synthesis: A Review. *Futur. J. Pharm. Sci.* **2020**, *6* (99). DOI: 10.1186/s43094-020-00108-z

(5) Bödeker, K. Lycopodin, Das Erste Alkaloïd Der Gefässkryptogamen. *Justus Liebigs Ann. der Chem.* **1881**, *208* (3), 363–367. DOI: 10.1002/jlac.18812080308

(6) Yang, H.; Carter, R. G.; Zakharov, L. N. Enantioselective Total Synthesis of Lycopodine. *J. Am. Chem. Soc.* **2008**, *130* (29), 9238–9239. DOI: 10.1021/ja803613w

(7) Permin, H.; Norn, S.; Kruse, E.; Kruse, P. R. On the History of Cinchona Bark in the Treatment of Malaria. *Dan. Medicinhist. Arbog.* **2016**, *44*, 9–30.

(8) Škubník, J.; Pavlíčková, V. S.; Ruml, T.; Rimpelová, S. Vincristine in Combination Therapy of Cancer: Emerging Trends in Clinics. *Biology*, **2021**, *10* (9), 849. DOI: 10.3390/biology10090849

(9) Ishikawa, H.; Colby, D. A.; Seto, S.; Va, P.; Tam, A.; Kakei, H.; Rayl, T. J.; Hwang, I.; Boger, D. L. Total Synthesis of Vinblastine, Vincristine, Related Natural Products, and Key Structural Analogues. *J. Am. Chem. Soc.* **2009**, *131* (13), 4904–4916. DOI: 10.1021/ja809842b

(10) Ma, X.; Gang, D. R. The Lycopodium Alkaloids. *Nat. Prod. Rep.* **2004**, *21* (6), 752–772. DOI: 10.1039/B409720N

(11) Chen, F.; Song, L.; Cheng, B. Huperzine Alkaloids: Forty Years of Total Syntheses. *Nat. Prod. Rep.*, **2024**, Advance Article. DOI: 10.1039/D3NP00029J

(12) Herzon, S.; Tun, M. K. M. The Pharmacology and Therapeutic Potential of (–)-Huperzine A. *J. Exp. Pharmacol.*, **2012**, *4*, 113-123. DOI: 10.2147/jep.s27084

(13) García-Ayllón, M. S.; Small, D. H.; Avila, J.; Sáez-Valero, J. Revisiting the Role of Acetylcholinesterase in Alzheimer's Disease: Cross-Talk With P-tau and β-Amyloid. *Front. Mol. Neurosci.* **2011**, *4* (22), 1-9. DOI: 10.3389/fnmol.2011.00022

(14) Talesa, V. N. Acetylcholinesterase in Alzheimer's Disease. *Mech. Ageing Dev.*, **2001**, *122* (16), 1961–1969. DOI: 10.1016/s0047-6374(01)00309-8

(15) McKinney, M.; Miller, J. H.; Yamada, F.; Tuckmantel, W.; Kozikowski, A. P. Potencies and Stereoselectivities of Enantiomers of Huperzine A for Inhibition of Rat Cortical Acetylcholinesterase. *Eur. J. Pharmacol.*, **1991**, *203* (2), 303–305. DOI: 10.1016/0014-2999(91)90730-E

(16) Tang, X. C.; De Sarno, P.; Sugaya, K.; Giacobini, E. Effect of Huperzine A, a New Cholinesterase Inhibitor, on the Central Cholinergic System of the Rat. *J. Neurosci. Res.* **1989**, *24* (2), 276–285. DOI: 10.1002/jnr.490240220

(17) Raves, M. L.; Harel, M.; Pang, Y.-P.; Silman, I.; Kozikowski, A. P.; Sussman, J. L. Structure of Acetylcholinesterase Complexed with the Nootropic Alkaloid, (–)-Huperzine A. *Nat. Struct. Biol.*, **1997**, *4* (1), 57–63. DOI: 10.1038/nsb0197-57

(18) Ayer, W. A. The Lycopodium Alkaloids. *Nat. Prod. Rep.*, **1991**, *8* (5), 455–463. DOI: 10.1039/NP9910800455

(19) Ayer, W. A.; Masaki, N.; Nkunika, D. S. Luciduline: A Unique Type of Lycopodium Alkaloid. *Can. J. Chem.* **1968**, *46* (23), 3631–3642. DOI: 10.1139/v68-602

(20) Castillo, M.; Gupta, R. N.; Ho, Y. K.; MacLean, D. B.; Spenser, I. D. Biosynthesis of Lycopodine. Incorporation of Δ^1-Piperideine and of Pelletierine. *Can. J. Chem.* **1970**, *48* (18), 2911–2918. DOI: 10.1139/v70-489

(21) Castillo, M.; Gupta, R. N.; Maclean, D. B.; Spenser, I. D. Biosynthesis of Lycopodine From Lysine And Acetate. The Pelletierine Hypothesis. *Can. J. Chem.* **1970**, *48* (12), 1893-1903. DOI: 10.1139/v70-312

(22) Marshall, W.; Nguyen, T.; Maclean, D. B.; Spenser, I. D. Biosynthesis of Lycopodine. The Question of the Intermediacy of Piperidine-2-Acetic Acid. *Can. J. Chem.* **1975**, *53* (1), 41–50. DOI: 10.1139/v75-005

(23) Hemscheidt, T.; Spenser, I. D. Biosynthesis of Lycopodine: Incorporation of Acetate via an Intermediate with C2v Symmetry. *J. Am. Chem. Soc.* **1993**, *115* (7), 3020–3021. DOI: 10.1021/ja00060a078

(24) Hemscheidt, T.; Spenser, I. D. A Classical Paradigm of Alkaloid Biogenesis Revisited: Acetonedicarboxylic Acid as a Biosynthetic Precursor of Lycopodine. *J. Am. Chem. Soc.* **1996**, *118* (7), 1799–1800. DOI: 10.1021/ja953735q

(25) Richards, J. C.; Spenser, I. D. The Stereochemistry of the Enzymic Decarboxylation of L-Arginine and of L-Ornithine. *Can. J. Chem.* **1982**, *60* (22), 2810–2820. DOI: 10.1139/v82-404

(26) W. A. Ayer and L. S. Trifonov, in Lycopodium Alkaloids, Academic Press, San Diego, 1994.

(27) Conroy, H. Biogenesis of Lycopodium Alkaloids. *Tetrahedron Lett*. **1960**, *1* (31), 34–37. DOI: 10.1016/S0040-4039(01)99301-3

(28) Dai, M.; Yang, Y. Total Syntheses of Lyconadins: Finding Efficiency and Diversity. *Synlett*. **2014**, *25* (15), 2093–2098. DOI: 10.1055/s-0034-1378319

(29) Zhang, X. M.; Guo, X.; Li, Y. Y.; Wang, S. H.; Zhang, F. M.; Li, B. S.; Tu, Y. Q. Construction of the Tetracyclic Core of the Lycopodium Alkaloid Annotinolide C. *Org. Chem. Front*. **2021**, *8* (11), 2510-2514. DOI: 10.1039/D1QO00087J

(30) (a) Beshore, D. C.; Smith, A. B. Total Syntheses of (+)-Lyconadin A and (–)-Lyconadin B. J. Am. Chem. Soc. 2007, 129 (14), 4148-4149. DOI: 0.1021/ja070336+ (b) Beshore, D. C.; Smith, A. B. The Lyconadins: Enantioselective Total Syntheses of(+)-Lyconadin A and (–)-Lyconadin B. J. Am. Chem. Soc. 2008, 130 (41), 13778-13789. DOI: 10.1021/ja804939r

(31) (a) Bisai, A.; West, S. P.; Sarpong, R. Unified Strategy for the Synthesis of the "Miscellaneous"LycopodiumAlkaloids: Total Synthesis of (±)-Lyconadin A. J. Am. Chem. Soc. 2008, 130 (23), 7222-7223. DOI: 10.1021/ja8028069 (b) West, S. P.; Bisai, A.; Lim, A. D.; Narayan, R. R.; Sarpong, R. Total Synthesis of (+)-Lyconadin A and Related Compoundsvia Oxidative C-N Bond Formation. J. Am. Chem. Soc. 2009, 131 (31), 11187-11194. DOI: 10.1021/ja903868n

(32) Nishimura, T.; Unni, A. K.; Yokoshima, S.; Fukuyama, T. Total Syntheses of Lyconadins A−C. J. Am. Chem. Soc. 2013, 135 (8), 3243-3247. DOI: 10.1021/ja312065m

(33) Cheng, X.; Waters, S. P. Pyridone Annulation via Tandem CurtiusRearrangement/6π-Electrocyclization:Total Synthesis of (–)-Lyconadin C. Org. Lett. 2013, 15 (16), 4226-4229. DOI: 10.1021/ol401954f

(34) Sarpong, R.; Haley, H. M. S.; Payer, S. E.; Papidocha, S. M.; Clemens, S.; Nyenhuis, J. Bioinspired Diversification Approach Toward the Total Synthesis of Lycodine-Type Alkaloids. *J. Am. Chem. Soc*. **2021**, *143* (12), 4732−4740. DOI: 10.1021/jacs.1c00457

(35) Rychnovsky, S. D.; DeForest, J. C.; Samame, R. A.; Suryn, G.; Burtea, A. Second-Generation Synthesis of (+)-Fastigiatine Inspired by Conformational Studies. *J. Org. Chem*. **2018**, *83* (16), 8914−8925. DOI: 10.1021/acs.joc.8b01144

(36) (a) Inubushi, Y.; Ishii, H.; Harayama, T.; Burnell, R. H.; Ayer, W. A.; Altenkirk, B. Structure of Fawcettimine: Correlation with Serratinine. *Tetrahedron Lett.*, **1967**, *8* (12), 1069–1072. DOI: 10.1016/S0040-4039(00)90638-5 (b) Ishii, H.; Yasui, B.; Harayama, T.; Inubushi, Y. Structure of Fawcettidine: Transformation of Serratinine into Fawcettidine. *Tetrahedron Lett.*, **1966**, *7* (49), 6215–6219. DOI: 10.1016/S0040-4039(00)70168-7 (c) Harayama, T.; Takatani, M.; Inubushi, Y. Stereoselective Syntheses of Lycopodium Alkaloids, (±)-Fawcettimine and (±)-8-Deoxyserratinine. *Tetrahedron Lett.*, **1979**, *20* (44), 4307–4310. DOI: 10.1016/s0040-4039(01)86574-6
(37) Heathcock, C. H.; Blumenkopf, T. A.; Smith, K. M. Total Synthesis of (±)-Fawcettimine. *J. Org. Chem.*, **1989**, *54* (7), 1548-1562.

(38) Ding, X.; Nguyen, S. T.; Williams, J. D.; Peet, N. P. Diels-Alder Reactions of Five-Membered Heterocycles Containing One Heteroatom. *Tetrahedron Lett.*, **2014**, *55* (51), 7002–7006. DOI: 10.1016/j.tetlet.2014.10.114

(39) Zaimoku, H.; Nishide, H.; Nishibata, A.; Goto, N.; Taniguchi, T.; Ishibashi, H. Syntheses of (±)-Serratine, (±)-Lycoposerramine T, and (±)-Lycopoclavamine B. *Org. Lett*., **2013**, *15* (9), 2140–2143. DOI: 10.1021/ol400628h

(40) Zhao, X.-H.; Zhang, Q.; Du, J.-Y.; Lu, X.-Y.; Cao, Y.-X.; Deng, Y.-H.; Fan, C.-A. Total Synthesis of (±)-Lycojaponicumin D and Lycodoline-Type *Lycopodium* Alkaloids. *J. Am. Chem. Soc.*, **2017**, *139* (20), 7095–7103. DOI: 10.1021/jacs.7b03280

(41) Tang, Y.; Xiong, J.; Zhang, J.-J.; Wang, W.; Zhang, H.-Y.; Hu, J.-F. Annotinolides A–C, Three Lycopodane-Derived 8,5-Lactones with Polycyclic Skeletons from Lycopodium Annotinum. *Org. Lett.* **2016**, *18* (17), 4376–4379. DOI: 10.1021/acs.orglett.6b02132

(42) Hardy, J.; Selkoe, D. J.; The Amyloid Hypothesis of Alzheimer's Disease: Progress and Problems on the Road to Therapeutics. *Science*, **2002**, *297* (5580), 353–356. DOI: 10.1126/science.1072994

(43) Cleary, J. P.; Walsh, D. M.; Hofmeister, J. J.; Shankar, G. M.; Kuskowski, M. A.; Selkoe, D. K.; Ashe, K. H. Natural Oligomers of the Amyloid-Beta Protein Specifically Disrupt Cognitive Function. *Nat. Neurosci.* **2005**, *8* (1), 79–84. DOI: 10.1038/nn1372

(44) Haass, C.; Selkoe, D. J. Soluble Protein Oligomers in Neurodegeneration: Lessons from the Alzheimer's Amyloid Beta-Peptide. *Nat. Rev. Mol. Cell Biol.* **2007**, *8* (2), 101–112. DOI: 10.1038/nrm2101

(45) Yan, R. Stepping Closer to Treating Alzheimer's Disease Patients with BACE1 Inhibitior Drugs. *Transl. Neurodegener.* **2016**, *5* (13), 1-11. DOI: 10.1186/s40035-016-0061-5

(46) Synder, S. A.; Qu, P. Concise and Stereoselective Total Syntheses of Annotinolides C, D, and E. *J. Am. Chem. Soc*. **2021**, *143* (31), 11951–11956. DOI: 10.1021/jacs.1c05942

(47) Kotha, S.; Gunta, R. Synthesis of Intricate Fused *N*-Heterocycles via Ring-Rearrangement Metathesis. *J. Org. Chem.* **2017**, *82* (16), 8527–8535. DOI: 10.1021/acs.joc.7b01299

(48) Anderson, E. D.; Boger, D. L. Inverse Electron Demand Diels-Alder Reactions of 1,2,3-Triazines: Pronounced Substituent Effects on Reactivity and Cycloaddition Scope. *J. Am. Chem. Soc.* **2011**, *133* (31), 12285–12292. DOI: 10.1021/ja204856a

(49) Chandrasekhar, S.; Reddy, C. R. Towards a Synthesis of Epothilone A: Asymmetric Synthesis of C(1) C(6) and C(7) C(15) Fragments. *Tetrahedron Asymmetry* **2002**, *13* (3), 261–268. DOI: 10.1016/S0957-4166(02)00095

(50) Beaver, M. G.; Buscagan, T. M.; Lavinda, O.; Woerpel, K. A. *Angew. Chem. Int. Ed.* **2016**, *55* (5), 1816–1819. DOI: 10.1002/anie.201507806

(51) Loy, N. S. Y.; Choi, S.; Kim, S.; Park, C.-M. The Synthesis of Pyrroles and Oxazoles Based on Gold α-Imino Carbene Complexes. *Chem. Commun.* **2016**, *52* (46), 7336-7339. DOI: 10.1039/c6cc01742h

(52) Quinones, R. E.; Glinkerman, C. M.; Zhu, K.; Boger, D. L. Direct Synthesis of β-Aminoenals Through Reaction of 1,2,3-Triazine with Secondary Amines. *Org. Lett.* **2017**, *19* (13), 3568–3571. DOI: 10.1021/acs.orglett.7b01543

(52) He, G.; Zhang, S. Y.; Nack, W. A.; Li, Q.; Chen, G. Use of a Readily Removable Auxiliary Group for the Synthesis of Pyrrolidones by the Palladium-Catalyzed Intramolecular Amination of Unactivated γ C(sp^3)–H Bonds. *Angew. Chem. Int. Ed.* **2013**, *52* (42), 11124–11128. DOI: 10.1002/anie.201305615

(53) Ferrer, M.; Roberts, R. S.; Sevilla, S. A Modular Synthesis of Novel 4-amino-7,8-dihydro-1,6-naphthyridin-5(6H)-ones as PDE4 Inhibitors. *Tetrahedron Lett.* **2013**, *54* (36), 4821–4825. DOI: 10.1016/j.tetlet2013.06.016

(54) Xu, Y.; Jing, D.; Chen, R.; Rashid, H. U.; Jiang, J.; Liu, X.; Wang, L.; Xie, P. Design, Synthesis and Evaluation of Novel Sophoridinic Imine Derivatives Containing Conjugated Planar Structure as Potent Anticancer Agents. *Bioorg. Med. Chem.* **2018**, *26* (14), 4136–4144. DOI: 10.1016/j.bmc.2018.07.001

(55) Song, B.; Li, L.-H.; Song, X.-R.; Qiu, Y.-F.; Zhong, M.-J.; Zhou, P.-X.; Liang, Y.-M. Zinc-Catalyzed [4+3] Cycloaddition with Concomitant Furan Annulation: Formation of Cyclohepta[b]Furans. *Chem. Eur. J.* **2014**, *20* (20), 5910–5913. DOI: 10.1002/chem.201402513

(56) Inoshita, T.; Goshi, K.; Morinaga, Y.; Umeda, Y.; Ishikawa, H. Enantioselective Construction of Octahydroquinolines via Trienamine-Mediated Diels-Alder Reactions. *Org. Lett.* **2019**, *21* (8), 2903–2907. DOI: 10.1021/acs.orglett.9b00932

(57) Niphakis, M. J.; Turunen, B. J.; Georg, G. I. Synthesis of 6- and 7-Membered Cyclic Enaminones: Scope and Mechanism. *J. Org. Chem.* **2010**, *75* (20), 6793–6805. DOI: 10.1021/jo100907u

(58) Liu, Y.; Lindsey, J. S. Northern-Southern to Synthetic Bacteriochlorins. *J. Org. Chem.* **2016**, *81* (23), 11882–11897. DOI: 10.1021/acs.joc.6b02334

(59) Murphy, R. A.; Sarpong, R. Heathcock-Inspired Strategies for the Synthesis of Fawcettimine-Type Lycopodium Alkaloids. *Chem. Eur. J.*, **2014**, *20* (1), 42–56. DOI: 10.1002/chem.201303975

(60) Li, H.; Wang, X.; Lei, X. Total Syntheses of Lycopodium Alkaloids (+)-Fawcettimine, (+)-Fawcettidine, and (−)-8-Deoxyserratinine. *Angew. Chem. Int. Ed.* **2011**, *51* (2), 491–495. DOI: 10.1002/anie.201106753.

(61) Dvir, H.; Jiang, H. L.; Wong, D. M.; Harel, M.; Chetrit, M.; He, X. C.; Jin, G. Y.; Yu, G. L.; Tang, X. C.; Silman, I.; Bai, D. L.; Sussman, J. L. X-Ray Structures of *Torpedo Californica* Acetylcholinesterase Complexed with (+)-Huperzine a and (−)-Huperzine B: Structural Evidence for an Active Site Rearrangement. *Biochem.*, **2002**, *41* (35), 10810–10818. DOI: 10.1021/bi020151+

(62) Taylor, R. E.; Galvin, G. M.; Hilfiker, K. A.; Chen, Y. A Formal Total Synthesis of Epothilone A: Enantioselective Preparation of the C1−C6 and C7−C12 Fragments. *J. Org. Chem.*, **1998**, *63* (25), 9580–9583. DOI: 10.1021/jo981461u

(63) Quiñones, R. E.; Glinkerman, C. M.; Zhu, K.; Boger, D. L. Direct Synthesis of β-Aminoenals through Reaction of 1,2,3-Triazine with Secondary Amines. *Org. Lett.*, **2017**, *19* (13), 3568–3571. DOI: 10.1021/acs.orglett.7b01543

(64) He, G.; Zhang, S.; Nack, W. A.; Li, Q.; Chen, G. Use of a Readily Removable Auxiliary Group for the Synthesis of Pyrrolidones by the Palladium-Catalyzed Intramolecular Amination of Unactivated γ C(Sp^3)–H Bonds. *Angew. Chem. Int. Ed.*, **2013**, *52* (42), 11124–11128. DOI: 10.1002/anie.201305615

(65) Song, B.; Li, L.-H.; Song, X.-R.; Qiu, Y.-F.; Zhong, M.-J.; Zhou, P.-X.; Liang, Y.-M. Zinc-Catalyzed [4+3] Cycloaddition with Concomitant Furan Annulation: Formation of Cyclohepta[*B*]Furans. *Chem. Eur. J.*, **2014**, *20* (20), 5910–5913. DOI: 10.1002/chem.201402513

(66) Zhang, Z.; Vitalii Smal; Pascal Retailleau; Arnaud Voituriez; Frison, G.; Angéla Marinetti; Guinchard, X. Tethered Counterion-Directed Catalysis: Merging the Chiral Ion-Pairing and Bifunctional Ligand Strategies in Enantioselective Gold(I) Catalysis. *J. Am. Chem. Soc.*, **2020**, *142* (8), 3797–3805. DOI: 10.1021/jacs.9b11154

(67) Nakajima, Y.; Inoue, T.; Nakai, K.; Mukoyoshi, K.; Hamaguchi, H.; Hatanaka, K.; Sasaki, H.; Tanaka, A.; Takahashi, F.; Kunikawa, S.; Usuda, H.; Moritomo, A.; Higashi, Y.; Inami, M.; Shirakami, S. Synthesis and Evaluation of Novel 1H-Pyrrolo[2,3-b]Pyridine-5-Carboxamide Derivatives as Potent and Orally Efficacious Immunomodulators Targeting JAK3. *Bioorg. Med. Chem.*, **2015**, *23* (15), 4871–4883. DOI: 10.1016/j.bmc.2015.05.034

(68) Benson, H.; Bones, K.; Churchill, G.; Ford, G.; Frodsham, L.; Janbon, S.; Millington, F.; Powell, L.; Raw, S. A.; Reid, J.; Stark, A.; Steven, A. Development of the Convergent, Kilogram-Scale Synthesis of an Antibacterial Clinical Candidate Using Enantioselective Hydrogenation. *Org. Process Res. Dev.*, **2020**, *24* (4), 588–598. DOI: 10.1021/acs.oprd.0c00029

(69) Girlanda-Junges, C.; Keyling-Bilger, F.; Schmitt, G.; Luu, B. Effect of Cyclohexenonic Long Chain Fatty Alcohols on Neurite Outgrowth. Study on Structure-Activity Relationship. *Tetrahedron*, **1998**, *54* (27), 7735–7748. DOI: 10.1016/S0040-4020(98)00406-2

(70) Liu, H.; Jiang, T.; Han, B.; Liang, S.; Zhou, Y. Selective Phenol Hydrogenation to Cyclohexanone over a Dual Supported Pd–Lewis Acid Catalyst. *Science*, **2009**, *326* (5957), 1250–1252. DOI: 10.1126/science.1179713

(71) Chen, Z.; Zeng, H.; Gong, H.; Wang, H.; Li, C. Palladium-Catalyzed Reductive Coupling of Phenols with Anilines and Amines: Efficient Conversion of Phenolic Lignin Model Monomers and Analogues to Cyclohexylamines. *Chem. Sci.*, **2015**, *6* (7), 4174–4178. DOI: 10.1039/c5sc00941c

(72) Qiu, Z.; Li, J.-S.; Li, C. Formal Aromaticity Transfer for Palladium-Catalyzed Coupling between Phenols and Pyrrolidines/Indolines. *Chem. Sci.*, **2017**, *8* (10), 6954–6958. DOI: 10.1039/c7sc02578e

(73) Amolins, M. W.; Peterson, L. B.; Blagg, B. S. J. Synthesis and Evaluation of Electron-Rich Curcumin Analogues. *Bioorg. Med. Chem.*, **2009**, *17* (1), 360–367. DOI: 10.1016/j.bmc.2008.10.057

1.8 Supplemental Figures

Table 1.1: Selected hydrogenation conditions.

H_2 (psi)	Solvent	Time (h)	Catalyst (mol%)	Additives	Results
150	CH_2Cl_2 (1 mL)	4	Pd/C (40)	1 equiv $FeCl_3$	SM
150	CH_2Cl_2 (1 mL)	4	Pd/C (40)	2 equiv $FeCl_3$	SM
150	CH_2Cl_2 (1 mL)	4	Pd/C (40)	1 equiv $FeBr_3$	SM
150	CH_2Cl_2 (1 mL)	4	Pd/C (40)	2 equiv $FeBr_3$	SM
150	CH_2Cl_2 (1 mL)	4	Pd/C (40)	1 equiv $FeCl_3$; 14 equiv TFA	SM
150	CH_2Cl_2 (1 mL)	4	Pd/C (40)	2 equiv $FeCl_3$; 14 equiv TFA	SM
150	CH_2Cl_2 (1 mL)	4	Pd/C (40)	1 equiv $FeBr_3$; 14 equiv TFA	SM
150	CH_2Cl_2 (1 mL)	4	Pd/C (40)	2 equiv $FeBr_3$; 14 equiv TFA	SM
150	CH_2Cl_2 (1 mL)	48	Pd/C (40)	1 equiv $FeCl_3$	SM
150	CH_2Cl_2 (1 mL)	48	Pd/C (40)	2 equiv $FeCl_3$	SM
150	CH_2Cl_2 (1 mL)	48	Pd/C (40)	1 equiv $FeBr_3$	SM
150	CH_2Cl_2 (1 mL)	48	Pd/C (40)	2 equiv $FeBr_3$	SM
150	CH_2Cl_2 (1 mL)	48	Pd/C (40)	1 equiv $FeCl_3$; 14 equiv TFA	SM
150	CH_2Cl_2 (1 mL)	48	Pd/C (40)	2 equiv $FeCl_3$; 14 equiv TFA	SM
150	CH_2Cl_2 (1 mL)	48	Pd/C (40)	1 equiv $FeBr_3$; 14 equiv TFA	SM

150	CH_2Cl_2 (1 mL)	48	Pd/C (40)	2 equiv $FeBr_3$; 14 equiv TFA	SM
150	CH_2Cl_2 (1 mL)	4	Pd/C (40)	-	SM
150	CH_2Cl_2 (1 mL)	4	Pd/C (40)	14 equiv TFA	SM
250	-	4	Pd/C (40)	5 equiv TFA	SM
250	-	4	Pd/C (40)	10 equiv TFA	SM
250	-	4	Pd/C (40)	14 equiv TFA	SM
250	CH_2Cl_2 (1 mL)	4	Pd/C (40)	5 equiv TFA	SM
250	CH_2Cl_2 (1 mL)	4	Pd/C (40)	10 equiv TFA	SM
250	CH_2Cl_2 (1 mL)	4	Pd/C (40)	14 equiv TFA	SM
500	CH_2Cl_2 (0.5 mL)	16	Pd/C (40)	14 equiv TFA	Over hydrogenation
500	CH_2Cl_2 (1 mL)	16	Pd/C (40)	14 equiv TFA	Over hydrogenation
500	CH_2Cl_2 (0.5 mL)	16	Pd/C (40)	14 equiv TFA	Over hydrogenation
500	CH_2Cl_2 (1 mL)	16	Pd/C (40)	14 equiv TFA	Over hydrogenation
500	CH_2Cl_2 (10 mL)	4	Pd/C (40)	5 equiv TFA	SM
500	CH_2Cl_2 (10 mL)	4	Pd/C (40)	10 equiv TFA	SM
500	CH_2Cl_2 (10 mL)	4	Pd/C (40)	14 equiv TFA	SM
500	CH_2Cl_2 (2 mL)	4	Pd/C (40)	5 equiv TFA	SM
500	CH_2Cl_2 (2 mL)	4	Pd/C (40)	10 equiv TFA	SM
500	CH_2Cl_2 (2 mL)	4	Pd/C (40)	14 equiv TFA	SM
500	-	4	Rh/char (40)	14 equiv TFA	SM
500	CH_2Cl_2 (1 mL)	16	Pd/C (20)	14 equiv TFA	SM/desired pdt/over hydrogenation mixture

250	CH_2Cl_2 (2 mL)	16	Pd/C (20)	14 equiv TFA	SM/desired pdt/over hydrogenation mixture
250	CH_2Cl_2 (10 mL)	16	Pd/C (20)	14 equiv TFA	Mostly SM
250	CH_2Cl_2 (1 mL)	16	Pd/C (30)	14 equiv TFA	Mostly over hydrogenation
250	**CH_2Cl_2 (2 mL)**	**16**	**Pd/C (30)**	**14 equiv TFA**	**2:1 desired pdt/over hydrogenation**
250	CH_2Cl_2 (10 mL)	16	Pd/C (30)	14 equiv TFA	1:1 desired pdt/over hydrogenation
250	CH_2Cl_2 (0.5 mL)	16	Pd/C (20)	14 equiv TFA	1:1 desired pdt/over hydrogenation
250	CH_2Cl_2 (1 mL)	4	Pd/C (20)	14 equiv TFA	Mostly SM; trace desired pdt
250	CH_2Cl_2 (2 mL)	4	Pd/C (20)	14 equiv TFA	Mostly SM; trace desired pdt
250	CH_2Cl_2 (0.5 mL)	4	Pd/C (40)	14 equiv TFA	SM
250	CH_2Cl_2 (1 mL)	4	Pd/C (40)	14 equiv TFA	SM
250	CH_2Cl_2 (2 mL)	4	Pd/C (40)	14 equiv TFA	SM
250	CH_2Cl_2 (2 mL)	4	Pd/C (30)	14 equiv TFA	SM
250	CH_2Cl_2 (2 mL)	16	Pd/C (20)	5 equiv TFA	SM
250	CH_2Cl_2 (2 mL)	16	Pd/C (20)	10 equiv TFA	SM
250	CH_2Cl_2 (2 mL)	16	Pd/C (20)	14 equiv TFA	SM
250	CH_2Cl_2 (2 mL)	16	Pd/C (30)	5 equiv TFA	SM
250	CH_2Cl_2 (2 mL)	16	Pd/C (30)	10 equiv TFA	SM
250	CH_2Cl_2 (2 mL)	16	Pd/C (30)	14 equiv TFA	SM

250	CH_2Cl_2 (2 mL)	16	Pd/C (40)	5 equiv TFA	SM
250	CH_2Cl_2 (2 mL)	16	Pd/C (40)	10 equiv TFA	SM
250	CH_2Cl_2 (2 mL)	16	Pd/C (40)	14 equiv TFA	SM
250	H_2O (2 mL)	16	Pd/C (20)	14 equiv TFA	SM
250	H_2O (2 mL)	16	Pd/C (40)	14 equiv TFA	SM
250	CH_2Cl_2 (2 mL)	16	Pd/C (20)	14 equiv HCl	SM
500	CH_2Cl_2 (10 mL)	16	Pd/C (40)	5 equiv TFA	SM
500	CH_2Cl_2 (10 mL)	16	Pd/C (40)	10 equiv TFA	SM
500	CH_2Cl_2 (10 mL)	16	Pd/C (40)	14 equiv TFA	SM
500	CH_2Cl_2 (2 mL)	16	Pd/C (40)	5 equiv TFA	Mostly SM; trace desired pdt
500	CH_2Cl_2 (2 mL)	16	Pd/C (40)	10 equiv TFA	Over hydrogenation
500	CH_2Cl_2 (2 mL)	16	Pd/C (40)	14 equiv TFA	Over hydrogenation
250	CH_2Cl_2 (2 mL)	48	Pd/C (20)	14 equiv TFA	SM
250	MeOH (2 mL)	48	Pd/C (20)	14 equiv TFA	SM
250	H_2O (2 mL)	48	Pd/C (20)	14 equiv TFA	SM
250	Dioxane (2 mL)	48	Pd/C (20)	14 equiv TFA	SM
250	THF (2 mL)	48	Pd/C (20)	14 equiv TFA	SM
250	Phenol (2 mL)	48	Pd/C (20)	14 equiv TFA	SM
250	$CHCl_3$ (2 mL)	48	Pd/C (20)	14 equiv TFA	SM
250	Cyclohexane (2 mL)	48	Pd/C (20)	14 equiv TFA	SM
250	EtOH (2 mL)	48	Pd/C (20)	14 equiv TFA	SM

Chapter 2 – Oxidative C–H Functionalization Towards the Synthesis of Protoberberine Alkaloids as Potential AMPK Inhibitors

2.1 Introduction

2.1.1 Background and Biological Activity

AMP-activated protein kinase (AMPK) earned its name from its function in allosteric activation triggered by AMP binding.[1,2] Since then, it has been predominantly recognized as a cellular energy status sensor, responding to energy stress signals characterized by increasing AMP and/or ADP levels coupled with decreasing ATP levels.[1,2] Alternative to the "canonical" mode of activation, recent attention has increasingly focused on "non-canonical" mechanisms that activate AMPK, such as those independent of AMP/ADP, including nutrient sensing (glucose, glycogen, amino acids, and fatty acids) and activation in response to cellular damage, including damage to lysosomes and nuclear DNA.[1,2] The initial discovery of AMPK dates back to 1973 when Ki-Han Kim at the University of Purdue observed the time-dependent inactivation of a partially purified preparation of acetyl-CoA carboxylase (ACC), a key regulatory enzyme in fatty acid synthesis, upon incubation with ATP.[1,2] Similarly, David Gibson from Indiana University reported analogous findings for 3-hydroxy-3-methylglutaryl-CoA (HMG-CoA) reductase, a key enzyme in isoprenoid synthesis, including cholesterol.[1,2] At that time, glycogen metabolism was the sole physiological process known to be regulated by protein phosphorylation, leading Kim and Gibson to speculate that their observations represented new instances of this phenomenon.[3,4] However, it was assumed that the protein kinases these two groups were investigating were distinct. Kim further reported that ACC kinase

was allosterically activated by AMP, proposing a mechanism to inhibit the energy-intensive pathway of fatty acid synthesis under conditions of limited cellular energy.[3,4] In contrast, Gibson provided evidence that HMG-CoA reductase kinase was itself activated by phosphorylation by an upstream kinase, marking only the second known example of a protein kinase cascade.[4] Finally, in 1987, Grahame Hardie's group correlated the findings and, 14 years after the initial observations, provided evidence that ACC and HMG-CoA reductase kinases were indeed the same entity and changed the name to AMP-activated protein kinase the following year.[4]

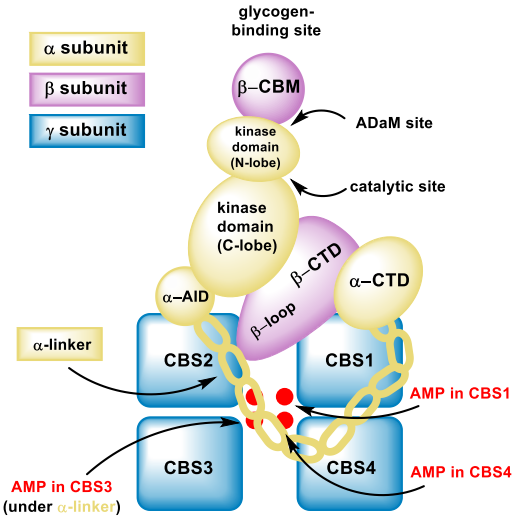

Figure 2.1: Heterotrimeric complex of AMPK.

AMPK exists as a heterotrimeric complex comprising one catalytic α-subunit and two regulatory β- and γ-subunits.[5,6] AMPK can consist of two isoforms each of α- and β-subunits, and three isoforms of the γ-subunit.[5,6] There are 12 distinct combinations of AMPK complexes in mammals, varying depending on tissue type, cell type, regulation mechanism, and biochemical properties.[5,6] The α-subunit encompasses the *N*-terminal kinase domain (KD) and a C-terminal region that binds the β and γ subunits, housing

crucial regulatory domains.[5,6] The β-subunit contains two conserved glycogen-binding domains (GBM) involved in glycogen sensing, along with a C-terminal domain that binds the α and γ subunits. Additionally, the β-subunit features a site at its *N*-terminus that facilitates AMPK's targeting to cellular membranes. The γ subunit comprises two Bateman domains conserved across species, each containing two cystathionine β-synthase repeats (CBS).[5,6] These four CBS repeats serve as distinct, universal adenine nucleotide binding sites, competitively binding AMP, ADP, or ATP.[6]

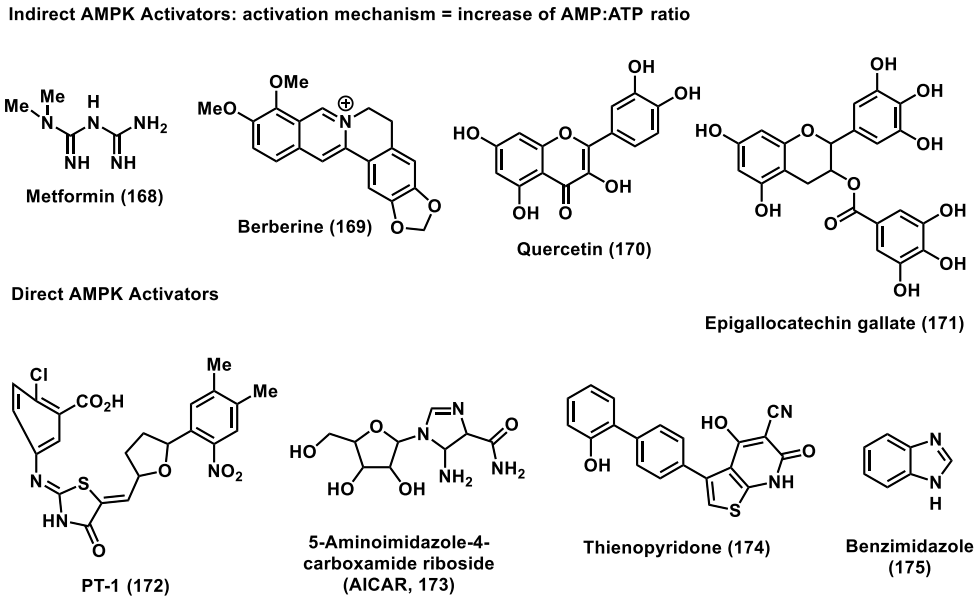

Figure 2.2: Selected examples of indirect and direct AMPK activators.

2.1.2 AMPK Modulators

Numerous pharmacological compounds have been identified that either indirectly enhance AMPK activity or bind to it directly, with some undergoing clinical trials or approved for use (Figure 2.1).[7] While initial attempts to pinpoint direct AMPK activators focused on compounds simulating nucleotide-dependent activation, the specifics of nucleotide binding sites remained elusive.[7] The first such activator discovered was 5-

aminoimidazole-4-carboxamide ribonucleotide (ZMP), a monophosphate derivative of the cell-permeable precursor AICAR.[7] This breakthrough popularized the use of AICAR as a pharmacological tool for exploring AMPK activation effects in cells.[7] Additionally, methotrexate can elevate ZMP levels by inhibiting the folate-dependent enzyme AICA ribotide transformylase/IMP cyclohydrolase (ATIC), which converts ZMP to IMP.[7] However, approaches aimed at increasing ZMP may inadvertently affect other AMP-sensitive enzymes, such as fructose 1,6-bisphosphatase and glycogen phosphorylase. It's now clear that some effects of AICAR on metabolic pathways are AMPK-independent, cautioning against solely relying on AICAR to demonstrate AMPK involvement in a specific pathway.[7]

In contrast, indirect modulators have gained more popularity for activating AMPK by elevating the AMP/ADP:ATP ratio through various mechanisms.[7] For instance, metformin (**168**), a widely used oral anti-diabetic agent, inhibits complex I (NADH:ubiquinone oxidoreductase) in mitochondria, thus reducing mitochondrial respiration and ATP production, ultimately activating AMPK. Metformin-induced AMPK activation hinges on uptake from circulation by organic cation transporters, whose activity crucially determines therapeutic effects across individuals.[7] These transporters are predominantly expressed in the liver, where activation necessitates the upstream kinase LKB1.[7] Conversely, the closely related and lipophilic biguanide phenformin possesses a greater capacity to enter cells and activate AMPK beyond hepatocytes, although its withdrawal from most countries ensued due to an elevated risk of lactic acidosis.[7] To augment AMPK activation outside the liver, various groups have endeavored to develop

metformin-like complex I inhibitors, such as R419.[7] Moreover, several plant-derived natural products commonly used in traditional herbal medicine indirectly activate AMPK by inhibiting mitochondrial respiration.[7,8] For instance, berberine (**169**), a quaternary ammonium salt from the protoberberine group of isoquinoline alkaloids, exhibits potent antibiotic, anti-inflammatory, and antioxidant activities.[8] It also heightens cancer cell sensitivity to antitumor reagents and mitigates hyperglycemia-induced human endothelial injury by enhancing AMPK activation.[8] Evident of these previous examples, AMPK activators have been thoroughly studied aligned with significant efforts to further develop them, but their counterparts remain underexplored.[8]

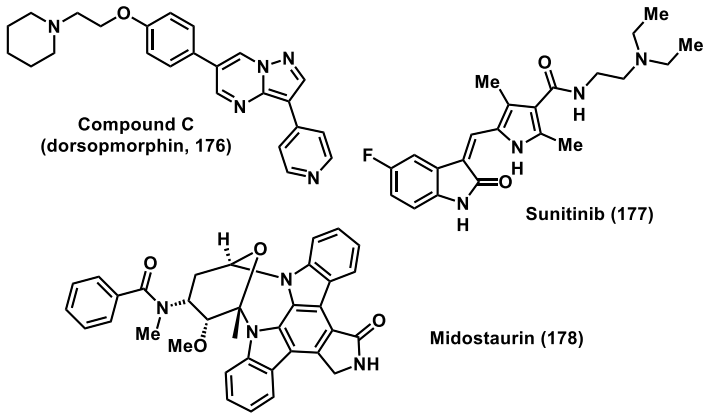

Figure 2.3: Structures of known AMPK inhibitors.

While genetic studies on AMPK's role in mouse cancer indicate its function as a tumor suppressor, protecting against cancer initiation, evidence suggests that it transitions into a tumor promoter once cancer is established.[9-13] As pinpointing the exact onset of cancer is challenging, AMPK activators may inadvertently facilitate tumor growth by shielding against metabolic, oxidative, and genotoxic stress.[9-13] The comprehension of this phenomenon has been hindered by the scarcity of well-characterized and specific AMPK

inhibitors, raising concerns regarding undiscovered processes in cancer studies and their potential impact on biological functions.[9-13] Over the past two decades, only three competitive inhibitors of 5'-AMP-activated protein kinase have been identified (Figure 2.2): dorsomorphin (compound C, **176**), sunitinib (**177**), and midostaurin (**178**).[9-13] However, these inhibitors exhibit limited structural similarity, posing challenges in accessing a diverse range of compounds for further investigation.[9-13] To address this limitation, we drew inspiration from berberine and its extensive natural product family of isoquinoline alkaloids. Given the bioactivity of its metabolic intermediates, there may be potential AMPK modulation properties within berberine's biosynthetic protoberberine precursors.[9-13] Based on initial findings, we anticipate that some derivatives could serve as AMPK inhibitors, aiding in a deeper understanding of their physiological processes.

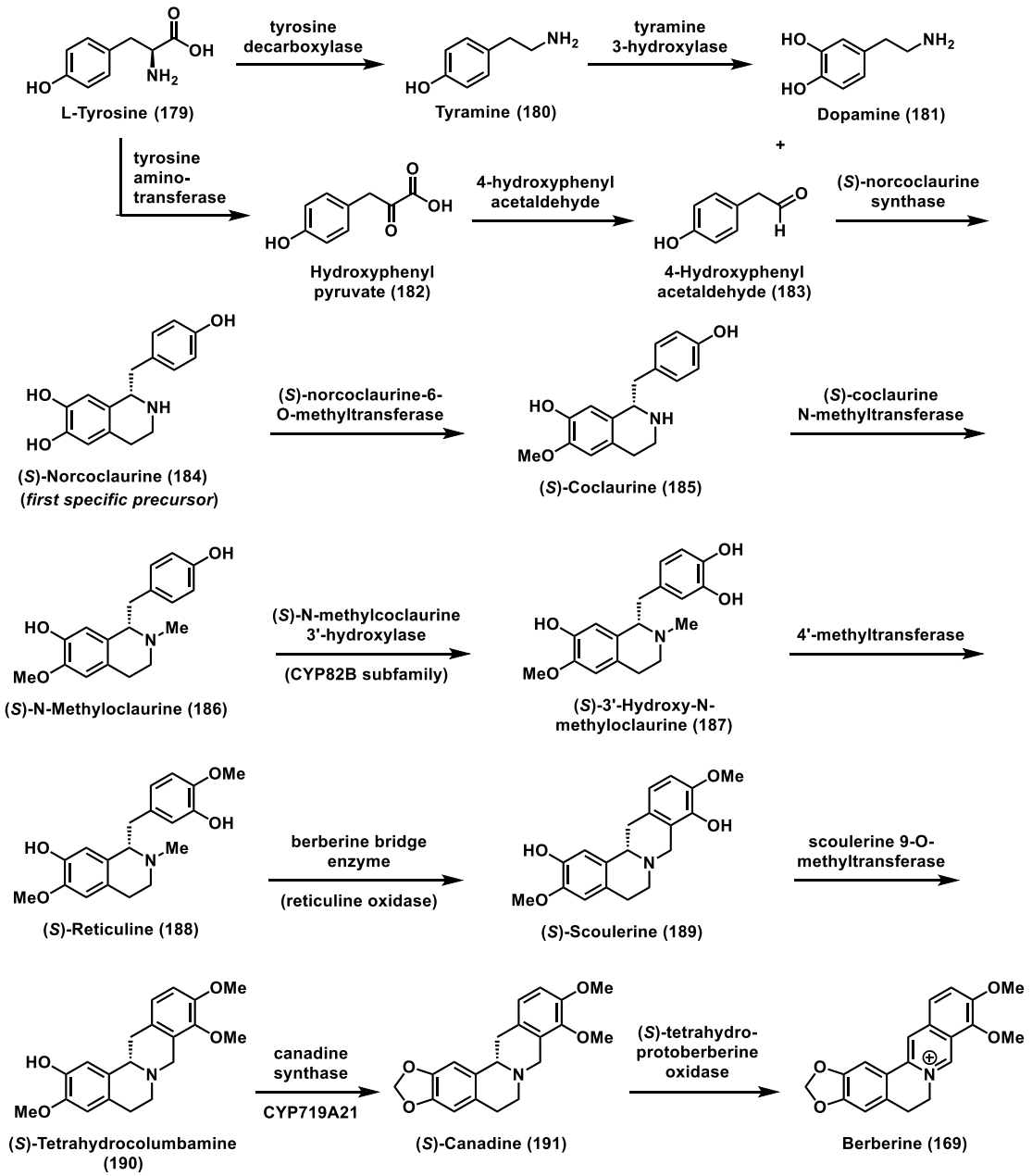

Scheme 2.1: Biosynthesis of berberine.

2.1.3 Biosynthesis

Microbial manufacturing is emerging as an attractive and environmentally friendly method for producing natural products. Recent studies have focused on enhancing the microbial production of berberine and its derivatives, yielding promising results.[14-20] Han

and Li conducted a study engineering 19 genes, including 12 heterologous ones from plants and bacteria, to achieve complete berberine biosynthesis in Saccharomyces cerevisiae.[14-20] Through this approach, they achieved a remarkable 643-fold increase in berberine titer to 1.08 mg/L by overexpressing bottleneck enzymes, scaling up fermentation, and applying post-fermentation heat treatment to strengthen the berberine supply chain.[14-20] Another strategy to enhance the production of valuable bioactive compounds like berberine involves manipulating genes encoding plant enzymes through metabolic engineering. Huang et al. modulated genes encoding the berberine bridge enzyme (BBE) to increase berberine production in the plant *Macleaya cordata*.[25] The BBE enzyme is pivotal in closing a saturated ring in the intermediates of berberine biosynthesis, specifically converting (*S*)-reticuline (**188**) to (*S*)-secoulerine (**189**).[25] Since the hydrocarbon backbone of berberine and other protoberberines is established at this stage, scientists have identified the gene encoding BBE as a critical target for metabolic engineering efforts.[25]

Additionally, berberine can be naturally sourced from various plants such as *Berberis vulgaris*, which produce significant amounts of this compound as a metabolite.[25] The synthesis of berberine begins with (*S*)-norcoclaurine (**184**), a primary precursor synthesized by the enzyme (*S*)-norcoclaurine synthase from dopamine and 4-hydroxyphenylacetaldehyde.[25] (*S*)-Norcoclaurine undergoes a series of methylation, hydroxylation, and methylation steps to transform into intermediate **188**.[25] The conversion of (*S*)-reticuline to (*S*)-secoulerine is a critical step in berberine biosynthesis, facilitated by the berberine bridge enzyme (BBE), which closes a saturated ring in the reticuline structure.[25] Subsequent steps involve the conversion of **189** to (*S*)-tetrahydrocolumbamine

(**190**) and (*S*)-canadine (**191**) catalyzed by enzymes scoulerine 9-O-methyltransferase and canadine synthase CYP719A21, respectively.[25] This updated biomimetic inspiration has led to numerous successful syntheses of berberine and its protoberberine precursors.[25]

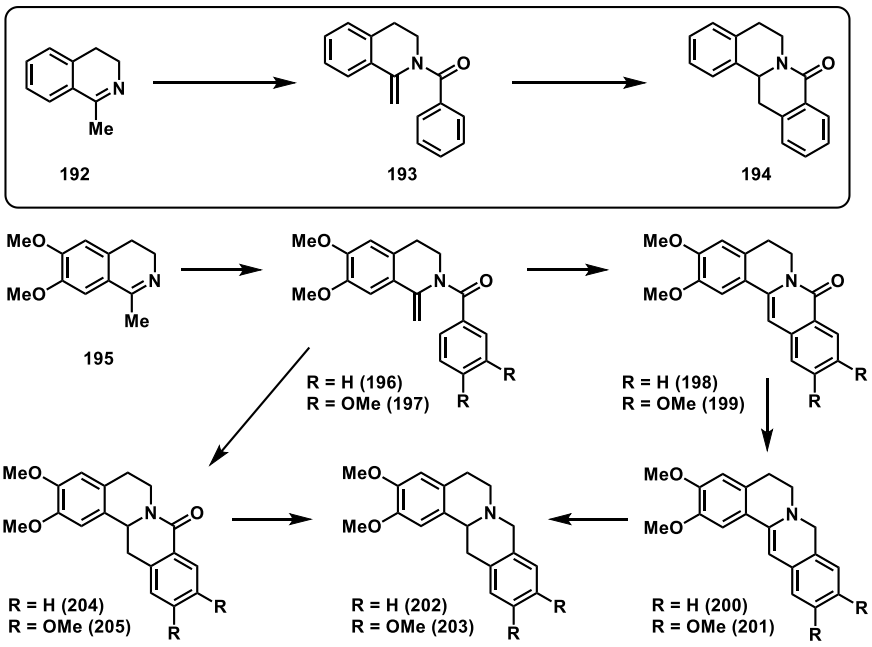

Scheme 2.2: Synthesis of protoberberine type alkaloids from 1973 by Ninomiya and Naito.

2.1.4 Previous Syntheses

One of the earliest documented attempts at synthesizing isoquinoline alkaloids dates back to Ninomiya and Naito in 1973 (Scheme 2.2), who aimed at producing xylopinine (**203**).[26] Their approach involved *N*-benzoylation of 1-methyl-3,4-dihydroisoquinoline (**192**), followed by low-pressure mercury lamp irradiation.[26] While this method yielded cyclized photoproduct **194** in a 70% yield, attempts with dimethoxy *N*-benzamide derivatives initially led to unstable intermediates **196** and **197** that were only isolated at 5% yield.[26] Instead of revisiting the synthesis, Ninomiya and Naito decided to push forward and examine the stability of the cyclized products (**198, 199, 204, 205**). When

the tetracyclic skeleton was built, they were able to finalize the synthesis through full reduction of lactam moiety over two steps–a method still utilized in modern protoberberine syntheses.[26]

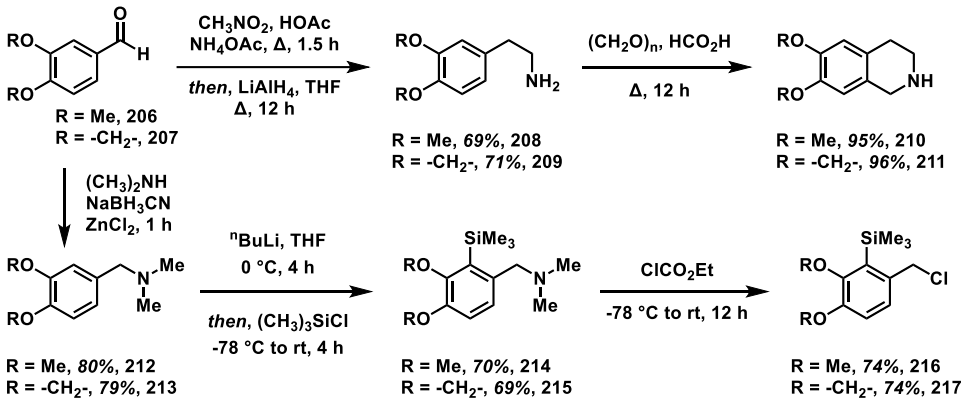

Scheme 2.3: Synthesis of precursors towards protoberberines.

Three decades later, Schore and colleagues embarked on constructing five different naturally occurring protoberberines in enantioenriched form through alkylation.[27] They utilized two different 2-trimethylsilylbenzyl chlorides (**216** and **217**) of four tetrahydroisoquinolines derivatized from Meyers' formamidine valinol methyl ether chiral auxiliary (Scheme 2.3).[27] The process began with a nitrostyrene reduction of **206** and **207** to 3,4-dialkoxyphenylethylamines **208** and **209**, followed by Pictet–Spengler cyclization to yield tetrahydroisoquinolines **210** and **211**.[27] The alkylating agents were formed from benzaldehydes through a series of reactions starting from the same benzaldehydes (**206** and **207**), ultimately leading to substituted benzyl chlorides **216** and **217** that were used for the enantioselective alkylation of tetrahydroisoquinolines.[27] This method resulted in predominantly natural protoberberine precursors and eventually was used successfully in

the synthesis of THIQ alkaloids (*S*)-(–)-tetrahydropalmatine (**225**), (*S*)-(–)-canadine (**191**), and (*S*)-(–)-sinactine (**229**) (Scheme 2.4).[27]

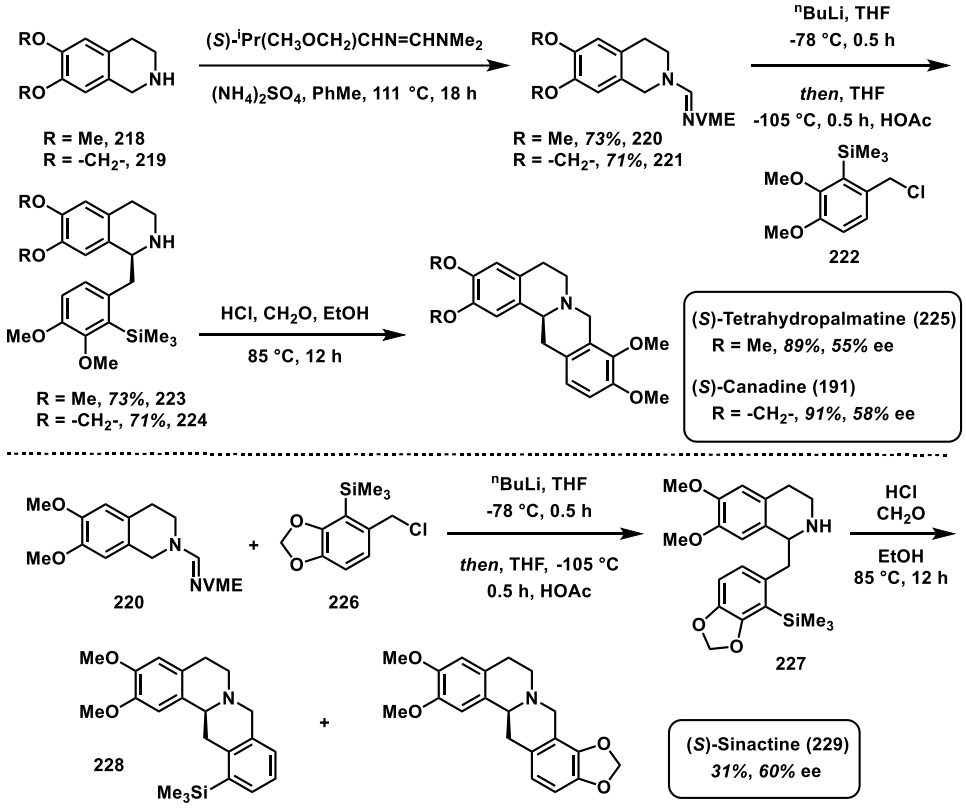

Scheme 2.4: Late-stage syntheses of Tetrahydropalmatine, Canadine, and Sinactine.

In 2014, Donohoe and colleagues achieved the synthesis of berberine hydrochloride in just five steps, with a versatile palladium-catalyzed enolate arylation as the key step (Scheme 2.5).[28] This approach enabled analogous syntheses of pseudocoptisine (**239**), tetrahydropseudocoptisine (**240**), dehydrocorydaline (**246**), palmatine (**247**), and an unnatural fluorinated analogue (**248**).[28] The synthesis towards these derivatives commenced with preparation of aryl bromide **232** and coupling partner **233**, followed by regioselective Friedel–Crafts acylation and α-arylation to **234**.[28] The desired isoquinoline intermediate **235** prior to berberine was constructed by hydrolysis of the acetal in **234** and

aromatization, ultimately yielding berberine chloride (**169**).[28] As they overlooked the overall approach, the two step process was converted to a one-pot coupling method for cyclization in 40% yield from the same starting materials **232** and **233**.

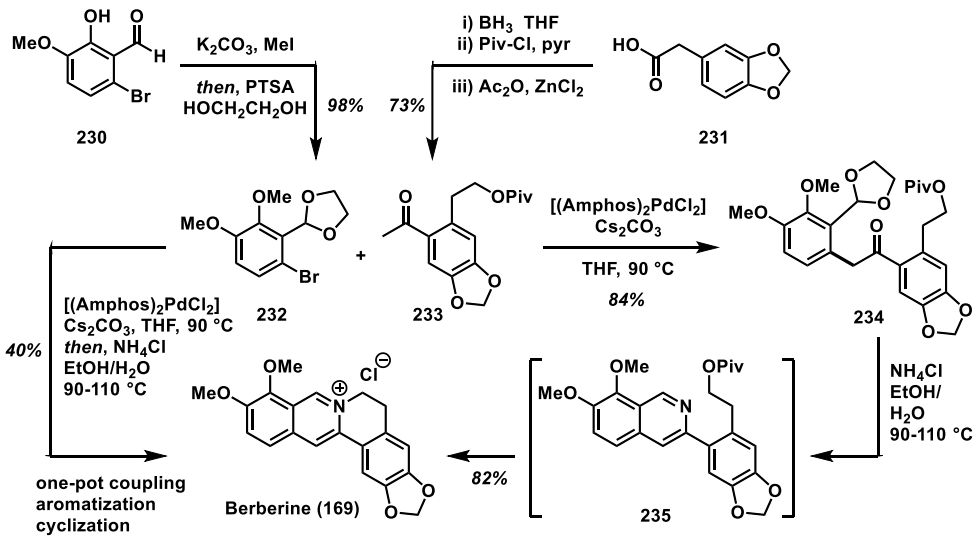

Scheme 2.5: Synthesis of Berberine chloride.

The derivatization of precursors to **236** and **237** allowed access to pseudocoptisine (**239**) after the cyclization step and tetrahydropseudocoptisine (**240**) upon reduction of the iminium salt (Scheme 2.6). The synthesis of alkaloids **246**, **247**, and **248** followed shortly after (Scheme 2.7).[28] Their first target, dehydrocorydaline (**246**), was constructed through a sequence of reactions after cyclization to isoquinoline **245** that began with a DIBAL-H reduction and finished with an *in situ* substitution upon chlorinating the pivalic protected alcohol.

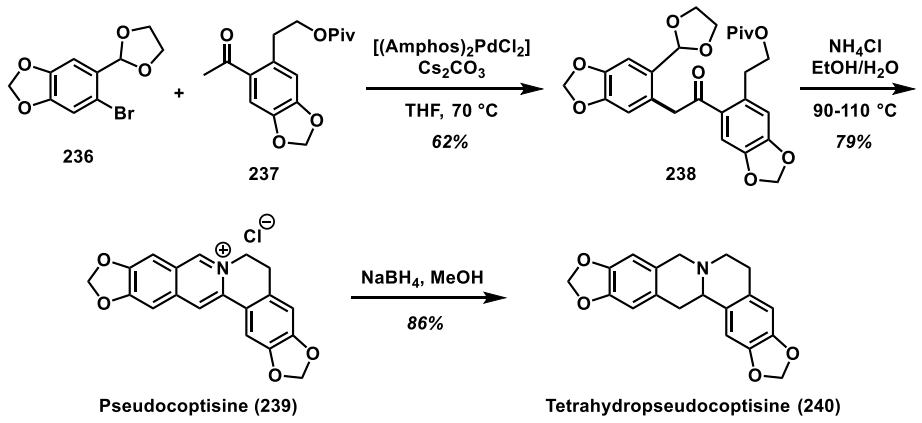

Scheme 2.6: Synthesis of Tetrahydropseudocoptisine.

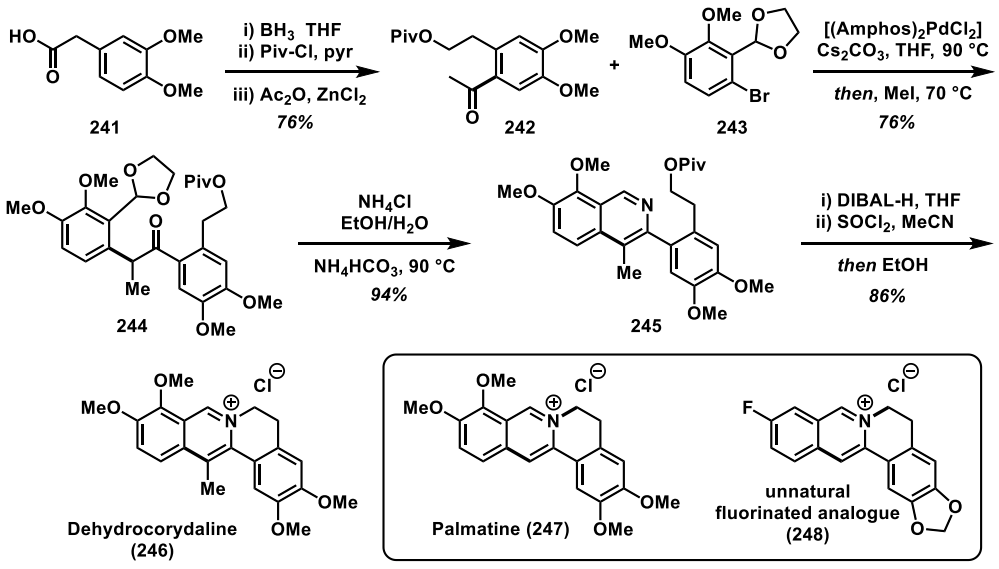

Scheme 2.7: Donohoe synthesis of Dehydrocorydaline, Palmatine, and fluorinated analogue.

More recently, Konno and colleagues synthesized berberine analogues through an intramolecular Heck reaction (Scheme 2.8).[29] The synthesis started off with a Jones oxidation of aldehyde **249** to carboxylic acid **250**. This was converted to an acyl chloride and substituted by an aminoacetal to arrive at **251**. Treated with acid, the acetal was cleaved and induced cyclization into isoquinolone **252**. Convergently, alkyl bromide **253** was formed through a series of transformations from aldehyde **254** and was used to perform the

N-alkylation of **252**.[29] The resulting tethered aryl bromide **257** was the key intermediate that set the stage for an intramolecular Heck reaction. This cross-coupling was facilitated by $Pd(OAc)_2$, DIPEA, and PPh_3, followed by consecutive reduction and aromatization to yield berberine (**169**).[29] Derivatization was achieved through deprotection, deacetylation, full reduction to the quinolizidine, or a combination thereof (Scheme 2.9).[29] While protoberberines have been studied for decades, recent focus on their anti-tumor and AMPK activation properties has led to the synthesis of specific analogues.[29] However, their complete bioactivity and availability are yet to be fully elucidated, highlighting the need for further research and the production of promising AMPK inhibiting counterparts.[29]

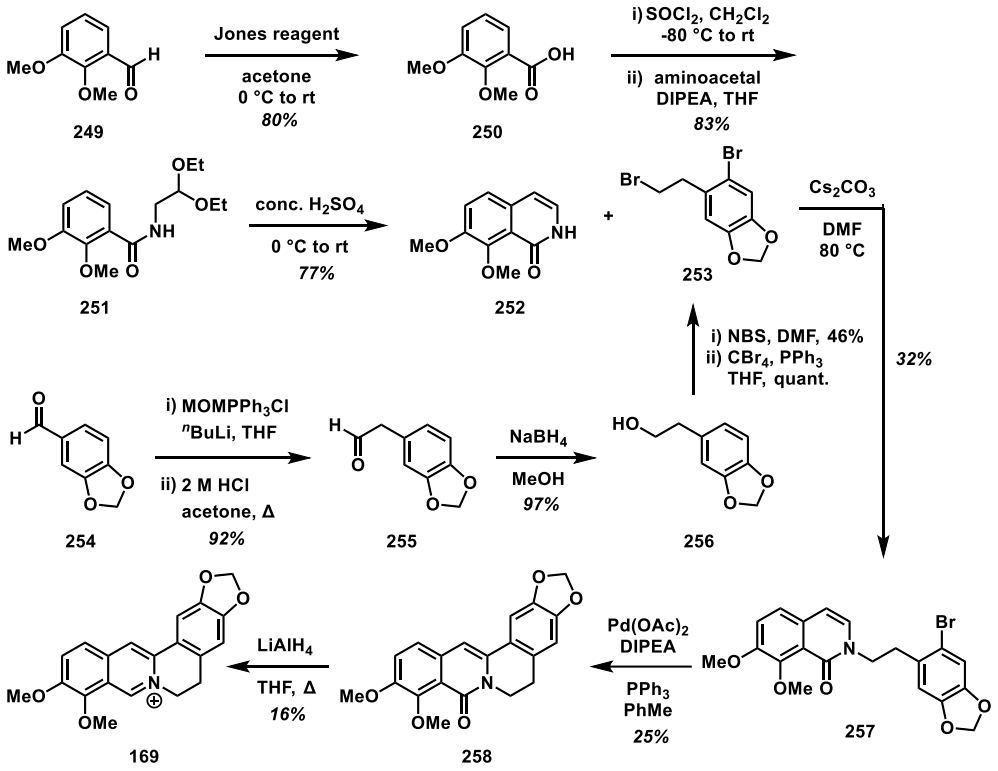

Scheme 2.8: Konno synthesis of berberine analogues *via* intramolecular Heck reaction.

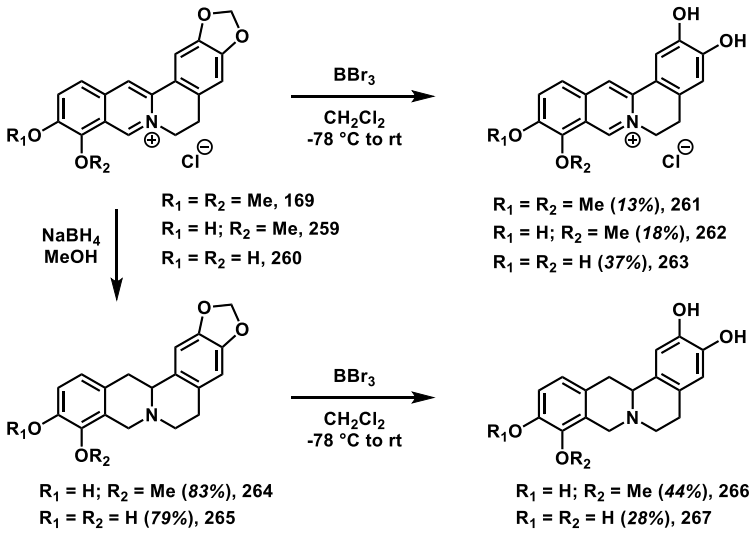

Scheme 2.9: Continued synthesis of Berberine analogues by Konno and co-workers.

2.1.5 Retrosynthetic Proposal

Building upon our previous research on α-arylation in our laboratory, our objective was to devise a versatile approach for synthesizing both natural and synthetic derivatives of protoberberine, focusing on this pivotal reaction. Starting from 2,3-dimethoxyberbine (**203**), we aimed to construct the core tetracyclic framework through the cyclization and reduction of the isoquinolone moiety. Introduction of the vinyl group in **268** was planned *via* a Suzuki C–C cross-coupling reaction involving a vinyl boroxine pyridine complex and aryl bromide **269**. In the final transform illustrated, the aryl bromide served as the primary intermediate resulting from the C–H functionalization of *N*-methoxybenzamide (**271**) with dimethoxy phenyl silyl enol ether **270**. These two building blocks were synthesized efficiently with high yields and could be further modified as needed. We anticipated challenges in modifying the *N*-methoxybenzamide due to steric hindrance at one of the two available ortho positions, where C–H activation occurs. To address this potential issue, we

explored the possibility of late-stage functionalization as an alternative strategy. Additionally, the delicate nature of these isoquinoline alkaloids posed difficulties during isolation, leading to varying yields ranging from low to moderate in several instances due to the need for multiple purification steps for a single experiment.

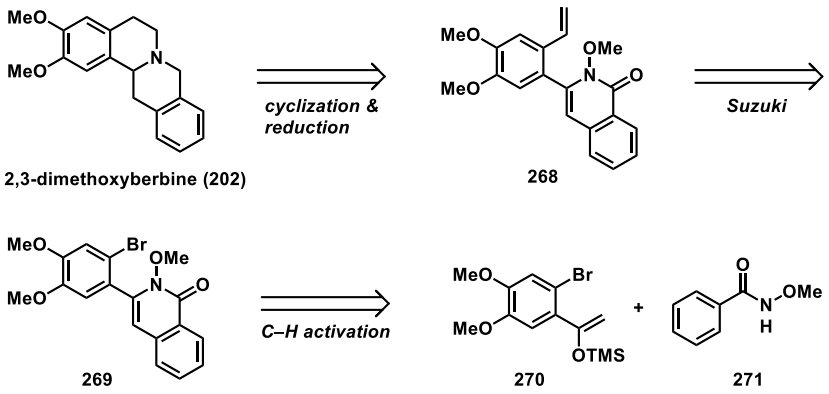

Scheme 2.10: Retrosynthetic analysis of 2,3-dimethoxyberberine.

2.2 Results and Discussion

2.2.1 Synthetic Approaches

We initiated our synthetic approach with construction of the silyl enol ether coupling partner. This process commenced with bromination of 3,4-dimethoxybenzaldehyde (**272**) using Br_2 in MeOH, resulting in 6-bromovertraldehyde (**273**), and was followed by a Grignard addition into the aldehyde handle to give secondary alcohol **274** in 98% yield. Subsequent steps involved a Swern oxidation of the alcohol **274** to yield phenyl ketone **275**, which was silylated under basic conditions to **270** in 89% yield. Alternatively, various *N*-methoxybenzamides were synthesized for the α-arylation step, typically through the conversion of the corresponding carboxylic acid into an acyl chloride, followed by a nucleophilic addition from O-methylhydroxylamine hydrochloride.

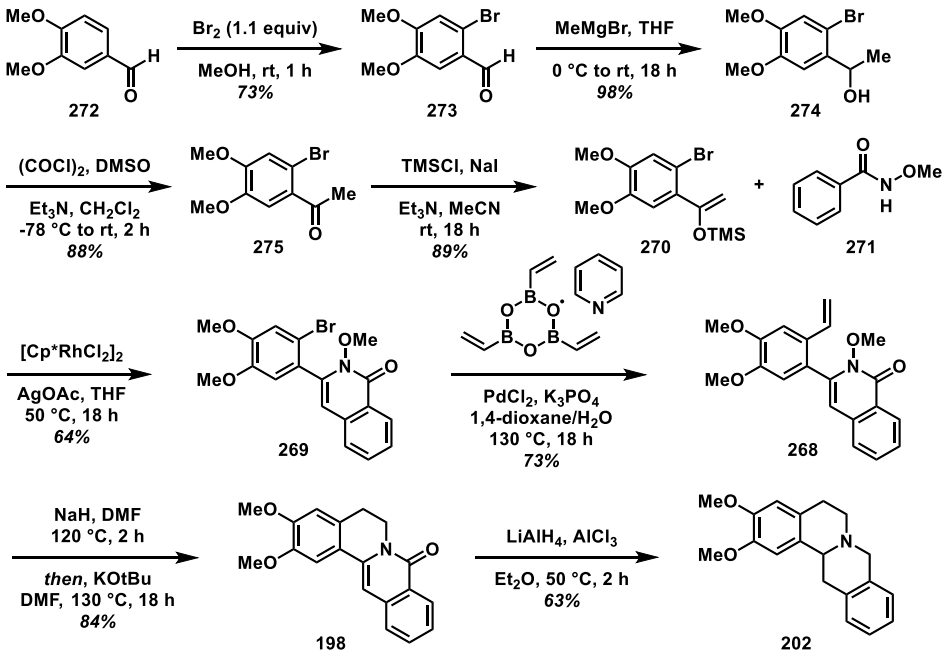

Scheme 2.11: Forward synthesis towards 2,3-dimethoxyberberine.

Additionally, a Suzuki cross-coupling with trivinylboroxin pyridine complex was performed on the unsubstituted N-methoxybenzamide, resulting in terminal alkene **268** in 73% yield (Scheme 2.11). This step initially yielded poor results, hypothesized to be due to the addition of water, which poisoned the catalyst. However, further investigation revealed that a higher water content in the solvent mixture was necessary, using a 1:1 mixture of 1,4-dioxane/H2O. Furthermore, optimizing the catalyst to $PdCl_2$ in correspondence with K_3PO_4 proved to be more favorable. Difficulty in separating the substrate and product led to subjecting the crude material to the same conditions again if conversion was incomplete. After thorough purification, an anionic 6π-electrocyclization provided access to the desired tetracyclic isoquinoline framework (**198**). Despite the challenges of the full reduction due to its sensitivity to air, adjusting temperature and time

while minimizing exposure to air led to the successful synthesis of 2,3-dimethoxyberbine (**202**) with a 63% yield.

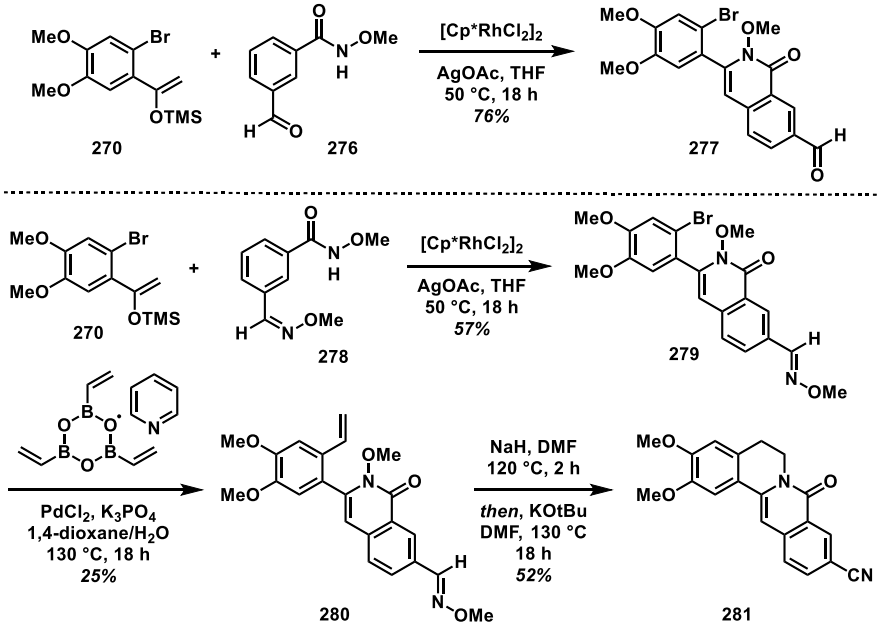

Scheme 2.12: Construction of cyanoisoquinolone.

From the three different *N*-methoxybenzamides, the α-arylated product substituted with an aldehyde (**277**) did not yield satisfactory results under any Suzuki conditions. The majority of the crude material comprised starting material, with only a minimal 5% yield of an unidentified side product, prompting a reassessment of our strategy. It is likely that the exposed aldehyde hindered the desired outcomes; thus, we opted to protect it by converting it to the oxime during the amidation step. Utilizing an excess of O-methylhydroxylamine salt, we obtained oxime (**278**) in a yield of 92%, which also exhibited better behavior during the C–H functionalization step (**279**). This modification resulted in a 25% yield of the desired vinylated oxime derivative **280** (Scheme 2.12).

Subsequently, the exchange underwent a one-pot cyclization/oxidation process, transforming the oxime into nitrile **281** with a moderate yield of 52%.

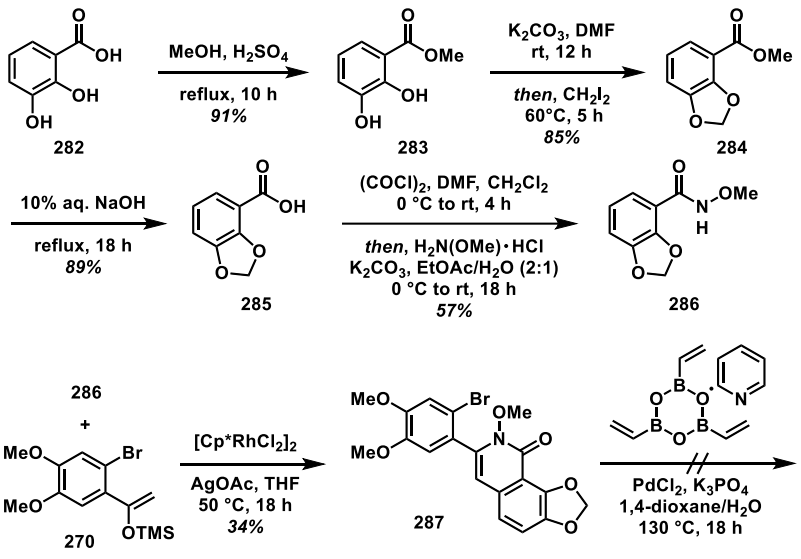

Scheme 2.13: Synthesis of dioxolane derivative.

Several attempts were made to introduce a 2,3-dioxolane group onto the benzamide starting material to investigate the steric effects during α-arylation (Scheme 2.13). For this purpose, 2,3-dihydroxybenzoic acid (**282**) underwent esterification with methanol and sulfuric acid, followed by treatment of benzoate **283** with diiodomethane and base to form dioxolane **284**. Subsequently, the benzoate was hydrolyzed back to carboxylic acid **285** and converted to the respective benzamide (**286**). Coupled with silyl enol ether **270**, the C–H functionalization of the dioxole derivative was achieved in about 34% yield (**287**), but no significant results were observed when treated under Suzuki cross-coupling conditions.

2.3 Conclusion and Future Direction

As the first key reaction of this synthetic approach, the mechanism of the oxidative C–H activation step has been further elucidated from previously reported work. Upon

recrystallization, these benzamides are bound to rhodium and form complex **A** facilitated by acetate ligands and generate acetic acid molecules responsible for activating the electron-rich silyl enol ether later in the process (Scheme 2.14). This is followed by C–H activation ortho to the directing group through concerted-metalation-deprotonation (CMD), which is the rate-limiting step. The enolate formed upon introduction of the silyl enol ether in complex **B** displaces nitrogen from the metal center and results in complex **C**. A single oxidation with AgOAc was then suspected to provide a favorable reductive elimination between the aromatic ring and α-keto position in complex **D**. Extrusion of the reactive intermediate **F** under heat and acidic conditions triggered the benzamide nitrogen to add into the reactive ketone to form a hemiaminal. This was followed by elimination upon workup, yielding desired α-arylated products.

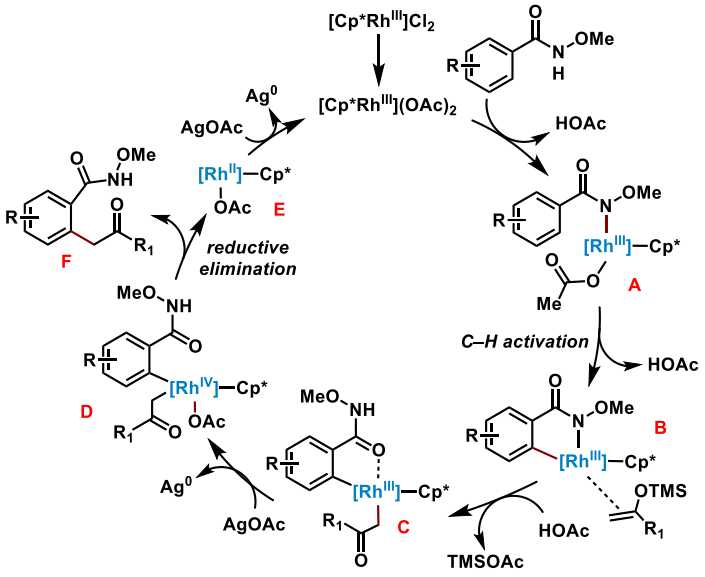

Scheme 2.14: Proposed mechanism of C–H functionalization.

The synthesis of protoberberine natural products represents a pivotal area of research that has seen significant advancements in recent years. With a focus on elucidating

the mechanistic intricacies of the anionic 6π-electrocyclization, we intend to shed light on the fundamental principles governing these reactions. Moreover, the exploration of oxoberberine alkaloid derivatives has emerged as a promising avenue for further investigation, inspired by the potential of these compounds as AMPK inhibitors. This endeavor not only expands our understanding of the biological significance of these compounds but also holds great promise for the development of new therapeutic agents targeting AMPK-related pathways. By combining insights from mechanistic studies with biological assays, we can accelerate the discovery of new derivatives with improved potency and selectivity, ultimately paving the way for the development of novel therapeutics for a range of diseases.

2.4 Experimental

2.4.1 General Information

2.4.1.1 Solvents and Reagents

Commercial reagents were purchased from MilliporeSigma, Acros Organics, Chem-Impex, TCI, Oakwood, and Alfa Aesar, and used without additional purification. Solvents were purchased from Fisher Scientific, Acros Organics, Alfa Aesar, and Sigma Aldrich. Tetrahydrofuran (THF), diethyl ether (Et_2O), acetonitrile (MeCN), dichloromethane (CH_2Cl_2), benzene, 1,4-dioxane, and triethylamine (Et_3N) were sparged with argon and dried by passing through alumina columns using argon in a Glass Contour (Pure Process Technology) solvent purification system. Dimethylformamide (DMF), dimethyl sulfoxide (DMSO), and dichloroethane (DCE) were purchased in Sure/Seal or

AcroSeal bottling and dispensed under N_2. Deuterated solvents were obtained from Cambridge Isotope Laboratories, Inc. or MilliporeSigma.

2.4.1.2 Reaction setup, progress monitoring, and product purification

In general, the catalytic reactions are not air- or moisture-sensitive; however, the iron and zinc salts are hygroscopic and quickly change color when being weighed and added to the reaction vessel. This influences how much metal catalyst is being added because their molecular weights increase on hydration. For consistency and rigor, the iron and zinc salts were weighed and added to vials inside a nitrogen-filled glovebox. All other reagents, including the solvent, were added outside the glovebox under open air. Reaction progresses were monitored using thin-layer chromatography (TLC) on EMD Silica Gel 60 F254 or Macherey–Nagel SIL HD (60 Å mean pore size, 0.75 mL/g specific pore volume, 5–17 μm particle size, with fluorescent indicator) silica gel plates. Visualization of the developed plates was performed under UV light (254 nm). Purification and isolation of products were performed via silica gel chromatography (both column and preparative thin-layer chromatography). Organic solutions were concentrated under reduced pressure on IKA® temperature-controlled rotary evaporator equipped with an ethylene glycol/water condenser.

2.4.1.3 Analytical instrumentation

Melting points were measured with the MEL-TEMP melting point apparatus. Proton nuclear magnetic resonance (^{1}H NMR) spectra, carbon nuclear magnetic resonance (^{13}C NMR) spectra and fluorine nuclear magnetic resonance (^{19}F NMR) spectra were recorded on Bruker Avance NEO 400 (not ^{1}H decoupled) or Bruker Avance 600 MHz

spectrometers (^{1}H decoupled). Chemical shifts (δ) are reported in ppm relative to the residual solvent signal (δ 7.26 for ^{1}H NMR, δ 77.16 for ^{13}C NMR in $CDCl_3$).[1] Data for ^{1}H NMR spectroscopy are reported as follows: chemical shift (δ ppm), multiplicity (s = singlet, d = doublet, t = triplet, q = quartet, m = multiplet, br = broad, dd = doublet of doublets, dt = doublet of triplets), coupling constant (Hz), integration. Data for ^{13}C and ^{19}F NMR spectroscopy are reported in terms of chemical shift (δ ppm). IR spectroscopic data were recorded on a NICOLET 6700 FT-IR spectrophotometer using a diamond attenuated total reflectance (ATR) accessory. Samples are loaded onto the diamond surface either neat or as a solution in organic solvent and the data acquired after the solvent had evaporated. High resolution accurate mass (ESI) spectral data were obtained from the Analytical Chemistry Instrumentation Facility at the University of California, Riverside, on an Agilent 6545 Q-TOF LC/MS instrument (supported by NSF grant CHE-1828782).

2.5 Experimental Procedures and Characterization Data

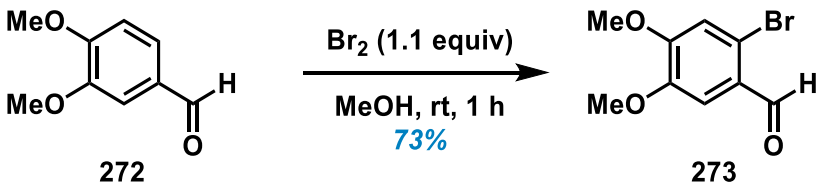

2-Bromo-4,5-dimethoxybenzaldehyde (273).[30] Br_2 (8.6 mL, 166 mmol, 1.1 equiv) was added slowly to a stirring solution of 3,4-dimethoxy benzaldehyde (25.0 g, 150 mmol, 1.0 equiv) in MeOH (250 mL, 0.60 M) over the course of 30 min, and then stirred at rt for 1 h. The reaction mixture was concentrated *in vacuo* and then filtered through a fritted funnel. The solids were washed with cold water and ether, affording the title compound as a white solid (26.7 g, 73%). ^{1}H NMR (500 MHz, $CDCl_3$) δ 10.19 (s, 1H), 7.41 (s, 1H), 7.06 (s,

1H), 3.96 (s, 3H), 3.92 (s, 3H). All other spectroscopic data are in accord with previously reported literature.

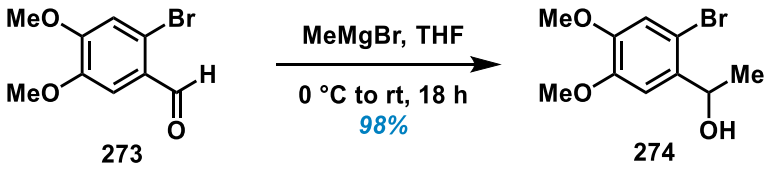

1-(2-Bromo-4,5-dimethoxyphenyl)ethan-1-ol (274).[31] As a modified procedure to Wang and coworkers, MeMgBr (8.8 mL, 26.1 mmol, 3 M) was added dropwise to a stirring solution of aldehyde **273** (5.34 g, 21.8 mmol) in THF (63 mL, .35 M) at 0 °C. The reaction was stirred at 0 °C for 30 min before warming to rt and stirring for 18 h. The reaction mixture was then quenched with sat. aq. NH_4Cl (15 mL) and the organic layer was separated. The aqueous phase was extracted with EtOAc (3 × 20 mL) and the combined organic layers washed with brine (3 × 10 mL), dried over anhydrous Na_2SO_4, filtered, and concentrated *in vacuo*. Purification by silica gel flash column chromatography (eluting with 0-30% EtOAc/hex). The product was isolated as a colorless oil (5.57 g, 98%). R_f = 0.23 (30% EtOAc/hex). ^{1}H NMR (500 MHz, $CDCl_3$) δ 7.10 (s, 1H), 6.96 (s, 1H), 5.17 (q, J = 6.4 Hz, 1H), 3.89 (s, 3H), 1.45 (d, J = 6.4 Hz, 3H). All other spectroscopic data are in accord with previously reported literature.

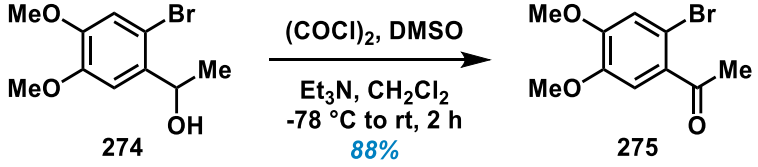

1-(2-Bromo-4,5-dimethoxyphenyl)ethan-1-one (275). DMSO (4.7 mL, 65.4 mmol) was added to a stirring solution of oxalyl chloride (2.8 mL, 32.7 mmol) in CH_2Cl_2 (100 mL) at -78 °C. The resulting mixture was stirred for 5 min before using the remaining amount of CH_2Cl_2 (120 mL) to add alcohol **274** (5.69 g, 21.8 mmol) dropwise over 10 min at -78 °C. The solution was stirred for 35 min for a total of approximately 40 min before adding Et_3N (15.2 mL, 109 mmol) dropwise at -78 °C. The reaction mixture was warmed to rt and then stirred for 30 min, which was then quenched with sat. aq. $NaHCO_3$ (20 mL). The layers were separated and the aqueous was extracted with CH_2Cl_2 (3 × 20 mL). The combined organic extract was dried over anhydrous Na_2SO_4, filtered, and concentrated *in vacuo*. Purification by silica gel flash column chromatography (eluting with 0-33% EtOAc/hex). The product was isolated as a white solid (5.01 g, 88%). R_f = 0.55 (33% EtOAc/hex). ^1H NMR (400 MHz, $CDCl_3$) δ 7.14 (s, 1H), 7.05 (s, 1H), 3.92 (s, 3H), 3.89 (s, 3H), 2.67 (s, 3H). HRMS (ESI): *m/z* $[M+H]^+$ calculated for $C_{10}H_{11}BrO_3$: 257.9892; found: 258.9932.

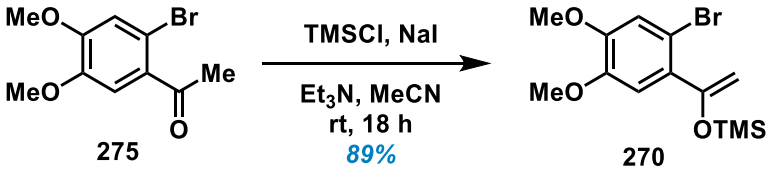

((1-(2-Bromo-4,5-dimethoxyphenyl)vinyl)oxy)trimethylsilane (270).[33] MeCN (62 mL) was added to a mixture of ketone **275** (10.8 g, 41.7 mmol, 1.0 equiv) and NaI (7.50 g, 50.0 mmol, 1.2 equiv) at rt and stirred for 5 min. Et_3N (8.7 mL, 62.5 mmol, 1.5 equiv) was added dropwise, followed by TMSCl (6.4 mL, 50.0 mmol, 1.2 equiv) and then stirred at rt for 18 h. The reaction was diluted with CH_2Cl_2 (30 mL) at 0 °C and then subsequently

quenched with sat. aq. NH_4Cl (30 mL). The solution was stirred for 5 min at 0 °C before separating the mixture. The aqueous layer was extracted with CH_2Cl_2 (3 × 10 mL), then the combined organic extract was washed with ice water (2 × 60 mL) and NH_4Cl (1 × 60 mL) before dried over anhydrous Na_2SO_4, filtered, and concentrated *in vacuo*. Purification by vacuum distillation (pressure: 200 mTorr, head temp: 218 °C). The product was isolated as a colorless oil (12.4 g, 89%). ^1H NMR (500 MHz, $CDCl_3$) δ 7.01 (s, 1H), 6.92 (s, 1H), 4.59 (d, J = 1.4 Hz, 1H), 4.54 (d, J = 1.4 Hz, 1H), 3.87 (s, 3H), 3.86 (s, 3H), 0.22 (s, 9H). ^{13}C NMR (600 MHz, $CDCl_3$) δ 155.6, 149.2, 147.9, 132.3, 115.9, 113.2, 96.2, 56.3, 0.28. HRMS (ESI): *m/z* $[M+H]^+$ calculated for $C_{13}H_{19}BrO_3Si$: 330.0274; found: 331.0346.

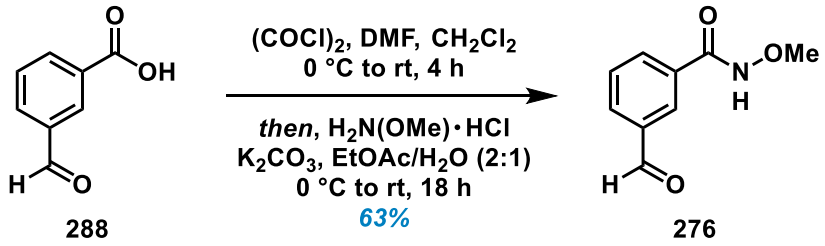

3-Formyl-*N*-methoxybenzamide (276).[34] To a solution of 3-formylbenzoic acid (1.01 g, 6.67 mmol, 1.0 equiv) in CH_2Cl_2 (22 mL, 0.3M) at 0 °C under N_2 was added dropwise oxalyl chloride (686 uL, 7.99 mmol, 1.2 equiv), followed by a catalytic amount of DMF. The reaction was allowed to stir at rt until completion (approximately 4 h). The mixture was concentrated *in vacuo* to afford the corresponding crude acid choride. *O*–methylhydroxylamine hydrochloride (557 mg, 6.67 mmol, 1.0 equiv) was added to a biphasic mixture of K_2CO_3 (1.84 g, 13.3 mmol, 2.0 equiv) in an EtOAc/H_2O (66 mL, 2:1, 0.1 M) solution. The resulting solution was cooled to 0 °C, followed by dropwise addition

of the crude acid chloride dissolved in a minimum amount of EtOAc. The reaction flask was rinsed once more with EtOAc before stirring the mixture at rt for 18 h. The phases were then separated and the aqueous layer was extracted with EtOAc (2 × 20 mL). The combined organic extract was dried over anhydrous Na_2SO_4, filtered, and then concentrated *in vacuo*. Purification by recrystallization (EtOAc/hex). The product was isolated as a white solid (754 mg, 63%). ^{1}H NMR (600 MHz, $CDCl_3$) δ 10.06 (s, 1H), 9.12 (bs, 1H), 8.24 (s, 1H), 8.07 (d, J = 7.8 Hz, 1H), 8.03 (d, J = 7.6 Hz, 1H), 7.64 (t, J = 7.8, 7.6 Hz, 1H), 3.92 (s, 3H). ^{13}C NMR (600 MHz, $CDCl_3$) δ 191.5, 136.6, 133.3, 129.8, 127.8, 64.9. HRMS (ESI): *m/z* $[M+H]^+$ calculated for $C_9H_9NO_3$: 179.0582; found: 180.0597.

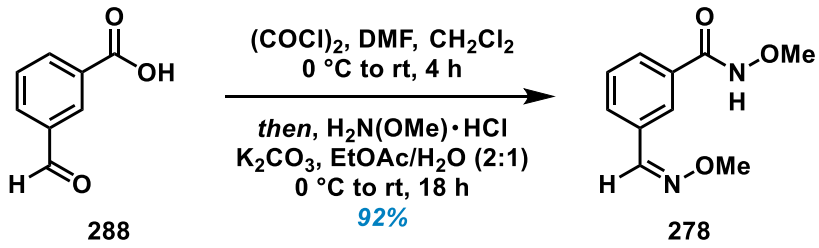

(Z)-*N*-Methoxy-3-((methoxyimino)methyl)benzamide (278).[34] To a solution of 3-formylbenzoic acid (10.0 g, 66.6 mmol, 1 equiv) in CH_2Cl_2 (222 mL, 0.3 M) at 0 °C under N_2 was added dropwise oxalyl chloride (6.9 mL, 79.9 mmol, 1.2 equiv), followed by a catalytic amount of DMF. The reaction was allowed to stir at rt until completion (approximately 4 h). The mixture was concentrated *in vacuo* to afford the corresponding crude acid choride. *O*–methylhydroxylamine hydrochloride (13.9 g, 167 mmol, 2.5 equiv) was added to a biphasic mixture of K_2CO_3 (36.8 g, 266 mmol, 4.0 equiv) in an EtOAc/H_2O (666 mL, 2:1, 0.1 M) solution. The resulting solution was cooled to 0 °C, followed by

dropwise addition of the crude acid chloride dissolved in a minimum amount of EtOAc. The reaction flask was rinsed once more with EtOAc before stirring the mixture at rt for 18 h. The phases were then separated and the aqueous layer was extracted with EtOAc (2 × 150 mL). The combined organic extract was dried over anhydrous Na_2SO_4, filtered, and then concentrated *in vacuo*. Purification by recrystallization (EtOAc/hex). The product was isolated as a white solid (12.8 g, 92%). ^{1}H NMR (600 MHz, $CDCl_3$) δ 8.06 (s, 1H), 7.93 (s, 1H), 7.75 (d, J = 7.7 Hz, 1H), 7.71 (d, J = 7.8 Hz, 1H), 7.44 (t, J = 7.7 Hz, 1H), 3.98 (s, 3H), 3.89 (s, 3H). ^{13}C NMR (600 MHz, $CDCl_3$) δ 147.6, 132.9, 130.5, 129.3, 128.4, 125.3, 64.7, 62.4. HRMS (ESI): *m/z* $[M+H]^+$ calculated for $C_{10}H_{12}N_2O_3$: 208.0848; found: 209.0914.

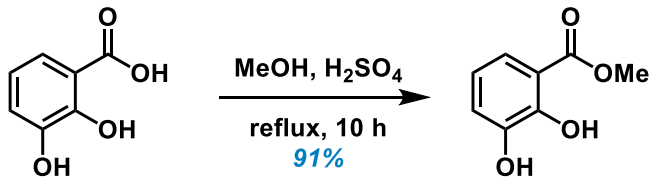

282 **283**

Methyl 2,3-dihydroxybenzoate (283).[35] Sulfuric acid (668 mg, 6.81 mmol, 0.21 equiv) was added dropwise to a stirring solution of 2,3-dihydroxybenzoic acid (**282**) (5.01 g, 32.4 mmol, 1.0 equiv) in anhydrous methanol (50 mL, 0.65 M) at rt under N_2 gas. The mixture was refluxed for 10 h before concentrating *in vacuo*. Purification by recrystallization (Et_2O). The product was isolated as a pink solid (5.494 g, 98%). ^{1}H NMR (600 MHz, $CDCl_3$) δ 8.89 (s, 1H), 7.36 (d, J = 7.9 Hz, 1H), 7.11 (d, J = 8.0 Hz, 1H), 6.80 (td, J = 8.0, 2.0 Hz, 1H), 6.27 (s, 1H), 3.95 (s, 3H). HRMS (ESI): *m/z* $[M+H]^+$ calculated for $C_8H_8O_4$:

168.0423; found: 169.0431. All other spectroscopic data are in accord with previously reported literature.

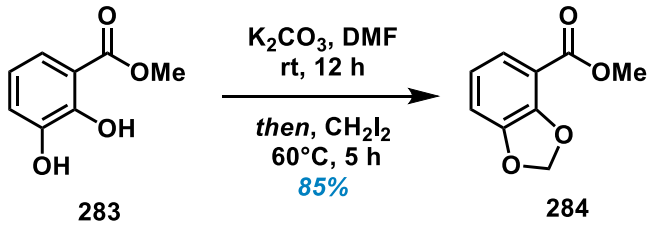

Methyl benzo[1,3]dioxole-4-carboxylate (284).[35] Add K_2CO_3 (3.45 g, 25.0 mmol, 3.0 equiv) to a stirring solution of dihydroxy benzoate **283** (1.40 g, 8.33 mmol, 1.0 equiv) in DMF (11 mL, 0.8 M) at rt. The reaction mixture was stirred for 12 h before adding a solution of diiodomethane (2.45 g, 9.16 mmol, 1.1 equiv) in DMF (7.0 mL, 1.2 M) dropwise at rt. The solution was then stirred at 60 °C for 5 h and quenched with water (20 mL). The mixture was transferred to a separatory funnel and extracted with EtOAc (3 × 20 mL). The combined organic extract was washed with water (2 × 20 mL), dried over anhydrous Na2SO4, filtered, and concentrated *in vacuo*. Purification by silica gel flash column chromatography (eluting with 100% CH_2Cl_2). The product was isolated as a white solid (1.27 g, 85%). R_f = 0.48 (100% CH_2Cl_2). ^{1}H NMR (500 MHz, $CDCl_3$) δ 7.41 (d, J = 8.1 Hz, 1H), 6.97 (d, J = 7.7 Hz, 1H), 6.86 (t, J = 7.7 Hz, 1H), 6.10 (s, 2H), 3.92 (s, 3H). HRMS (ESI): *m/z* $[M+H]^+$ calculated for $C_9H_8O_4$: 180.0423; found: 181.0428.

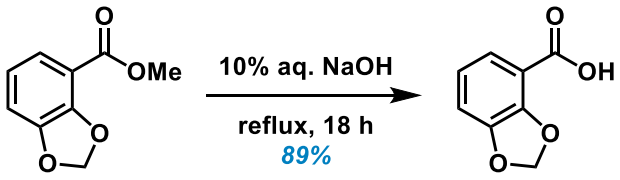

284 285

Benzo[1,3]-dioxole-4-carboxylic acid (285).[35] A mixture of benzoate **284** (3.28 g, 18.2 mmol, 1.0 equiv) in 10% NaOH solution (22 mL, 0.83 M) was refluxed o/n and then cooled to rt. The reaction mixture was transferred to an Erlenmeyer flask, titrated until precipitation (approximately pH 4), and diluted with H_2O. The resulting precipitate was filtered out and washed with cold 1 M HCl. Purification by recrystallization (EtOAc). The product was isolated as a tan solid (2.09 mg, 89%). ^{1}H NMR (500 MHz, $CDCl_3$) δ 7.46 (dd, J = 8.2, 1.2 Hz, 1H), 7.03 (dd, J = 7.7, 1.2 Hz, 1H), 6.90 (t, J = 7.7 Hz, 1H), 6.14 (s, 2H). HRMS (ESI): *m/z* $[M+H]^+$ calculated for $C_8H_6O_4$: 166.0266; found: 167.0271.

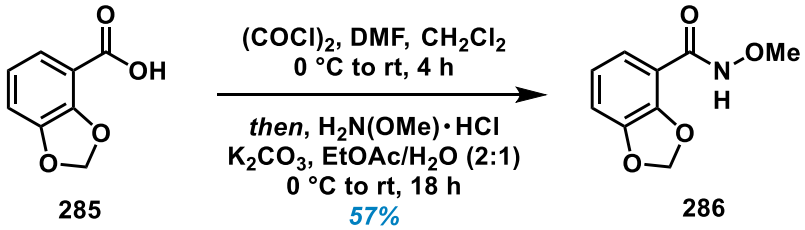

285 286

***N*-Methoxybenzo[1,3]dioxole-4-carboxamide (286).**[34] To a solution of carboxylic acid **285** (2.10 g, 12.6 mmol, 1.0 equiv) in CH_2Cl_2 (42 mL, 0.3 M) at 0 °C under N_2 was added dropwise oxalyl chloride (1.3 mL, 15.2 mmol, 1.2 equiv), followed by a catalytic amount of DMF. The reaction was allowed to stir at rt until completion (approximately 4 h). The mixture was concentrated *in vacuo* to afford the corresponding crude acid choride. *O*–methylhydroxylamine hydrochloride (1.05 g, 12.6 mmol, 1.0 equiv) was added to a

biphasic mixture of K_2CO_3 (3.48 g, 25.2 mmol, 2.0 equiv) in an EtOAc/H_2O (126 mL, 2:1, 0.1 M) solution. The resulting solution was cooled to 0 °C, followed by dropwise addition of the crude acid chloride dissolved in a minimum amount of EtOAc. The reaction flask was rinsed once more with EtOAc before stirring the mixture at rt for 18 h. The phases were then separated and the aqueous layer was extracted with EtOAc (2 × 40 mL). The combined organic extract was dried over anhydrous Na_2SO_4, filtered, and then concentrated *in vacuo*. Purification by recrystallization (EtOAc/hex). The product was isolated as a white solid (698 mg, 57%). ^{1}H NMR (500 MHz, $CDCl_3$) δ 9.48 (s, 1H), 7.59 (dd, J = 6.6, 2.8 Hz, 1H), 7.00 – 6.93 (m, 2H), 6.09 (s, 2H), 3.90 (s, 3H). HRMS (ESI): *m/z* $[M+H]^+$ calculated for $C_9H_9NO_4$: 195.0532; found: 196.0535.

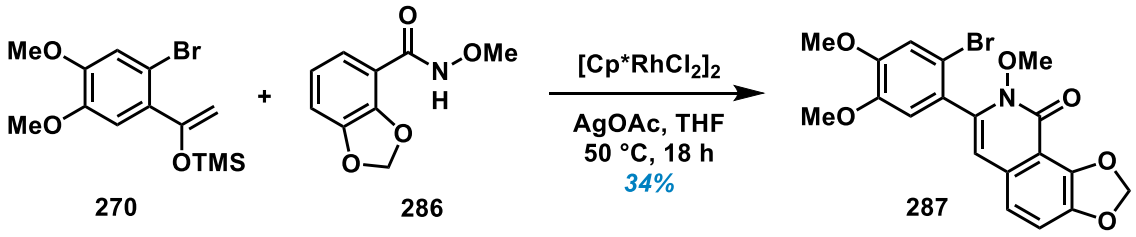

7-(2-Bromo-4,5-dimethoxyphenyl)-8-methoxy-[1,3]dioxolo[4,5-h]isoquinolin-9(8H)-one (287). A mixture of *N*-methoxybenzamide **286** (200 mg, 1.02 mmol, 1.0 equiv), AgOAc (509 mg, 2.25 mmol, 2.2 equiv), and $[Cp^*RhCl_2]_2$ (31.5 mg, 0.051 mmol, 5 mol%) was dissolved in THF (5.0 mL, 0.2 M) and stirred at rt for 1 min. Silyl enol ether **270** (407 mg, 1.23 mmol, 1.2 equiv) was added to the mixture while stirring and then heated at 50 °C for 18 h. The reaction mixture was then cooled to rt before filtering it through a silica plug using CH_2Cl_2 (5 mL) and subsequently EtOAc (5 mL). The filtrate was then

concentrated *in vacuo*, diluted with CH_2Cl_2 (10 mL), treated with concentrated HCl (165 µL, 1 equiv), and concentrated *in vacuo* once more. Purification by silica gel flash column chromatography (eluting with 0-50% acetone/hex). The product was isolated as a white solid (151 mg, 34%). R_f = 0.38 (50% acetone/hex). ^{1}H NMR (500 MHz, $CDCl_3$) δ 7.19 (d, *J* = 8.2 Hz, 1H), 7.12 (s, 1H), 7.03 (d, *J* = 8.3 Hz, 1H), 6.93 (s, 1H), 6.31 (s, 1H), 6.26 (d, *J* = 8.3 Hz, 2H), 3.94 (s, 3H), 3.88 (s, 3H), 3.79 (s, 3H). HRMS (ESI): *m/z* $[M+H]^+$ calculated for $C_{19}H_{16}BrNO_6$: 433.0161; found: 434.0219.

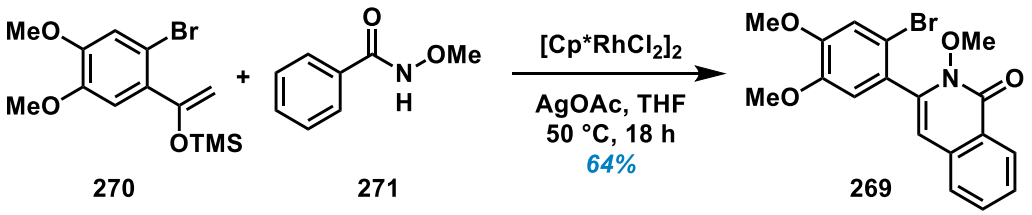

270 271 269

3-(2-Bromo-4,5-dimethoxyphenyl)-2-methoxyisoquinolin-1(2H)-one (269).[34] A mixture of unsubstituted *N*-methoxybenzamide **271** (300 mg, 1.98 mmol, 1 equiv), AgOAc (727 mg, 4.37 mmol, 2.2 equiv), and $[Cp^*RhCl_2]_2$ (61.1 mg, 0.099 mmol, 5 mol%) was dissolved in THF (10 mL, 0.2 M) and stirred at rt for 1 min. Silyl enol ether **270** (789 mg, 1.38 mmol, 1.2 equiv) was added to the mixture while stirring and then heated at 50 °C for 18 h. The reaction mixture was then cooled to rt before filtering it through a silica plug using CH_2Cl_2 (5 mL) and subsequently EtOAc (5 mL). The filtrate was then concentrated *in vacuo*, diluted with CH_2Cl_2 (10 mL), treated with concentrated HCl (165 µL, 1 equiv), and concentrated *in vacuo* once more. Purification by silica gel flash column chromatography (eluting with 0-66% EtOAc/hex). The product was isolated as a tan solid (499 mg, 64%). R_f = 0.44 (66% EtOAc/hex). ^{1}H NMR (700 MHz, $CDCl_3$) δ 8.49 (d, *J* = 8.0 Hz, 1H), 7.67 (t, *J* = 7.6 Hz, 1H), 7.58 – 7.48 (m, 2H), 7.14 (s, 1H), 6.95 (s, 1H), 6.43

(s, 1H), 3.95 (s, 3H), 3.87 (s, 3H), 3.81 (s, 3H). ^{13}C NMR (176 MHz, $CDCl_3$) δ 158.8, 150.4, 148.1, 140.9, 135.6, 132.6, 127.9, 127.0, 126.9, 126.5, 125.9, 115.4, 114.5, 114.3, 107.9, 63.9, 56.4, 56.4. HRMS (ESI): *m/z* $[M+H]^+$ calculated for $C_{18}H_{16}BrNO_4$: 389.0263; found: 390.0269.

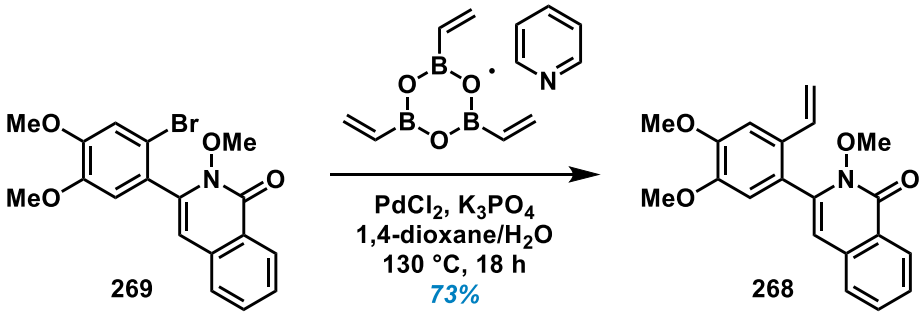

3-(4,5-Dimethoxy-2-vinylphenyl)-2-methoxyisoquinolin-1(2H)-one (268).[36] $PdCl_2$ (4.56 mg, 0.026 mmol, 0.05 equiv) was added to a solution of aryl halide **269** (200 mg, 0.514 mmol, 1.0 equiv) in 1,4-dioxane (5.1 mL, 0.1 M) at rt and stirred for 20 min. K_3PO_4 (327 mg, 1.54 mmol, 3.0 equiv) and trivinylboroxin pyridine (186 mg, 0.771 mmol, 1.5 equiv) were added to the mixture and then diluted with H_2O (5.1 mL, 0.1 M). The reaction flask was sealed and heated at 130 °C for 18 h before quenching with H_2O (10 mL). The solution was then extracted with CH_2Cl_2 (3 × 10 mL) and EtOAc (3 × 10 mL). The combined organic extract was dried over anhydrous Na_2SO_4, filtered, and concentrated *in vacuo*. Purification by silica gel flash column chromatography (eluting with 0-50% acetone/hex). The product was isolated as a tan solid (210 mg, 73%). R_f = 0.56 (50% acetone/hex). ^{1}H NMR (400 MHz, $CDCl_3$) δ 8.49 (ddd, *J* = 8.7, 1.3, 0.7 Hz, 1H), 7.67 (ddd, *J* = 8.7, 7.1, 1.3 Hz, 1H), 7.53 (m, 2H), 7.18 (s, 1H), 6.89 (s, 1H), 6.68 (dd, *J* = 17.4, 11.0 Hz, 1H), 6.37 (d, *J* = 0.7 Hz, 1H), 5.65 (dd, *J* = 17.4, 0.9 Hz, 1H), 5.17 (dd, *J* = 11.0, 0.9

Hz, 1H), 4.00 (s, 3H), 3.90 (s, 3H), 3.72 (s, 3H). HRMS (ESI): *m/z* $[M+H]^+$ calculated for $C_{20}H_{19}NO_4$: 337.1314; found: 338.1359.

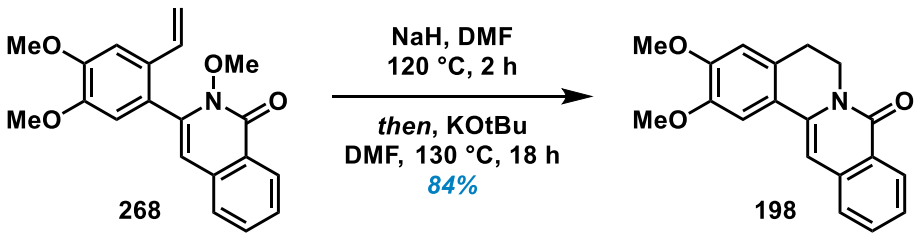

2,3-Dimethoxy-5,6-dihydro-8H-isoquinolin-8-one (198). DMF (2 mL, 0.37 M) was added to a mixture of isoquinolone **268** (250 mg, 0.741 mmol, 1.0 equiv) and 60% NaH (60 mg, 1.48 mmol, 2.0 equiv) at rt and then stirred at 130 °C for at least 2 h. The reaction mixture was then concentrated *in vacuo* before adding KOtBu (25.0 mg, 0.222 mmol, 0.3 equiv) in DMF (2 mL, 0.37 M) and then stirred at 130 °C for 18 h. After cooling to rt, the reaction was quenched with H_2O (20 mL) and extracted with EtOAc (3 x 10 mL). The combined organic extract was washed with brine (2 × 30 mL), dried over anhydrous Na_2SO_4, filtered, and concentrated *in vacuo*. Purification by silica gel flash column chromatography (eluting with 25% acetone/hex). The product was isolated as a tan solid (191 mg, 84%). R_f = 0.22 (25% acetone/hex). ^{1}H NMR (700 MHz, $CDCl_3$) δ 8.43 (d, *J* = 8.1 Hz, 1H), 7.63 (t, *J* = 7.5 Hz, 1H), 7.57 (d, *J* = 8.0 Hz, 1H), 7.44 (t, *J* = 7.6 Hz, 1H), 7.28 (s, 1H), 6.89 (s, 1H), 6.75 (s, 1H), 4.37 (t, *J* = 6.3 Hz, 2H), 4.00 (s, 3H), 3.95 (s, 3H), 2.95 (t, *J* = 6.3 Hz, 2H). ^{13}C NMR (700 MHz, $CDCl_3$) δ 162.4, 150.5, 148.7, 137.6, 136.9, 132.4, 128.9, 128.2, 126.4, 126.1, 124.8, 122.52, 110.7, 108.1, 101.6, 56.4, 56.2, 39.9, 28.3. HRMS (ESI): *m/z* $[M+H]^+$ calculated for $C_{19}H_{17}NO_3$: 307.1208; found: 308.1237.

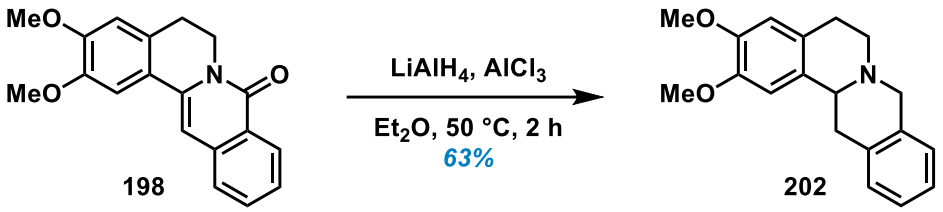

2,3-Dimethoxy-5,8,13,13a-tetrahydro-6H-isoquinoline (202). $AlCl_3$ (97.0 mg, 0.729 mmol, 11.2 equiv) was added to a stirring solution of $LiAlH_4$ (83.0 mg, 2.19 mmol, 33.7 equiv) in Et_2O (16 mL, 0.004 M). The isoquinolone **(198)** (20.0 mg, 0.065 mmol, 1.0 equiv) was then added to the ethereal AlH_3 mixture and stirred at 40 °C for 2 h. The reaction mixture was then cooled to rt and then quenched with H_2O (1 mL), 2 M NaOH (1 mL), and H_2O (3 mL) again. The solution was filtered through a fritted funnel and extracted with EtOAc (3 × 5 mL). The combined organic extract was dried over anhydrous Na_2SO_4, filtered, and concentrated *in vacuo*. Purification by silica gel preparative TLC (eluting with 25% acetone/CH_2Cl_2). R_f = 0.22 (25% acetone/CH_2Cl_2). The product was isolated as a tan solid (12.0 mg, 63%). ^{1}H NMR (500 MHz, $CDCl_3$) δ 7.25-7.23 (m, 3H), 7.18 (d, *J* = 5.6 Hz, 1H), 6.84 (s, 1H), 6.72 (s, 1H), 4.13 (d, *J* = 14.9 Hz, 4H), 4.00 (s, 3H), 3.97 (s, 3H), 3.85 (d, *J* = 15.0 Hz, 1H), 3.74 (d, *J* = 9.8 Hz, 1H), 3.43 (dd, *J* = 16.2, 4.0 Hz, 1H), 3.30 – 3.21 (m, 2H), 3.02 (dd, *J* = 16.2, 11.4 Hz, 1H), 2.81 – 2.69 (m, 2H). ^{13}C NMR (600 MHz, $CDCl_3$) δ 162.4, 150.5, 148.6, 137.6, 136.9, 132.4, 128.9, 128.2, 126.4, 126.1, 124.7, 122.5, 110.6, 108.0, 101.7, 56.4, 56.2, 39.9, 28.3. HRMS (ESI): *m/z* $[M+H]^+$ calculated for $C_{19}H_{21}NO_2$: 295.1572; found: 296.1614.

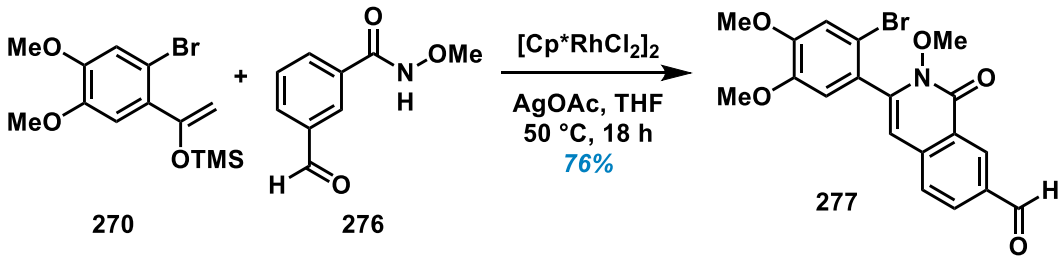

3-(2-Bromo-4,5-dimethoxyphenyl)-2-methoxy-1-oxo-1,2-dihydroisoquinoline-7-carbaldehyde (277). A mixture of amide **276** (100 mg, 0.558 mmol, 1 equiv), AgOAc (278 mg, 1.23 mmol, 2.2 equiv), and $[Cp^*RhCl_2]_2$ (17.1 mg, 0.028 mmol, 5 mol%) was dissolved in THF (2.8 mL, 0.2 M) and stirred at rt for 1 min. Silyl enol ether **270** (222 mg, 0.670 mmol, 1.2 equiv) was added to the mixture while stirring and then heated at 50 °C for 18 h. The reaction mixture was then cooled to rt before filtering it through a silica plug using CH_2Cl_2 (3 mL) and subsequently EtOAc (3 mL). The filtrate was then concentrated *in vacuo*, diluted with CH_2Cl_2 (10 mL), treated with concentrated HCl (46.5 µL, 1 equiv), and concentrated *in vacuo* once more. Purification by silica gel flash column chromatography (eluting with 0-30% acetone/hex). The product was isolated as a tan solid (178 mg, 76%). R_f = 0.23 (30% acetone/hex). ^{1}H NMR (600 MHz, $CDCl_3$) δ 10.15 (s, 1H), 8.94 (d, *J* = 1.7 Hz, 1H), 8.18 (dd, *J* = 8.2, 1.7 Hz, 1H), 7.66 (d, *J* = 8.2 Hz, 1H), 7.15 (s, 1H), 6.94 (s, 1H), 6.50 (s, 1H), 3.96 (s, 3H), 3.88 (s, 3H), 3.84 (s, 3H). ^{13}C NMR (600 MHz, $CDCl_3$) δ 191.2, 158.4, 150.7, 148.2, 144.1, 140.1, 134.7, 133.3, 130.2, 127.6, 126.9, 125.2, 115.4, 114.1, 113.9, 107.5, 64.2, 56.5, 56.4. HRMS (ESI): *m/z* $[M+H]^+$ calculated for $C_{19}H_{16}BrNO_5$: 417.0212; found: 417.0245.

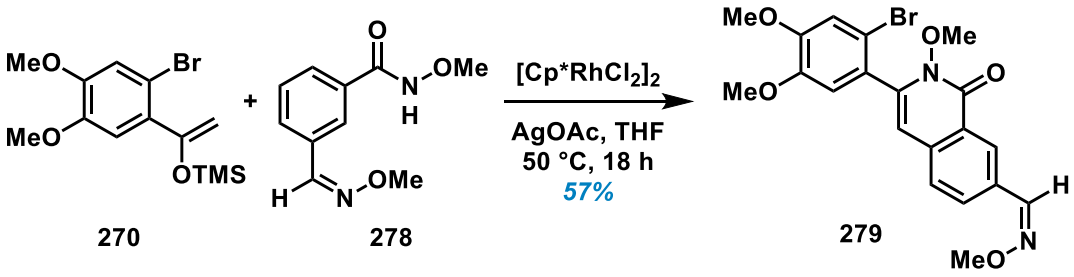

270 278 279

(Z)-3-(2-Bromo-4,5-dimethoxyphenyl)-2-methoxy-1-oxo-1,2-dihydroisoquinoline-7-carbaldehyde O-methyl oxime (279).[34] A mixture of amide **278** (300 mg, 1.44 mmol, 1 equiv), AgOAc (716 mg, 3.17 mmol, 2.2 equiv), and $[Cp^*RhCl_2]_2$ (45.0 mg, 0.072 mmol, 5 mol%) was dissolved in THF (7.2 mL, 0.2 M) and stirred at rt for 1 min. Silyl enol ether **270** (573 mg, 1.73 mmol, 1.2 equiv) was added to the mixture while stirring and then heated at 50 °C for 18 h. The reaction mixture was then cooled to rt before filtering it through a silica plug using CH_2Cl_2 (5 mL) and subsequently EtOAc (5 mL). The filtrate was then concentrated *in vacuo*, diluted with CH_2Cl_2 (10 mL), treated with concentrated HCl (120 μL, 1 equiv), and concentrated *in vacuo* once more. Purification by silica gel flash column chromatography (eluting with 0-50% EtOAc/hex). The product was isolated as a white solid (.271 g, 42%). R_f = 0.34 (50% EtOAc/hex). ^{1}H NMR (600 MHz, $CDCl_3$) δ 8.49 (d, *J* = 1.7 Hz, 1H), 8.19 (s, 1H), 8.06 (dd, *J* = 8.3, 1.7 Hz, 1H), 7.53 (d, *J* = 8.3 Hz, 1H), 7.14 (s, 1H), 6.94 (s, 1H), 6.43 (s, 1H), 4.01 (s, 3H), 3.95 (s, 3H), 3.87 (s, 3H), 3.81 (s, 3H). ^{13}C NMR (600 MHz, $CDCl_3$) δ 158.5, 150.5, 148.1, 147.8, 141.7, 136.6, 131.2, 129.6, 127.9, 127.1, 126.9, 125.6, 115.4, 114.3, 114.1, 107.7, 64.0, 62.4, 56.4, 56.4. HRMS (ESI): *m/z* $[M+H]^+$ calculated for $C_{20}H_{19}BrN_2O_5$: 446.0477; found: 447.0528.

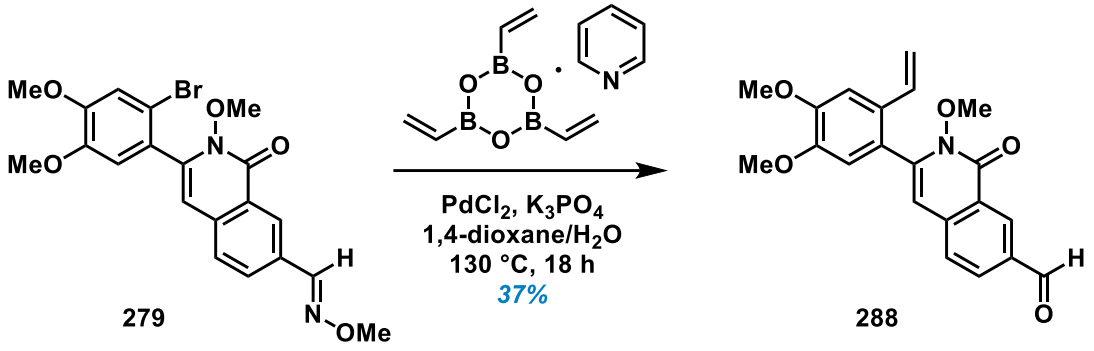

3-(4,5-Dimethoxy-2-vinylphenyl)-2-methoxy-1-oxo-1,2-dihydroisoquinoline-7-carbaldehyde (288). $PdCl_2$ (3.96 mg, 0.022 mmol, 0.05 equiv) was added to a solution of aryl halide **279** (200 mg, 0.447 mmol, 1.0 equiv) in 1,4-dioxane (4.5 mL, 0.1 M) at rt and stirred for 20 min. K_3PO_4 (285 mg, 1.34 mmol, 3.0 equiv) and trivinylboroxin pyridine (161 mg, 0.671 mmol, 1.5 equiv) were added to the mixture and then diluted with H_2O (7.5 mL, 0.06 M). The reaction flask was sealed and heated at 130 °C for 18 h before quenching with H_2O (10 mL). The solution was then extracted with CH_2Cl_2 (3 × 10 mL) and EtOAc (3 × 10 mL). The combined organic extract was dried over anhydrous Na_2SO_4, filtered, and concentrated *in vacuo*. Purification by silica gel flash column chromatography (eluting with 0-40 acetone/hex). The product was isolated as a tan solid (60.4 mg, 37%). R_f = 0.27 (40% acetone/hex). ^{1}H NMR (600 MHz, $CDCl_3$) δ 9.07 (d, *J* = 1.7 Hz, 1H), 8.33 (dd, *J* = 8.3, 1.8 Hz, 1H), 7.62 (d, *J* = 8.3 Hz, 1H), 7.18 (s, 1H), 6.89 (s, 1H), 6.64 (dd, *J* = 17.3, 11.0 Hz, 1H), 6.45 (s, 1H), 5.66 (d, *J* = 17.3 Hz, 1H), 5.20 (d, *J* = 11.0 Hz, 1H), 4.00 (s, 3H), 3.91 (s, 3H), 3.72 (s, 3H). HRMS (ESI): *m/z* $[M+H]^+$ calculated for $C_{21}H_{19}NO_5$: 365.1263; found: 366.1357.

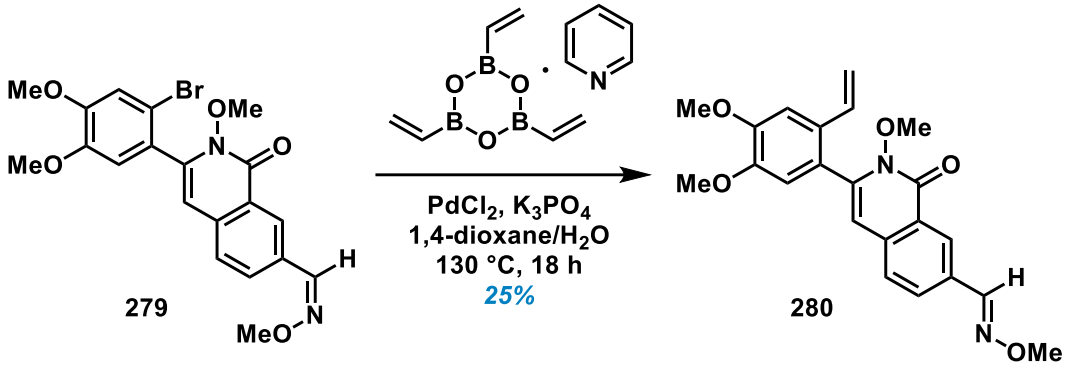

3-(4,5-Dimethoxy-2-vinylphenyl)-2-methoxy-1-oxo-1,2-dihydroisoquinoline-7-carbaldehyde O-methyl oxime (280). $PdCl_2$ (3.96 mg, 0.022 mmol, 0.05 equiv) was added to a solution of aryl halide **279** (200 mg, 0.447 mmol, 1.0 equiv) in 1,4-dioxane (4.5 mL, 0.1 M) at rt and stirred for 20 min. K_3PO_4 (285 mg, 1.34 mmol, 3.0 equiv) and trivinylboroxin pyridine (161 mg, 0.671 mmol, 1.5 equiv) were added to the mixture and then diluted with H_2O (7.5 mL, 0.06 M). The reaction flask was sealed and heated at 130 °C for 18 h before quenching with H_2O (10 mL). The solution was then extracted with CH_2Cl_2 (3 × 10 mL) and EtOAc (3 × 10 mL). The combined organic extract was dried over anhydrous Na_2SO_4, filtered, and concentrated *in vacuo*. Purification by silica gel flash column chromatography (eluting with 0-40% acetone/hex). The product was isolated as a tan solid (44.0 mg, 25%). R_f = 0.63 (40% acetone/hex). ^{1}H NMR (600 MHz, $CDCl_3$) δ 8.48 (d, *J* = 1.7 Hz, 1H), 8.19 (s, 1H), 8.05 (dd, *J* = 8.5, 1.6 Hz, 1H), 7.50 (d, *J* = 8.5 Hz, 1H), 7.17 (s, 1H), 6.88 (s, 1H), 6.67 (dd, *J* = 17.3, 11.0 Hz, 1H), 6.37 (s, 1H), 5.65 (d, *J* = 17.3 Hz, 1H), 5.18 (d, *J* = 11.0 Hz, 1H), 4.01 (s, 3H), 3.99 (s, 3H), 3.89 (s, 3H), 3.71 (s, 3H). HRMS (ESI): *m/z* $[M+H]^+$ calculated for $C_{22}H_{22}N_2O_5$: 394.1529; found: 395.1581.

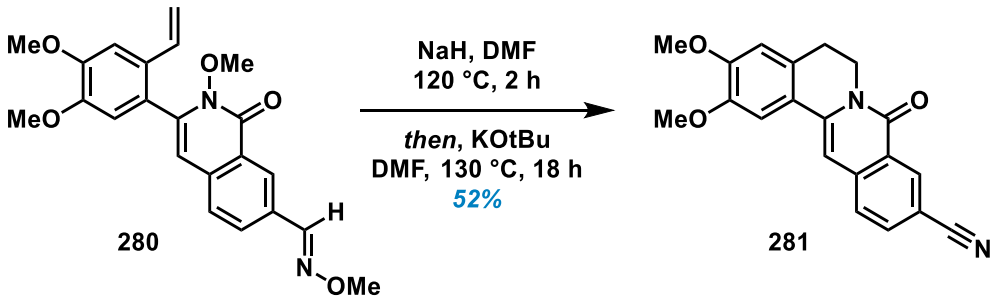

2,3-Dimethoxy-8-oxo-5,8-dihydro-6H-isoquinolino[3,2-a]isoquinoline-10-carbonitrile (281). DMF (0.5 mL, 0.2 M) was added to a mixture of isoquinolone **280** (40.0 mg, 0.101 mmol, 1.0 equiv) and NaH (8.10 mg, 0.203 mmol, 2.0 equiv) at rt and then stirred at 130 °C for 2 h. The reaction mixture was then concentrated *in vacuo* before adding KOtBu (3.40 mg, 0.030 mmol, 0.3 equiv) in DMF (0.5 mL, 0.2 M) and then stirred at 130 °C for 18 h. After cooling to rt, the reaction was quenched with H_2O (10 mL) and extracted with EtOAc (3 × 5 mL). The combined organic extract was washed with brine (1 × 15 mL), dried over anhydrous Na_2SO_4, filtered, and concentrated *in vacuo*. Purification by silica gel flash column chromatography (eluting with 0-66% EtOAc/hex). The product was isolated as a tan solid (19.1 mg, 52%). R_f = 0.29 (66% EtOAc/hex). ^{1}H NMR (400 MHz, $CDCl_3$) δ 8.72 (d, *J* = 1.8 Hz, 1H), 7.77 (dd, *J* = 8.3, 1.8 Hz, 2H), 7.62 (d, *J* = 8.3, 2H), 7.27 (s, 1H), 6.87 (s, 1H), 6.77 (s, 1H), 4.36 (t, *J* = 6.5 Hz, 2H), 4.00 (s, 3H), 3.96 (s, 3H), 2.97 (t, *J* = 6.5 Hz, 2H). HRMS (ESI): *m/z* $[M+H]^+$ calculated for $C_{20}H_{16}N_2O_3$: 332.1157; found: 333.1230.

2.6 NMR Spectra

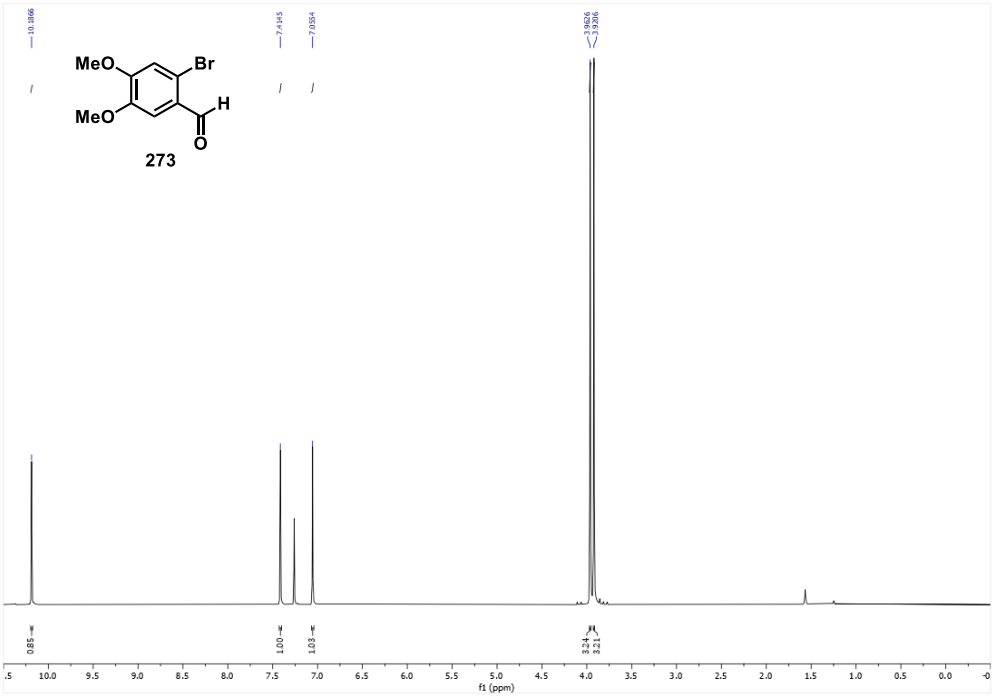

Figure 2.4: 2-Bromo-4,5-dimethoxybenzaldehyde (**273**); ^{1}H NMR (500 MHz, $CDCl_3$) at 24.8 °C.

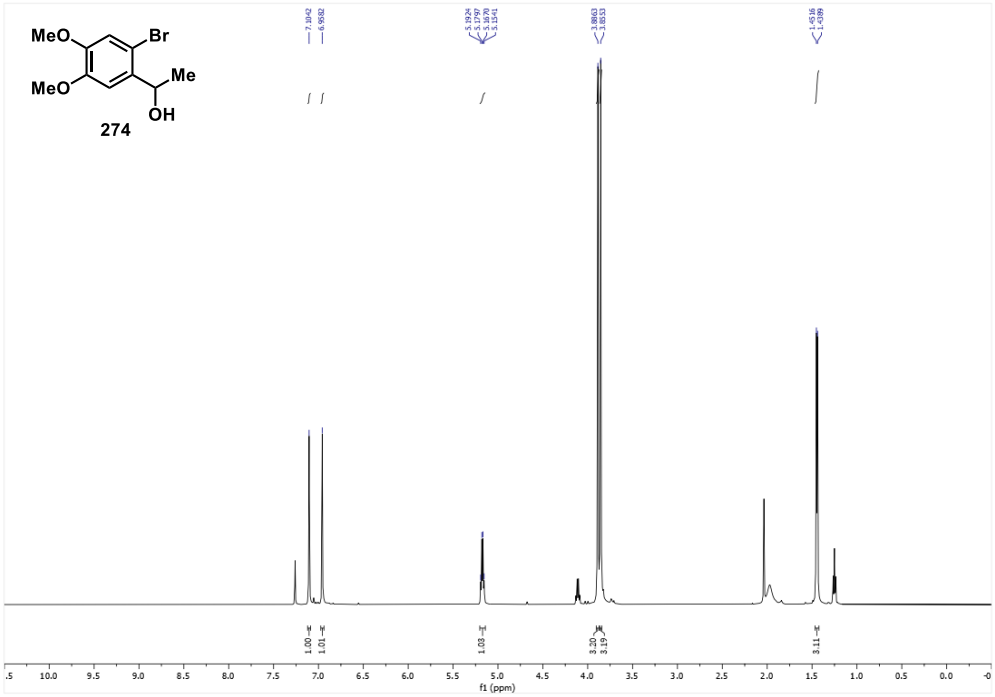

Figure 2.5: 1-(2-Bromo-4,5-dimethoxyphenyl)ethan-1-ol (**274**); ^{1}H NMR (500 MHz, $CDCl_3$) at 24.8 °C.

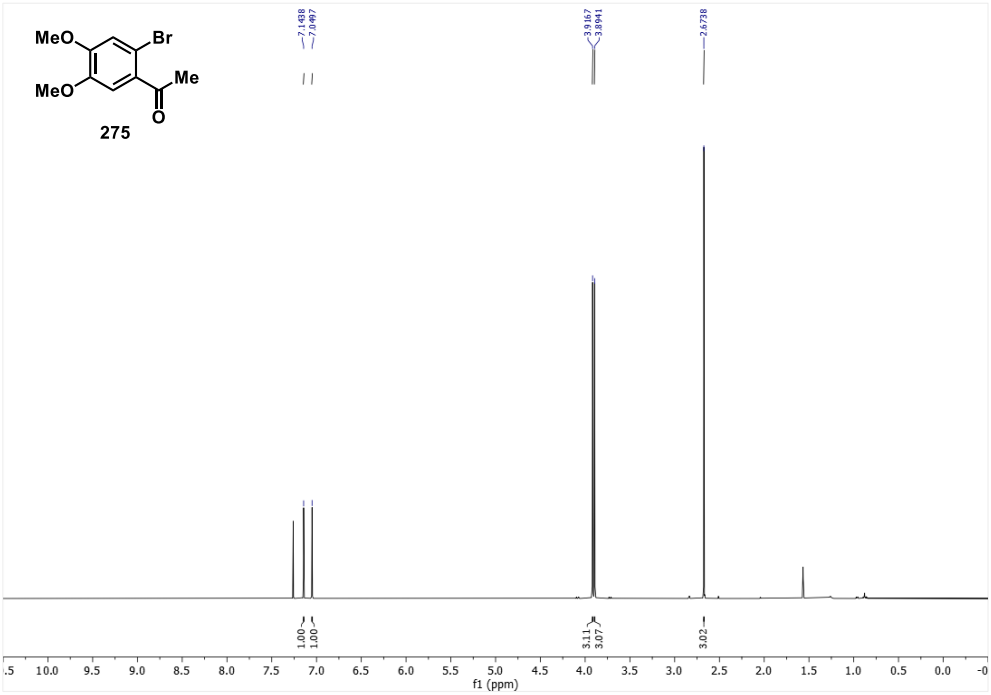

Figure 2.6: 1-(2-Bromo-4,5-dimethoxyphenyl)ethan-1-one (**275**); ^{1}H NMR (400 MHz, $CDCl_3$) at 21.9 °C.

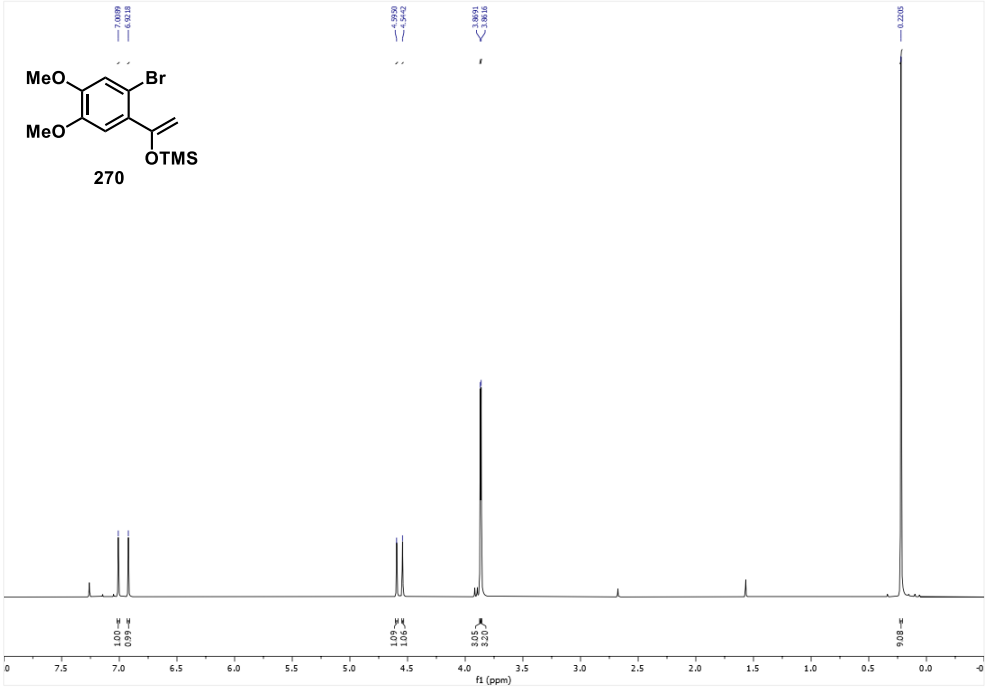

Figure 2.7: ((1-(2-Bromo-4,5-dimethoxyphenyl)vinyl)oxy)trimethylsilane (**270**); ^{1}H NMR (500 MHz, $CDCl_3$) at 24.8 °C.

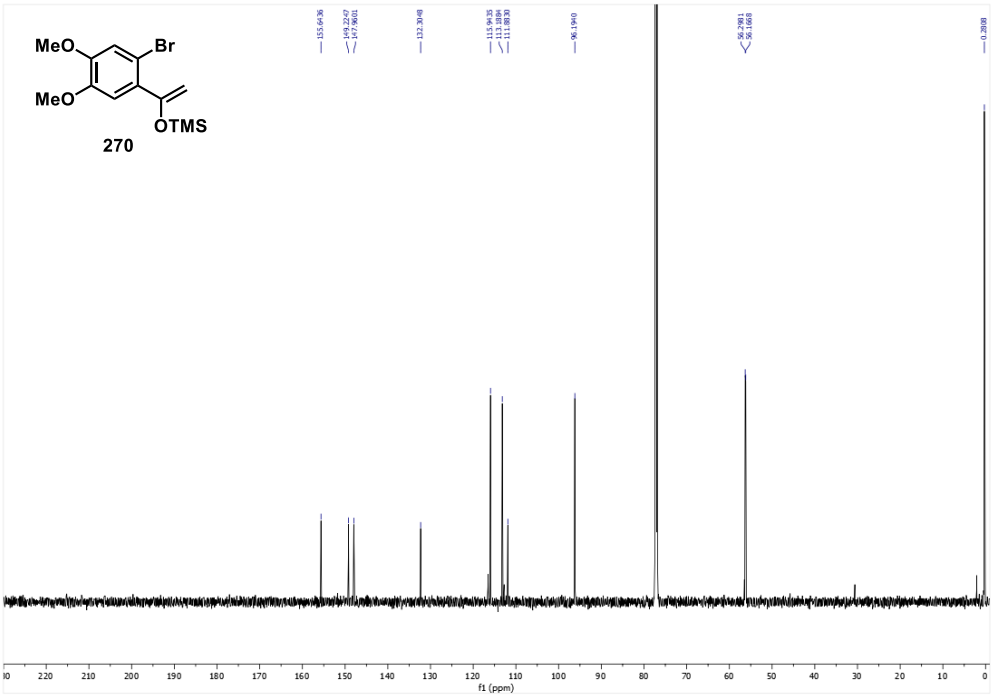

Figure 2.8: ((1-(2-Bromo-4,5-dimethoxyphenyl)vinyl)oxy)trimethylsilane (**270**); ^{13}C NMR (500 MHz, $CDCl_3$) at 24.8 °C.

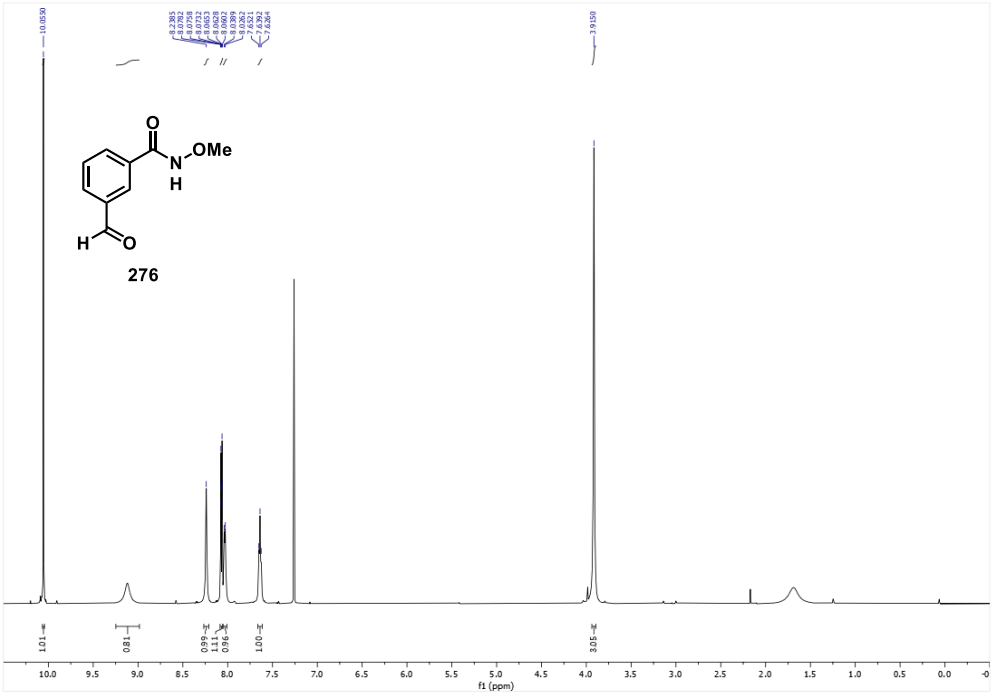

Figure 2.9: 3-Formyl-*N*-methoxybenzamide (**276**); ^{1}H NMR (600 MHz, $CDCl_3$) at 24.8 °C.

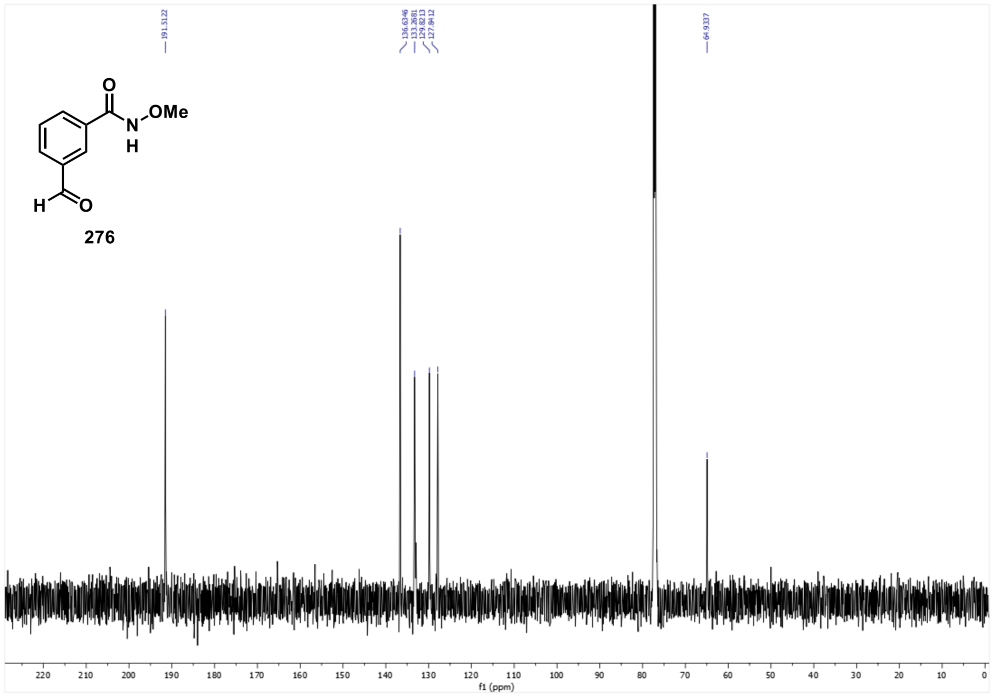

Figure 2.10: 3-Formyl-*N*-methoxybenzamide (**276**); ^{13}C NMR (600 MHz, $CDCl_3$) at 24.8 °C.

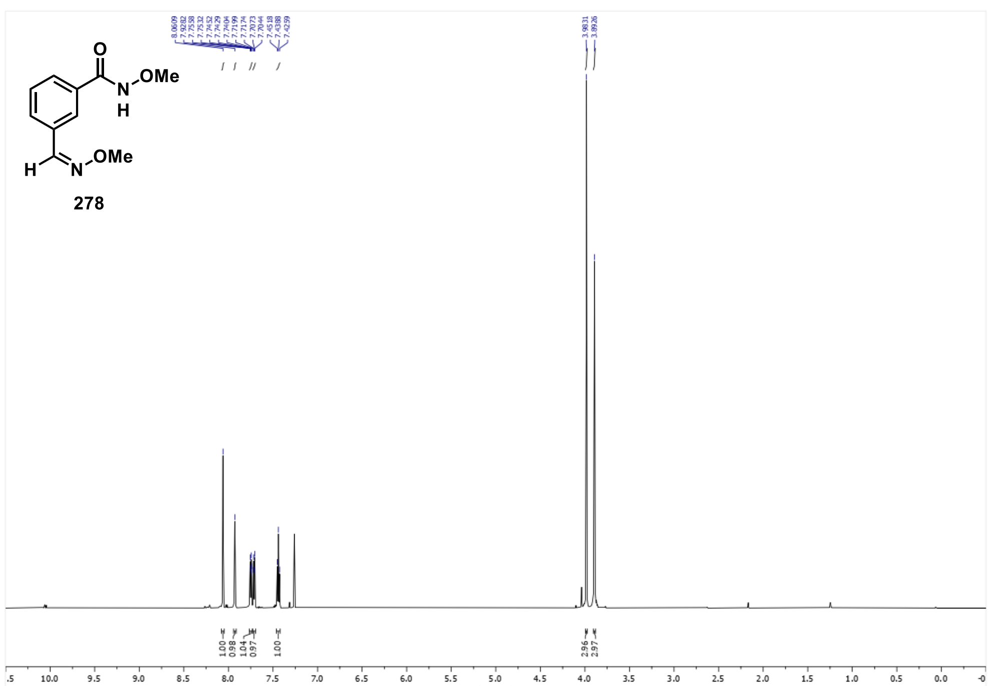

Figure 2.11: (Z)-*N*-Methoxy-3-((methoxyimino)methyl)benzamide (**278**); ^{1}H NMR (600 MHz, $CDCl_3$) at 24.8 °C.

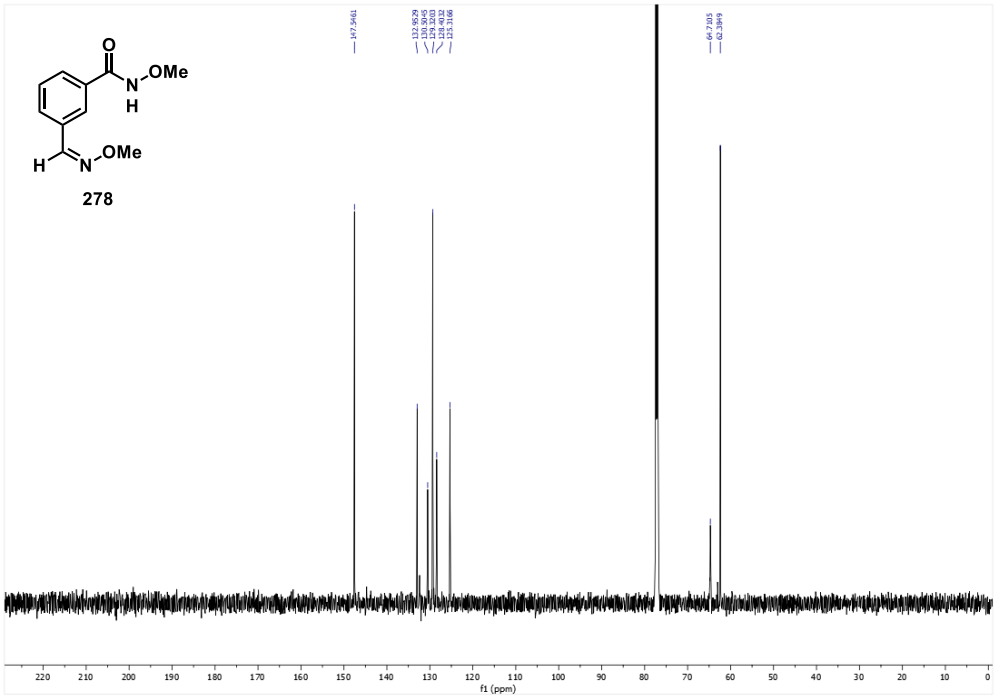

Figure 2.12: (Z)-*N*-Methoxy-3-((methoxyimino)methyl)benzamide (**278**); ^{13}C NMR (600 MHz, $CDCl_3$) at 24.8 °C.

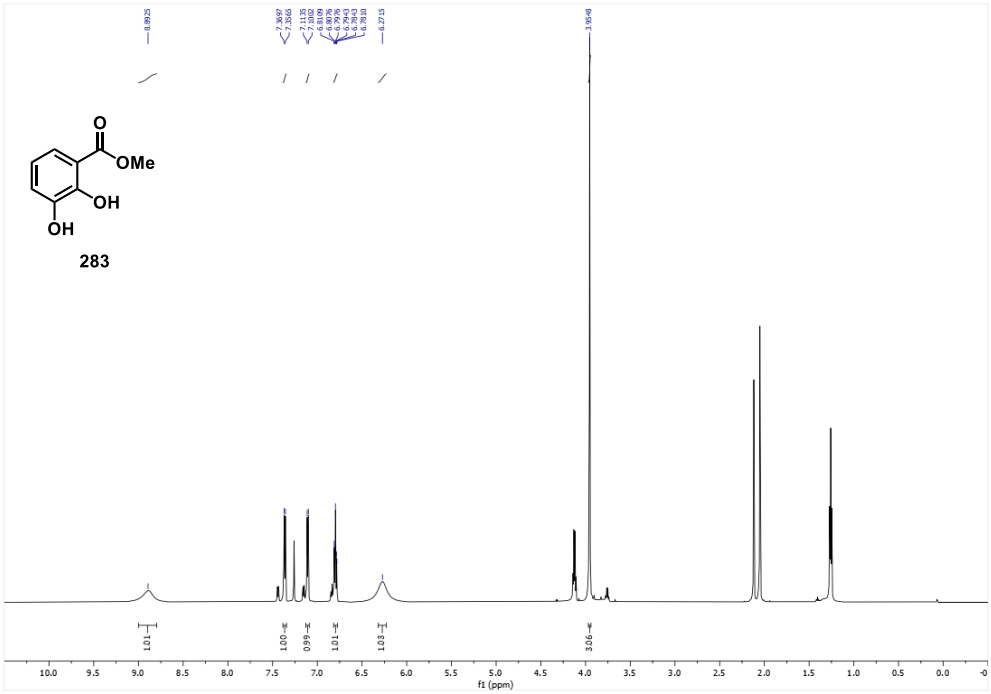

Figure 2.13: Methyl 2,3-dihydroxybenzoate (**283**); ^{1}H NMR (600 MHz, $CDCl_3$) at 24.8 °C.

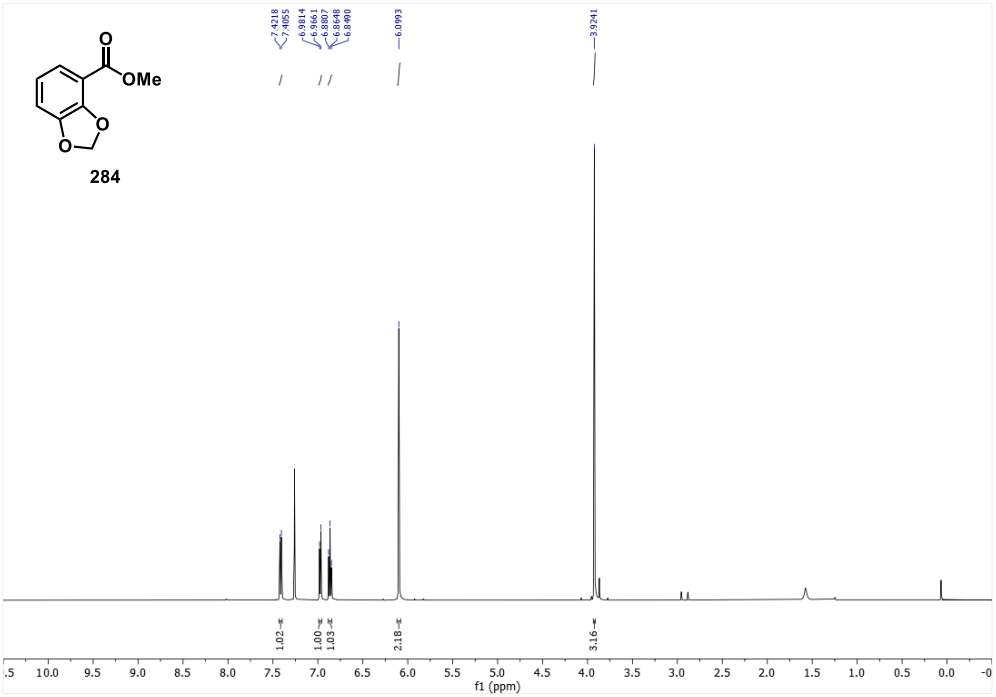

Figure 2.14: Methyl benzo[1,3]dioxole-4-carboxylate (**284**); ^{1}H NMR (500 MHz, $CDCl_3$) at 24.8 °C.

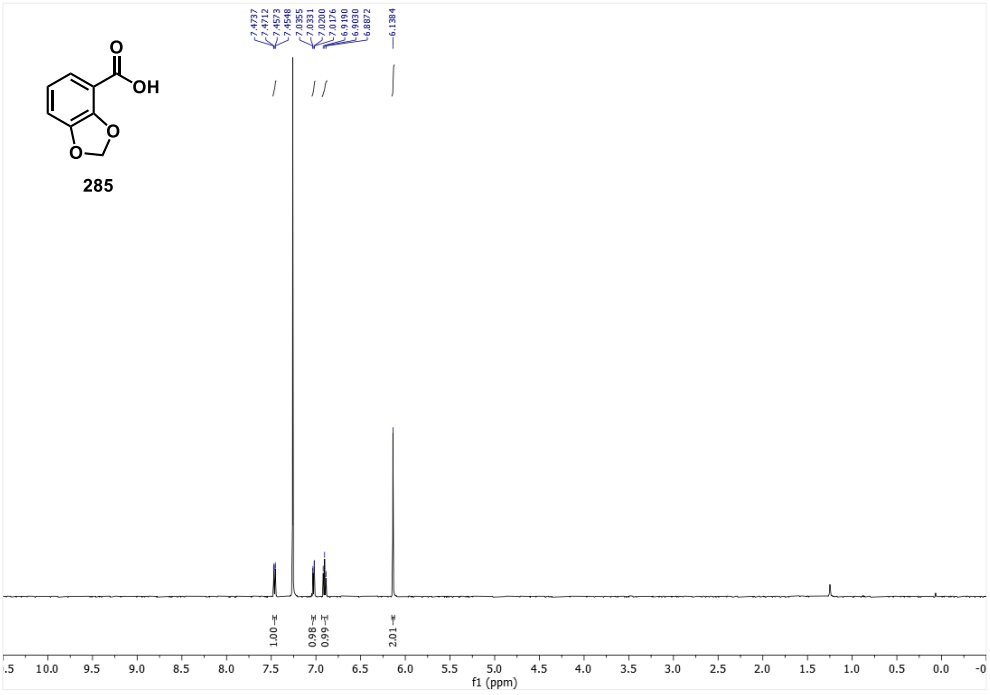

Figure 2.15: Benzo[1,3]-dioxole-4-carboxylic acid (**285**); ^{1}H NMR (500 MHz, $CDCl_3$) at 24.8 °C.

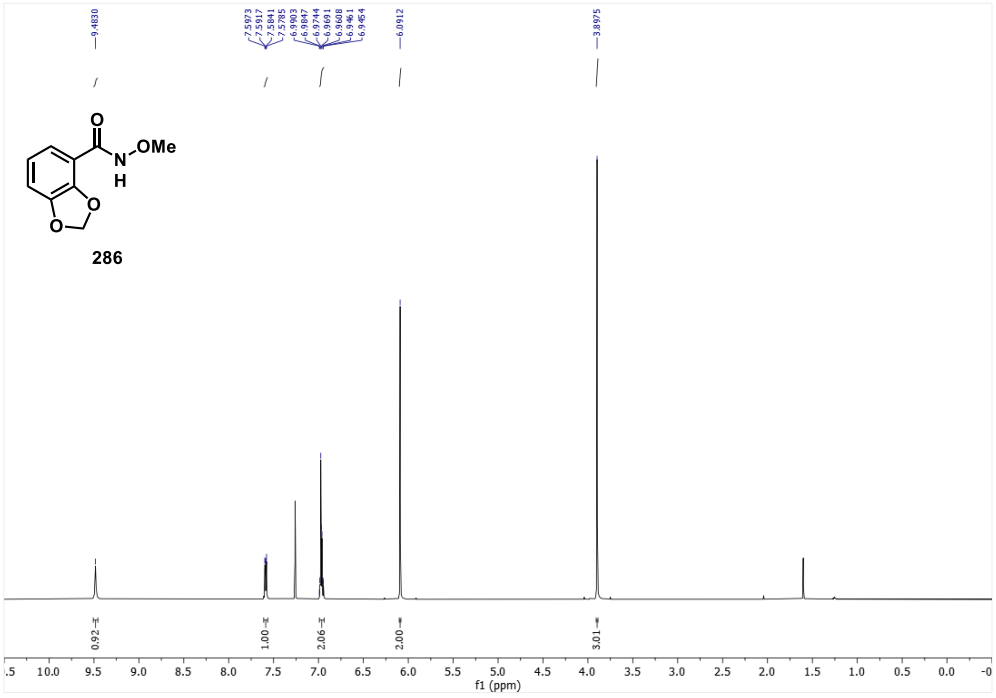

Figure 2.16: N-Methoxybenzo[1,3]dioxole-4-carboxamide (**286**); ^{1}H NMR (500 MHz, $CDCl_3$) at 24.8 °C.

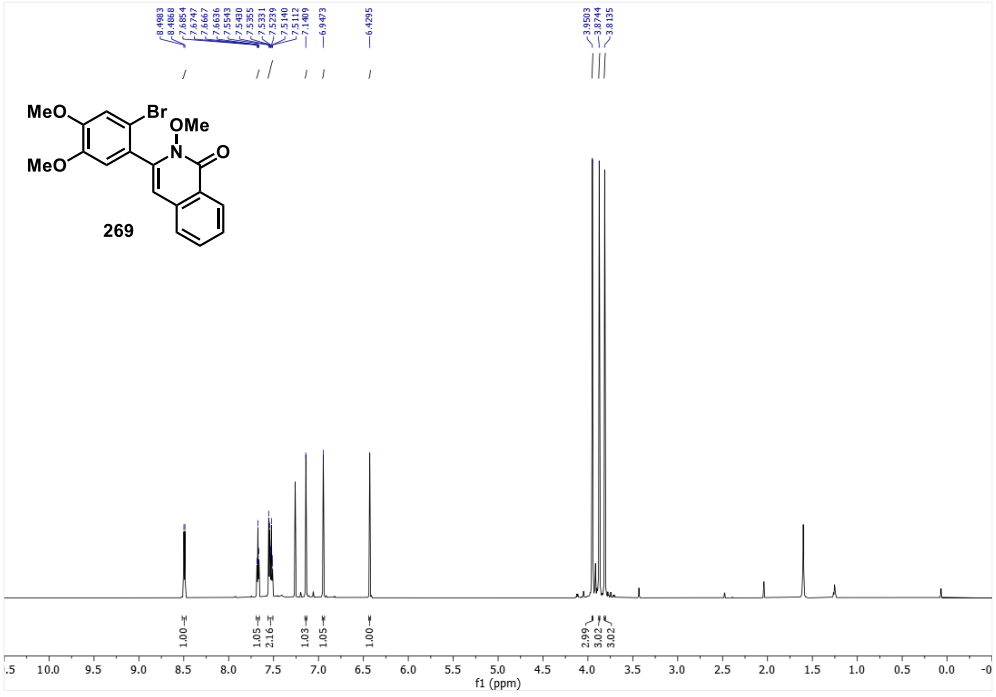

Figure 2.17: 3-(2-Bromo-4,5-dimethoxyphenyl)-2-methoxyisoquinolin-1(2H)-one (**269**); ^{1}H NMR (700 MHz, $CDCl_3$) at 24.8 °C.

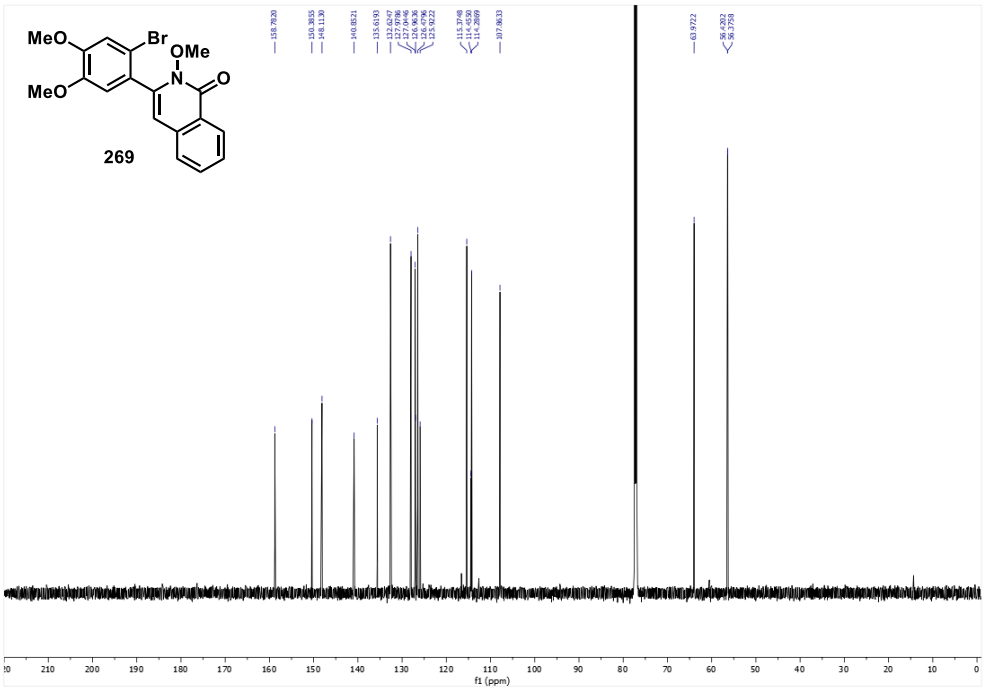

Figure 2.18: 3-(2-Bromo-4,5-dimethoxyphenyl)-2-methoxyisoquinolin-1(2H)-one (**269**); ^{13}C NMR (700 MHz, $CDCl_3$) at 24.8 °C.

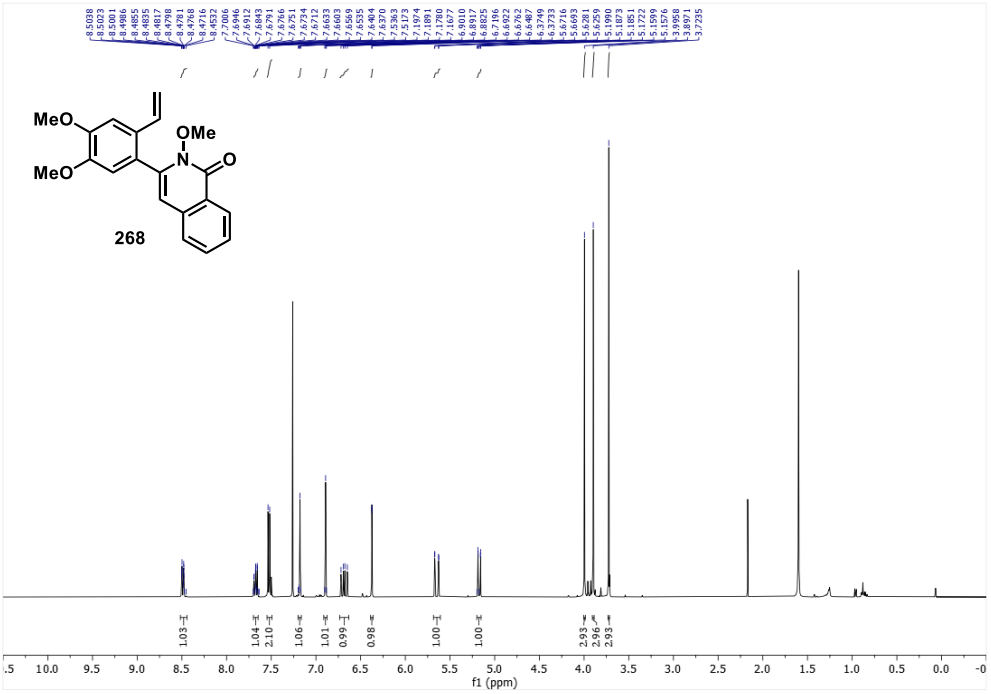

Figure 2.19: 3-(4,5-Dimethoxy-2-vinylphenyl)-2-methoxyisoquinolin-1(2H)-one (**268**); ^{1}H NMR (400 MHz, $CDCl_3$) at 21.9 °C.

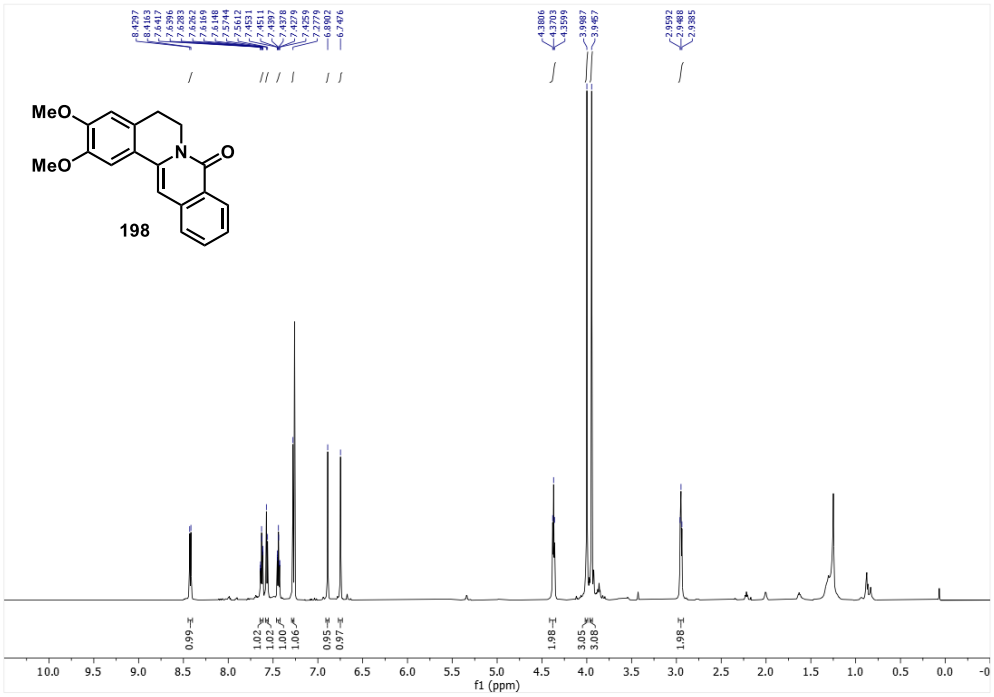

Figure 2.20: 2,3-Dimethoxy-5,6-dihydro-8H-isoquinolin-8-one (**198**); ^{1}H NMR (700 MHz, $CDCl_3$) at 24.8 °C.

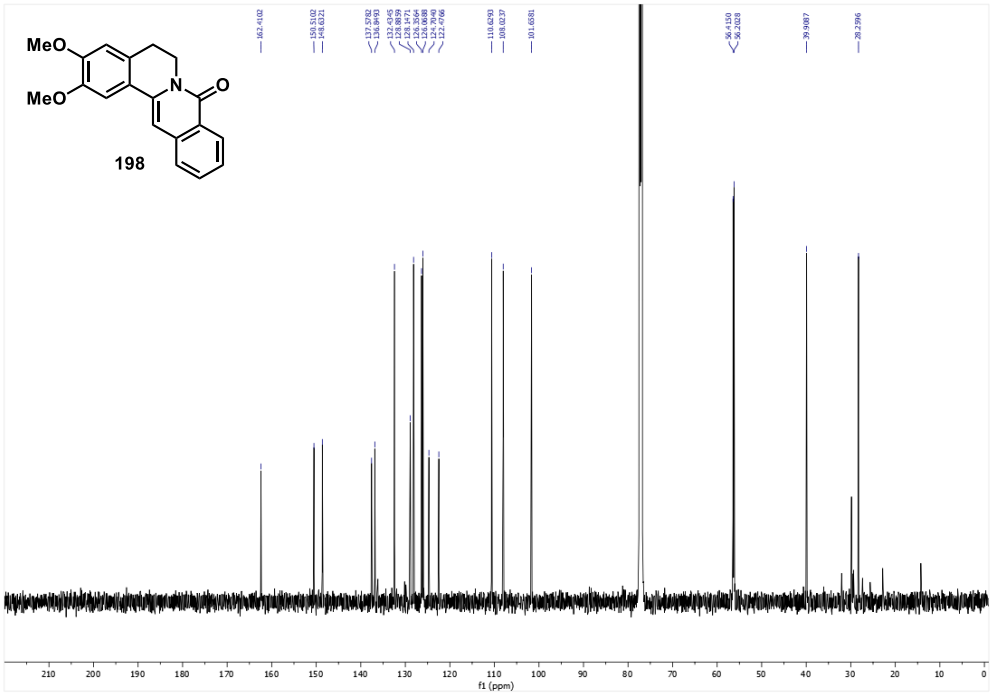

Figure 2.21: 2,3-Dimethoxy-5,6-dihydro-8H-isoquinolin-8-one (**198**); ^{13}C NMR (700 MHz, $CDCl_3$) at 24.8 °C.

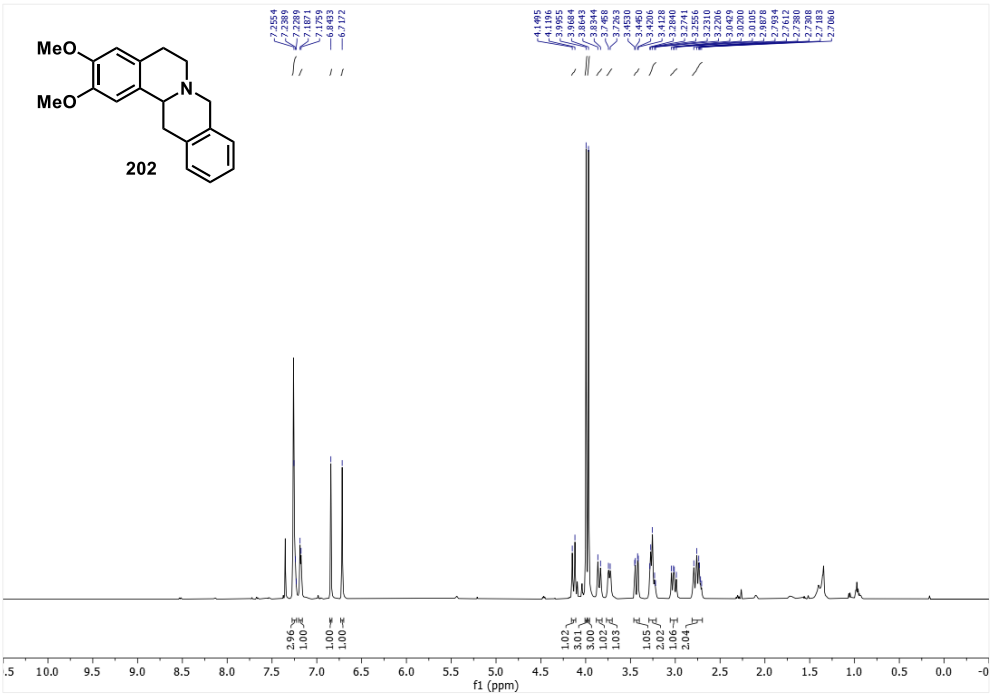

Figure 2.22: 2,3-Dimethoxy-5,8,13,13a-tetrahydro-6H-isoquinoline (**202**); ^{1}H NMR (500 MHz, $CDCl_3$) at 24.8 °C.

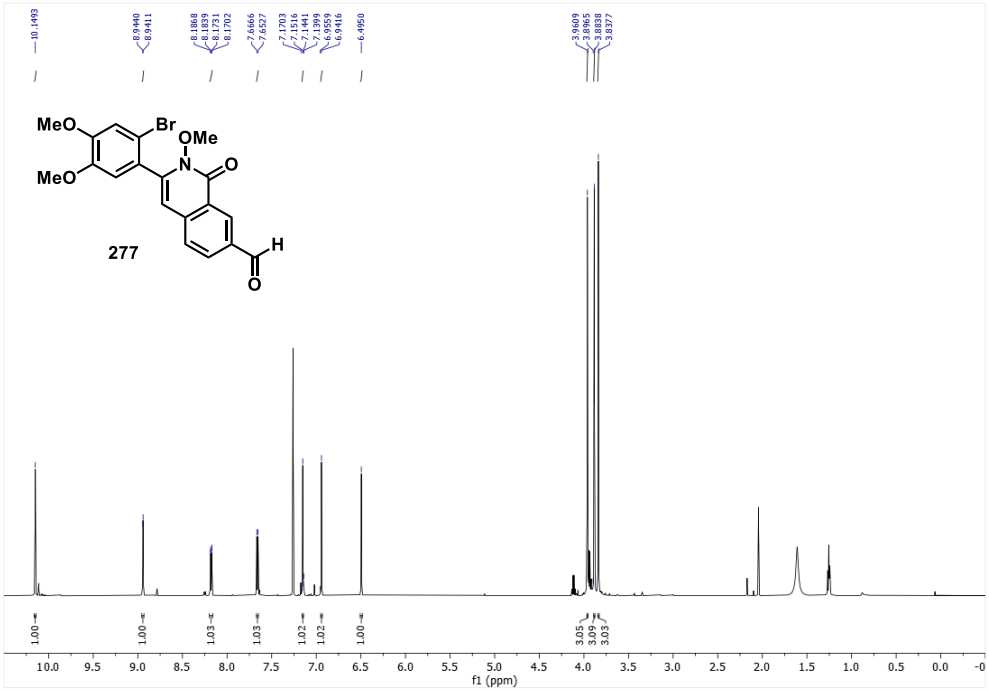

Figure 2.23: 3-(2-Bromo-4,5-dimethoxyphenyl)-2-methoxy-1-oxo-1,2-dihydroisoquinoline-7-carbaldehyde (**277**); ^{1}H NMR (600 MHz, $CDCl_3$) at 24.8 °C.

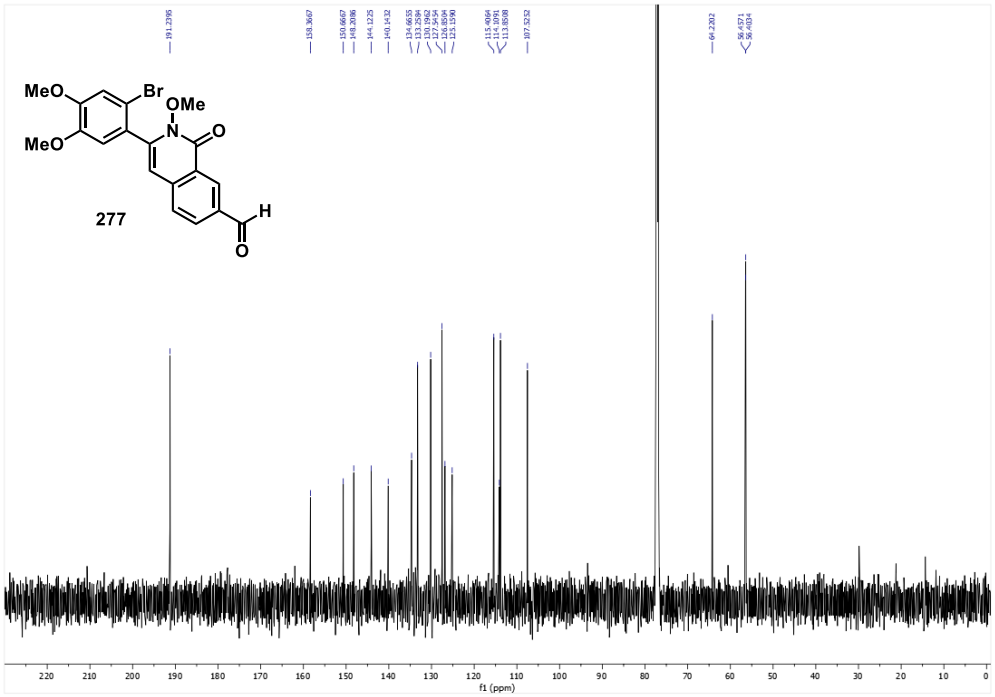

Figure 2.24: 3-(2-Bromo-4,5-dimethoxyphenyl)-2-methoxy-1-oxo-1,2-dihydroisoquinoline-7-carbaldehyde (**277**); ^{13}C NMR (600 MHz, $CDCl_3$) at 24.8 °C.

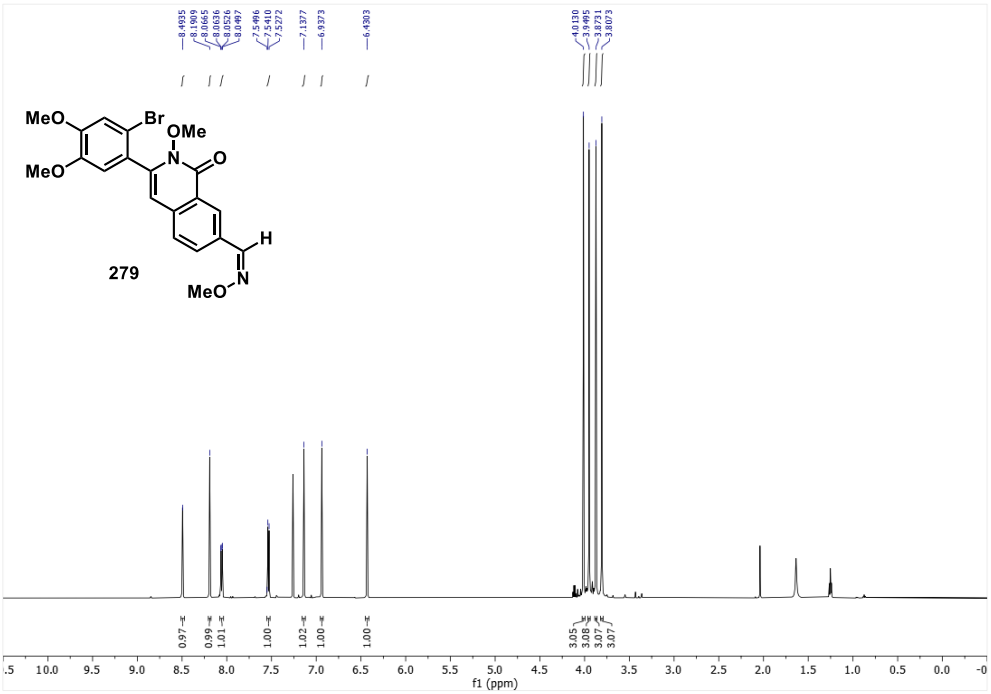

Figure 2.25: (Z)-3-(2-Bromo-4,5-dimethoxyphenyl)-2-methoxy-1-oxo-1,2-dihydroisoquinoline-7-carbaldehyde O-methyl oxime (**279**); ^{1}H NMR (600 MHz, $CDCl_3$) at 24.8 °C.

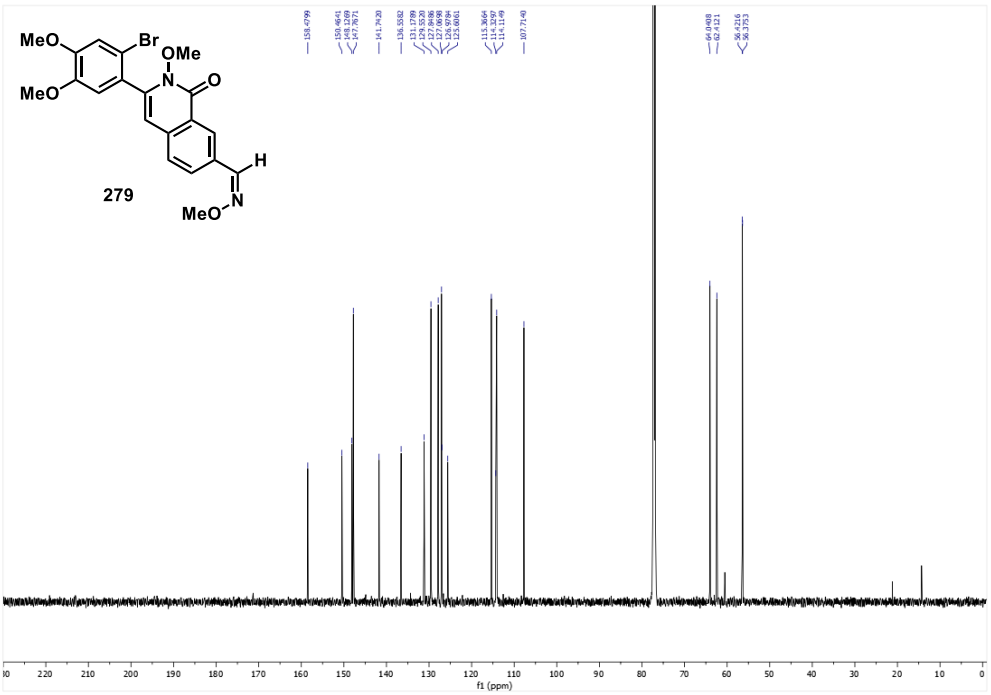

Figure 2.26: (Z)-3-(2-Bromo-4,5-dimethoxyphenyl)-2-methoxy-1-oxo-1,2-dihydroisoquinoline-7-carbaldehyde O-methyl oxime (**279**); ^{13}C NMR (600 MHz, $CDCl_3$) at 24.8 °C.

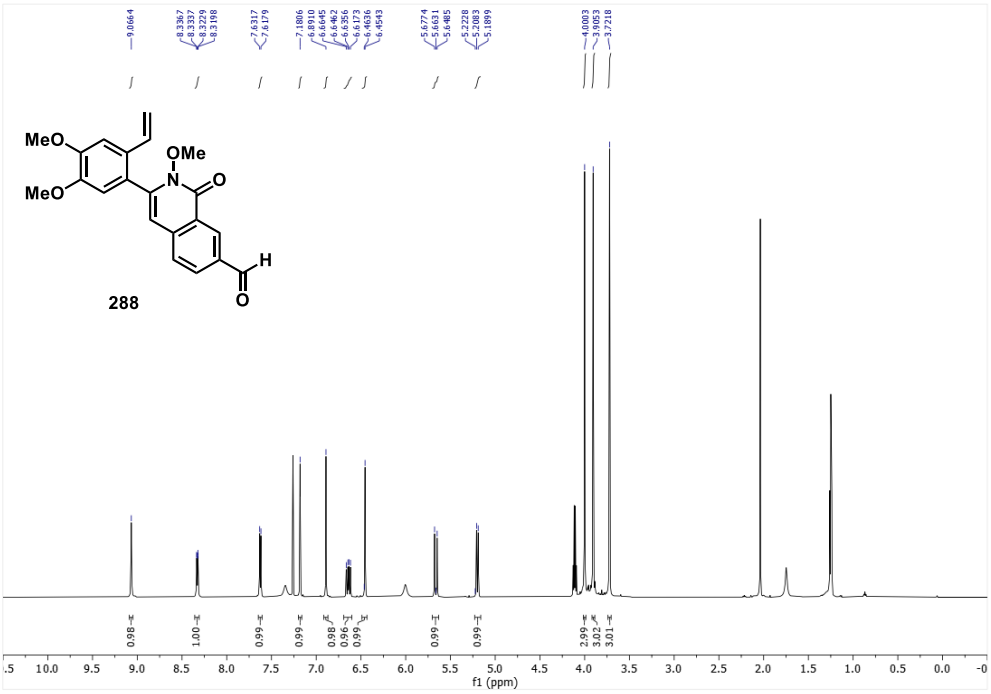

Figure 2.27: 3-(4,5-Dimethoxy-2-vinylphenyl)-2-methoxy-1-oxo-1,2-dihydroisoquinoline-7-carbaldehyde (**288**); ^{1}H NMR (600 MHz, $CDCl_3$) at 24.8 °C.

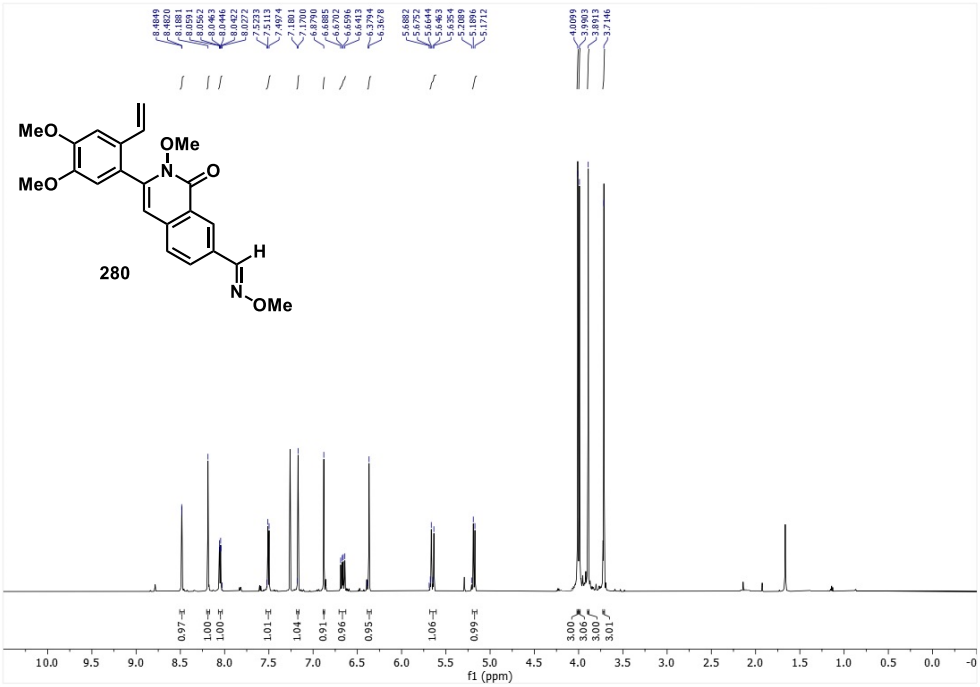

Figure 2.28: 3-(4,5-Dimethoxy-2-vinylphenyl)-2-methoxy-1-oxo-1,2-dihydroisoquinoline-7-carbaldehyde O-methyl oxime (**280**); ^{1}H NMR (600 MHz, $CDCl_3$) at 24.8 °C.

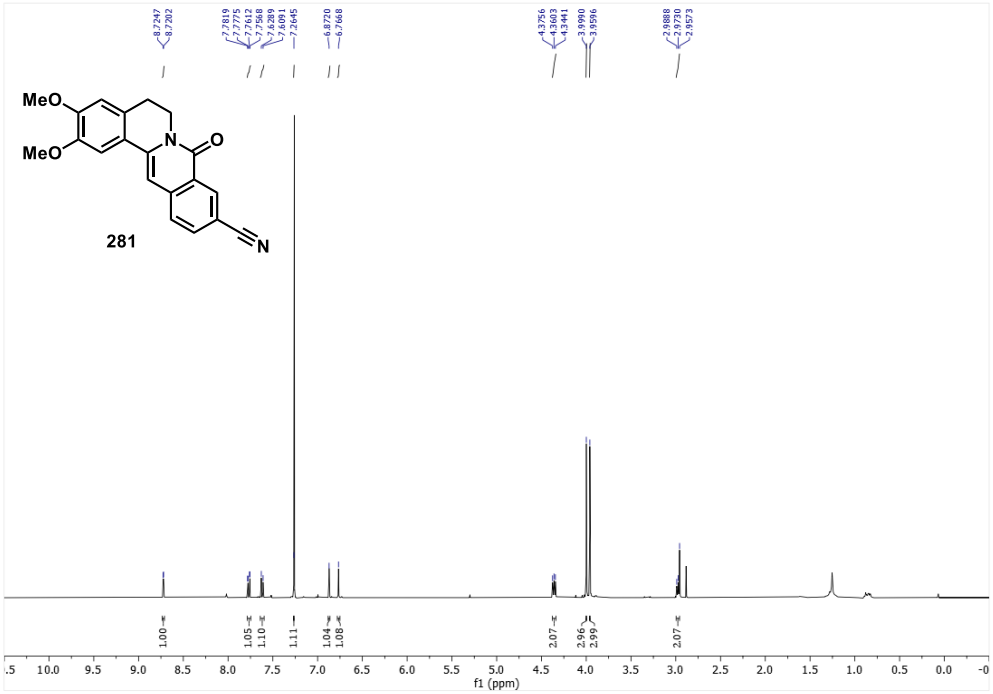

Figure 2.29: 2,3-Dimethoxy-8-oxo-5,8-dihydro-6H-isoquinolino[3,2-a]isoquinoline-10-carbonitrile (**281**); ^{1}H NMR (400 MHz, $CDCl_3$) at 21.9 °C.

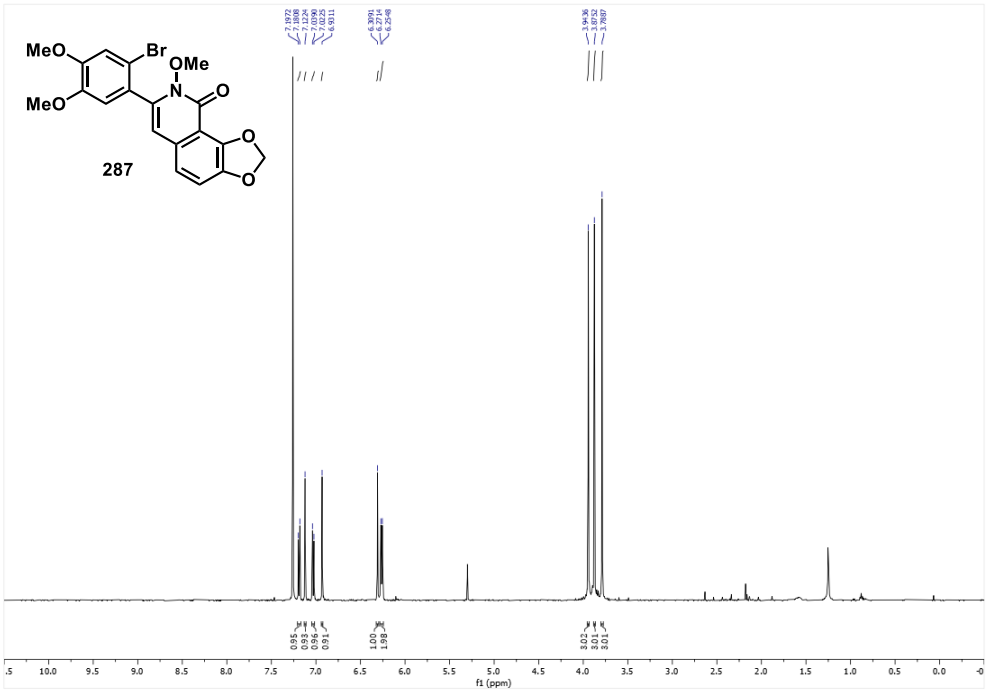

Figure 2.30: 7-(2-Bromo-4,5-dimethoxyphenyl)-8-methoxy-[1,3]dioxolo[4,5-h]isoquinolin-9(8H)-one (**287**); ^{1}H NMR (500 MHz, $CDCl_3$) at 24.8 °C.

2.7 References

(1) Zhang, E.; Jin, L.; Wang, Y.; Tu, J.; Zheng, R.; Ding, L.; Fang, Z.; Fan, M.; Al-Abdullah, I.; Natarajan, R.; Ma, K.; Wang, Z.; Riggs, A. D.; Shuck, S. C.; Yang, L.; Huang, W. Intestinal AMPK Modulation of Microbiota Mediates Crosstalk with Brown Fat to Control Thermogenesis. *Nat. Commun.,* **2022**, *13* (1), 1135. DOI: 10.1038/s41467-022-28743-5

(2) Steinberg, G. R.; Hardie, D. G. New Insights into Activation and Function of the AMPK. *Nat. Rev. Mol. Cell Biol.*, **2022**, 1–18. DOI: 10.1038/s41580-022-00547-x

(3) Carlson, C. A.; Kim, K.-H. Regulation of Hepatic Acetyl Coenzyme a Carboxylase by Phosphorylation and Dephosphorylation. *J. Biol. Chem.*, **1973**, *248* (1), 378–380. DOI: 10.1016/s0021-9258(19)44486-4

(4) Beg, Z. H.; Allmann, D. W.; Gibson, D. M. Modulation of 3-hydroxy-3-methylglutaryl coenzyme: a reductase activity with cAMP and with protein fractions of rat liver cytosol. *Biochem. Biophys. Res. Comm.*, **1973**, *54* (4), 1362–1369. DOI: 10.1016/0006-291x(73)91137-6

(5) Tarasiuk, O.; Miceli, M.; Di Domizio, A.; Nicolini, G. AMPK and Diseases: State of the Art Regulation by AMPK-Targeting Molecules. *Biology,* **2022**, *11* (7), 1041. DOI: 10.3390/biology11071041

(6) Kim, J.; Yang, G.; Kim, Y.; Kim, J.; Ha, J. AMPK Activators: Mechanisms of Action and Physiological Activities. *Exp. Mol. Med.*, **2016**, *48* (4), 224. DOI: 10.1038/emm.2016.16

(7) Steinberg, G. R.; Carling, D. AMP-Activated Protein Kinase: The Current Landscape for Drug Development. *Nat. Rev. Drug Discov.*, **2019**, *18* (7), 527–551. DOI: 10.1038/s41573-019-0019-2

(8) Jin, Y.; Liu, S.; Ma, Q.; Xiao, D.; Chen, L. Berberine Enhances the AMPK Activation and Autophagy and Mitigates High Glucose-Induced Apoptosis of Mouse Podocytes. *Eur. J. Pharmacol.*, **2017**, *794*, 106-114. DOI: 10.1016/j.ejphar.2016.11.037

(9) Sanz-Gómez, M.; Aledavood, E.; Beroiz-Salaverri, M.; Lagartera, L.; Vega-Martín, E.; Gil-Ortega, M.; Cumella, J.; Pérez, C.; Luque, F. J.; Estarellas, C.; Fernández-Alfonso, M. S.; Castro, A. Novel Indolic AMPK Modulators Induce Vasodilatation through Activation of the AMPK–ENOS–NO Pathway. *Sci. Rep.*, **2022**, *12* (1), 4225. DOI: 10.1038/s41598-022-07077-8

(10) Gongol, B.; Sari, I.; Bryant, T.; Rosete, G.; Marin, T. AMPK: An Epigenetic Landscape Modulator. *Int. J. Mol. Sci.*, **2018**, *19* (10), 3238. DOI: 10.3390/ijms19103238

(11) Rana, S.; Blowers, E. C.; Natarajan, A. Small Molecule Adenosine 5′-Monophosphate Activated Protein Kinase (AMPK) Modulators and Human Diseases. *J. Med. Chem.*, **2014**, *58* (1), 2–29. DOI: 10.1021/jm401994c

(12) Heidary Moghaddam, R.; Samimi, Z.; Asgary, S.; Mohammadi, P.; Hozeifi, S.; Hoseinzadeh-Chahkandak, F.; Xu, S.; Farzaei, M. H. Natural AMPK Activators in Cardiovascular Disease Prevention. *Front. Pharmacol.*, **2022**, *12*. DOI: 10.3389/fphar.2021.738420

(13) Vara-Ciruelos, D.; Russell, F. M.; Hardie, D. G. The Strange Case of AMPK and Cancer: Dr Jekyll or Mr Hyde? *Open Biol.*, **2019**, *9* (7), 190099. DOI: 10.1098/rsob.190099

(14) Laderoute, K.; Calaoagan, J. M.; Madrid, P. B.; Klon, A. E.; Ehrlich, P. J. SU11248 (Sunitinib) Directly Inhibits the Activity of Mammalian 5'-AMP-Activated Protein Kinase (AMPK). *Cancer Biol. Ther.*, **2010**, *10* (1), 68–76. DOI: 10.4161/cbt.10.1.12162

(15) Manley, P. W.; Weisberg, E.; Sattler, M.; Griffin, J. D. Midostaurin, a Natural Product-Derived Kinase Inhibitor Recently Approved for the Treatment of Hematological Malignancies. *Biochem.*, **2017**, *57* (5), 477–478. DOI: 10.1021/acs.biochem.7b01126

(16) Meng, G.; Liu, C.; Qin, S.; Dong, M.; Wei, X.; Zheng, M.; Qin, L.; Wang, H.; He, X.; Zhang, Z. An Improved Synthesis of Sunitinib Malate via a Solvent-Free Decarboxylation Process. *Res. Chem. Intermed.*, **2015**, *41* (11), 8941–8954. DOI: 10.1007/s11164-015-1939-z

(17) Valipour,M.; Khatir, Z. Z.; Abdollahi, E.; Ayati, A. Recent Applications of Protoberberines as Privileged Starting Materials for the Development of Novel Broad-Spectrum Antiviral Agents: A Concise Review (2017–2023). *ACS Pharmacol. Transl. Sci.*, **2024**, *7* (1), 48-71. DOI: 10.1021/acsptsci.3c00292

(18) Roy, N. S.; Choi, I.; Um, T.; Jeon, M. J.; Kim, B.; Kim, Y. D.; Yu, J.; Kim, S.; Kim, N. Gene Expression and Isoform Identification of PacBio Full-Length CDNA Sequences for Berberine Biosynthesis in Berberis Koreana. *Plants*, **2021**, *10* (7), 1314–1314. DOI: 10.3390/plants10071314

(19) Singh,S.; Pathak,N.; Fatima, E.; Negi, A. S. Plant Isoquinoline Alkaloids: Advances in the Chemistry and Biology of Berberine. *Eur. J. Med. Chem.*, **2021**, *226*, 113839. DOI: 10.1016/j.ejmech.2021.113839

(20) Roy, N. S.; Park, N.-I.; Kim, N.-S.; Park, Y.; Kim, B.-Y.; Kim, Y.-D.; Yu, J.-K.; Kim, Y.-I.; Um, T.; Kim, S.; Choi, I.-Y. Comparative Transcriptomics for Genes Related to Berberine and Berbamine Biosynthesis in Berberidaceae. *Plants*, **2022**, *11* (20), 2676. DOI: 10.3390/plants11202676

(21) Winkler, A.; Łyskowski, A.; Riedl, S.; Puhl, M.; Kutchan, T. M.; Macheroux, P.; Gruber, K. A Concerted Mechanism for Berberine Bridge Enzyme. *Nat. Chem. Bio.*, **2008**, *4* (12), 739–741. DOI: 10.1038/nchembio.123

(22) Han, J.; Li, S. De Novo Biosynthesis of Berberine and Halogenated Benzylisoquinoline Alkaloids in Saccharomyces Cerevisiae. *Commun. Chem.*, **2023**, *6* (1). DOI: 10.1038/s42004-023-00821-9

(23) Sharma, M.; Koul, A.; Sharma, D.; Kaul, S.; Swamy, M. K.; Dhar, M. K. Metabolic Engineering Strategies for Enhancing the Production of Bio-Active Compounds from Medicinal Plants. *Nat. Bioact. Compd.*, **2019**, 287–316. DOI: 10.1007/978-981-13-7438-8_12

(24) Mora-Vásquez, S.; Wells-Abascal, G. G.; Espinosa-Leal, C.; Cardineau, G. A.; García-Lara, S. Application of Metabolic Engineering to Enhance the Content of Alkaloids

in Medicinal Plants. *Metab. Eng. Commun.*, **2022**, *14*, e00194. DOI: 10.1016/j.mec.2022.e00194

(25) Huang, P.; Liu, W.; Xu, M.; Jiang, R.; Xia, L.; Wang, P.; Li, H.; Tang, Z.; Zheng, Q.; Zeng, J. Modulation of Benzylisoquinoline Alkaloid Biosynthesis by Overexpression Berberine Bridge Enzyme in Macleaya Cordata. *Sci. Rep.*, **2018**, *8* (1). DOI: 10.1038/s41598-018-36211-8

(26) Ninomiya, I.; Naito, T. Novel Total Synthesis of Protoberberine-Type Alkaloids. *J. Chem. Soc.*, **1973**, No. 4, 137–137. DOI: 10.1039/c39730000137

(27) Cutter, P. S.; Miller, R. Bryan.; Schore, N. E. Synthesis of Protoberberines Using a Silyl-Directed Pictet–Spengler Cyclization. *Tetrahedron*, **2002**, *58* (8), 1471–1478. DOI: 10.1016/s0040-4020(02)00010-8

(28) Gatland, A. E.; Pilgrim, B. S.; Procopiou, P. A.; Donohoe, T. J. Short and Efficient Syntheses of Protoberberine Alkaloids Using Palladium-Catalyzed Enolate Arylation. *Angew. Chem. Int. Ed.*, **2014**, *53* (52), 14555–14558. DOI: 10.1002/anie.201409164

(29) Tajiri, M.; Yamada, R.; Hotsumi, M.; Makabe, K.; Konno, H. The Total Synthesis of Berberine and Selected Analogues, and Their Evaluation as Amyloid Beta Aggregation Inhibitors. *Eur. J. Med. Chem.*, **2021**, *215*, 113289. DOI: 10.1016/j.ejmech.2021.113289

(30) Martins, G. M.; Zeni, G.; Back, D. F.; Teodoro Saul Kaufman; Silveira, C. C. Expedient Iodocyclization Approach toward Polysubstituted 3*H*-Benzo[*E*]Indoles. *Adv. Synth. Catal.*, **2015**, *357* (14-15), 3255–3261. DOI: 10.1002/adsc.201500275

(31) Chang, X.; Ma, P.; Chen, H.; Li, C.; Wang, P. Asymmetric Synthesis and Application of Chiral Spirosilabiindanes. *Angew. Chem.*, **2020**, *132* (23), 9022–9025. DOI: 10.1002/ange.202002289

(32) Lee, C.-L. K.; Loh, T.-P. Gram-Scale Synthesis of (−)-Epibatidine. *Org. Lett.*, **2005**, *7* (14), 2965–2967. DOI: 10.1021/ol0508911

(33) Kou, X.; Kou, K. G. M. α-Arylation of Silyl Enol Ethers via Rhodium(III)-Catalyzed C–H Functionalization. *ACS Catal.*, **2020**, *10* (5), 3103–3109. DOI: 10.1021/acscatal.9b05622

(34) Huang, Z.; Liu, Y.; Li, Y.; Xiong, L.; Cui, Z.; Song, H.; Liu, H.; Zhao, Q.; Wang, Q. Synthesis, Crystal Structures, Insecticidal Activities, and Structure−Activity Relationships of Novel *N*′-*Tert*-Butyl-*N*′-Substituted-Benzoyl-*N*-[Di(Octa)Hydro]Benzofuran{(2,3-Dihydro)Benzo[1,3]([1,4])Dioxine}Carbohydrazide Derivatives. *J. Agric. Food Chem.*, **2010**, *59* (2), 635–644. DOI: 10.1021/jf104196t

(35) Li, L.; Okumu, A.; Dellos-Nolan, S.; Li, Z.; Karmahapatra, S.; English, A.; Yalowich, J. C.; Wozniak, D. J.; Mitton-Fry, M. J. Synthesis and Anti-Staphylococcal Activity of Novel Bacterial Topoisomerase Inhibitors with a 5-Amino-1,3-Dioxane Linker Moiety. *Bioorg. Med. Chem. Lett.*, **2018**, *28* (14), 2477–2480. DOI: 10.1016/j.bmcl.2018.06.003

(36) Wu, L.-H.; Cheng, J.-K.; Shen, L.; Shen, Z.-L.; Loh, T.-P. Visible Light-Mediated Trifluoromethylation of Fluorinated Alkenes via C−F Bond Cleavage. *Adv. Synth. Catal.*, **2018**, *360* (20), 3894–3899. DOI: 10.1002/adsc.201800740

(37) Zhou, S.; Tong, R. A General, Concise Strategy That Enables Collective Total Syntheses of over 50 Protoberberine and Five Aporhoeadane Alkaloids within Four to Eight Steps. *Chem. Eur. J.*, **2016**, *22* (21), 7084–7089. DOI: 10.1002/chem.201601245

Chapter 3 – Co-Catalyzed C–H Functionalization of *N*-Methoxybenzamides with Electron-Rich Ynamides

3.1 Introduction

3.1.1 Applications of C–H Functionalization

Transition-metal-catalyzed synthetic transformations represent versatile strategies for discovering and developing new molecules across various applications.[1-5] However, their typical reliance on prefunctionalized starting materials to control chemo- and regio-selectivity poses inherent challenges. This approach is constrained by the limited availability of prefunctionalized precursors compared to unfunctionalized feedstock chemicals, restricting their applicability to complex molecules like natural products or pharmaceuticals. To overcome these limitations, chemists have developed a broad range of methods for installing synthetically useful functional handles.[1-5] Many of these methods involve multistep procedures, which can lead to reduced step-economy, synthetic inefficiency, and waste. Thus, there is a growing need for new catalytic methods enabling direct functionalization of typically inert C−H bonds.

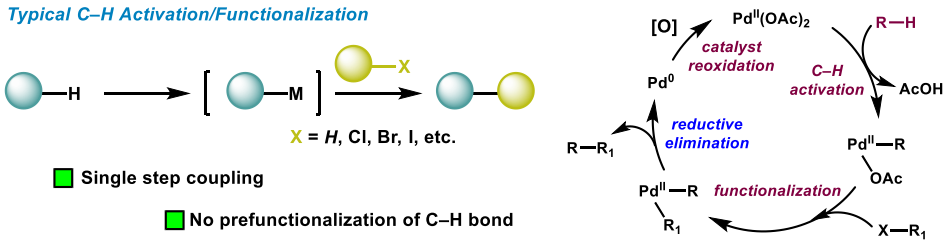

Figure 3.1: Generalization of typical C−H functionalization.

Despite the conventional view of C−H bonds as inert, recent advancements have led to the development of synthetic methods capable of direct C−H bond functionalization

with various coupling partners. This advancement offers significant improvements in step-economy and overall sustainability, enabling innovative synthetic routes and strategic disconnections (Figure 3.1).[1-5] However, many developed methods are limited to relatively simple substrates with few functional groups or limited molecular complexity.

Late-stage functionalization (LSF) has emerged as a valuable approach, allowing chemoselective transformations on complex molecules without the need for installing functional groups solely to facilitate the reaction.[1-5] The collective goal of LSF is to achieve chemoselective transformations on complex molecules without the need for installing functional groups exclusively for this purpose.[1-5] This approach allows for more effective use of synthetic resources and contributes to the overall sustainability of synthetic methodologies.[1-5] While transition-metal-catalyzed synthetic transformations offer versatile strategies for molecule discovery, overcoming the limitations associated with prefunctionalized starting materials is essential for expanding their applicability to complex molecular systems.[1-5] The development of efficient catalytic methods for direct C−H bond functionalization represents a promising avenue for achieving this goal and advancing the field of synthetic chemistry.

The capacity to selectively modify individual C−H bonds within complex molecular environments enables the efficient synthesis of diverse compound libraries with minimal effort and time.[6] Moreover, when paired with modular coupling partners, this approach facilitates combinatorial strategies in SARs and exploration of chemical space.[6] By introducing subtle molecular modifications through C−H functionalization reactions, adjustments in pharmacokinetic and physicochemical properties such as potency,

selectivity, solubility, and stability become feasible.[6,7] The advent of innovative techniques like high-throughput experimentation and modern chemoinformatics further enhances the potential of C−H functionalization reactions in discovering and developing biologically relevant molecules.[6,7]

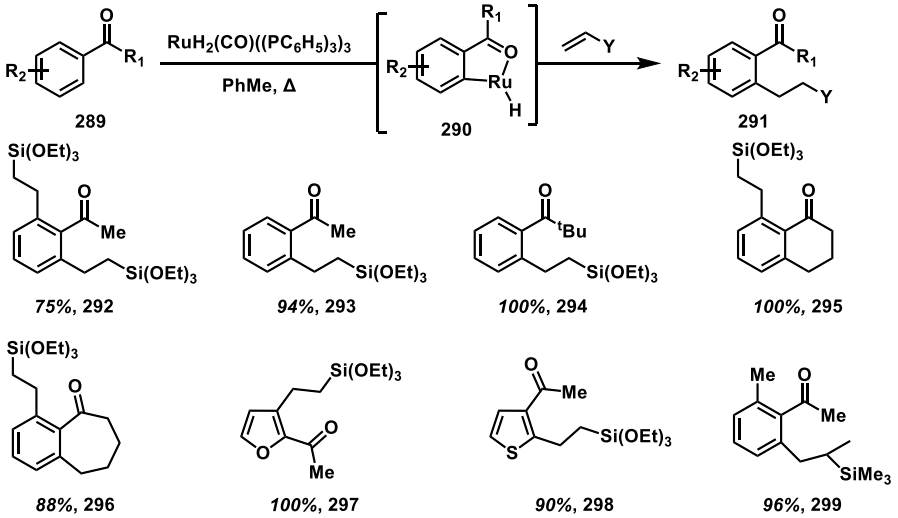

Scheme 3.1: Ruthenium-catalyzed *ortho*-alkylation of aryl ketones by Murai and co-workers.

3.1.2 C(sp^2)−H Alkenylation Strategies

The challenge of efficiently functionalizing C−H bonds arises from their high bond dissociation enthalpy and their presence throughout organic molecules.[8-11] A common approach to address this challenge involves employing a directing group, typically a weakly coordinating Lewis-basic group.[8-11] This group coordinates to the transition-metal catalyst, guiding reactivity towards a specific C−H bond. Although template directing groups exist that can direct reactivity to more distal C−H bonds, typically this method allows functionalization at the position *ortho*-, or in other words the closest C−H bond to the directing group substituent. An early instance of such reactivity was reported by Murai and co-workers in 1993, showcasing the *ortho*-alkylation of aryl ketone substrates (**289**)

using ruthenium catalysis (Scheme 3.1).[8-11] This involves ruthenium complex **290** as an intermediate after C−H activation, which is disconnected from the arene upon migratory insertion leading to alkylated examples (**291**). Subsequently, numerous reports of directed C−H activation have emerged, employing various transition metals, directing groups, and coupling partners, thereby expanding the chemistry feasible with directed C−H functionalization.[11] More recently, there has been an increased emphasis on developing methodologies that can accommodate sensitive functional groups and greater structural complexity.[11] This allows for the utilization of this chemistry in the late-stage functionalization and diversification of molecules.[11]

Despite the wide array of C−H functionalization techniques available, our laboratory's prior research on the α-arylation of electron-rich silyl enol ethers has motivated us to explore the *ortho* C−H activation of *N*-methoxybenzamides using alternative electron-rich substrates. Over the past two decades, metal-catalyzed C−H alkenylation and cyclization protocols have been extensively studied.[12] Various transition metals, in conjunction with directing groups, have yielded significant and valuable results in terms of reactivity and selectivity.[12] A wide range of chemists developed diverse protocols for the alkenylation of simple molecules, and once optimal reaction conditions were established, these methods were extended to facilitate the late-stage functionalization of molecules with greater structural complexity. Yu et al. reported the palladium-catalyzed C−H alkenylation of phenylacetic amides (**300**) with unactivated alkenes, involving the functionalization of two C(sp^2)−H bonds (Scheme 3.2).[20] The use of substoichiometric quantities of pyridine and quinoline ligands proved crucial for achieving satisfactory results in terms of reactivity

and selectivity. The reaction was conducted at 100 °C, employing oxygen as a terminal oxidant, and one equivalent of $Cu(OAc)_2$ as a co-oxidant in DCE as the solvent.[20] This methodology was successfully applied to the olefination of ibuprofen (**303**), naproxen (**304**), and ketoprofen (**305**) analogs, resulting in good yields and moderate linear-to-branched olefin selectivity.[20] It is noteworthy that the C−H olefination reaction using unactivated alkenes remains a challenging aspect of organic synthesis methodology.

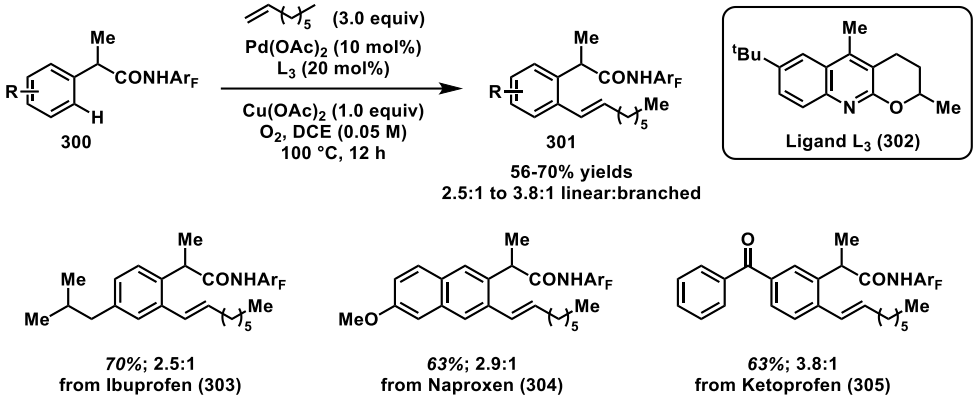

Scheme 3.2: Palladium-catalyzed *ortho*-alkenylation with unactivated olefins.

Yi and co-workers introduced an alternative approach to access *ortho*-alkenylated phenols (**309**) in 2012 using ruthenium catalysis, where alcohols (**307**) and diols (**308**) were employed in a dehydrative mechanism instead of directly using alkenes as reagents (Scheme 3.3).[21] Initially, the authors focused on the alkylation of phenols with alcohols, and upon optimizing this reaction, they expanded the method to produce styrenes and benzofuran derivatives via a tandem alkylation/dehydrogenation process.[21] A notable aspect of both reactions was the utilization of cyclopentene as a sacrificial hydrogen acceptor during the C−H activation step.[21] Alcohols yielded olefinated products (**309**), while 1,2-diols led to benzofuran derivatives (**310**). The developed alkenylation reaction

proved successful for six different substrates using two distinct approaches: alkenylation of the drug-like molecule and utilizing the drug molecule as the alkenylation partner.[21]

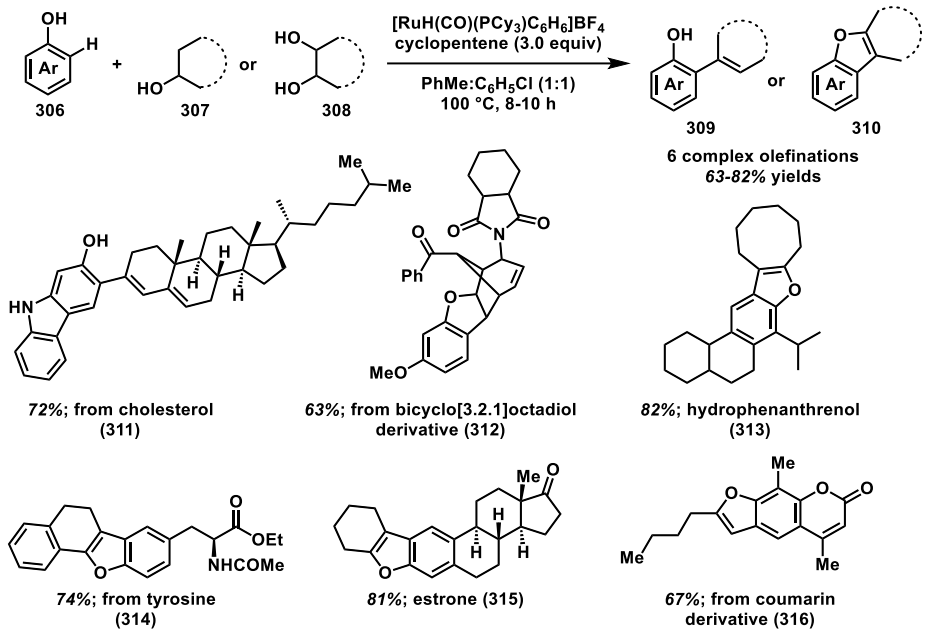

Scheme 3.3: Ruthenium-catalyzed *ortho*-alkenylation by Yi and co-workers.

Recently, Hou et. al reported the scandium-catalyzed dearomative spiro-annulation of quinolines (**317**) with alkynes (Scheme 3.4).[22] The quinoline group of starting materials resembling **317** served as a directing group, enabling ortho-selective C−H activation with an enantiopure cyclopentadienyl scandium catalyst, followed by alkenylation via alkyne insertion.[22] The intermediate **319** was formed through intramolecular 1,2-addition of the scandium-alkenyl bond to the C−N double bond of the quinoline ring, which eventually yielded dearomatized enantioenriched products (**318**).[22] Excellent yields and enantioselectivities were achieved using simple starting materials, while good yields and modest to good enantioselectivities were obtained for more complex molecules like **321**.

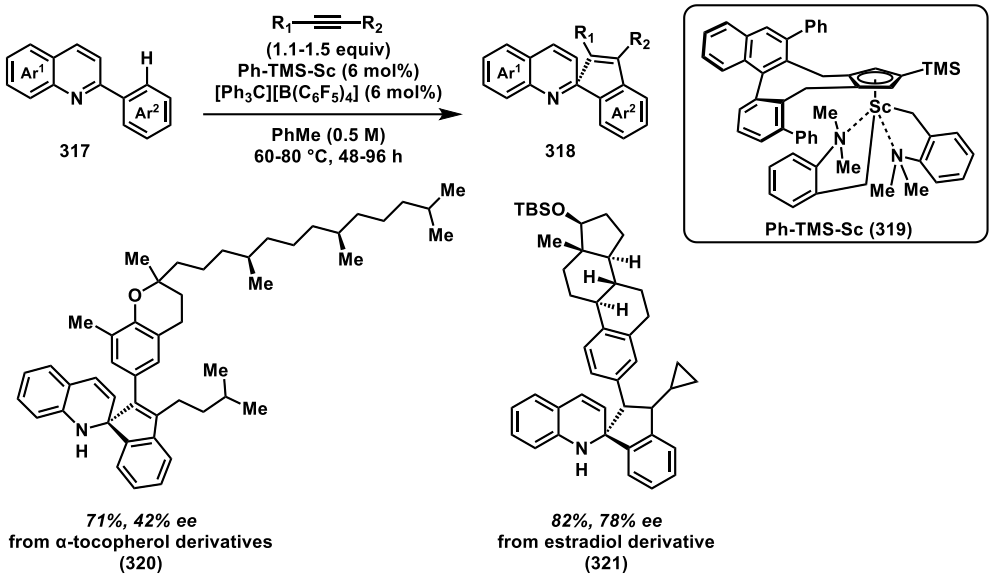

Scheme 3.4: Scandium-catalyzed *ortho*-alkenylation and spiro-annulation.

Using manganese catalysis and NaOAc as an additive, Ackermann and collaborators reported Mn(I)-catalyzed hydroarylation of alkynes (**323**) using N-(2-pyridine)tryptophan derivatives (**322**) (Scheme 3.5).[23] Complex peptides containing a tryptophan coupling partner yielded product yields of 65−88% (**324**), including peptides containing another tryptophan unit that regioselectively afforded products using N-(2-pyridine) as a directing group.[23] The reaction also tolerated biomolecule-derived alkyne, obtaining five mixed tryptophan derivatives in 72−95% yield. Additionally, self-assembled macrocyclization was described for the formation of 16 cyclic peptides (**327**) ranging from 15 to 22-membered ring sizes (**328**), achieving yields of 37−74% (**329**, **330**, and **331**).[23] These methods show successful developments in the area of C–H functionalization, specifically by incorporating the use of less toxic metals in attempts to uphold the "12 Principles of Green Chemistry".

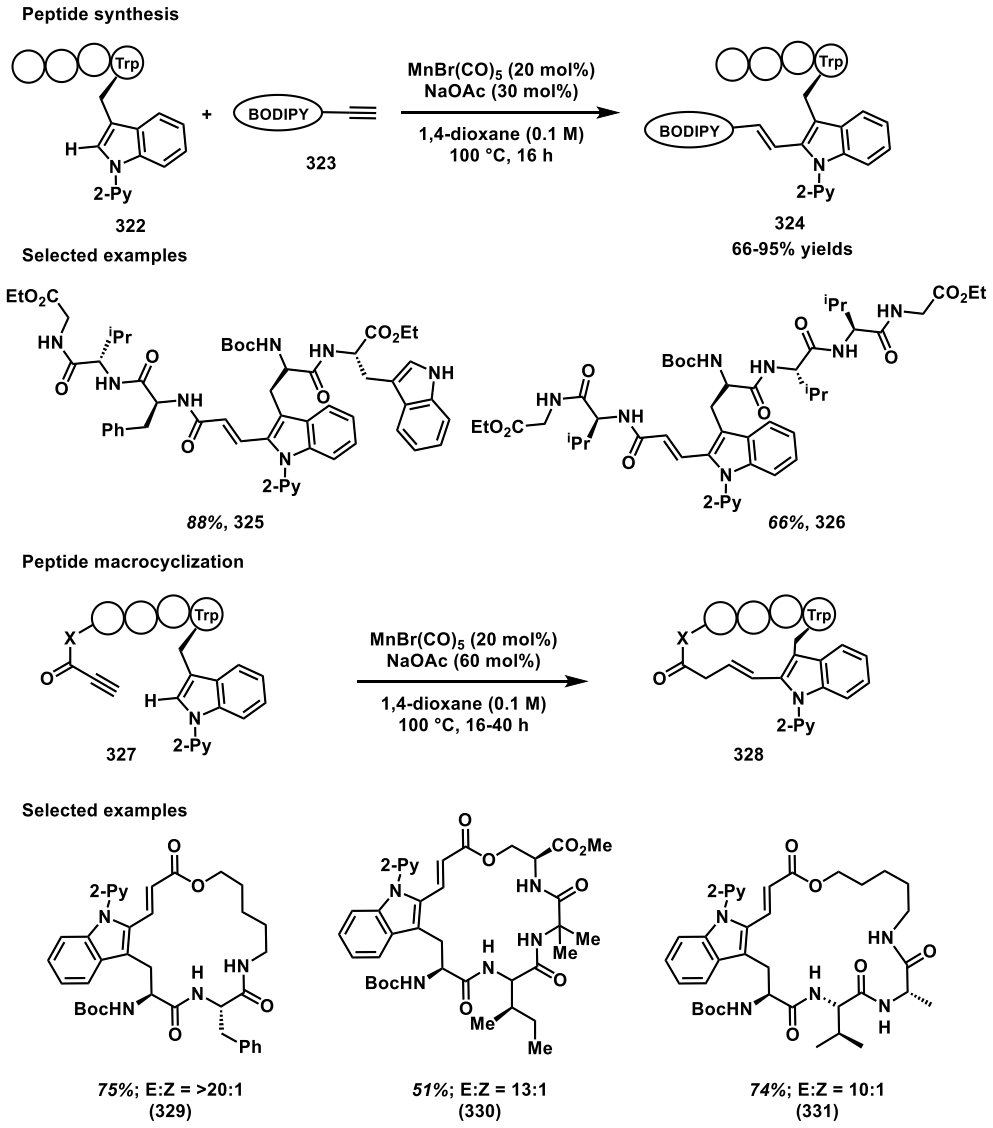

Scheme 3.5: Manganese-catalyzed C2 directed C(sp^2)–H alkenylation with bioactive derivatives.

3.1.3 Cobalt as an Alternative to Precious Metals

In recent years, the utilization of 3d and 4d transition series metal catalysts for activating and functionalizing unreactive C–H bonds has emerged as a critical tool for synthesizing numerous important compounds, including various heterocyclic compounds, through efficient alkyne annulation reactions. These catalysts offer high efficiency, step, and atom economy, making them highly desirable.[24] Their efficiency stems from lower

catalyst loading, mild reaction conditions, excellent selectivity, and tolerance towards functional groups. Due to their high abundance, low cost, and lower toxicity compared to noble metal catalysts, first-row transition metals such as copper, nickel, iron, and cobalt have garnered significant attention and have been successfully developed as attractive alternatives.[24] Cobalt, in particular, and its compounds play pivotal roles in various applications, including permanent magnets, cell phones, high-geared alloys (Stellite), rechargeable batteries, cancer treatment, hydrocarbon desulfurization processes, nitrous oxide elimination, and the promising technology of converting natural gas into liquid hydrocarbons, owing to their unique catalytic properties.[24]

Cobalt exhibits greater reactivity and lower toxicity compared to its counterpart, rhodium. Moreover, cobalt is approximately 300,000 times more abundant than rhodium, which is the rarest non-radioactive metal.[24] Elemental cobalt, priced at $0.334 per gram, is also significantly cheaper than rhodium, which costs $153.44 per gram, making it a cost-effective option for various conversion reactions facilitated by transition metal catalysts of the 2nd and 3rd rows, such as cross-coupling reactions.[24] Cobalt stands out as one of the most effective catalysts for inert C–H bond activation reactions reported to date. Due to cobalt's lower electronegativity compared to analogous group 9 elements, it forms more nucleophilic organometallic Co-intermediates.[24] These intermediates pave the way for new reaction pathways in metal-catalyzed C–H activations, leading to significantly improved positional and chemoselectivities.

3.1.4 C−H Functionalization of Electron-Rich Species

As previously mentioned, Kou and co-workers pioneered the first α-arylation of silyl enol ethers via C−H activation using a rhodium(III) catalyst. Unlike conventional electron-deficient alkene and alkyne substrates, electron-rich silyl enol ethers posed unique mechanistic challenges, which were addressed by incorporating a silver salt additive. Employing ketone-derived enol silanes led to the formation of 3-substituted dihydroisoquinolones, offering a complementary approach to existing methods utilizing enol esters. In most instances, the oxygens of the enol ester derivatives are masked with electron-withdrawing groups, presumably to reduce electron density at the alkene and facilitate the migratory insertion step. Alternative strategies for acylating aromatic C–H bonds involve α-sulfonyloxy- or α-chloroketones, as well as carbene precursors derived from carbonyl compounds. While C–H functionalization with electron-rich alkenes is uncommon, examples documented by the Fagnou and Marsden labs exist and have yet to be further scrutinized. With this method established, we decided to look at more electron rich substrates to further understand the extent of reactivity with these *N*-methoxybenzamides.

Parallel to simple alkynes, we came across research conducted by the Wang group at Sun Yat-Sen University on cobalt-catalyzed C(sp2)–H activation of vinyl phenols (**332** and **336**) with ynamides (**334** and **337**). This resulted in both oxidative [5+2] annulation and dearomative [3+2] spiroannulation, which were either sterically or electronically influenced (Scheme 3.6). In both instances, regioselectivity favored insertion on the ynamide β-carbon (**335** and **338**), which was opposite of the expected reactivity compared

to typical alkynes because it involved two electron-rich centers coming together. In addition to this anomaly, the increased electron density of the ynamides provided an interesting avenue for venturing into the use of more electron-rich species in this methodology. Our investigations were then geared toward C–H functionalization of *N*-methoxybenzamides with ynamides to recreate this unusual regioselectivity towards the synthesis of isoquinolones.

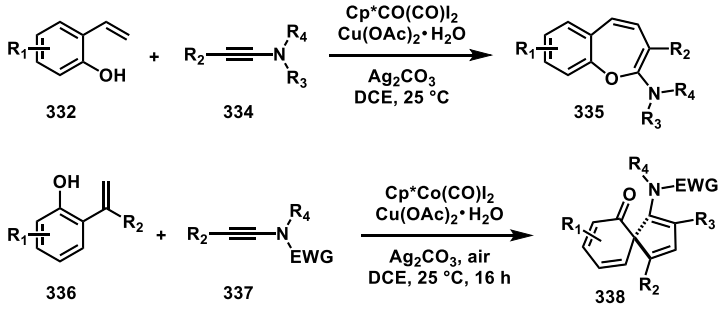

Scheme 3.6: Cobalt-catalyzed [5+2] C–H annulation and [3+2] spiro-annulation by Wang and co-workers.

3.1.5 Synthesis of Isoquinolones by Cobalt-Catalyzed C−H Activation

Coupled with certain amide direct groups, there are a variety of heterocyclic products that can accessed through C–H activation. Isoquinolones are one of the most desired scaffolds in natural product synthesis and have been more recently been synthesized by this method. In 2016, Ackermann and co-workers devised an economical and environmentally friendly oxidative annulation procedure for synthesizing 2-(isoquinolon-2-yl)pyridine-*N*-oxides (**341**) from 2-benzamidopyridine *N*-oxide (**339**) and both internal and terminal alkynes (**340**).[23] The catalyst employed was the cost-effective and readily available $Co(OAc)_2$, with 1 atm of oxygen serving as the sacrificial oxidant, resulting in the generation of water as the sole byproduct (Scheme 3.7). Furthermore, the optimized conditions proved to be applicable across a wide range of coupling partners,

encompassing benzamides and alkynes. Notably, high regioselectivity was achieved when employing terminal alkynes, leading to the selective formation of the 3-substituted derivatives (**342-348**). The reaction exhibited good tolerance towards silyl (**343**), aliphatic alkynes (**344**), ester (**345**), ether (**346**), and acid groups (**347**). However, amides with electron-withdrawing groups (EWGs) exhibited reduced yields. Meta-substituted amides demonstrated good regioselectivity, yielding 7-substituted isoquinolones (**359** and **360**). The pyridine-*N*-oxide moiety could be readily replaced through treatment with potassium-tert-butoxide, thereby extending the utility of this methodology to the cost-effective synthesis of 21,22-dimethoxyrosettacin. The investigation into the regioselectivity observed with terminal alkynes involved DFT studies, revealing **365** and **367** as the pivotal transition states.[23] This phenomenon can be elucidated by considering the regioselectivity and the involvement of a cobalt(III) complex. The higher energy transition states **366** and **368** distinctly ruled out the formation of other regioisomers and the participation of the Co(II) state during the migratory insertion step subsequent to *ortho*-cobaltation.

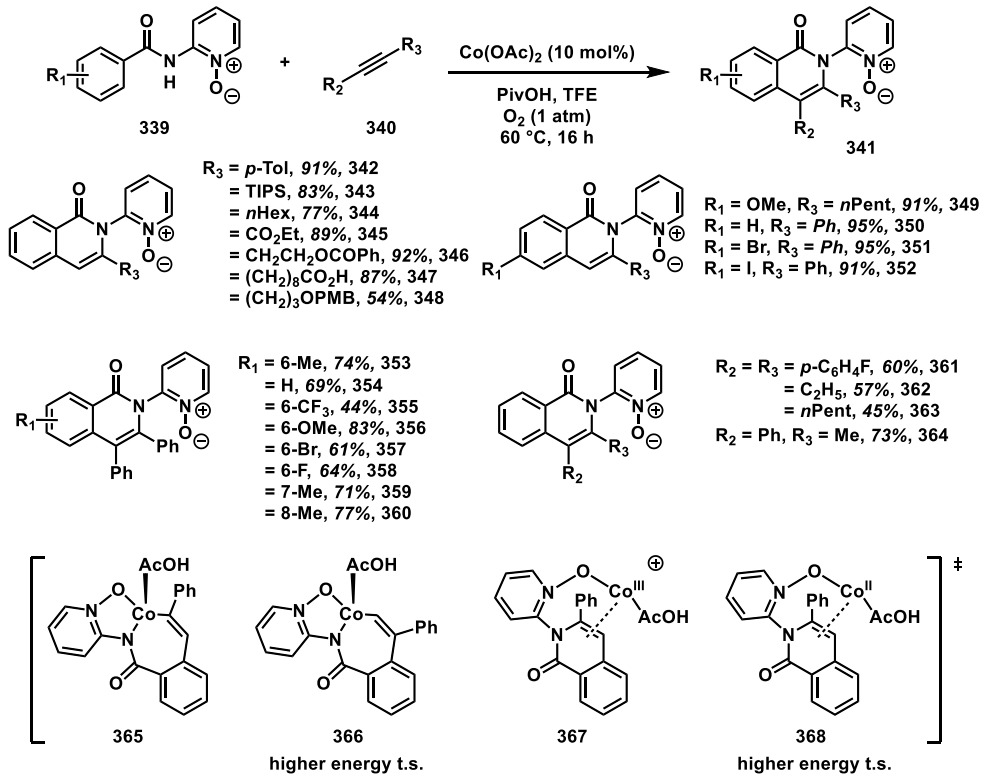

Scheme 3.7: Synthesis of isoquinolones using a cobalt system by Ackermann and co-workers.

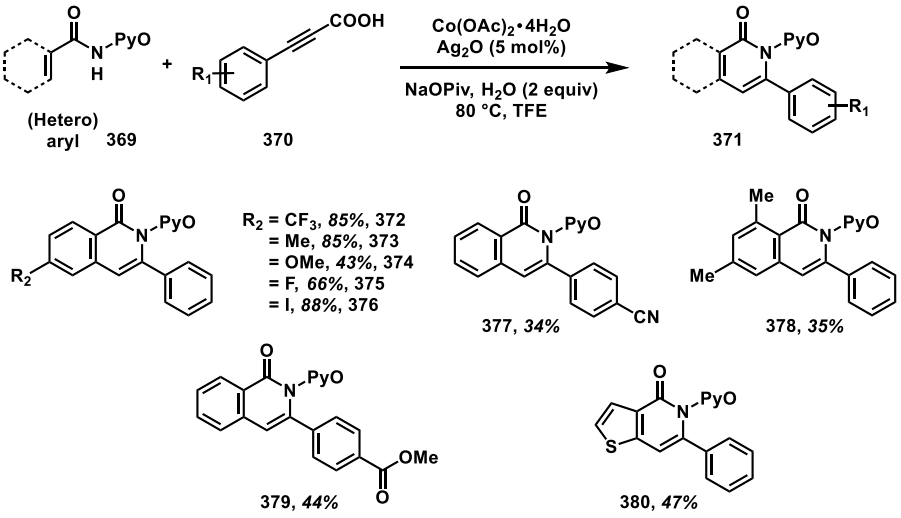

Scheme 3.8: Synthesis of isoquinolones from *N*-(pyridyl)-*N*-oxide)benzamides by Hao and co-workers.

Shortly after, Hao and co-workers demonstrated another cobalt-catalyzed method for synthesizing isoquinolones **371** from N-(pyridyl-N-oxide)benzamides **369** and alkynyl

carboxylic acids **370** (Scheme 3.8). This C–H activation/cyclization protocol employed readily available and inexpensive $Co(OAc)_2 \cdot 4H_2O$ as the catalyst, proceeding through a 6-endodig cyclization with the pyridine *N*-oxide moiety as the directing group.[25] The electron density on the benzamide core did not reveal any discernible trend in the yield, while meta-substituents maintained the regioselectivity, inducing functionalization at the less substituted ortho-position. The proposed mechanism invoked a standard CMD and migratory insertion process that was followed by oxidation with Ag_2O in order to set the stage for reductive elimination. This sequence yielded selected isoquinoline examples (**372-380**) with the desired regioselectivity inserting at the carbon adjacent to an EWG.[25]

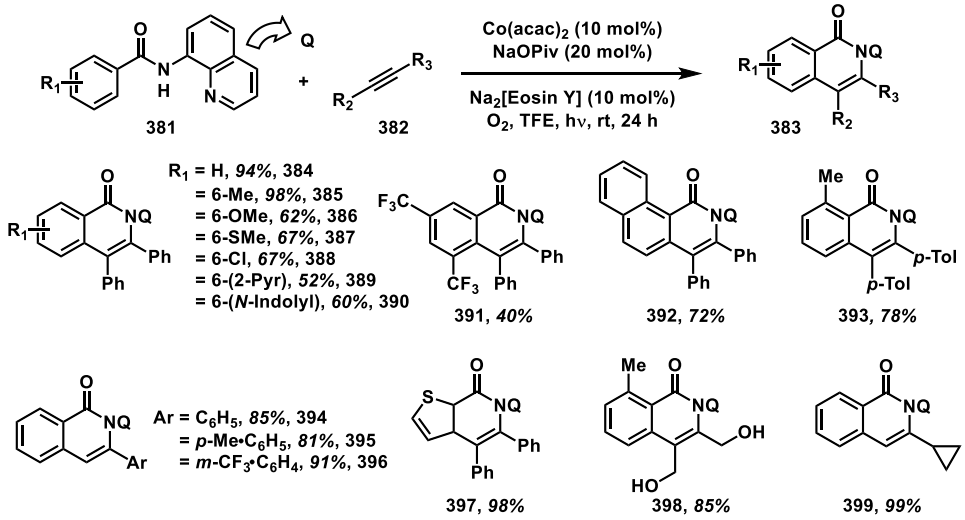

Scheme 3.9: Metal oxidant-free cobalt-catalyzed isoquinolone synthesis by Sundararaju and co-workers.

One commonality among these instances is the reliance on an external oxidant to restore cobalt to its active catalytic oxidation state. To address this challenge, Sundararaju and co-workers introduced the first metal oxidant-free cobalt-catalyzed synthesis of *N*-(quinolin-8-yl)isoquinolinones **383** in 2018 (Scheme 3.9).[25] Although still requiring the use of an oxidant, they were able to use oxygen as the sole oxidizing agent by employing an

eosin-based photocatalytic cycle and allowing the reaction to proceed at room temperature. Under the optimized conditions, the protocol yielded satisfactory product yields when employing various *N*-(quinolin-8-yl)benzamides (**381**) and alkynes, including diynes (**382**). The benzamides utilized encompassed substituents with varying electron densities, as well as heterocyclic substituents (**384-390**). Meta-substituted analogs, in this context, yielded a mixture of products resulting from the competitive activation of both *ortho*-C(sp^2)–H bonds, consistently favoring the less sterically hindered bonds. The reaction also demonstrated good compatibility with heterocyclic amides (**394-396**).[25] The alkynes explored included terminal alkynes or (symmetric/unsymmetric) internal alkynes, and high regioselectivity was noted in the case of aryl acetylenes. The protocol exhibited effectiveness with other directing groups as well, such as 2-benzamidopyridine-1-oxide and *N*-(2-(4,5-dihydrooxazol-2-yl)phenyl)benzamide, yielding moderate yields.

Although there are many examples of simple internal and terminal alkynes used with C–H functionalization, there are no reports of using ynamides to construct isoquinolones. These cyclized products present an electron-rich system with an amine handle for additional transformations, while the use of *N*-methoxybenzamides also contributes as an internal oxidant for cobalt-catalysis.

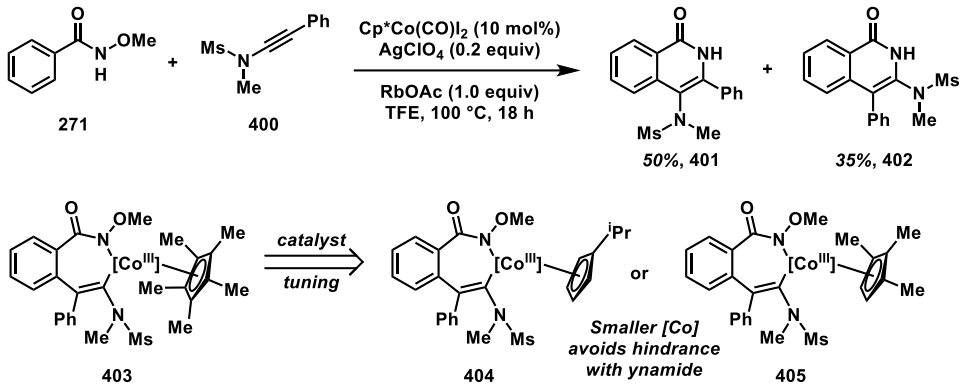

Scheme 3.10: Preliminary results and future catalyst adjustments.

3.2 Results and Discussion

3.2.1 Unprecedented Reactivity with Ynamides

We made a significant discovery involving the Co-catalyzed coupling of hydroxamic ester and ynamide, resulting in the identification of a regioisomer of the isoquinolone. This regioisomer had not been previously observed in either Rh(III)/(I) or Rh(III)/(IV)/(II) catalysis paradigms, underscoring the unique reactivity exhibited by cobalt. The emergence of this new regioisomer is believed to be attributed to the smaller atomic radius of cobalt compared to rhodium. This size disparity enables cobalt to occupy the bulkier side of the alkene post-ynamide insertion. Another possibility is coordination between the ynamide nitrogen-bearing sulfonate group and the cobalt metal center, where we aim to further investigate these pathways by exploring Co-catalysts featuring smaller Cp^{iPr} (**404**) and Cp^{Me3} (**405**) ligands (Scheme 3.10). These ligands can mitigate steric bulk, offering a promising avenue to access 3-aminoisoquinolones, for which no synthetic methods currently exist.

Initial attempts at C–H activation involved the utilization of $AgSbF_6$ as the primary silver salt, accompanied by two different additives: CsOAc and AcOH. The selection of

TFE as the solvent was influenced by previous reports on cobalt catalysis, as it was anticipated that they would complement each other. Various combinations of reaction temperature, time, and solvents were tested to determine the optimal conditions, ultimately identifying RbOAc in TFE at temperatures not exceeding 85 °C as the most favorable. While silver salts were found to enhance reactivity, they were deemed not essential for achieving regioselectivity or overall reactivity. Elevated temperatures beyond 85 °C consistently resulted in lower conversions and isolated yields, likely due to the sensitivity of the ynamides in solution. Interestingly, varying the concentration had minimal impact on the reaction, with the original concentration of 0.1 M proving to be the optimal choice. Subsequently, additives were screened to promote regioselectivity while also aiming to increase the overall reaction yield. Despite exploring numerous combinations and unique silver salts, the current results demonstrate an 85% conversion rate using $AgClO_4$ and RbOAc, with the desired regioisomer constituting 50% and the undesired regioisomer accounting for 35%.

Although we discovered that the presence of silver salts is not necessary for this method, it does increase the overall yield alongside RbOAc. We continued to try different equivalences and silver additives like $AgSbF_6$, AgOPiv, AgOTf, AgC_2O_3, and $AgNO_3$ but none could overcome the results given by a catalytic amount of $AgClO_4$. At one point we decided to test some of those silver salts with other acetates but it is evident that RbOAc allows the reaction to proceed at a much higher yield compared to CsOAc, $Cu(OAc)_2$, $Mn(OAc)_2$, and $Zn(OAc)_2$. The addition of base with RbOAc does not have an effect on the overall reactivity, but the absence of acetate greatly reduces the yield. Combinations of

K_3PO_4 with CsOAc or NaOAc only achieved trace amounts of the desired regioisomer. Alternatives to these acetate salts like CsOPiv, CsF, and $NaSbF_6$ only give conversions less than 20% or no reactivity at all. We have yet to elucidate why the rubidium is the obvious choice in reactivity with a near 100% conversion from starting material but will be transitioning to improve regioselectivity from catalyst tuning.

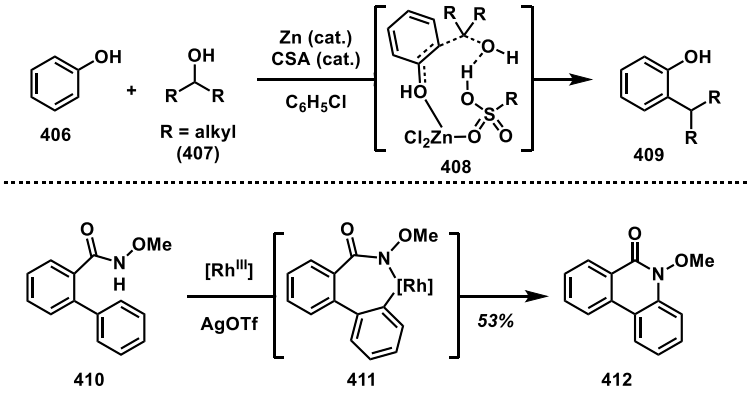

Scheme 3.11: Observed hydrogen bond scaffolding and 7-membered cyclometalate.

3.3 Conclusions and Future Direction

As we look forward, our synthetic efforts will be towards constructing ligands for a variety of cobalt and rhodium complexes. Smaller ligands could mitigate steric hindrance that we assume plays a role in regioselectivity. Electronic changes to potential cobalt complexes could also improve the speed of reductive elimination by providing stability to the active catalyst once ejecting the aminoisoquinolone. Moreover, instead of relying on preinstalled internal directing functionalities to guide reactivity, we propose to advance a Co-catalyzed C–H functionalization strategy to transform native electron-poor azines and electron-rich azoles, which builds on our laboratory's recent success in enhancing reactivity and altering site-selectivity of a Zn-catalyzed Friedel–Crafts alkylation to afford

new $C(sp^2)$–$C(sp^3)$ bonds when using camphorsulfonic acid co-catalyst to assemble a hydrogen bonding network (Scheme 3.11).

We have observed successful C–H functionalization, where the reaction proceeds via a 7-membered cyclometalate. Consequently, we anticipate that the hydrogen bond-supported cyclometalate may serve as a plausible intermediate for subsequent C–C bond formation. This scaffolding catalysis, facilitated by hydrogen bonding, will be tested with electron-rich azoles, leveraging their superior hydrogen bond donor ability compared to amides (Scheme 3.12). Hydrazide derivatives will act as co-catalysts to bring the arene and metal into proximity. Unlike conventional scaffolding catalysis, which relies on reversible covalent bond formation, the proposed methods exploit non-covalent interactions to directly functionalize heterocycles.

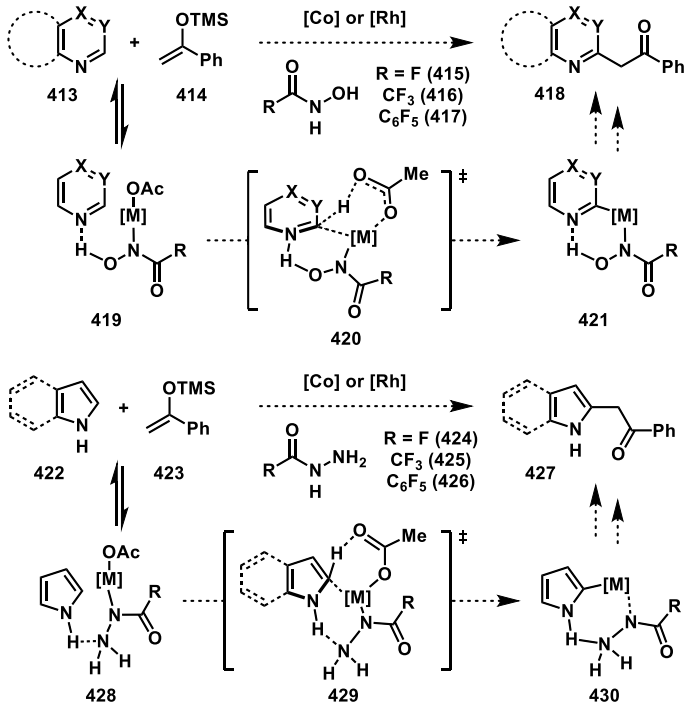

Scheme 3.12: Application towards electron-poor azines and electron-rich azoles.

3.4 Experimental

3.4.1 General Information

3.4.1.1 Solvents and Reagents

Commercial reagents were purchased from MilliporeSigma, Acros Organics, Chem-Impex, TCI, Oakwood, and Alfa Aesar, and used without additional purification. Solvents were purchased from Fisher Scientific, Acros Organics, Alfa Aesar, and Sigma Aldrich. Tetrahydrofuran (THF), diethyl ether (Et_2O), acetonitrile (MeCN), dichloromethane (CH_2Cl_2), benzene, 1,4-dioxane, and triethylamine (Et_3N) were sparged with argon and dried by passing through alumina columns using argon in a Glass Contour (Pure Process Technology) solvent purification system. Dimethylformamide (DMF), dimethyl sulfoxide (DMSO), and dichloroethane (DCE) were purchased in Sure/Seal or AcroSeal bottling and dispensed under N_2. Deuterated solvents were obtained from Cambridge Isotope Laboratories, Inc. or MilliporeSigma.

3.4.1.2 Reaction setup, progress monitoring, and product purification

In general, the catalytic reactions are not air- or moisture-sensitive; however, the iron and zinc salts are hygroscopic and quickly change color when being weighed and added to the reaction vessel. This influences how much metal catalyst is being added because their molecular weights increase on hydration. For consistency and rigor, the iron and zinc salts were weighed and added to vials inside a nitrogen-filled glovebox. All other reagents, including the solvent, were added outside the glovebox under open air. Reaction progresses were monitored using thin-layer chromatography (TLC) on EMD Silica Gel 60 F254 or Macherey–Nagel SIL HD (60 Å mean pore size, 0.75 mL/g specific pore volume,

5–17 μm particle size, with fluorescent indicator) silica gel plates. Visualization of the developed plates was performed under UV light (254 nm). Purification and isolation of products were performed via silica gel chromatography (both column and preparative thin-layer chromatography). Organic solutions were concentrated under reduced pressure on IKA® temperature-controlled rotary evaporator equipped with an ethylene glycol/water condenser.

3.4.1.3 Analytical instrumentation

Melting points were measured with the MEL-TEMP melting point apparatus. Proton nuclear magnetic resonance (^{1}H NMR) spectra, carbon nuclear magnetic resonance (^{13}C NMR) spectra and fluorine nuclear magnetic resonance (^{19}F NMR) spectra were recorded on Bruker Avance NEO 400 (not ^{1}H decoupled) or Bruker Avance 600 MHz spectrometers (^{1}H decoupled). Chemical shifts (δ) are reported in ppm relative to the residual solvent signal (δ 7.26 for ^{1}H NMR, δ 77.16 for ^{13}C NMR in $CDCl_3$).[1] Data for ^{1}H NMR spectroscopy are reported as follows: chemical shift (δ ppm), multiplicity (s = singlet, d = doublet, t = triplet, q = quartet, m = multiplet, br = broad, dd = doublet of doublets, dt = doublet of triplets), coupling constant (Hz), integration. Data for ^{13}C and ^{19}F NMR spectroscopy are reported in terms of chemical shift (δ ppm). IR spectroscopic data were recorded on a NICOLET 6700 FT-IR spectrophotometer using a diamond attenuated total reflectance (ATR) accessory. Samples are loaded onto the diamond surface either neat or as a solution in organic solvent and the data acquired after the solvent had evaporated. High resolution accurate mass (ESI) spectral data were obtained from the

Analytical Chemistry Instrumentation Facility at the University of California, Riverside, on an Agilent 6545 Q-TOF LC/MS instrument (supported by NSF grant CHE-1828782).

3.5 Experimental Procedures and Characterization Data

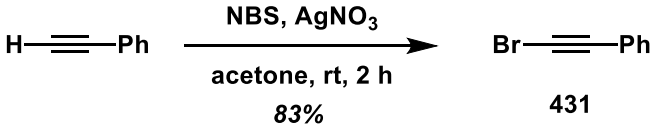

(Bromoethynyl)benzene (431).[30] *N*-bromosuccinimide (12.6 g, 70.5 mmol, 1.2 equiv) and $AgNO_3$ (1.00 g, 5.88 mmol, 0.1 equiv) were added to a stirring solution of phenylacetylene (6.45 mL, 58.8 mmol, 1.0 equiv) in acetone (196 mL, 0.3 M) at rt and in the absence of light. After stirring at rt for 1 h, an additional quantity of $AgNO_3$ (1.00 g, 5.88 mmol, 0.1 equiv) was added to the mixture and stirred for 1 h at rt. The reaction mixture was then filtered through a fritted funnel and transferred to a separatory funnel. The filtrate was extracted with CH_2Cl_2 (3 × 200 mL) and the combined organic extract was dried over anhydrous Na_2SO_4, filtered, and concentrated *in vacuo*. Purification by silica gel flash chromatography (eluting with 100% hex). The product was isolated as a (8.78 g, 83 %). R_f = 0.61 (100% hex). ^{1}H NMR (500 MHz, $CDCl_3$) δ 7.49 – 7.43 (m, 1H), 7.32 (qd, *J* = 8.8, 7.8, 3.5 Hz, 1H). All other spectroscopic data are in accord with previously reported literature.

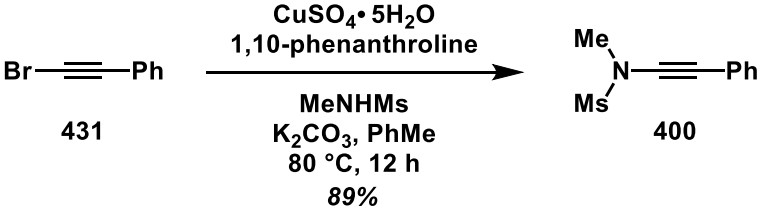

***N*-Methyl-*N*-(phenylethynyl)methanesulfonamide (400).**[30] A mixture of *N*–methylmethanesulfonamide (2.7 mL, 29.6 mmol, 1.2 equiv), $CuSO_4$ (394 mg, 2.47 mmol, 0.1 equiv), H_2O (0.22 mL, 12.4 mmol, 0.5 equiv), and 1,10-phenanthroline (890 mg, 4.94 mmol, 0.2 equiv) was diluted with toluene (27 mL, 0.93 M) and then treated with bromoalkyne **431** (4.47 g, 24.7 mmol, 1.0 equiv) and K_2CO_3 (8.53 g, 61.8 mmol, 2.5 equiv). The reaction mixture was stirred at 80 °C for 18 h and then cooled to rt before filtering through Celite. The filtrate was concentrated *in vacuo*. Purification by silica gel flash chromatography (eluting with 0-25% EtOAc/hex). The product was isolated as a (4.62 g, 89%). R_f = 0.38 (25% EtOAc/hex). ^{1}H NMR (400 MHz, $CDCl_3$) δ 7.45 – 7.37 (m, 1H), 7.36 – 7.28 (m, 1H), 3.30 (s, 2H), 3.13 (s, 1H). All other spectroscopic data are in accord with previously reported literature.

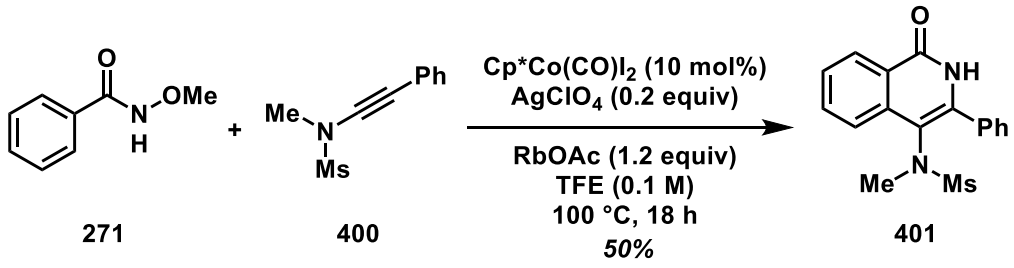

271 400 401

***N*-Methyl-*N*-(1-oxo-3-phenyl-1,2-dihydroisoquinolin-4-yl)methanesulfonamide (401).** Cp*Co(CO)I_2 (4.78 mg, 0.01 mmol, 10 mol%), RbOAc (17.3 mg, 0.120 mmol, 1.2 equiv), and $AgClO_4$ (4.15 mg, 0.02 mmol, 0.2 equiv) were added to a mixture of *N*-methoxy benzamide (**271**) (15.1 mg, 0.100 mmol, 1.0 equiv) and ynamide **400** (25.1 mg, 0.120 mmol, 1.2 equiv) in an oven-dried 4 mL vial equipped with a stir bar at rt. The reaction flask was then charged with HFIP (1 mL, 0.1 M), capped, and stirred at 100 °C

for 18 h. The reaction mixture was filtered through a 3 cm silica plug with CH_2Cl_2 and EtOAc (acetone if needed). Purification by silica gel flash chromatography (eluting with 0-50% acetone/hex). The product was isolated as a (16.4 mg, 50%). R_f = 0.29 (50% acetone/hex). ^{1}H NMR (400 MHz, $CDCl_3$) δ 9.00 (s, 1H), 8.40 (dt, *J* = 8.1, 1.1 Hz, 1H), 7.81 (d, *J* = 3.6 Hz, 1H), 7.62 – 7.46 (m, 6H), 3.30 (s, 3H), 2.95 (s, 4H).

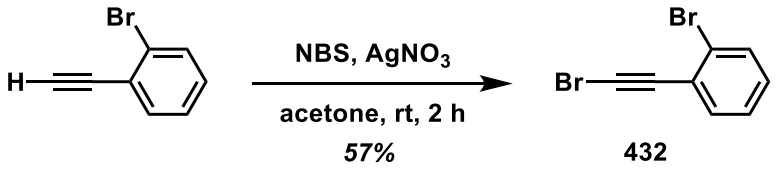

1-Bromo-2-(bromoethynyl)benzene (432). *N*-bromosuccinimide (3.91 g, 33.1 mmol, 1.2 equiv) and $AgNO_3$ (469 mg, 2.76 mmol, 0.1 M) were added to a stirring solution of 1-bromo-2-ethynylbenzene (3.5 mL, 27.6 mmol, 1.0 equiv) in acetone (196 mL, 0.3 M) at rt and in the absence of light. After stirring at rt for 1 h, an additional quantity of $AgNO_3$ (469 mg, 2.76 mmol, 0.1 M) was added to the mixture and stirred for another 1 h at rt. The reaction mixture was then filtered through a fritted funnel and concentrated *in vacuo*. Purification by silica gel flash chromatography (eluting with 100% hex. The product was isolated as a slightly orange oil (4.084 g, 57 %). R_f = 0.55 (100% hex). ^{1}H NMR (400 MHz, $CDCl_3$) δ 7.57 (dd, *J* = 8.0, 1.3 Hz, 1H), 7.48 (dd, *J* = 7.5, 1.8 Hz, 1H), 7.26 (td, *J* = 7.5, 1.3 Hz, 1H), 7.19 (td, J = 8.0, 1.8 Hz, 1 H).

3.6 NMR Spectra

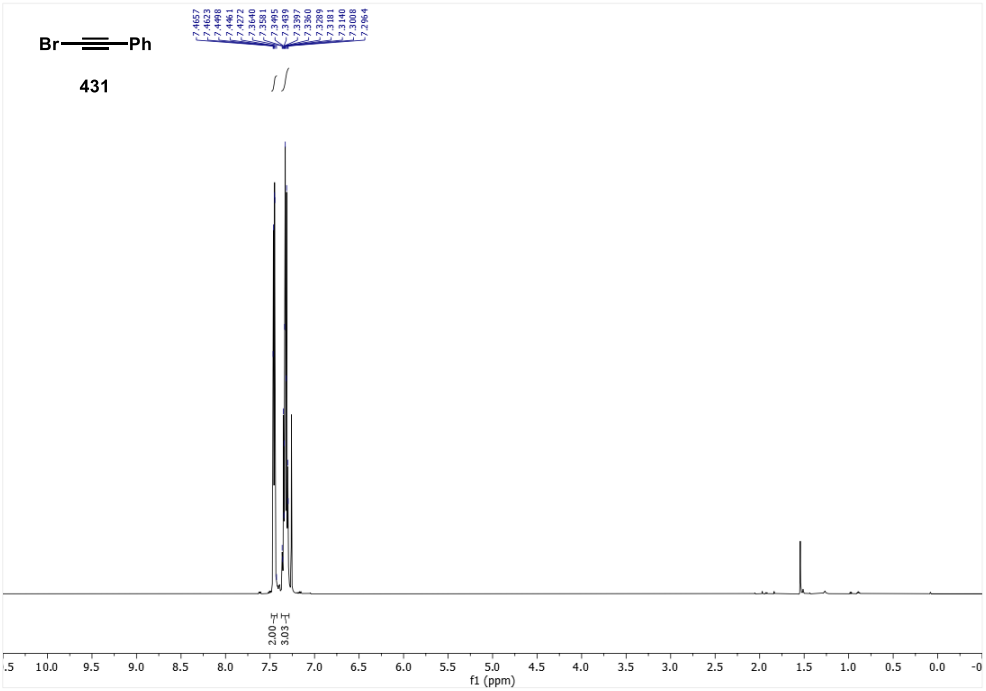

Figure 3.2: (Bromoethynyl)benzene (**431**); ^{1}H NMR (500 MHz, $CDCl_3$) at 24.8 °C.

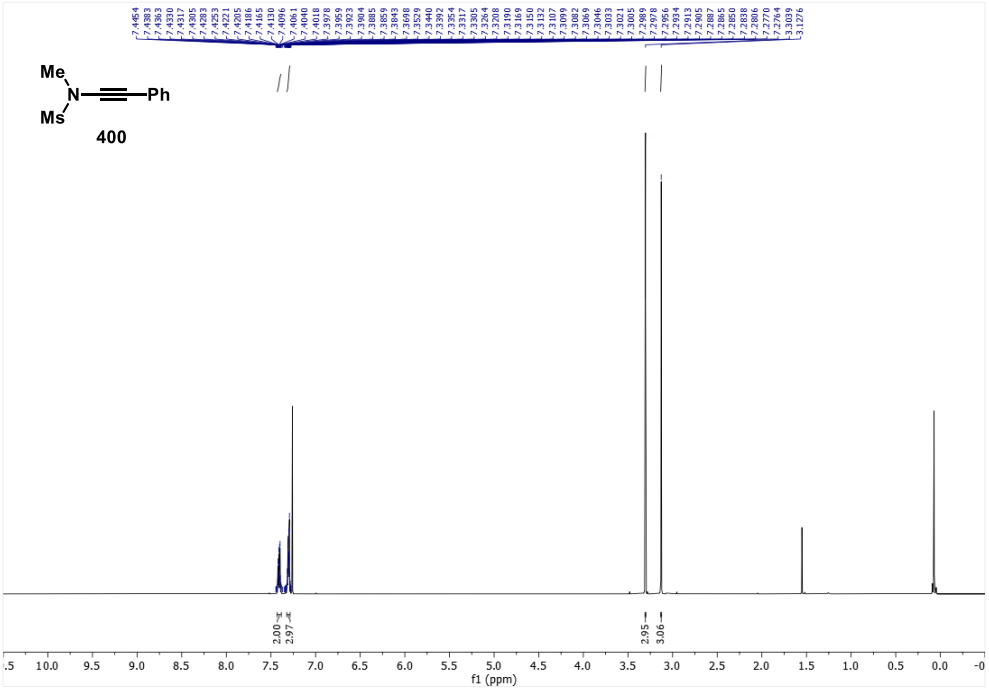

Figure 3.3: N-Methyl-*N*-(phenylethynyl)methanesulfonamide (**400**); ^{1}H NMR (400 MHz, $CDCl_3$) at 21.9 °C.

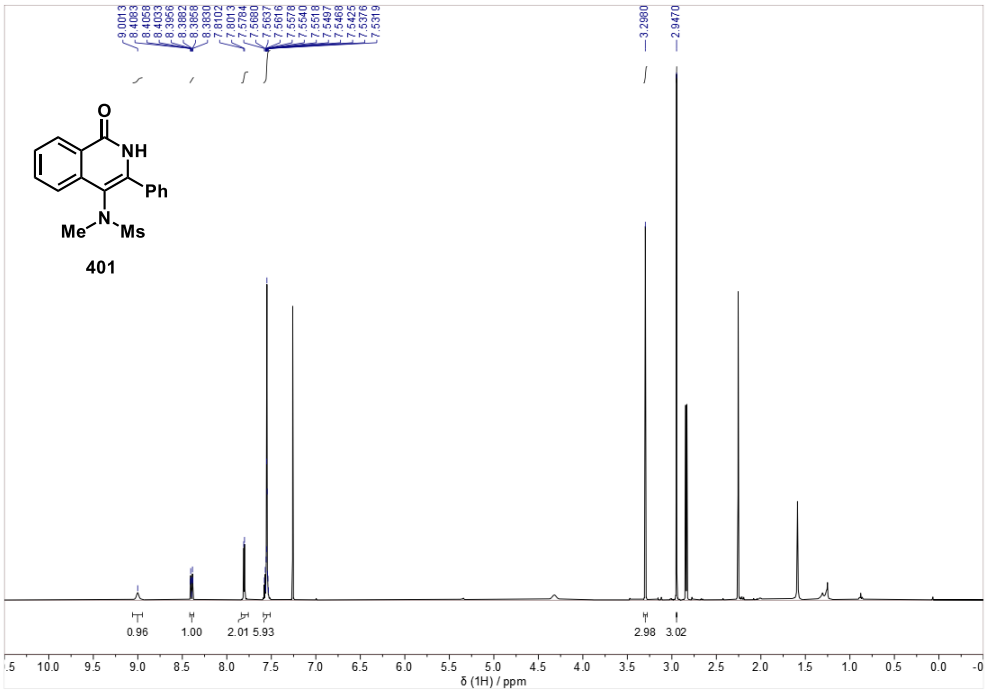

Figure 3.4: N-Methyl-*N*-(1-oxo-3-phenyl-1,2-dihydroisoquinolin-4-yl)methanesulfonamide (**401**); ^{1}H NMR (400 MHz, $CDCl_3$) at 21.9 °C.

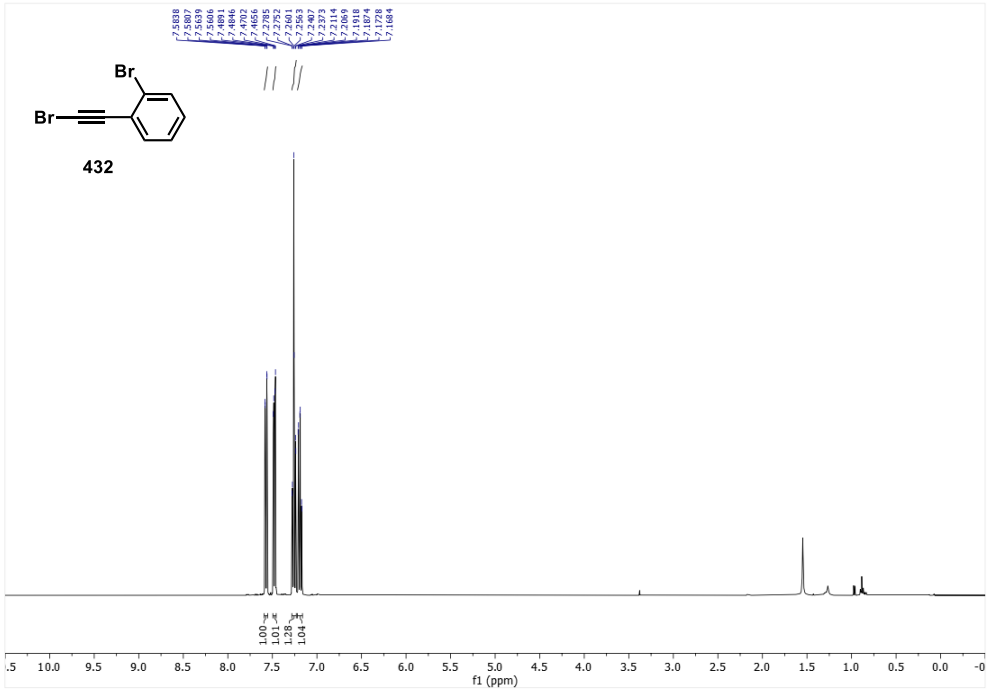

Figure 3.5: 1-Bromo-2-(bromoethynyl)benzene (**432**); ^{1}H NMR (400 MHz, $CDCl_3$) at 21.9 °C.

3.7 References

(1) Docherty, J. H.; Lister, T. M.; Mcarthur, G.; Findlay, M. T.; Domingo-Legarda, P.; Kenyon, J.; Choudhary, S.; Larrosa, I. Transition-Metal-Catalyzed C–H Bond Activation for the Formation of C–C Bonds in Complex Molecules. *Chem. Rev.*, **2023**, *123* (12), 7692-7760. DOI: 10.1021/acs.chemrev.2c00888

(2) Nicolaou, K. C. Organic Synthesis: The Art and Science of Replicating the Molecules of Living Nature and Creating Others like Them in the Laboratory. *Proc. R. Soc. A: Math. Phys. Eng.*, **2014**, *470* (2163), 20130690–20130690. DOI: 10.1098/rspa.2013.0690

(3) Campeau, L.-C.; Hazari, N. Cross-Coupling and Related Reactions: Connecting Past Success to the Development of New Reactions for the Future. *Organometallics*, **2018**, *38* (1), 3–35. DOI: 10.1021/acs.organomet.8b00720

(4) Levi, P. G.; Cullen, J. M. Mapping Global Flows of Chemicals: From Fossil Fuel Feedstocks to Chemical Products. *Environ. Sci. Technol.*, **2018**, *52* (4), 1725–1734. DOI: 10.1021/acs.est.7b04573

(5) Zhang, L.; Ritter, T. A Perspective on Late-Stage Aromatic C–H Bond Functionalization. *J. Am. Chem. Soc.*, **2022**, *144* (6), 2399–2414. DOI: 10.1021/jacs.1c10783

(6) Beck, H.; Härter, M.; Haß, B.; Schmeck, C.; Baerfacker, L. Small Molecules and Their Impact in Drug Discovery: A Perspective on the Occasion of the 125th Anniversary of the Bayer Chemical Research Laboratory. *Drug Discov. Today*, **2022**, *27* (6). DOI: 10.1016/j.drudis.2022.02.015

(7) Ertl, P.; Schuffenhauer, A. Estimation of Synthetic Accessibility Score of Drug-like Molecules Based on Molecular Complexity and Fragment Contributions. *J. Cheminform.*, **2009**, *1* (1), 8. DOI: 10.1186/1758-2946-1-8

(8) Murai, S.; Kakiuchi, F.; Sekine, S.; Tanaka, Y.; Kamatani, A.; Sonoda, M.; Chatani, N. Efficient Catalytic Addition of Aromatic Carbon-Hydrogen Bonds to Olefins. *Nature*, **1993**, *366* (6455), 529–531. DOI: 10.1038/366529a0

(9) Guimond, N.; Gorelsky, S. I.; Fagnou, K. Rhodium(III)-Catalyzed Heterocycle Synthesis Using an Internal Oxidant: Improved Reactivity and Mechanistic Studies. *J. Am. Chem. Soc.*, **2011**, *133* (16), 6449–6457. DOI: 10.1021/ja201143v

(10) Webb, N. J.; Marsden, S. P.; Raw, S. A. Rhodium(III)-Catalyzed C–H Activation/Annulation with Vinyl Esters as an Acetylene Equivalent. *Org. Lett.*, **2014**, *16* (18), 4718–4721. DOI: 10.1021/ol502095z

(11) Lou, S.-J.; Luo, G.; Yamaguchi, S.; An, K.; Masayoshi Nishiura; Hou, Z. Modular Access to Spiro-Dihydroquinolines via Scandium-Catalyzed Dearomative Annulation of Quinolines with Alkynes. *J. Am. Chem. Soc.*, **2021**, *143* (48), 20462–20471. DOI: 10.1021/jacs.1c10743

(12) Carral-Menoyo, A.; Sotomayor, N.; Lete, E. Cp*Co(III)-Catalyzed C–H Hydroarylation of Alkynes and Alkenes and Beyond: A Versatile Synthetic Tool. *ACS Omega* **2020**, *5* (39), 24974–24993. DOI: 10.1021/acsomega.0c03639

(13) Zhang, Y.; Szostak, M. Synthesis of Natural Products by C−H Functionalization of Heterocycless. *Chem. Eur. J.*, **2022**, *28* (22). DOI: 10.1002/chem.202104278

(14) Koronatov, A. N.; Rostovskii, N. V.; Khlebnikov, A. F.; Novikov, M. S. Rh(II)-Catalyzed Ring Expansion of Pyrazoles with Diazocarbonyl Compounds as a Method for the Preparation of 1,2-Dihydropyrimidines. *J. Org. Chem.*, **2018**, *83* (16), 9210–9219. DOI: 10.1021/acs.joc.8b01228

(15) Yi, C. S.; Lee, D. W. Intermolecular Dehydrative Coupling Reaction of Aryl Ketones with Cyclic Alkenes Catalyzed by a Well-Defined Cationic Ruthenium−Hydride Complex: A Novel Ketone Olefination Method via Vinyl C−H Bond Activation. *Organometallics*, **2010**, *29* (8), 1883–1885. DOI: 10.1021/om100051h

(16) Culkin, D. A.; Hartwig, J. F. Palladium-Catalyzed α-Arylation of Carbonyl Compounds and Nitriles. *Acc. Chem. Res.*, **2003**, *36* (4), 234–245. DOI: 10.1021/ar0201106

(17) Bellina, F.; Rossi, R. Transition Metal-Catalyzed Direct Arylation of Substrates with Activated Sp^3-Hybridized C−H Bonds and Some of Their Synthetic Equivalents with Aryl Halides and Pseudohalides. *Chem. Rev.*, **2009**, *110* (2), 1082–1146. DOI: 10.1021/cr9000836

(18) Johansson, Carin C. C.; Colacot, Thomas J. Metal-Catalyzed α-Arylation of Carbonyl and Related Molecules: Novel Trends in C−C Bond Formation by C−H Bond Functionalization. *Angew. Chem. Int. Ed.*, **2010**, *49* (4), 676–707. DOI: 10.1002/anie.200903424

(19) Novak, P.; Martin, R. Pd-Catalyzed α-Arylation of Carbonyl and Related Compounds: Recent Developments and Perspectives. *Curr. Org. Chem.*, **2011**, *15* (18), 3233–3262. DOI: 10.2174/138527211797248021

(20) Lu, M. Z.; Chen, X. R.; Xu, H.; Dai, H. X.; Yu, J. Q. Ligand-Enabled: Ortho-C-H Olefination of Phenylacetic Amides with Unactivated Alkenes. *Chem. Sci.*, **2018**, *9*, 1311−1316. DOI: 10.1039/C7SC04827K

(21) Walton, J. W.; Jonathan. Ruthenium-Catalyzed*Ortho*-Alkylation of Phenols with Alcohols by Dehydrative Coupling. *Angew. Chem.*, **2012**, *51* (49), 12166–12168. DOI: 10.1002/anie.201206246

(22) Lou, S.-J.; Luo, G.; Yamaguchi, S.; An, K.; Masayoshi Nishiura; Hou, Z. Modular Access to Spiro-Dihydroquinolines via Scandium-Catalyzed Dearomative Annulation of Quinolines with Alkynes. *J. Am. Chem. Soc.*, **2021**, *143* (48), 20462–20471. DOI: 10.1021/jacs.1c10743

(23) Wang, H.; Pesciaioli, F.; Oliveira, J. C. A.; Warratz, S.; Ackermann, L. Synergistic Manganese(I) C−H Activation Catalysis in Continuous Flow: Chemoselective Hydroarylation. *Angew. Chem. Int. Ed.*, **2017**, *56* (47), 15063–15067. DOI: 10.1002/anie.201708271

(24) Daily Metal Prices. Accessed July 19, 2023. https://www.dailymetalprice.com/

(25) Kalsi, D.; Dutta, S.; Barsu, N.; Rueping, M.; Sundararaju, B. Room-Temperature C–H Bond Functionalization by Merging Cobalt and Photoredox Catalysis. *ACS Catal.*, **2018**, *8* (9), 8115–8120. DOI: 10.1021/acscatal.8b02118

(26) Carral-Menoyo, A.; Sotomayor, N.; Lete, E. Cp*Co(III)-Catalyzed C–H Hydroarylation of Alkynes and Alkenes and Beyond: A Versatile Synthetic Tool. *ACS Omega* **2020**, *5* (39), 24974–24993. DOI: 10.1021/acsomega.0c03639

(27) Han, X.-L.; Liu, X.-G.; Lin, E.; Chen, Y.; Chen, Z.; Wang, H.; Li, Q. Cp*Co(III)-Catalyzed Oxidative [5+2] Annulation: Regioselective Synthesis of 2-Aminobenzoxepines *Via* C–H/O–H Functionalization of 2-Vinylphenols with Ynamides. *Chem. Comm.*, **2018**, *54* (82), 11562–11565. DOI: 10.1039/c8cc06807k

(28) Lin, P.-P.; Han, X.-L.; Ye, G.-H.; Li, J.-L.; Li, Q.; Wang, H. Cp*Co(III)-Catalyzed Dearomative [3 + 2] Spiroannulation of 2-Alkenylphenols with Ynamides via C–H Activation. *J. Org. Chem.*, **2019**, *84* (20), 12966–12974. DOI: 10.1021/acs.joc.9b01750

(29) Kaplaneris, N.; Kaltenhäuser, F.; Sirvinskaite, G.; Fan, S.; De Oliveira, T.; Conradi, L.-C.; Ackermann, L. Late-Stage Stitching Enabled by Manganese-Catalyzed C─H Activation: Peptide Ligation and Access to Cyclopeptides. *Sci. Adv.*, **2021**, *7* (9). DOI: 10.1126/sciadv.abe6202

(30) Beltran, F.; Andna, L.; Miesch, L. Spirocyclization of Keto-Ynesulfonamides Promoted by Quaternary Ammonium Salts. *Org. Chem. Front.*, **2019**, *6* (3), 373–376. DOI: 10.1039/c8qo00937f

(31) Ujwaldev, S. M.; Harry, N. A.; Divakar, M. A.; Anilkumar, G. Cobalt-Catalyzed C–H Activation: Recent Progress In Heterocyclic Chemistry. *Catal. Sci. Technol.*, **2018**, *8*, 5983. DOI: 10.1039/c8cy01418c

3.8 Supplemental Figures

Table 3.1: Optimization of Reaction Conditions (time, temperature, solvent, conc.).

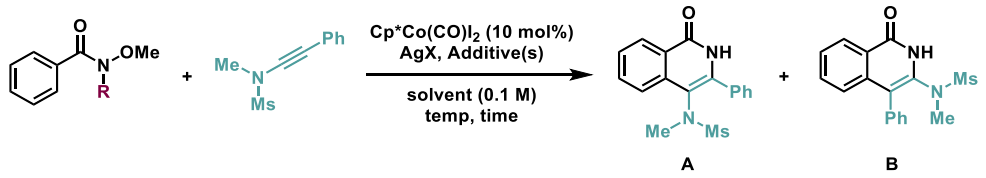

R	Catalyst (10 mol%)	AgX (equiv)	Additive (s)	Solvent	Temp (°C)	Time (h)	A (%)	B (%)
H	$Cp^*Co(CO)I_2$	--	--	TFE	100	18	0	0
H	$Cp^*Co(CO)I_2$	$AgSbF_6$ (0.2)	CsOAc (1.0), AcOH (9.6)	TFE	100	18	0	0
H	$Cp^*Co(CO)I_2$	$AgSbF_6$ (1.0)	CsOAc (1.0), AcOH (9.6)	TFE	100	18	0	0
H	$Cp^*Co(CO)I_2$	$AgSbF_6$ (2.2)	CsOAc (1.0), AcOH (9.6)	TFE	100	18	0	0
H	$Cp^*Co(CO)I_2$	--	CsOAc (1.0), AcOH (9.6)	TFE	100	18	0	0
H	$Cp^*Co(CO)I_2$	$AgSbF_6$ (0.2)	CsOAc (1.0), AcOH (1.0)	TFE	100	18	0	0
H	$Cp^*Co(CO)I_2$	$AgSbF_6$ (1.0)	CsOAc (1.0), AcOH (1.0)	TFE	100	18	0	0
H	$Cp^*Co(CO)I_2$	$AgSbF_6$ (2.2)	CsOAc (1.0), AcOH (1.0)	TFE	100	18	0	0

Me	$Cp^*Co(CO)I_2$	--	CsOAc (1.0), AcOH (9.6)	TFE	100	18	0	0
Me	$Cp^*Co(CO)I_2$	$AgSbF_6$ (0.2)	CsOAc (1.0), AcOH (9.6)	TFE	100	18	0	0
Me	$Cp^*Co(CO)I_2$	$AgSbF_6$ (1.0)	CsOAc (1.0), AcOH (9.6)	TFE	100	18	0	0
Me	$Cp^*Co(CO)I_2$	$AgSbF_6$ (2.2)	CsOAc (1.0), AcOH (9.6)	TFE	100	18	0	0
Me	$Cp^*Co(CO)I_2$	--	CsOAc (1.0), AcOH (1.0)	TFE	100	18	0	0
Me	$Cp^*Co(CO)I_2$	$AgSbF_6$ (0.2)	CsOAc (1.0), AcOH (1.0)	TFE	100	18	0	0
Me	$Cp^*Co(CO)I_2$	$AgSbF_6$ (1.0)	CsOAc (1.0), AcOH (1.0)	TFE	100	18	0	0
Me	$Cp^*Co(CO)I_2$	$AgSbF_6$ (2.2)	CsOAc (1.0), (9.6)	TFE	100	18	0	0
H	$Cp^*Co(CO)I_2$	$AgSbF_6$ (0.2)	CsOAc (1.0)	DCE	100	18	0	0
H	$Cp^*Co(CO)I_2$	$AgSbF_6$ (0.2)	CsOAc (1.0)	MeOH	100	18	0	0
H	$Cp^*Co(CO)I_2$	$AgSbF_6$ (0.2)	CsOAc (1.0)	1,3-dioxolane	100	18	0	0
H	$Cp^*Co(CO)I_2$	$AgSbF_6$ (0.2)	CsOAc (1.0)	HFIP	100	18	0	0
H	$Cp^*Co(CO)I_2$	$AgSbF_6$ (0.2)	CsOAc (1.0)	TFE/cat. H_2O	100	18	trace	trace
H	$Cp^*Co(CO)I_2$	$AgSbF_6$ (0.2)	CsOAc (1.0)	DMF	100	18	0	0
H	$Cp^*Co(CO)I_2$	$AgSbF_6$ (0.2)	CsOAc (1.0)	fluoroben-zene	100	18	17[a]	14[a]

H	$Cp^*Co(CO)I_2$	$AgSbF_6$ (0.2)	CsOAc (1.0)	THF	100	18	0	0
H	$Cp^*Co(CO)I_2$	$AgSbF_6$ (0.2)	CsOAc (1.0)	1,4-dioxane	100	18	0	0
H	$Cp^*Co(CO)I_2$	$AgSbF_6$ (0.2)	CsOAc (1.0)	CH_3CN	100	18	0	0
H	$Cp^*Co(CO)I_2$	$AgSbF_6$ (0.2)	CsOAc (1.0)	DCE	80	18	0	0
H	$Cp^*Co(CO)I_2$	$AgSbF_6$ (0.2)	CsOAc (1.0)	MeOH	80	18	0	0
H	$Cp^*Co(CO)I_2$	$AgSbF_6$ (0.2)	CsOAc (1.0)	1,3-dioxolane	80	18	0	0
H	$Cp^*Co(CO)I_2$	$AgSbF_6$ (0.2)	CsOAc (1.0)	TFE	80	18	22	19
H	$Cp^*Co(CO)I_2$	$AgSbF_6$ (0.2)	CsOAc (1.0)	HFIP	80	18	0	0
H	$Cp^*Co(CO)I_2$	$AgSbF_6$ (0.2)	CsOAc (1.0)	TFE/cat. H_2O	80	18	trace	trace
H	$Cp^*Co(CO)I_2$	$AgSbF_6$ (0.2)	CsOAc (1.0)	DCE	65	18	0	0
H	$Cp^*Co(CO)I_2$	$AgSbF_6$ (0.2)	CsOAc (1.0)	MeOH	65	18	0	0
H	$Cp^*Co(CO)I_2$	$AgSbF_6$ (0.2)	CsOAc (1.0)	1,3-dioxolane	65	18	0	0
H	$Cp^*Co(CO)I_2$	$AgSbF_6$ (0.2)	CsOAc (1.0)	TFE	100	72	0	0
H	$Cp^*Co(CO)I_2$	$AgSbF_6$ (0.4)	CsOAc (1.0)	TFE	100	72	trace	0
H	$Cp^*Co(CO)I_2$	$AgClO_4$ (0.2)	NaOAc (1.0)	HFIP	100	18	0	0
H	$Cp^*Co(CO)I_2$	$AgClO_4$ (0.2)	NaOAc (1.0)	MeOH	100	18	0	0
H	$Cp^*Co(CO)I_2$	$AgClO_4$ (0.2)	NaOAc (1.0)	DCE	100	18	trace	0
H	$Cp^*Co(CO)I_2$	$AgClO_4$ (0.2)	NaOAc (1.0)	PhMe	100	18	0	0
H	$Cp^*Co(CO)I_2$	$AgClO_4$ (0.2)	NaOAc (1.0)	HFIP/TFE (1:1)	100	18	0	0
H	$Cp^*Co(CO)I_2$	$AgClO_4$ (0.2)	NaOAc (1.0)	DCE/TFE (1:1)	100	18	0	0

H	$Cp^*Co(CO)I_2$	$AgClO_4$ (0.2)	NaOAc (1.0)	PhMe/TFE (1:1)	100	18	0	0
H	$Cp^*Co(CO)I_2$	$AgClO_4$ (0.2)	RbOAc (1.0)	TFE	85	48	12	5
H	**$Cp^*Co(CO)I_2$**	**--**	**RbOAc (1.2)**	**TFE**	**85**	**48**	**32**	**18**
H	$Cp^*Co(CO)I_2$	--	RbOAc (2.0)	TFE	85	48	30	17
H	$Cp^*Co(CO)I_2$	--	RbOAc (1.2)	TFE	85	96	20	16
H	$Cp^*Co(CO)I_2$	--	RbOAc (1.2)	TFE	100	96	12	9
H	$Cp^*Co(CO)I_2$	$AgClO_4$ (0.2)	RbOAc (1.0)	TFE	100	96	12	9
H	$Cp^*Co(CO)I_2$	--	RbOAc (1.2)	TFE (0.03 M)	85	48	25	15
H	$Cp^*Co(CO)I_2$	--	RbOAc (1.2)	TFE (0.05 M)	85	48	41	23
H	$Cp^*Co(CO)I_2$	--	RbOAc (1.2)	TFE (0.2 M)	85	48	33	21
H	$Cp^*Co(CO)I_2$	--	RbOAc (1.2)	TFE (0.03 M)	100	18	14	9
H	$Cp^*Co(CO)I_2$	--	RbOAc (1.2)	TFE (0.05 M)	100	18	22	14
H	$Cp^*Co(CO)I_2$	--	RbOAc (1.2)	TFE (0.2 M)	100	18	23	16
H	$Cp^*Co(CO)I_2$	$AgSbF_6$ (0.2)	CsOAc (1.0)	TFE	85	48	22	13
H	$Cp^*Co(CO)I_2$	--	RbOAc (1.2)	TFE	100	48	22	16
H	$Cp^*Co(CO)I_2$	$AgClO_4$ (0.2)	RbOAc (1.0)	HFIP	100	18	0	0
H	$Cp^*Co(CO)I_2$	$AgClO_4$ (0.2)	RbOAc (1.0)	DCE	100	18	0	0
H	$Cp^*Co(CO)I_2$	$AgClO_4$ (0.2)	RbOAc (1.0)	CH_2Cl_2	100	18	0	0
H	$Cp^*Co(CO)I_2$	$AgClO_4$ (0.2)	RbOAc (1.0)	MeOH	100	18	0	0
H	$Cp^*Co(CO)I_2$	$AgClO_4$ (0.2)	RbOAc (1.0)	$MeNO_2$	100	18	0	0
H	$Cp^*Co(CO)I_2$	$AgClO_4$ (0.2)	RbOAc (1.0)	1,4-dioxane	100	18	0	0
H	$Cp^*Co(CO)I_2$	$AgClO_4$ (0.2)	RbOAc (1.0)	1,3-dioxolane	100	18	0	0
H	$Cp^*Co(CO)I_2$	$AgClO_4$ (0.2)	RbOAc (1.0)	THF	100	18	0	0
H	$Cp^*Co(CO)I_2$	$AgClO_4$ (0.2)	RbOAc (1.0)	CHCN	100	18	0	0

H	Cp*Co(CO)I_2	$AgClO_4$ (0.2)	RbOAc (1.0)	$PhCF_3$	100	18	0	0
H	Cp*Co(CO)I_2	$AgClO_4$ (0.2)	RbOAc (1.0)	HFIP	80	18	0	0
H	Cp*Co(CO)I_2	$AgClO_4$ (0.2)	RbOAc (1.0)	MeOH	80	18	0	0
H	Cp*Co(CO)I_2	$AgClO_4$ (0.2)	RbOAc (1.0)	$MeNO_2$	80	18	0	0

[a] = isolated yield

Table 3.2: Optimization of Additives (silver salts, acetates, bases).

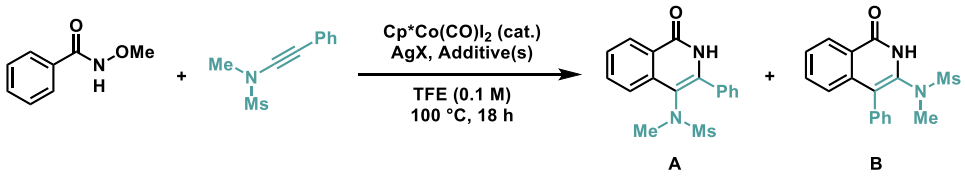

Catalyst (10 mol%)	AgX (equiv)	Additive(s) (equiv)	A (%)	B (%)
Cp*Co(CO)I_2	AgOAc (1.0)	--	0	0
Cp*Co(CO)I_2	AgOAc (2.0)	--	0	0
Cp*Co(CO)I_2	--	$Cu(OAc)_2$ (0.5)	0	0
Cp*Co(CO)I_2	--	$Cu(OAc)_2$ (1.0)	0	0
Cp*Co(CO)I_2	--	$Cu(OAc)_2$ (2.0)	0	0
Cp*Co(CO)I_2	--	$Mn(OAc)_2$ (1.0)	0	0
Cp*Co(CO)I_2	--	$Mn(OAc)_2$ (2.0)	0	0
Cp*Co(CO)I_2	--	$Mn(OAc)_3 \cdot H_2O$	0	0
Cp*Co(CO)I_2	--	$Zn(OAc)_2$ (1.0)	0	0
Cp*Co(CO)I_2	--	CsOPiv (1.0)	16[a]	11[a]
Cp*Co(CO)I_2	AgOPiv (1.2)	--	0	0
Cp*Co(CO)I_2	AgOPiv (2.0)	--	0	0
Cp*Co(CO)I_2	--	CsOAc (1.0), K_3PO_4 (0.5)	< 10	0
$[Cp^*CoI_2]_2$ (5 mol%)	--	CsOAc (1.0)	19[a]	14[a]
Cp*Co(CO)I_2	$AgSbF_6$ (1.2)	--	0	0

$Cp^*Co(CO)I_2$	$AgSbF_6$ (2.2)	--	0	0
$Cp^*Co(CO)I_2$	AgOTf (0.2)	--	31 (23[a])	19 (16[a])
$Cp^*Co(CO)I_2$	$AgBF_4$ (0.2)	--	20	14
$Cp^*Co(CO)I_2$	$AgPF_6$ (0.2)	--	27	19
$Cp^*Co(CO)I_2$	$AgClO_4$ (0.2)	--	31 (29[a])	21 (17[a])
$Cp^*Co(CO)I_2$	$AgNO_3$ (1.0)	--	0	0
$Cp^*Co(CO)I_2$	$AgNO_3$ (0.2)	--	35	23
$Cp^*Co(CO)I_2$	AgOPiv (0.2)	--	24	17
$Cp^*Co(CO)I_2$	AgOAc (1.0)	--	19	14
$Cp^*Co(CO)I_2$	AgOAc (2.2)	--	14	0
$Cp^*Co(CO)I_2$	Ag_2CO_3 (0.1)	--	39	27
$Cp^*Co(CO)I_2$	AgOTf (0.2)	CsOPiv (1.0)	19	14
$Cp^*Co(CO)I_2$	AgOPiv (0.2)	CsOPiv (1.0)	24	15
$Cp^*Co(CO)I_2$	$AgClO_4$ (0.2)	NaOAc (1.0)	46	38
$Cp^*Co(CO)I_2$	$AgClO_4$ (0.2)	KOAc (1.0)	36	27
$Cp^*Co(CO)I_2$	Ag_2CO_3 (0.1)	NaOAc (1.0)	27	22
$Cp^*Co(CO)I_2$	$AgSbF_6$ (0.2)	NaOAc (1.0)	10	0
$Cp^*Co(CO)I_2$	$AgNO_3$ (0.2)	NaOAc (1.0)	26	22
$Cp^*Co(CO)I_2$	$AgClO_4$ (0.2)	NaOAc (1.0)	3	2
$Cp^*Co(CO)I_2$ (5 mol%)	$AgClO_4$ (0.1)	NaOAc (0.5)	12	8
$Cp^*Co(CO)I_2$ (7.5 mol%)	$AgClO_4$ (0.15)	NaOAc (1.0)	24	15
$Cp^*Co(CO)I_2$ (5 mol%)	$AgClO_4$ (0.1)	NaOAc (1.0)	11	8
$Cp^*Co(CO)I_2$ (20 mol%)	$AgClO_4$ (0.4)	NaOAc (1.0)	30[a]	18[a]
$Cp^*Co(CO)I_2$	**$AgClO_4$ (0.2)**	**RbOAc (1.0)**	**50[a]**	**35[a]**
$Cp^*Co(CO)I_2$	$AgSbF_6$ (0.2)	RbOAc (1.0)	8	5
$Cp^*Co(CO)I_2$	--	RbOAc (1.2)	19	13

$Cp^*Co(CO)I_2$	$AgSbF_6$ (0.2)	--	0	0
$Cp^*Co(CO)I_2$	$AgClO_4$ (0.2)	CsOAc (1.0)	0	0
$Cp^*Co(CO)I_2$	$AgClO_4$ (2.2)	CsOAc (1.0)	0	0
$Cp^*Co(CO)I_2$	$AgClO_4$ (0.2)	CsOAc (1.0)	0	0
$Cp^*Co(CO)I_2$	$AgClO_4$ (2.2)	CsOAc (1.0)	0	0
$Cp^*Co(CO)I_2$	$AgClO_4$ (0.2)	CsOAc (1.0)	0	0
$Cp^*Co(CO)I_2$	$AgClO_4$ (0.2)	CsOAc (1.0)	0	0
$Cp^*Co(CO)I_2$	$AgClO_4$ (0.2)	CsOAc (1.0)	0	0
$Cp^*Co(CO)I_2$	$AgClO_4$ (0.2)	--	0	0
$Cp^*Co(CO)I_2$	$AgSbF_6$ (0.2)	CsF (1.0)	6	4
$Cp^*Co(CO)I_2$	$AgBF_4$ (0.2)	CsF (1.0)	15	10
$Cp^*Co(CO)I_2$	$AgBF_4$ (0.1)	CsF (1.0)	7	5
$Cp^*Co(CO)I_2$	AgF (0.2)	RbOAc (1.0)	13	9
$Cp^*Co(CO)I_2$	--	RbOAc (1.0)	20	13
$Cp^*Co(CO)I_2$	--	CsF (0.2), RbOAc (1.0)	38	25
$Cp^*Co(CO)I_2$	--	$NaSbF_6$ (0.2)	0	0
$Cp^*Co(CO)I_2$	--	$NaSbF_6$ (1.2)	0	0
$Cp^*Co(CO)I_2$	AgF (0.2)	CsF (0.2), $NaSbF_6$ (1.0)	5	4
$Cp^*Co(CO)I_2$	$AgBF_4$ (0.2)	$NaSbF_6$ (1.0)	6	0
$Cp^*Co(CO)I_2$	$AgClO_4$ (0.2)	$NaSbF_6$ (1.0)	0	0
$Cp^*Co(CO)I_2$	$AgSbF_6$ (0.2)	$NaSbF_6$ (1.0)	0	0
$Cp^*Co(CO)I_2$	$AgSbF_6$ (0.2)	$NaSbF_6$ (1.0)	0	0
$Cp^*Co(CO)I_2$	AgOAc (0.2)	$NaSbF_6$ (1.0)	0	0
$Cp^*Co(CO)I_2$	AgF (0.2)	NaOAc (1.0)	19	12
$Cp^*Co(CO)I_2$	$AgBF_4$ (1.2)	AgF (0.2)	11	7
$Cp^*Co(CO)I_2$	--	CsF (0.2), NaOAc (1.0)	24	10

$Cp^*Co(CO)I_2$	--	LiOAc (0.2)	11	4
$Cp^*Co(CO)I_2$	--	LiOAc (1.2)	28	22
$Cp^*Co(CO)I_2$	AgF	LiOAc (1.0)	20	15
$Cp^*Co(CO)I_2$	--	CsF (0.45), LiOAc (1.0)	40	25
$Cp^*Co(CO)I_2$	$AgClO_4$ (0.2)	LiOAc (1.0)	31	26
$Cp^*Co(CO)I_2$	$AgBF_4$(0.2)	LiOAc (1.0)	0	0
$Cp^*Co(CO)I_2$	AgOTf (0.2)	LiOAc (1.0)	16	11
$Cp^*Co(CO)I_2$	AgOTf (0.2)	RbOAc (1.0)	11	8

[a] = isolated yield